Lecture Notes in Earth System Sciences
LNESS

Majid Naeimi
Jakob Flury *Editors*

Global Gravity Field Modeling from Satellite-to-Satellite Tracking Data

EXTRAS ONLINE

Springer

Lecture Notes in Earth System Sciences

More information about this series at http://www.springer.com/series/10529

Majid Naeimi · Jakob Flury
Editors

Global Gravity Field Modeling from Satellite-to-Satellite Tracking Data

Springer

Editors
Majid Naeimi
Institut für Erdmessung
Leibniz Universität Hannover
Hannover
Germany

Jakob Flury
Institut für Erdmessung
Leibniz Universität Hannover
Hannover
Germany

Additional material to this book can be downloaded from http://extras.springer.com.

ISSN 2193-8571 ISSN 2193-858X (electronic)
Lecture Notes in Earth System Sciences
ISBN 978-3-319-49940-6 ISBN 978-3-319-49941-3 (eBook)
DOI 10.1007/978-3-319-49941-3

Library of Congress Control Number: 2016957489

Printed on acid-free paper

This Springer imprint is published by Springer Nature
The registered company is Springer International Publishing AG
The registered company address is: Gewerbestrasse 11, 6330 Cham, Switzerland

Foreword

The satellite gravimetry mission GRACE marks the beginning of a new level of engagement of geodesy in climate research. Since its launch in 2002, GRACE is delivering uninterrupted series of rather detailed maps of temporal variations of the Earth's gravity field. They reflect changes in the continental water cycle, quantify mass losses and gains of glaciers and the ice shields of Greenland and Antarctica, and allow to discriminate the steric from the mass component of global sea level rise and determine postglacial land uplift. Important statements on sea level rise and global ice mass balance in the IPCC report 2013 [62] are based on GRACE data.

The measurement principle of GRACE is high-precision intersatellite tracking between its two low-orbiting satellites. GRACE is now in its final mission phase and will hopefully be followed in 2017 or 2018 by an almost identical mission. This is a necessity, for time series of thirty years and more are required to unambiguously identify climate-related signals. Therefore, in order to ensure continuity of such data, preparations have started toward concepts for a mission thereafter. Very likely, it will again be based on the principle of 'satellite-to-satellite tracking between low-orbiting satellites (SST low-low).' In addition, the goal will be to make it a mission superior to GRACE in terms of spatial and temporal resolution and measurement precision. This will ask for improved concepts in terms of technology, data analysis, and interpretation.

In order to get young scientists interested and prepared for such a mission, Prof. Jakob Flury, the speaker of the Collaborative Research Center 1128, together with Dr. Majid Naeimi took the initiative for the autumn school 'Global Gravity Field Modeling from Satellite-to-Satellite Tracking Data.' The aim of Collaborative Research Center 1128 'Relativistic Geodesy and Gravimetry with Quantum Sensors' funded by the Deutsche Forschungsgemeinschaft (DFG) is to explore new frontiers of the determination of the Earth's gravitational field and of monitoring the global and regional mass redistribution. Thus, the autumn school fits perfectly to its agenda.

But why exactly 'satellite-to-satellite tracking'? Let me say a few words about the history of this so successful technique. Since Newton, it is well known that the

orbit of any artificial satellite orbiting the Earth is perfectly analogous to the free fall of an apple from a tree or a prism in a vacuum tube of an absolute gravimeter. Tracking the orbital motion of a satellite is therefore analogous to the measurement of the free fall of a test mass in the laboratory. Both types of experiments, tracking of satellites and as free-fall experiments in the laboratory, are applied in practice in order to determine the attraction of the Earth. However, the satellite experiment is confronted with two fundamental obstacles: First, while it is relatively easy in a laboratory to follow the complete free fall of a prism using, e.g., laser interferometry, it is almost impossible to get a long and evenly distributed sequence of tracking data to a satellite from an observatory on Earth, the limitations being visibility and weather conditions. Thus, only in a complicated patchwork of observations collected from many tracking stations, data taken from several satellites, and using various types of tracking techniques, it became possible, step by step, to derive comprehensive gravity models. The development in the USA is described in two fascinating volumes, edited by Henriksen [58]. The situation changed with the advent of GPS in the nineties. From then on, any low-orbiting satellite could be tracked from the configuration of GPS satellites at high altitude, uninterruptedly, and even three dimensional. Second, as expressed by Newton's inverse-squared distance law, the signal strength of gravity gets rapidly weaker with the square of the distance from the Earth. As a consequence, at satellite altitude, only a highly damped version of the Earth's gravity field can be observed. This is and was an intrinsic limitation of any type of satellite gravimetry. Therefore to obtain the Earth's gravity field with high accuracy and high spatial resolution, this damping issue should be resolved. One measure is, of course, to use satellites orbiting the Earth at lowest possible orbits, just to be as close to the attracting Earth's masses as possible. A second countermeasure is 'differentiation,' i.e.. either satellite gradiometry or satellite-to-satellite tracking.

Gravity field determination from space is as old as space age itself. It started with the first missions Sputnik 1 and Sputnik 2 in 1957. Taking their radio Doppler signal, the Earth's oblateness could be deduced with an unprecedented accuracy making more than 100 years lasting effort of geodetic arc measurements and triangulation obsolete ([23] or [102], see also [63]). However, refined gravity recovery, i.e., the construction of models beyond solely the determination of J2, turned out to be a complicated and long journey, again [58]. The development of geopotential modeling is described in [118]. In 1960 [3], the idea was spelled out of using tracking between spacecraft for gravity field determination. It became more concrete in [160]. What does it help? Measuring the relative motion between satellites eliminates the major and well-known gravitational effect, that of the spherical, slightly flattened Earth, which is almost identical for the two spacecraft. This leads to a strong amplification of the short-wavelength signal part of the Earth's gravity field relative to the remaining long-wavelength features. In a mathematical sense, it is like differentiation or like measuring the gravity gradient along the line connecting the two satellites. From the point of view of Fourier series analysis, it is the well-known effect of differentiation resulting in a multiplication of the series elements by their wave number, e.g. [20]. On invitation of NASA,

leading Earth scientists gathered in Williamstown in 1969 to formulate a vision for a future Earth science program from space [80]. Satellite-to-satellite tracking was an element of this report. It is still worthwhile to read this report because it is truly visionary both in terms of the identification of the Earth science objectives and the ideas of their realization using new satellite mission concepts. The ideas of the Williamstown report were the basis of concrete program elements in 1972 in NASA's EOPAP report [109]. There, dedicated satellite gravimetry took shape, the so-called GRAVSAT mission ideas of satellite-to-satellite tracking in the high–low and low–low mode and satellite gradiometry. Analyzing the tracking data from Earth to the Apollo lunar orbiters for the purpose of gravity field recovery can be regarded the first realization of a high–low satellite-to-satellite tracking experiment [108]. Other high–low tracking tests were between the relay satellite ATS-6 and Apollo/Soyuz [150] and between ATS-6 and Geos-3 [51, 94, 128, 134, 159]. A first, not quite successful attempt of low–low tracking was the gravimetric use of the data of the docking experiment between the Apollo and Soyuz spacecraft [156].

In Europe, the first initiative in this direction was a summer school on satellite geodynamics in Lannion in 1974 sponsored by the French space agency CNES, where leading European geodesists and geophysicists discussed ideas about dedicated satellite gravimetry missions and their theoretical background, [4]. In 1978, it followed a workshop on Space Oceanography, Navigation and Geodynamics (SONG) organized by the European Space Agency [37]; it was the first step toward an ESA Earth observation program, and satellite-to-satellite tracking and gradiometry were on its agenda [127]. In parallel, ESA ran a first study mission and system definition study of a low–low satellite-to-satellite tracking experiment for gravity field determination, called SLALOM [5]. The idea was laser tracking from the space shuttle to two passive compact cannon ball satellites.

A theoretical milestone was [100]: Meissl formulated a framework connecting the spectral representation of various gravity functionals, such a geoid heights, gravity anomalies, and gravity gradients at altitude and at the Earth's surface, in a systematic way in terms of spherical harmonics. Later, this framework was denoted Meissl scheme [126], see also [124, 125]. Other important theoretical contributions and simulation work on satellite-to-satellite tracking were [26, 27, 50, 74, 79, 107, 130, 135, 152].

However, the necessary technology was not yet mature enough to get a dedicated low–low SST gravity mission approved. An analysis of the state of the art took place in a workshop organized by the US National Research Council: applications of a dedicated gravitational satellite mission [113], followed by several mission proposals in the years thereafter. While the European side concentrated on satellite gradiometry, i.e., the measurement of the relative gravitational acceleration between several test masses inside one satellite, the US American side pursued the realization of a low–low satellite-to-satellite mission, from 1979 on as Gravity Research Mission (GRM). Of great importance were simulation studies showing the potential of such a mission for determining temporal variations of the gravity field, caused by mass transport processes in system Earth, such as ice melting, sea level

rise, and glacial isostatic adjustment [32, 154]. In 2002, GRACE was launched, the first low–low satellite-to-satellite tracking mission, the beginning of an amazing success story [140]. In 2012, the NASA GRAIL mission employed the same mission and sensor concept to the determination of the lunar gravity field [166].

The autumn school, supported by the Wilhelm und Else Heraeus foundation, took place from October 4 to 9, 2015, at the Physikzentrum in Bad Honnef, Germany. The organizers succeeded to attract as teachers five of the leading experts in this field. In their lectures, the participants were introduced into the basic alternative approaches of data analysis as well as into the characteristics, strength, and limitations of these methods. Furthermore, in order to deepen insight, they together with coworkers prepared and supervised labs. In a series of evening talks, additional selected topics were presented, ranging from future technology via advanced methodology, relativistic modeling to Earth application. About fifty students from 16 countries participated in the autumn school. Their unanimous conclusion is well prepared, perfectly organized, good atmosphere, and very useful.

Special thanks go to Prof. Flury and Dr. Naeimi, to all lecturers and their coworkers, and to the Physikzentrum and Wilhelm und Else Heraeus foundation.

Munich, Germany Reiner Rummel
June 2016

Preface

The present book collects the lecture notes of the international Wilhelm und Else Heraeus autumn school 'Global Gravity Field Modeling from Satellite-to-Satellite Tracking Data,' held from October 4 to 9, 2015, in Bad Honnef, Germany. The first ideas of the autumn school (the initial plan was a summer school) came up in November 2013 during an internal discussion in Hannover on the requirements for the GRACE/GRACE Follow-On Mock Data Challenge project[1] in the Collaborative Research Center (Sonderforschungsbereich) 1128 'Relativistic Geodesy and Gravimetry with Quantum Sensors (geo-Q)' of Leibniz Universität Hannover.[2] The idea soon attracted attention, and we received positive feedback from experts of the field.

In a rather short period of application time, we received many applications from around the world and we are pleased for hosting over fifty participants from Germany, USA, Switzerland, Austria, India, China, Iran, Russia, Bulgaria, Netherlands, Poland, Brazil, Luxembourg, Canada, and Sweden.

The main goal of the autumn school was to provide a basis to the interested students and geodesists for analyzing SST data from current and future satellite missions. The emphasis was put on different approaches for the recovery of the Earth's gravity field. These techniques are the acceleration approach, the energy balance approach, and the classical (variational) approach. In addition, the related subjects of orbit determination and parameter estimation were included.

The school started on Sunday 4 October with an opening talk by Prof. Reiner Rummel about the spherical harmonic analysis and gravity field determination and was followed by a 5-day intensive program. Core topic lectures on each morning

[1] http://www.geoq.uni-hannover.de/mock.html

[2] http://www.geoq.uni-hannover.de

were complemented by more numerical and practical exercises in the afternoon. The chapters of this book are based on the core topic lectures given on each day as follows:

1. **Parameter Estimation for Satellite Gravity Field Modeling**, by Prof. Jürgen Kusche and Anne Springer, University of Bonn, Germany

This chapter gives first a general overview about Gauss–Markov models and their use in the presence of observation noise. Variance component estimation, regularization, and biased estimation are addressed. Exercises at the end of the chapter give more insight into the applications for gravity field determination from GRACE data.

2. **Precise Orbit Determination**, by Prof. Adrian Jäggi and Dr. Daniel Arnold, University of Bern, Switzerland

Here, the general issues of orbit modeling such as the treatment of tracking data, orbit representation techniques, and the orbit determination problem together with gravity field parameterization are considered. Two exercises for a deeper understanding of orbit determination are added.

3. **The Classical Variational Approach**, by Prof. Srinivas Bettadpour and Christopher McCullough, University of Texas at Austin, USA

The basic principles of the classical approach used by processing centers such as CSR and GFZ are discussed, followed by numerical exercises for more understanding.

4. **The Acceleration Approach**, by Dr. Matthias Weigelt, Institut für Erdmessung, Leibniz Universität Hannover, Hannover, Germany

A comprehensive overview about the acceleration approach including the strengths and drawbacks of this method is provided in this chapter. Approximate and rigorous solutions using this approach are discussed, with the exercises on the numerical aspects.

5. **The Energy Balance Approach**, by Prof. Christopher Jekeli, Ohio State University, USA

This chapter reviews the energy integral for the derivation of potential differences along the satellite orbit and for gravity field determination. Aspects of this approach including the separation of the temporal variations, the rotational potential, kinetic potential, and dissipative forces are described. Similar to other chapters, exercises provide more understanding about the numerical details of the method.

Acknowledgements

We would like to thank all the lecturers for contributing to the autumn school, for providing great lectures and exercises as well as for the fruitful discussions. Their great efforts to provide these lecture notes will certainly make this book as a long-lasting reference in satellite gravimetry. We also thank all attendees of the school who, with their enthusiasm, created a scientific and friendly atmosphere during the school.

A special thank goes to Wilhelm und Else Heraeus Foundation for generously hosting the school. We also acknowledge the support by Prof. Karsten Danzman from Albert Einstein Institute in Hannover who suggested the inspiring venue of Physikzentrum Bad Honnef, Germany. Finally, the support for typesetting by Richu Mary Shelly is gratefully acknowledged.

Data and Material for Exercises

All data and programs for the exercises as well as their solutions (if provided) are available at the following online repositories:

www.geoq.uni-hannover.de/autumnschool-data
http://extras.springer.com

For Chap. 2, the related files can be downloaded from:

http://aiuws.unibe.ch/WEHeraeusAS2015/Chapter2-OrbitDetermination.zip

Hannover, Germany
August 2016

Majid Naeimi
Jakob Flury

Contents

Contributors

Daniel Arnold Astronomical Institute, University of Bern, Bern, Switzerland

Srinivas Bettadpur Center for Space Research (CSR), The University of Texas at Austin, Austin, USA

Christopher Jekeli School of Earth Sciences, The Ohio State University, Columbus, USA

Adrian Jäggi Astronomical Institute, University of Bern, Bern, Switzerland

Jürgen Kusche Institute for Geodesy and Geoinformation, Bonn University, Bonn, Germany

Christopher McCullough Center for Space Research (CSR), The University of Texas at Austin, Austin, USA

Anne Springer Institute for Geodesy and Geoinformation, Bonn University, Bonn, Germany

Matthias Weigelt Institut für Erdmessung, Leibniz Universität Hannover, Hannover, Germany

Chapter 1
Parameter Estimation for Satellite Gravity Field Modeling

Jürgen Kusche and Anne Springer

Abstract In simple words, *parameter estimation* is the process of extracting well-defined best 'guesses' of geophysical or measurement-system related values from uncertain and erroneous, conflicting and possibly at the same time incomplete data. These data may provide information on the sought-for parameters by way of direct observation, but much more often this relation is very indirect. Anyway, we know that we can never know 'true' parameters but we are satisfied with 'estimates' as long as these are 'best' in some way, like having the least spread for a given breed of data errors.

This itself is a challenge common to all natural sciences (and most social sciences where 'empirical' studies are relevant). In satellite gravity field determination, the most relevant sought-for quantity is a geophysical field that has an infinite number of degrees of freedom and no preferred degree of truncation—this renders the application of standard and centuries-old methods such as least squares more complicated. This also continues to create confusion among data analysts from different backgrounds. Constructive approximation theory, rooted in functional analysis, provides a modern approach of breaking down the problem to a finite number of parameters without the uneasy feeling of 'omitting' something important. But the error bounds provided by approximation theory depend on such abstract ideas as kernel functions that describe the smoothness of a space.

Least-squares methods are by no means the single unchallenged approach in satellite gravity analysis, due to the reason just mentioned. However, they are straightforward to apply, and they lead to error estimates that at least offer a way to address the uncertainty introduced by real measurement systems.

J. Kusche (✉) · A. Springer
Institute for Geodesy and Geoinformation, Bonn University, Bonn, Germany
e-mail: kusche@geod.uni-bonn.de

A. Springer
e-mail: springer@geod.uni-bonn.de

M. Naeimi and J. Flury (eds.), *Global Gravity Field Modeling from Satellite-to-Satellite Tracking Data*, Lecture Notes in Earth System Sciences,
DOI 10.1007/978-3-319-49941-3_1

Least squares methods, in our view, allow to tackle some of today's challenges in satellite gravity data analysis, like (1) efficiently dealing with large amounts of data and of sought-for parameters, (2) quantifying the effect of data errors and so-called background model errors on spherical harmonics and derived science results more or less comprehensively, and (3) 'consistently' combining data sets from different instruments, satellites, and processing chains, in the presence of inconsistencies that are 'known' but hard to pinpoint and too costly to remove from a first principles point of view.

The development of the least squares method originated in a need for fitting techniques that materialized already in ancient times, with the first astronomical/geodetic observations that relate to the radius of the Earth and the orbital radii of the Earth and the Moon [109]. Later, and well-known in geodesy, meridional arc measurements were carried out in order to determine the flattening of the ellipsoidal Earth. For these measurements, one could not simply derive the parameter of interest from a single measurement and average the data. *Laplace* (1749–1827) developed several fitting techniques, aiming at e.g. minimizing the maximum error between fitted ellipsoid and data, and later, minimizing the average absolute value of the errors subject to constraining the sum of them to zero. Much of this work was influenced by *Boscovitch* (1711–1787) who, less known to us today, worked on the same problem and developed first principles of what we would call adjustment theory. *Legendre* (1752–1833) published the method of normal equations for least squares to be applied in the analysis of arc measurements, and *Gauss* (1777–1855) developed the method of weighted least squares as we know it today, albeit without relying to matrix notation at that time. He applied LS to his determinations of planetary and asteroid orbits, and of course in the adjustment of large-scale trigonometric surveys.

These lecture notes were compiled on the occasion of the International Autumn School 'Global Gravity Field Modeling from Satellite-to-Satellite Tracking Data', organized by DFG's SFB 'geo-Q' at October 4–9, 2015 in Bad Honnef, Germany. Our aim was to give students with different background an introduction to some concepts from parameter estimation that are common and useful for analyzing satellite gravity data (i.e. typically solving for sets of spherical harmonic coefficients). The focus was on concepts, and technical proofs were avoided.

1.1 Notation

Vectors are denoted by $\mathbf{a}$, $\mathbf{x}$ and matrices by capital letters, $\mathbf{A}$, $\mathbf{X}$, etc. Although it would be more consistent, we refrain from distinguishing between random variables and their realizations.

$E(\cdot)$ and $D(\cdot)$ are expectation and dispersion (covariance) operators. By $\hat{\cdot}$ we denote an estimated quantity. Note that $\hat{c}^2$ differs from $\widehat{c^2}$.

Spherical harmonics are $Y_{nm}(\lambda, \theta)$, i.e. for $m > 0$ these are the $C_{nm}(\lambda, \theta)$, for $m < 0$ the $S_{nm}(\lambda, \theta)$. They are considered as fully normalized (we drop the overbar).

1.2 Literature

Adjustment problems are addressed in various scientific fields and, thus, there is a vast amount of literature on this topic. Here, a selective and inevitably incomplete overview on publications relevant in the field of geodesy is given.

A tutorial on the history of least squares adjustment including several examples based on typical geodetic problems (e.g. related to the shape of the Earth) is provided by [109]. For an introduction into the field of adjustment theory and statistics we recommend a comprehensive textbook written by a scientist deeply involved in the development of satellite geodesy [85]. [13] approaches the topic from an applied mathematician's perspective, concentrating on discrete least squares problems including the design of efficient solvers. Among the contributions focusing on gravity field determination we would like to highlight [127] who discusses numerical strategies for large adjustment problems with a focus on decorrelation and iterative solution. [22] expands this work and addresses several aspects of least squares gravity field estimation in a massive parallel programming concept. Quality measures that can be applied to both unconstrained and constrained global gravity analyses/solutions are reviewed by [19].

As gravity field recovery from satellite data represents an ill-posed problem regularization is a key issue. An in-depth study on regularization applied to the GOCE problem was published by [33]. For an optimal choice of the regularization parameters Variance-Component Estimation (VCE) proved to be a good choice. In his groundbreaking paper of 1979 [40] suggested the VCE iterative procedure most common in use until today. For a theoretical derivation and justification of VCE within the Maximum Likelihood framework [84] is a good reference. Deeper insights into VCE and a comparison to Lerch's optimal weighting are given by [87] who also introduces a Monte Carlo approach for variance-component estimation. A comprehensive discussion of several VCE techniques with application to gravity modeling was published by [145] and also includes hypothesis testing for auxiliary parameters.

1.3 Gauss-Markov Model

One of the most important models in the statistical analysis of measured data $y_i, i = 1 \ldots n$ is the *Gauss-Markov Model*, or in brief *GMM*. Many books have been written on statistical data analysis in general, on the GMM, on the famous least squares method and its application in geodesy, adjustment theory, but in the the discussion below we will strictly follow the excellent work by Karl-Rudolf Koch, *Parameter estimation and hypothesis testing in linear models* [85].

What is not in the mixed bag presented here, is the application of parameter estimation theory to modern problems of geodesy that cannot be formulated through the GMM: mixed integer-float estimation as in GNSS ambiguity resolution problems, estimation with multiplicative noise as e.g. in radar altimetry and InSAR, classification problems as in altimetry and remote sensing.

1.3.1 Assumptions Underlying the Gauss-Markov Model

In the GMM one assumes that (1) the mathematical expectation of the data (loosely speaking, the error-free data) can be related linearly to a set of unknown but fixed parameters $x_j,\ j = 1 \ldots m$, and (2) and that we have at our hand a knowledge of the variances and covariances of the data errors, up to some common factor.

The analysis framework provided by the GMM is much more general as e.g. considered in time series analysis. The data that are considered to provide information (*inference*) on the parameters may be collected at the same time at different locations, at different times from the same instrument, or simply a combination of any of these situations.

1.3.1.1 Formulation of the Gauss-Markov Model

Writing data and parameters in vector notation, the above translates into the most basic formulation of the GMM,

$$E(\mathbf{y}) = \mathbf{A}\mathbf{x} \qquad \text{and} \qquad D(\mathbf{y}) = \sigma^2\mathbf{I}\,, \tag{1.1}$$

with $\mathbf{y} = n \times 1$ data vector, $\mathbf{x} = m \times 1$ parameter vector, $\mathbf{A} = n \times m$ full-rank observation equation matrix or design matrix, and the variance factor σ^2. In the above, we assume that all observations have the same error variance and that they are uncorrelated with respect to each other.

As a reminder, the expectation $E(\mathbf{y})$ and the covariance matrix $D(\mathbf{y})$ of the observations are

$$E(\mathbf{y}) = \int \mathbf{y}\ p(\mathbf{y})\ d\mathbf{y} \qquad \text{and} \qquad D(\mathbf{y}) = E\left((\mathbf{y} - E(\mathbf{y}))(\mathbf{y} - E(\mathbf{y}))^T\right)\,.$$

Loosely speaking, the expectation $E(\mathbf{y})$ is what we would obtain by averaging an infinite number of data vectors, where the frequency of the occurence of a certain measured outcome is given by the probability density function $p(\mathbf{y})$. The covariance (or dispersion) matrix is what we would obtain by averaging an infinite number of samples of the deviation of the data vector to its expectation (the data errors), taken to the outer product. On the diagonal, $D(y_i) = D(y_i, y_i) = E(y_i - E(y_i))^2 = E(e_i^2)$ is the error variance, on the off-diagonal $D(y_i, y_j) = E((y_i - E(y_i)(y_j - E(y_j)) = E(e_i e_j)$ the data error covariance. In the above, it is assumed to be zero.

On introducing the (unknown) observation errors $e_i, i = 1 \ldots n$, this may be recast as

$$\mathbf{y} + \mathbf{e} = \mathbf{A}\mathbf{x} \qquad \text{with} \qquad E(\mathbf{e}) = \mathbf{0} \qquad \text{and} \qquad D(\mathbf{e}) = \mathbf{C_{ee}} = \sigma^2\mathbf{I}\,. \tag{1.2}$$

In other words, for the i-th observation, $D(e_i) = E(e_i^2)$ is what we would obtain by averaging an infinite number $k \to \infty$ of ${e_i^{(k)}}^2$, and $D(e_i, e_j) = E(e_i e_j)$ by averaging the $e_i^{(k)} e_j^{(k)}$.

1.3.1.2 Properties of the Gauss-Markov Model

In Eq. (1.1), $\mathbf{y}$ is a vector of observed measurement values. The matrix $\mathbf{A}$ must be given, it realizes our—possibly hypothetical—understanding of the mathematical and physical relation of the data to some set of 'explaining' parameters $\mathbf{x}$—the model that relates observables to (sometimes called) hidden parameters. Here, we will consider only the most common case with $n > m$; i.e. more data than parameters to be estimated. Obviously, different formulations of the model are possible and this affects the definition of $\mathbf{x}$.

Example Fitting a polynomial to a set of measurement a first model reads

$$y(t_i) + \varepsilon_i = a_0 + (t_i - t_0)a_1 + \frac{1}{2}(t_i - t_0)^2 a_2$$

while a second one can be formulated as

$$y(t_i) + \varepsilon_i = b_0 + t_i b_1 + t_i^2 b_2.$$

It is clear that $a_0 = b_0$, $a_1 + 2t_0 a_2 = b_1$, $\frac{1}{2}t_0^2 a_2 = b_2$. In the first model of the example, the rows $\mathbf{a}_i$ of the design matrix that correspond to the ith measurement, are made up by the entries 1 (corresponding to a_0), $(t_i - t_0)$, and $\frac{1}{2}(t_i - t_0)^2$.

Parameters $\mathbf{x}$ are considered as fixed, i.e. unknown but deterministic and non-random quantities in the above. This differs in the Bayesian approach, where the parameters are considered as stochastic and, consequently, a PDF has to be specified for them. In the Bayesian terminology, the above model would be written as

$$E(\mathbf{y}|\mathbf{x}) = \mathbf{A}\mathbf{x} \qquad \text{and} \qquad D(\mathbf{y}|\sigma^2) = \sigma^2 \mathbf{I}$$

where $\cdot|\mathbf{x}$ and $\cdot|\sigma^2$ means *under the condition that the unknown parameters* $\mathbf{x}$ *and* σ^2 *are given*.

An evenly sampled sequence of measurements $y_i = y(t_i)$ (e.g. ranging data in satellite gravimetry) can be related to the spherical harmonics of the gravity field c_{nm} and s_{nm}, and this is ultimately done when the final parameter estimation step is performed. On the other hand, one may view at the stream of data from a time series perspective, and fit, e.g. within a certain time window of p consecutive samples, simple models (e.g. simple polynomials, Chebyshev polynomials) that disregard the gravity field. Without introducing the error contributions, the system above would read $\mathbf{y} = \mathbf{A}\mathbf{x}$; it is inconsistent and has no solution (at least not for a given, measured data vector). For the moment we assume $\mathbf{A}$ has full rank; this assumption can be later relaxed.

Observation errors $\mathbf{e}$ are unknown by definition. Also, in the formulation we do not have to assume the errors to be normally distributed. In the GMM, data errors are considered as stochastic but the only assumption that we make is that their expectation is zero and that their covariance matrix is given up to some factor. In particular, we don't have to assume the errors follow a normal distribution. The above implies that

$$E(\mathbf{e}) = \int \mathbf{e}\; p(\mathbf{e})\; d\mathbf{e} = \mathbf{0} \qquad \text{and} \qquad D(\mathbf{e}) = E(\mathbf{e}\mathbf{e})^T = \sigma^2 \mathbf{I}.$$

The variance factor σ^2 can be assumed as unknown and estimated. In fact its value is not required in the standard solution to the GMM, and therefore it can be estimated from the fit of the observed data to the 'predicted data'. In practice, the variance factor is often identified with an overall scaling factor for the a-priori accuracy of the observations, and we expect to estimate a factor close to one in case our a-priori assumption on the data error variance was a good one. At the same time, this means if we believe we know σ^2 in advance, it is still a good test to estimate it. In the above, the error covariance matrix is assumed as diagonal; this can be relaxed soon.

1.3.1.3 Generalization of the Gauss-Markov Model

In the GMM it is possible to relate each single observation y_i to the unknown parameters. But in applications, one may have several observations within one equation. There are more general models that relate linear functionals of 'original' data to unknowns, e.g. $\mathbf{By} + \mathbf{e} = \mathbf{Ax}$ but we do not consider them here. One example are multiplicative noise models, e.g. $y_i = \varepsilon_i \mathbf{a_i^T x}$ with $E(\varepsilon_i) = 1$, that are needed for representing speckle noise of radar measurements.

Moreover, in reality, the entries of the matrix $\mathbf{A}$ will often contain measured quantities. For example, in satellite gravity field determination, typically the orbit of a satellite is required to build the entries of matrix $\mathbf{A}$. It is a known fact that such errors may be critical, but in the standard GMM, errors of this kind are not taken into account. There are more general statistical models, e.g. the Gauss-Helmert model or the Errors-in-Variables and Total Least Squares models ($\mathbf{y} + \mathbf{e} = (\mathbf{A} + \mathbf{E})\mathbf{x}$ with $E(\mathbf{E}) = 0$) where one can account for random errors in the design matrix, but these are usually more difficult to apply. In gravity field determination, it is much more common to parameterize such errors, i.e. to relate them to deterministic parameters and thus augment the parameter vector.

1.3.2 Parameter Estimation in the Gauss-Markov Model

For the above model, since we do not know the 'real value' of the data or of the data errors, it is only possible to derive a statistical *estimate* $\hat{\mathbf{x}}$ of the parameter vector $\mathbf{x}$.

The value that we obtain for this estimate depends on the unknown data errors and its deviation from the expectation is thus uncertain. Therefore, we also would like to derive a measure for the statistical uncertainty with which $\hat{\mathbf{x}}$ has been obtained. Typically, this means we derive an estimate for the covariance matrix $D(\hat{\mathbf{x}})$.

In order to do so, we need to apply some sort of statistical theory, which is to say to adopt some principle for arriving at an estimate that minimizes a quantity which can be reasonably interpreted. In other words, we need to cast 'plausibility' into a mathematical framework. Fortunately, for the above model, the principle of *best linear unbiased estimation (BLUE)*, the *least-squares method*, and the *maximum likelihood method (ML) on assuming a Gaussian pdf for the errors* all arrive at the same estimate $\hat{\mathbf{x}}$ for the parameters:

$$\hat{\mathbf{x}} = \left(\mathbf{A}^T\mathbf{A}\right)^{-1}\mathbf{A}^T\mathbf{y}. \tag{1.3}$$

An estimate is called unbiased whenever $E(\hat{\mathbf{x}}) = \mathbf{x}$. This means, assuming we collect more and more data (of the same kind), the estimate will get closer and closer to the true value. In the case we discuss here, this means

$$E(\hat{\mathbf{x}}) = E\left(\left(\mathbf{A}^T\mathbf{A}\right)^{-1}\mathbf{A}^T\mathbf{y}\right) = \left(\mathbf{A}^T\mathbf{A}\right)^{-1}\mathbf{A}^T\mathbf{A}\mathbf{x} = \mathbf{x}$$

which, as expected, tells that the estimate is unbiased. In the GMM the above estimate is often called a *linear regression*. The estimate is obtained as a weighted linear combination of the data. If the data errors are normally distributed, the errors of the estimate will be so as well. Obviously, for computing $\hat{\mathbf{x}}$ it is not required to know the variance factor.

The above estimate is often written with normal equation matrix $\mathbf{N}$ and right-hand side vector $\mathbf{r}$ as

$$\hat{\mathbf{x}} = (\mathbf{N})^{-1}\mathbf{r} \quad \text{with} \quad \mathbf{N} = \mathbf{A}^T\mathbf{A} \quad \text{and} \quad \mathbf{r} = \mathbf{A}^T\mathbf{y}.$$

Or, in order to emphasize the linear nature of the estimate this can be reformulated as

$$\hat{\mathbf{x}} = \mathbf{L}\mathbf{y} \quad \text{with} \quad \mathbf{L} = \left(\mathbf{A}^T\mathbf{A}\right)^{-1}\mathbf{A}^T\,.$$

Example Assume, for the moment, we have measured values of the gravitational potential, obtained at a given constant (geocentric) satellite altitude r. With other words, we assume the data is given on a sphere with radius r encompassing the Earth (in so-called space-wise approaches, one 'projects' data observed at varying orbital height to the height of a mean orbital sphere, think of employing a reference vertical gradient of the potential times altitude difference). We would like to determine the spherical harmonic coefficients v_{nm} of the gravity field. In this—strongly simplified—case, the model reads for a single observation $y_i = y(\lambda_i, \theta_i)$

$$y_i + e_i = \sum_{n=0}^{\infty} \sum_{m=-n}^{n} \left(\frac{a}{r}\right)^{n+1} Y_{nm}(\lambda_i, \theta_i)\ v_{nm}, \tag{1.4}$$

and a is the reference radius associated with the coefficients. Here we use

$$Y_{nm}(\lambda, \theta) = \begin{matrix} P_{nm}(\cos\theta)\cos(m\lambda) \\ P_{n|m|}(\cos\theta)\sin(|m|\lambda) \end{matrix} \quad \text{and} \quad v_{nm} = \begin{matrix} c_{nm} \\ s_{n|m|} \end{matrix} \quad \text{for} \quad \begin{matrix} m \geq 0 \\ m < 0 \end{matrix}.$$

Obviously, we have to truncate the series to some finite degree $\bar{n}$, in order to 'fit into the GMM framework'. Then, the estimate

$$\hat{\mathbf{x}} = \begin{bmatrix} \hat{v}_{00} \\ \vdots \\ \hat{v}_{\bar{n}\bar{n}} \end{bmatrix}$$

is obtained from the above with realizing that

$$\mathbf{y} = \begin{bmatrix} y(\lambda_1, \theta_1) \\ \vdots \\ y(\lambda_n, \theta_n) \end{bmatrix} \quad \text{and} \quad \mathbf{A} = \begin{bmatrix} \left(\frac{a}{r}\right)^1 Y_{00}(\lambda_1, \theta_1) & \ldots & \left(\frac{a}{r}\right)^{\bar{n}+1} Y_{\bar{n}\bar{n}}(\lambda_1, \theta_1) \\ & & \\ \left(\frac{a}{r}\right)^1 Y_{00}(\lambda_n, \theta_n) & \ldots & \left(\frac{a}{r}\right)^{\bar{n}+1} Y_{\bar{n}\bar{n}}(\lambda_n, \theta_n) \end{bmatrix}.$$

It is interesting to note that the least squares estimate $\hat{\mathbf{x}} = \mathbf{N}^{-1}\mathbf{r} = \mathbf{W}\mathbf{r}$ apparently looks like a discretized integral over the data, with a particular choice of integration weights:

$$\hat{\mathbf{r}} = \mathbf{A}^T\mathbf{y} = \begin{bmatrix} \hat{r}_{00} \\ \vdots \\ \hat{r}_{\bar{n}\bar{n}} \end{bmatrix} \quad \text{with} \quad r_{nm} = \sum_i \left(\frac{a}{r}\right)^{n+1} Y_{nm}(\lambda_i, \theta_i)\ y_i$$

and

$$\mathbf{N} = \begin{bmatrix} N_{00;00} & \ldots & N_{00;\bar{n}\bar{n}} \\ & & \\ N_{00;\bar{n}\bar{n}} & \ldots & N_{\bar{n}\bar{n};\bar{n}\bar{n}} \end{bmatrix}$$

with

$$N_{nm;n'm'} = \sum_i \left(\frac{a}{r}\right)^{n+n'+2} Y_{nm}(\lambda_i, \theta_i) Y_{n'm'}(\lambda_i, \theta_i).$$

Again, this resembles the well known integral $\int_\Omega Y_{nm}(\cdot) Y_{n'm'}(\cdot) d\cdot$.

It is quite obvious from the above that the choice of the reference radius a affects the condition of the normal equation system. The closer we chose a to the satellite orbital height r, the more will $\frac{a}{r}$ and $\left(\frac{a}{r}\right)^{n+n'+2}$ approach unity. With the spherical harmonics normalized, all main diagonal entries will be of the same magnitude. Yet,

the price we have to pay is that the coefficients determined in this way describe the potential at satellite height. Once we would employ them to, e.g. derive geoid heights, we have to apply the $\left(\frac{a}{r}\right)^{n+1}$ to them. There is no way to escape *downward continuation* and the increasing instability for higher degrees that it adds.

Assuming the observations as temporally uncorrelated, and given as a long time series (collected along a satellite orbit over many years), it is numerically most efficient to assemble the normal equation system 'on-the-fly', in batches or even for single observations. A single observations can be written as

$$y_i + e_i = \mathbf{a}_i^T \mathbf{x} \tag{1.5}$$

with $\mathbf{a}_i^T$ being one row of the design matrix. This means, the corresponding normal equation system is

$$\mathbf{N}_i = \mathbf{a}_i \mathbf{a}_i^T \quad \mathbf{r}_i = \mathbf{a}_i \mathbf{y}. \tag{1.6}$$

The outer product can be computed very efficiently using library routines, and $\mathbf{N} = \sum_i \mathbf{N}_i$ can be updated on the fly. Furthermore, whenever the observations in a satellite gravity determination problem are distributed very dense, on similar heights, and without a polar gap, and assuming they are weighted per area, the normal equation matrix will appear as near block diagonal. In fact, conditions of *discrete orthogonality* have to be met to create a block diagonal matrix that allows to use specially designed solvers.

Example Estimating spherical harmonic coefficients from simulated, error-free values of the gravitational potential along a given satellite orbit using the relationship of Eq. (1.4) results into a near block diagonal normal equation matrix as shown in Fig. 1.1. Even (uneven) coefficients of the same order are highly correlated.

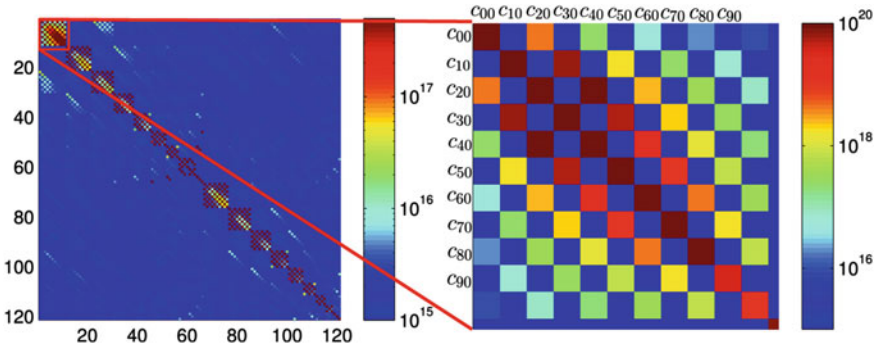

Fig. 1.1 Example of the normal equation matrix for estimating spherical harmonic coefficients from simulated gravitational potential using Eq. (1.4). The gravitational potential was simulated along a real GRACE orbit of one month at an altitude of about 480 km with a sampling of 60 s. The presented normal equation matrix was computed up to degree and order $\bar{n} = 10$. The parameter vector is sorted order-wise and contains first all cosine components and then all sine components. Particularly high correlations exist between even (uneven) coefficients of the same order

1.3.3 Deriving the Estimator Through the Maximum-Likelihood Method

As has been said before, the estimator Eq. (1.3) can be derived from various principles, which means that it features a broad spectrum of optimality properties. This explains its popularity.

In the following, we chose the Maximum-Likelihood (ML) method to derive the estimator. The reason for this is of didactic nature; the ML method is often used to derive efficient estimators in other problems, such as those with multiplicative noise or where estimators for extreme values are sought.

In the ML method, we have to assume we know the pdf of the observations. In problems of satellite gravity, we usually assume the noise is Gaussian ($\mathcal{N}(\cdot)$). This means, we add to the model Eq. (1.2) the assumption

$$\mathbf{y} \sim \mathcal{N}(\mathbf{A}\mathbf{x}, \sigma^2\mathbf{I}) \tag{1.7}$$

where $\sim$ means 'is distributed as'. In ML, the pdf of the observations is viewed upon as a function of the parameters ($\mathbf{x}$ and σ^2 in case of the GMM) for given (i.e. the observed) data $\mathbf{y}$. The parameters are then chosen as those for which the probability to observe the given data is biggest. In the general case, this leads to an optimization problem that is often solved numerically, but for the GMM an analytical solution exists which coincides with the LS estimator. In satellite gravity, the ML principle simply translates as: upon all possible gravity fields the one that has the highest probability to generate the observed orbits and ranging data is the one that we chose.

With the definition of the multivariate Gaussian PDF, and with what has been said before, the Likelihood function is

$$L(\mathbf{y}, \mathbf{x}, \sigma^2) = \frac{1}{(2\pi\sigma^2)^{n/2}}\, e^{-\frac{(\mathbf{y}-\mathbf{A}\mathbf{x})^T(\mathbf{y}-\mathbf{A}\mathbf{x})}{2\sigma^2}} . \tag{1.8}$$

Now the ML estimates for $\mathbf{x}$ and σ^2 are to be found by maximizing the above. It is allowed and common to replace L by the log-Likelihood $\ln L$, since both functions can be easily shown to have extrema at the same positions. With this, we have to equate the partial derivatives of $\ln L$ to zero:

$$\frac{\partial \ln L(\mathbf{y}, \mathbf{x}, \sigma^2)}{\partial \mathbf{x}} = \mathbf{0} \quad \text{and} \quad \frac{\partial \ln L(\mathbf{y}, \mathbf{x}, \sigma^2)}{\partial \sigma^2} = 0 . \tag{1.9}$$

We obtain

$$\ln L(\mathbf{y}, \mathbf{x}, \sigma^2) = -\frac{n}{2}\ln 2\pi - \frac{n}{2}\ln\sigma^2 - \frac{1}{2\sigma^2}(\mathbf{y} - \mathbf{A}\mathbf{x})^T(\mathbf{y} - \mathbf{A}\mathbf{x})$$

and the conditions:

$$\frac{\partial \ln L(\mathbf{y}, \mathbf{x}, \sigma^2)}{\partial \mathbf{x}} = -\frac{1}{2\sigma^2}\frac{\partial}{\partial \mathbf{x}}\left(-2\mathbf{y}^T\mathbf{A}\mathbf{x} + \mathbf{x}^T\mathbf{A}^T\mathbf{A}\mathbf{x}\right) = \mathbf{0}$$

and

$$\frac{\partial \ln L(\mathbf{y}, \mathbf{x}, \sigma^2)}{\partial \sigma^2} = -\frac{n}{2\sigma^2} + \frac{1}{2\sigma^4}(\mathbf{y} - \mathbf{A}\mathbf{x})^T(\mathbf{y} - \mathbf{A}\mathbf{x}) = 0.$$

From the first condition, one obtains readily the estimate Eq. (1.3). From the second condition, one obtaines

$$\widehat{\sigma^2}_{ML} = \frac{1}{n}\left(\mathbf{y} - \mathbf{A}\hat{\mathbf{x}}\right)^T\left(\mathbf{y} - \mathbf{A}\hat{\mathbf{x}}\right).$$

The ML estimate for the variance factor σ^2 can be shown to be biased. This is an example where different estimation principles lead to different results in practice. We tend to use the unbiased estimator as discussed below in practical applications. But the unbiased one will then obviously not maximize the probability to obtain the observed data. For all estimation problems that are more complicated than the simple Gaussian linear model, additive noise case, we have to live with the ambiguity of estimators, and the estimator should be chosen based on the relevance of the underlying principle for the problem in question.

Gaussianity of noise is often taken for granted, owing to the central limits theorem that states that in case of many, equally important error sources adding up with arbitrary pdf, the limit will be Gaussian. There are many counterexamples in real applications where this is not valid; radar observing systems is a typical one (Speckle noise). More important possibly in satellite gravity, it has been shown several times that geophysical 'noise', i.e. signal anomalies with respect to climatology or simple models, is not Gaussian.

1.3.4 Unbiased Estimate of the Variance Factor

An unbiased estimate for the variance factor, which means $E(\widehat{\sigma^2}) = \sigma^2$, is found from the data residuals $\hat{\mathbf{e}} = \mathbf{y} - \mathbf{A}\hat{\mathbf{x}}$ as

$$\widehat{\sigma^2} = \frac{\Omega}{n - m} \quad \text{with} \quad \Omega = \left(\mathbf{y} - \mathbf{A}\hat{\mathbf{x}}\right)^T\left(\mathbf{y} - \mathbf{A}\hat{\mathbf{x}}\right). \tag{1.10}$$

Here, Ω is the residual square sum, or RSS, with the residuals representing estimates of the errors (the errors remain unknown). On assuming the data error pdf is normal, the residuals will be normally distributed, and it can be shown that $\widehat{\sigma^2}$ follows a χ^2-distribution. Therefore, in a practical problem, it is a good idea to check whether the histogram of the residuals $\hat{\mathbf{e}}$ resembles a Gaussian.

Estimation of the variance factor represents a problem where different estimation principles yield different estimators: The Maximum-Likelihood estimate for $\widehat{\sigma^2}$ would read $\frac{\Omega}{n}$, but it is not an unbiased estimate. Rather than the unbiased estimate for $\widehat{\sigma^2}$ from Eq. (1.10) the square root of this is usually considered in applications, but it is, strictly speaking, not necessarily a unbiased estimate of σ.

Finally, realizing that $\hat{\mathbf{x}} = \mathbf{L}\mathbf{y}$, we note that the error covariance matrix of the estimate $\hat{\mathbf{x}}$ will be

$$D(\hat{\mathbf{x}}) = \mathbf{L}D(\mathbf{y})\mathbf{L}^T = \left(\mathbf{A}^T\mathbf{A}\right)^{-1}\mathbf{A}^T(\sigma^2\mathbf{I})\mathbf{A}\left(\mathbf{A}^T\mathbf{A}\right)^{-1} = \sigma^2\left(\mathbf{A}^T\mathbf{A}\right)^{-1} \tag{1.11}$$

or

$$D(\hat{\mathbf{x}}) = \mathbf{C}_{\hat{\mathbf{x}}} = \sigma^2\mathbf{N}^{-1}\,.$$

With our estimate for σ^2, we obtain

$$\hat{\mathbf{C}}_{\hat{\mathbf{x}}} = \widehat{\sigma^2}\mathbf{N}^{-1}\,.$$

1.3.5 Outer Product or Sample Representation of the Variance-Covariance Matrix

Let $\mathbf{a}$ be a vector of random variables, e.g. the data vector $\mathbf{y}$, an estimate of the parameter vector $\hat{\mathbf{x}}$ or based on this, an estimate for some linear functional of the parameters $\hat{\mathbf{z}}$ (see later).

In satellite gravimetry, a representation $\mathbf{C}_{\mathbf{aa}}$ of the variance-covariance matrix (VCM) of $\mathbf{a}$ is required for many applications, for gravity analysis, error propagation to functionals, for data assimilation and so on. It is considered a product of the analysis that can be exchanged with other analysists.

By definition, the covariance matrix of $\mathbf{a}$ reads

$$D(\mathbf{a}) = E\left((\mathbf{a} - E(\mathbf{a}))(\mathbf{a} - E(\mathbf{a}))^T\right)\,.$$

Now assuming we have a sufficiently large set of sample realizations $\mathbf{a}_{(i)}$ of $\mathbf{a}$, this suggests that

$$\bar{\mathbf{C}}_{\mathbf{aa}} = \frac{1}{N_i}\sum(\mathbf{a}_{(i)} - \bar{\mathbf{a}})(\mathbf{a}_{(i)} - \bar{\mathbf{a}})^T$$

with

$$\bar{\mathbf{a}} = \frac{1}{N_i}\mathbf{a}_{(i)}$$

provides an approximation to $D(\mathbf{a})$ in the sense of $N_i \to \infty$. The above, $\bar{\mathbf{C}}_{\mathbf{aa}}$, represents a rank-$N_i$ approximation in outer-product representation. It is sometimes called

Monte Carlo representation of the VCM. This representation has some advantages and disadvantages:

Pros:

- The sample representation is extremely easy to apply, e.g. in error propagation. For example, error propagation of SH coefficient errors to radial orbit errors, important in radar altimetry, can be realized through N_i orbit integration and a final averaging.
- It applies to nonlinear error propagation in the same way.
- Samples do not necessarily have to be independent of each other. This opens the way to advanced Monte Carlo sampling schemes like Gibbs sampling or Metropolis-Hastings.

Cons:

- $\bar{\mathbf{C}}_{\mathbf{aa}}$ as above is rank-deficient. Even if the number of samples reaches the dimension of the matrix, there is no guarantee that the matrix has full rank.
- It is difficult to find useable rules for how many samples are required in a particular problem, in order to have a good approximation.

1.4 Gauss-Markov Model with Observation Weighting

In many applications, observations of very different nature (e.g. from different sensors, measurements of different physical quantities) are to be combined. On the one hand, assuming we know that certain observations are less accurate than others, it appears natural to take this into account in the design of the estimator. On the other hand, when we have observations of different physical nature, a simple change of the units for one data set would lead to different results which is unwanted. The GMM, to accommodate for this situation, can be cast into the more general notation

$$E(\mathbf{y}) = \mathbf{A}\mathbf{x} \qquad \text{and} \qquad D(\mathbf{y}) = \sigma^2 \mathbf{P}^{-1} \,. \tag{1.12}$$

Here, our assumption is that we know—up to some overall factor—the covariance matrix $\mathbf{P}^{-1}$ of the data. This is to say, we know the specific variances of the data and we know (or assume to know) the correlations between the observations. The above model assumes implicitly that the inverse of the covariance matrix exists (it is the positive definite weight matrix $\mathbf{P}$); so we cannot have zero variances which would correspond to 'perfect' data.

In order to derive estimators and other properties for the above model, it is common to factorize the weight matrix, and reformulate the above first in the original form. With the Cholesky factorization $\mathbf{G}$ of $\mathbf{P}$ we obtain

$$\mathbf{P} = \mathbf{G}\mathbf{G}^T, \qquad \bar{\mathbf{A}} = \mathbf{G}^T\mathbf{A}, \qquad \bar{\mathbf{y}} = \mathbf{G}^T\mathbf{y}, \qquad \text{and} \qquad \bar{\mathbf{e}} = \mathbf{G}^T\mathbf{e}$$

and the above GMM can be transformed as

$$E(\bar{\mathbf{y}}) = \bar{\mathbf{A}}\mathbf{x} \quad \text{and} \quad D(\bar{\mathbf{y}}) = \sigma^2\mathbf{I}\,.$$

Therefrom, we then obtain that the respective (BLUE, ML, LS)- estimate for the parameter vector follows in the well-known form

$$\hat{\mathbf{x}} = \left(\bar{\mathbf{A}}^T\bar{\mathbf{A}}\right)^{-1}\bar{\mathbf{A}}^T\bar{\mathbf{y}} = \left(\mathbf{A}^T\mathbf{P}\mathbf{A}\right)^{-1}\mathbf{A}^T\mathbf{P}\mathbf{y}. \tag{1.13}$$

Similar, we obtain the variance factor

$$\widehat{\sigma^2} = \frac{\Omega}{n-m} \tag{1.14}$$

with

$$\Omega = \left(\bar{\mathbf{y}} - \bar{\mathbf{A}}\hat{\mathbf{x}}\right)^T\left(\bar{\mathbf{y}} - \bar{\mathbf{A}}\hat{\mathbf{x}}\right) = \left(\mathbf{y} - \mathbf{A}\hat{\mathbf{x}}\right)^T\mathbf{P}\left(\mathbf{y} - \mathbf{A}\hat{\mathbf{x}}\right) = \hat{\mathbf{e}}^T\mathbf{P}\hat{\mathbf{e}}^T \tag{1.15}$$

and the covariance matrix of the parameter vector

$$D(\hat{\mathbf{x}}) = \mathbf{C}_{\hat{\mathbf{x}}} = \sigma^2\left(\mathbf{A}^T\mathbf{P}\mathbf{A}\right)^{-1} \quad \text{and} \quad \hat{\mathbf{C}}_{\hat{\mathbf{x}}} = \widehat{\sigma^2}\left(\mathbf{A}^T\mathbf{P}\mathbf{A}\right)^{-1}. \tag{1.16}$$

These estimates are at the core of countless software packages. From a practical point of view, we observe that if we are only interested in $\hat{\mathbf{x}}$, it is not necessary to explicitly calculate the inverse of the normal equation matrix. Rather, the problem is formulated as solving the normal equations according to

$$\left(\mathbf{A}^T\mathbf{P}\mathbf{A}\right)\hat{\mathbf{x}} = \mathbf{A}^T\mathbf{P}\mathbf{y} \quad \text{or} \quad \mathbf{N}\hat{\mathbf{x}} = \mathbf{r}.$$

This can be achieved through Cholesky decomposition, or through iterative solvers (e.g. the conjugate gradient method, or the least squares CG method).

In many applications, the data vector is composed of a finite set of independent observations groups $\mathbf{y}_i$, e.g. collected from measurements to different satellites, using different instruments, or both. In this case the data covariance matrix can be assumed as block-diagonal and reads

$$D(\mathbf{y}) = \sigma^2\begin{bmatrix}\mathbf{P}_1^{-1} & & \\ & \cdots & \\ & & \mathbf{P}_k^{-1}\end{bmatrix}.$$

In this case it is easy to show that the normal equation matrix and right-hand side can be build as

$$\mathbf{N} = \mathbf{A}^T\mathbf{P}\mathbf{A} = \sum_{i=1}^{k} \mathbf{A}_i^T\mathbf{P}_i\mathbf{A}_i \quad \text{and} \quad \mathbf{r} = \mathbf{A}^T\mathbf{P}\mathbf{y} = \sum_{i=1}^{k} \mathbf{A}_i^T\mathbf{P}_i\mathbf{y}_i.$$

We call this process *assembling* the normal equations. When assembling the normal equations in a large problem, it is common to discard the observations afterwards (i.e. compute the normals 'on the fly'). On the other hand, estimating σ^2 requires computing the RSS, and this requires to compare the original observations with their predictions, using the GMM estimate. It is possible to show that

$$\Omega = \mathbf{y}^T\mathbf{P}\mathbf{y} - \mathbf{y}^T\mathbf{P}\mathbf{A}^T\hat{\mathbf{x}} = \mathbf{y}^T\mathbf{P}\mathbf{y} - \mathbf{r}^T\hat{\mathbf{x}}.$$

In other words, it would suffice to compute the *observation square sum* $\mathbf{y}^T\mathbf{P}\mathbf{y}$ during the assembly of the normal equations—storing the $\mathbf{y}$ is not necessary.

1.4.1 Additional Considerations

Correlation between observations or groups of observations lead to a number of practical questions: the contribution of each group to the estimate, the structure of the normal equation matrix, and possible decorrelation procedures. Likewise, correlation between parameters or groups of parameters is an interesting issue to discuss.

1.4.1.1 Covariance of the Adjustment Residuals

The adjustment residuals

$$\hat{\mathbf{e}} = \mathbf{y} - \mathbf{A}\hat{\mathbf{x}}$$

differ from zero, since the observations have errors but also the estimated parameters and therefore the predicted observations have errors. Straightforward error propagation tells that

$$\mathbf{D}(\hat{\mathbf{e}}) = \mathbf{C}_{\hat{\mathbf{e}}} = \mathbf{D}(\mathbf{y}) + \mathbf{A}\mathbf{D}(\hat{\mathbf{x}})\mathbf{A}^T = \sigma^2\left(\mathbf{P}^{-1} + \mathbf{A}(\mathbf{A}^T\mathbf{P}\mathbf{A})^{-1}\mathbf{A}\right).$$

In other words, an empirical analysis of the observation residuals in terms of auto- and cross-covariance (say, leading to $\bar{\mathbf{C}}_{\hat{\mathbf{e}}}$), can be used to assess the data covariance $\sigma^2\mathbf{P}^{-1}$ whenever the second term can be neglected.

Example The adjustment residuals of the above example for error free simulated gravitational potential decrease for increasing maximum degree $\bar{n}$ as shown in Fig. 1.2.

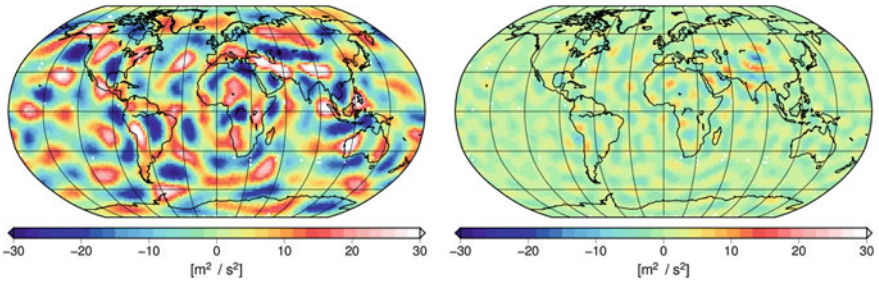

(a) $\bar{n} = 10$ (b) $\bar{n} = 20$

Fig. 1.2 As also described in the example above gravitational potential was simulated from Eq. (1.4) up to $\bar{n} = 30$ along a satellite orbit in 480 km altitude with a temporal resolution of 60 s. In **a** the adjustment residuals for solving the normal equations up to degree and order $\bar{n} = 10$ are visualized spatially. In **b** the normal equations are solved up to degree and order $\bar{n} = 20$. Obviously, the higher the maximum degree $\bar{n}$ of the series of spherical harmonics, the better also small features can be resolved. The spatial correlations also imply temporal correlations along the satellite orbit

1.4.1.2 Contribution of a Single Data Set

It can be immediately seen that each individual data set (i), in a multi-sensor or multi-satellite analysis, adds to the overall solution with the weighting

$$\mathbf{T}_i = \mathbf{A}_i^T \mathbf{P}_i \mathbf{A}_i (\mathbf{A}^T \mathbf{P} \mathbf{A})^{-1} = \mathbf{N}_i \mathbf{N}^{-1} \,. \tag{1.17}$$

It is obvious that $\sum_i \mathbf{T}_i = \mathbf{I}$, and $\sum_i \text{trace}\mathbf{T}_i = m$ (number of parameters). It is therefore common to associate

$$m_i = \text{trace}\mathbf{T}_i = \sum_j t_{i;j} \tag{1.18}$$

with the *overall contribution* of the i-th data set, and the j-th diagonal entries of the $\mathbf{T}_i$

$$t_{i;j} = (\mathbf{T}_i)_{jj} \tag{1.19}$$

with the *contribution* of the i-th data set to the j-th parameters, although this is a simplification. Observing matrix reordering rules under the trace operator, we may write $m_i = \text{trace}(\mathbf{G}_i^T \mathbf{A}_i \mathbf{N}^{-1} \mathbf{A}_i^T \mathbf{G}_i) = \text{trace}(\mathbf{G}_i^T \mathbf{A}_i \mathbf{U}_i)$. $\mathbf{U}_i$ contains in each of its columns the solution of the full normal equations with the i-th right hand side, assuming a unit data vector (1 in the i-th row, zero otherwise). This is to say the, once we have a software that solves the normal equation and gives us access to the partial right-hand sides, we can compute contribution numbers. When the parameters of the GMM are the spherical harmonics, this gives rise to the popular triangle contribution plots.

1.4.1.3 Observation Weighting and Filtering

In the more general GMM with observation weighting, either the application of the weight matrix $\mathbf{P}$ or of its Cholesky factor $\mathbf{G}$ to $m+1$ vectors is required: to the m column vectors of the design matrix plus the data vector. Assembling the normal equations can be recast as

$$\mathbf{N} = \mathbf{A}^T(\mathbf{PA}) \qquad \text{and} \qquad \mathbf{r} = \mathbf{A}^T(\mathbf{Py})$$

or

$$\mathbf{N} = \left(\mathbf{A}^T\mathbf{G}\right)\left(\mathbf{G}^T\mathbf{A}\right) \qquad \text{and} \qquad \mathbf{r} = \left(\mathbf{A}^T\mathbf{G}\right)\left(\mathbf{G}^T\mathbf{y}\right)$$

This may pose a numerical problem whenever the bandwith of the weight matrix (number of nonzero entries) is large, i.e. in cases where many observations are present (e.g. millions) and these observations are correlated over long time intervals.

Consider the second formulation. The application of $\mathbf{G}$ to either the a_{ij} or to the y_i can be written as

$$\bar{z}_i = \sum_{j=1}^{m} g_{ji} z_j \ .$$

We may instead seek to design a 'simple filter' that approximates the above matrix vector operation, e.g. in the form (see [127] for a much more comprehensive discussion)

$$\tilde{z}_i = \sum_{i-k}^{i+k} h_k z_i \ .$$

Whether this is possible, and to what extent (i.e. how big the effect of 'incorrect' weighting is on the estimate is), depends on the matrix $\mathbf{P}$ of course.

On the other hand, usually one has an idea about observation correlations rather than the weighting in the first place. This means we start with $\mathbf{C_{yy}} = \mathbf{P}^{-1}$ and try to avoid the inversion of this matrix in the first place. So, the application of the filter has to mimic the application of $\mathbf{C}^{-1}$ (or of its Cholesky factor) to a vector. We speak of *decorrelation filtering*.

The filter that mimics the multiplication with the Cholesky factor $\mathbf{G}$, when applied to the correlated observation errors, would have the effect of removing the correlation. In other words, the filter one seeks is a whitening filter. It is thus common to consider the observation residuals as an approximation to the correlated data noise, compute an empirical power spectral density (PSD), and then design a filter such that the PSD of the filtered residuals is as white as possible.

1.4.1.4 Truncated GMM

It may not be possible to consider all parameters that are unknown in the real-world problem as 'unknowns' in the GMM. This raises the question whether, and under which conditions, such model approximations lead to biased estimates. Let us assume the 'correct' GMM reads

$$E(\mathbf{y}) = \begin{bmatrix}\mathbf{A}_1 & \mathbf{A}_2\end{bmatrix}\begin{bmatrix}\mathbf{x}_1 \\ \mathbf{x}_2\end{bmatrix} \quad \text{and} \quad D(\mathbf{y}) = \sigma^2\mathbf{I}$$

with the $u \times 1$ parameter vector, while we estimate only the $k \times 1$ first portion of the parameter vector in the 'truncated' GMM

$$E(\mathbf{y}) = \mathbf{A}_1\mathbf{x}_1 \quad \text{and} \quad D(\mathbf{y}) = \sigma^2\mathbf{I}$$

which leads to the 'truncated' estimates

$$\tilde{\mathbf{x}}_1 = (\mathbf{A}_1^T\mathbf{A}_1)^{-1}\mathbf{A}_1^T\mathbf{y} \qquad \tilde{\mathbf{e}} = \mathbf{A}_1\hat{\mathbf{x}}_1 - \mathbf{y}\ .$$

It is easy to show that

$$E(\tilde{\mathbf{x}}_1) = \mathbf{x}_1 + (\mathbf{A}_1^T\mathbf{A}_1)^{-1}\mathbf{A}_1^T\mathbf{A}_2\mathbf{x}_2.$$

This means, the estimate $\tilde{\mathbf{x}}_1$ in the 'truncated' model is systematically biased, since the term on the right-hand side (the bias) is not a random but a fixed quantity. However, the estimate is unbiased under the condition that either (1) $\mathbf{x}_2 = \mathbf{0}$ or (2) $\mathbf{A}_1^T\mathbf{A}_2 = \mathbf{0}$. The last condition simply means that the original 'correct' GMM can be partitioned into two independent models (the normal equation matrix would be block-diagonal), and that the two portions of the parameter vector would be obtained uncorrelated w.r.t. each other.

Moreover one can show that

$$E(\tilde{\Omega}) = E(\tilde{\mathbf{e}}^T\tilde{\mathbf{e}}) = \sigma^2(n-k) + \mathbf{x}_2^T\mathbf{A}_2^T(\mathbf{I} - \mathbf{A}_1(\mathbf{A}_1^T\mathbf{A}_1)^{-1}\mathbf{A}_1^T)\mathbf{A}_2\mathbf{x}_2\ .$$

In other words, the statistical expectation of the RSS is bigger than $\sigma^2(n-k)$. This leads to the rule: If σ^2 is known and we obtain an estimate for it in the GMM which is significantly bigger than what we know, this may mean that the model is underparameterized.

Example In the case of measured values of the gravitational potential, that we discussed before, the entries of $\mathbf{A}_1^T\mathbf{A}_2$ are made up by the sums

$$\sum_i \left(\frac{a}{r}\right)^{n+n'} Y_{nm}(\lambda_i, \theta_i)Y_{n'm'}(\lambda_i, \theta_i)$$

for $n \leq \bar{n}$ and $n' > \bar{n}$. This means, again, whether the truncation effect is significant depends largely on whether the data distribution and weighting resembles integration on the sphere (then we would have orthogonality).

1.4.1.5 Common and Local Parameters

As was mentioned earlier, in satellite geodesy it is quite common to partition the data (vector) into different groups; i.e. according to specific observation sensors, techniques, or satellites. Similar, often the unknown parameters of the problem can be partitioned. While common parameters $\mathbf{x}^{(c)}$ refer to those parameters that are linked to all data sets (such as the spherical harmonic coefficients in a gravity field determination problem), local parameters $\mathbf{x}_k^{(l)}$ contain all those which are specific to a particular observation group k only (such as arc-dependent parameters, e.g. the initial state vector, or instrumental biases). Due to numerical reasons, it is very popular to separate these within the GMM.

Assuming k uncorrelated observation groups, and superscripts (c) and (l) referring to common and local, the GMM in this case can be written as

$$E(\mathbf{y}) = E\begin{bmatrix}\mathbf{y}_1\\ \dots \\ \mathbf{y}_k\end{bmatrix} = \begin{bmatrix}\mathbf{A}_1^{(l)} & \mathbf{0} & \dots & \mathbf{A}_1^{(c)}\\ \dots & \dots & \dots & \dots \\ \mathbf{0} & \dots & \mathbf{A}_k^{(l)} & \mathbf{A}_k^{(c)}\end{bmatrix}\begin{bmatrix}\mathbf{x}_1^{(l)}\\ \dots \\ \mathbf{x}_k^{(l)}\\ \mathbf{x}^{(c)}\end{bmatrix} \tag{1.20}$$

and

$$D(\mathbf{y}) = D\begin{bmatrix}\mathbf{y}_1\\ \dots \\ \mathbf{y}_k\end{bmatrix} = \sigma^2\begin{bmatrix}\mathbf{P}_1^{-1} & & \\ & \cdots & \\ & & \mathbf{P}_k^{-1}\end{bmatrix}.$$

Of course, the estimate for the entire parameter vector $\hat{\mathbf{x}}$ is found as

$$\hat{\mathbf{x}} = \left(\mathbf{A}^T\mathbf{P}\mathbf{A}\right)^{-1}\mathbf{A}^T\mathbf{P}\mathbf{y}.$$

With the above described partitioning of the data vector, design matrix and weight matrix, is possible to recast the normal equations for the common parameters in the reduced form

$$\left(\sum_{i=1}^{k}\bar{\mathbf{N}}_i^{(cc)}\right)\hat{\mathbf{x}}^{(c)} = \sum_{i=1}^{k}\bar{\mathbf{r}}_i^{(c)} \quad \text{or} \quad \bar{\mathbf{N}}^{(cc)}\hat{\mathbf{x}}^{(c)} = \bar{\mathbf{r}}^{(c)} \tag{1.21}$$

with

$$\bar{\mathbf{N}}_i^{(cc)} = \mathbf{A}_i^{(c)T}\mathbf{P}_i\mathbf{A}_i^{(c)} - \mathbf{A}_i^{(c)T}\mathbf{P}_i\mathbf{A}_i^{(l)}\left(\mathbf{A}_i^{(l)T}\mathbf{P}_i\mathbf{A}_i^{(l)}\right)^{-1}\mathbf{A}_i^{(l)T}\mathbf{P}_i\mathbf{A}_i^{(c)} \tag{1.22}$$

and

$$\bar{\mathbf{r}}_i^{(c)} = \mathbf{A}_i^{(c)T}\mathbf{P}_i\mathbf{y}_i - \mathbf{A}_i^{(c)T}\mathbf{P}_i\mathbf{A}_i^{(l)}\left(\mathbf{A}_i^{(l)T}\mathbf{P}_i\mathbf{A}_i^{(l)}\right)^{-1}\mathbf{A}_i^{(l)T}\mathbf{P}_i\mathbf{y}_i. \tag{1.23}$$

The i-th local parameter vector follows from substituting the estimate of the common parameter vector according to

$$\left(\mathbf{A}_i^{(l)T}\mathbf{P}_i\mathbf{A}_i^{(l)}\right)\hat{\mathbf{x}}_i^{(l)} = \mathbf{A}_i^{(l)T}\mathbf{P}_i\mathbf{y}_i - \mathbf{A}_i^{(l)T}\mathbf{P}_i\mathbf{A}_i^{(c)}\hat{\mathbf{x}}^{(c)} = \mathbf{A}_i^{(l)T}\mathbf{P}_i(\mathbf{y}_i - \mathbf{A}_i^{(c)}\hat{\mathbf{x}}^{(c)}). \tag{1.24}$$

The normal equations for the local parameters of group i appear as if we would only solve the data $\mathbf{y}_i$ of group i for these parameters, with a correction term $\mathbf{A}_i^{(c)}\hat{\mathbf{x}}^{(c)}$ on the right hand side. The data are reduced for the theoretical observations predicted by the estimated global parameters. This obviously comes down to a *reduction-backsubstitution* procedure. It is extremely common in applications where many local parameters are to be estimated, since the size of the normal equations systems to be solved is reduced to the number of the common parameters.

The covariance matrices for the global and local parameters of group i are found, from error propagation, as

$$D(\hat{\mathbf{x}}^{(c)}) = \sigma^2\left(\bar{\mathbf{N}}^{(cc)}\right)^{-1}$$

and

$$D(\hat{\mathbf{x}}_i^{(l)}) = \sigma^2\left(\left(\bar{\mathbf{N}}_i^{(ll)}\right)^{-1} + \left(\bar{\mathbf{N}}_i^{(ll)}\right)^{-1}\bar{\mathbf{N}}_i^{(lc)}\left(\bar{\mathbf{N}}^{(cc)}\right)^{-1}\bar{\mathbf{N}}_i^{(cl)}\left(\bar{\mathbf{N}}_i^{(ll)}\right)^{-1}\right) \tag{1.25}$$

with

$$\bar{\mathbf{N}}_i^{(ll)} = \mathbf{A}_i^{(l)T}\mathbf{P}_i\mathbf{A}_i^{(l)} \qquad \bar{\mathbf{N}}_i^{(lc)} = \mathbf{A}_i^{(l)T}\mathbf{P}_i\mathbf{A}_i^{(c)}.$$

And, from error propagation, we obtain as well the cross-covariance matrix between the common and the local parameters,

$$C\left(\hat{\mathbf{x}}^{(l)}, \hat{\mathbf{x}}_i^{(c)}\right) = \sigma^2\left(\bar{\mathbf{N}}_i^{(ll)}\right)^{-1}\bar{\mathbf{N}}_i^{(lc)}\left(\bar{\mathbf{N}}^{(cc)}\right)^{-1}. \tag{1.26}$$

Example In satellite gravimetry, it is common to estimate so called empirical $^1/_{\text{rev}}$. (once-per-revolution), $^2/_{\text{rev}}$., etc. parameters, which are simply meant to absorb remaining systematic errors in the observation time series. Similary, per orbital arc (i.e. observation group i) state vector and instrument bias parameters are estimated together with the harmonics. Do these parameters absorb (part of) the gravity signal? A formal answer can be gained by studying the correlation between the estimated harmonics (in the common vector) and the local parameters.

1.4.2 Linear Functionals

Often we are interested in linear functionals of an estimate $\hat{\mathbf{x}}$,

$$\hat{\mathbf{z}} = \mathbf{B}\hat{\mathbf{x}} \,. \tag{1.27}$$

Assuming $\hat{\mathbf{x}}$ is a linear combination of the data $\mathbf{y}$, then the same holds for $\hat{\mathbf{z}}$ and we error propagation leads to

$$D(\hat{\mathbf{z}}) = \mathbf{B}D(\hat{\mathbf{x}})\mathbf{B}^T \qquad \text{and} \qquad \mathbf{C}_{\hat{\mathbf{z}}} = \mathbf{B}\mathbf{C}_{\hat{\mathbf{x}}}\mathbf{B}^T. \tag{1.28}$$

Assuming $\mathbf{C}_{\hat{\mathbf{x}}}$ is given in outer product representation we can write

$$\bar{\mathbf{C}}_{\hat{\mathbf{z}}\hat{\mathbf{z}}} = \frac{1}{N_i}(\mathbf{B}\hat{\mathbf{x}}_{(i)} - \overline{\mathbf{B}\hat{\mathbf{x}}})(\mathbf{B}\hat{\mathbf{x}}_{(i)} - \overline{\mathbf{B}\hat{\mathbf{x}}})^T.$$

Example Many functionals of gravity, when expressed in so-called spherical approximation and parameterized through a truncated spherical harmonic expansion, are linear, e.g. gravity anomalies

$$\delta g(\lambda_i, \theta_i) = \sum_{n=0}^{\bar{n}} \sum_{m=-n}^{n} \frac{n-1}{a} \, Y_{nm}(\lambda_i, \theta_i) \, v_{nm} \,.$$

Obviously, matrix $\mathbf{B}$ maps the SH coefficients v_{nm} to a (regular) grid. This implies that not only the errors (variances) of gridded quantities can be propagated from the covariance matrix of harmonics, but also the correlations between grid values. In fact such correlations will strongly depend on the spatial distance of the grid nodes, and they may be quite high for neighboring grid points. It advisable to propagate to a regular grid, along parallels. This would allow computing Legendre functions only once. Several numerical tricks may be played along this line.

1.4.3 Nonlinear Problem

In many real-world applications, the original model however reads

$$\mathbf{y} + \mathbf{e} = f(\mathbf{x}). \tag{1.29}$$

Linearization about a given reference solution $\mathbf{x}_0$ with theoretical observations $\mathbf{y}_0 = f(\mathbf{x}_0)$ leads to

$$\delta\mathbf{y} + \mathbf{e} + \mathbf{s} = \mathbf{F}\delta\mathbf{x} \tag{1.30}$$

with

$$\mathbf{F} = \left.\frac{\partial \mathbf{y}}{\partial \mathbf{x}}\right|_{\mathbf{x}_0}, \qquad \delta\mathbf{y} = \mathbf{y} - \mathbf{y}_0, \qquad \text{and} \qquad \delta\mathbf{x} = \mathbf{x} - \mathbf{x}_0 \, .$$

It is important to understand that the linearization error $\mathbf{s}$ is not a stochastic quantity. The estimate for the parameter increment is usually sought as

$$\widehat{\delta\mathbf{x}} = \left(\mathbf{A}^T\mathbf{P}\mathbf{A}\right)^{-1}\mathbf{A}^T\mathbf{P}\delta\mathbf{y} \, . \tag{1.31}$$

With this, we choose as the new reference solution

$$\mathbf{x}_1 = \mathbf{x}_0 + \widehat{\delta\mathbf{x}}$$

and the process is iterated until convergence is reached (or it is clear that it will not be reached).

Example In satellite gravity field determination, the most common approach to link observations $\mathbf{y}$ and parameters $\mathbf{x}$ is the *variational equations approach*. Let us assume the parameters can be grouped as

$$\mathbf{x} = \begin{bmatrix} \mathbf{z}(t_i) \\ \mathbf{a} \\ \mathbf{p} \end{bmatrix}$$

where $\mathbf{z}(t_i)$ are state vector unknowns (orbit and velocity at the begin of a satellite arc or analysis interval, e.g. 0 h 0 m 0 s every day), $\mathbf{a}$ are force model parameters (e.g. spherical harmonic coefficients), and $\mathbf{p}$ are additional parameters directly related to the measurements (e.g. instrumental bias). The above mentioned linearized observation equations then read

$$\mathbf{y} + \mathbf{e} + \mathbf{s} = \mathbf{y}_0 + \left(\frac{\partial \mathbf{y}}{\partial \mathbf{z}}\right)\boldsymbol{\Phi}(t, t_i)(\mathbf{z}(t_i) - \mathbf{z}_0(t_i)) + \left(\frac{\partial \mathbf{y}}{\partial \mathbf{z}}\right)\mathbf{S}(t)(\mathbf{a} - \mathbf{a}_0) + \left(\frac{\partial \mathbf{y}}{\partial \mathbf{p}}\right)(\mathbf{p} - \mathbf{p}_0) \, .$$

Here, $\boldsymbol{\Phi}(t, t_i)$ and $\mathbf{S}(t)$ are the transition matrix and sensitivity matrix that need to be determined by numerical integration along with the orbit:

$$\boldsymbol{\Phi}(t, t_i) = \left(\frac{\partial \mathbf{z}(t)}{\partial \mathbf{z}(t_i)}\right) \qquad \text{and} \qquad \mathbf{S}(t) = \left(\frac{\partial \mathbf{z}(t)}{\partial \mathbf{a}}\right) \, .$$

This can finally be written as $\mathbf{y} + \tilde{\mathbf{e}} = \mathbf{A}\mathbf{x}$.

1.4.4 Variance-Component Estimation

As we have seen, in the GMM it is not required to know the variance factor, as it drops out in the estimation of the parameter vector, and it can be estimated from the residual square sum. This, however, is true only if a single, overall factor, is unknown. As has been mentioned before, in satellite gravimetry we have often to deal with data from multiple instruments or even multiple satellites within a single GMM. Moreover, often we have an idea of the instrument noise but it is hard to assess the errors introduced by background models, additional corrections relying on auxiliary data, and so on. This all leads to the situation that we would prefer to estimate a variance factor *per observation group*. Observations groups may even represent different time periods of the same instrument and satellite; e.g. data collected along subsequent orbital arcs. For example, varying ionospheric activity may affect microwave measurement noise in ways hard to predict, so that it appears natural that some days or arcs have a higher noise level than others.

The method of variance-component estimation (VCE), developed almost independently in various scientific disciplines like geodesy, agricultural /econometrics, and medical statistics, has been frequently applied to this problem. The idea of VCE is to formulate a more general joint estimation problem where, in addition to the $\mathbf{x}$, two or more unknown parameters within the data covariance matrix are to be estimated. These parameters are usually considered as multiplicative to certain structure matrices, such that a linear combination makes up the data covariance matrix. Different estimation principles like BIQUE (best invariant quadratic unbiased estimate), ML, or the Bayesian approach lead to different estimates in the same model.

In this context we will consider only a single model, where observation groups are considered as uncorrelated with respect to each other, and where only the overall variance factor per group is sought. It is the model which has been considered when we discussed partitioning into global and local parameters with

$$E(\mathbf{y}) = E\begin{bmatrix}\mathbf{y}_1\\ \dots\\ \mathbf{y}_k\end{bmatrix} = \begin{bmatrix}\mathbf{A}_1^{(l)} & \mathbf{0} & \dots & \mathbf{A}_1^{(c)}\\ \dots & \dots & \dots & \dots\\ \mathbf{0} & \dots & \mathbf{A}_k^{(l)} & \mathbf{A}_k^{(c)}\end{bmatrix}\begin{bmatrix}\mathbf{x}_1^{(l)}\\ \dots\\ \mathbf{x}_k^{(l)}\\ \mathbf{x}^{(c)}\end{bmatrix} \tag{1.32}$$

and

$$D(\mathbf{y}) = D\begin{bmatrix}\mathbf{y}_1\\ \dots\\ \mathbf{y}_k\end{bmatrix} = \begin{bmatrix}\sigma_1^2\mathbf{P}_1^{-1} & & \\ & \cdots & \\ & & \sigma_k^2\mathbf{P}_k^{-1}\end{bmatrix}.$$

In other words, next to $\mathbf{x}$ we seek $\boldsymbol{\sigma} = (\sigma_1^2, \dots, \sigma_k^2)^T$.

It is clear that this is a difficult problem. For example, the estimates for $\boldsymbol{\sigma}$ have to be strictly positive. It is further not obvious under which circumstances the problem has full rank. Moreover, as the relative size of the variance factors (the weighting of

the different groups with respect to each other) will undoubtly affect the estimate of $\mathbf{x}$, an iterative approach may be required.

An iterative solution that converges to the ML estimate in the above problem (and to the MINQE estimate, if it exists) has been given in [87], following work by [40, 84]. The method is as follows:

- Select start values $\sigma_j^{2[0]}$, $j = 1, \ldots, k$.
- Then, for $p = 0, \ldots$ iterate:
  - the computation of the local and global parameters $\hat{\mathbf{x}}_j^{(l)[p]}$, $\hat{\mathbf{x}}^{(c)[p]}$, and of the data residuals $\hat{\mathbf{e}}_j^{[p]}$ within all groups.
  - the computation of the group redundancy numbers $r_j^{[p]}$,

$$r_j = -\text{trace}\frac{\partial \hat{\mathbf{e}}_j}{\partial \mathbf{y}_j} = n_j - \frac{1}{\sigma_j^2}\text{trace}\tilde{\mathbf{A}}_j^T \mathbf{P}_j \tilde{\mathbf{A}}\mathbf{N}^{-1}. \tag{1.33}$$

  - the computation of the variance-components $\sigma_j^{2[p]}$,

$$\sigma_j^2 = \frac{\hat{\mathbf{e}}_j \mathbf{P}_j \hat{\mathbf{e}}_j}{r_j}. \tag{1.34}$$

1.5 Regularization and Biased Estimation

In the following we will briefly look at three different concepts of estimation that differ from the BLUE as discussed before:

- Tikhonov-type regularization (Kaula-type regularization)
- Truncated Singular Value Decomposition
- Estimation with prior information

Biased estimation is a well-known concept in satellite gravity determination. The reason for this is, chosing a biased estimator allows one to decrease the variance of the estimate and thus its sensitivity with respect to data errors. In satellite gravimetry, data are collected at satellite altitude where the gravity field is damped (increasingly for higher harmonics). Mathematically speaking, determination of harmonics from satellite data represents an ill-posed problem, and so are all related problems (determination of surface mass, of gravity anomalies). This translates in ill-conditioned normal equations systems and large variances and covariances for the estimated parameters. In fact, in many cases the unbiased LS estimates would lead to wildly oscillating harmonics. In biased estimation we know that the result is not unbiased but we can dramatically reduce this sensitivity.

1.5.1 Tikhonov Estimator

Let us consider the GMM as above, and the popular Tikhonov estimator

$$\hat{\mathbf{x}}^+ = \left(\mathbf{A}^T\mathbf{P}\mathbf{A} + \mathbf{R}\right)^{-1}\mathbf{A}^T\mathbf{P}\mathbf{y} \tag{1.35}$$

with $\mathbf{R}$ being positive definite, and in most applications diagonal. The expectation is

$$E(\hat{\mathbf{x}}^+) = \left(\mathbf{A}^T\mathbf{P}\mathbf{A} + \mathbf{R}\right)^{-1}\mathbf{A}^T\mathbf{P}\mathbf{A}\mathbf{x} = \mathbf{x} - \left(\mathbf{A}^T\mathbf{P}\mathbf{A} + \mathbf{R}\right)^{-1}\mathbf{R}\mathbf{x} \neq \mathbf{x}\,. \tag{1.36}$$

This gives rise to define the *bias* of $\hat{\mathbf{x}}$ as

$$\mathbf{b}_{\hat{\mathbf{x}}^+} = E(\hat{\mathbf{x}}^+ - \mathbf{x}) = \left(\mathbf{A}^T\mathbf{P}\mathbf{A} + \mathbf{R}\right)^{-1}\mathbf{R}\mathbf{x}. \tag{1.37}$$

The bias $\mathbf{b}_{\hat{\mathbf{x}}}$ characterizes important properties of the estimator, and it would be good to know it. Unfortunately it depends on the unknown true parameter vector and so it remains elusive. Many researchers have proposed to work with a first-order approximation, by replacing the true vector on the right hand side by its Tikhonov estimate

$$\mathbf{b}^{[1]}_{\hat{\mathbf{x}}} = \left(\mathbf{A}^T\mathbf{P}\mathbf{A} + \mathbf{R}\right)^{-1}\mathbf{R}\hat{\mathbf{x}}^+.$$

We would like to mention that, when regularizing an already linearized problem, the choice of the linearization point becomes important. This is so since one usually applies regularization to the determination of $\delta\mathbf{x} = \mathbf{x} - \mathbf{x}_0$, which is then biased towards zero, while one is finally interested in $\mathbf{x} = \mathbf{x}_0 + \delta\mathbf{x}$ (which is then biased towards $\mathbf{x}_0$).

The covariance matrix of the estimator is found from linear error propagation as

$$D(\hat{\mathbf{x}}^+) = \left(\mathbf{A}^T\mathbf{P}\mathbf{A} + \mathbf{R}\right)^{-1}\mathbf{A}^T\mathbf{P}\mathbf{A}\left(\mathbf{A}^T\mathbf{P}\mathbf{A} + \mathbf{R}\right)^{-1}\,.$$

Let us recall the definition of the covariance matrix

$$D(\hat{\mathbf{x}}^+) = E\left((\hat{\mathbf{x}}^+ - E(\hat{\mathbf{x}}^+))(\hat{\mathbf{x}}^+ - E(\hat{\mathbf{x}}^+))^T\right)\,.$$

The covariance matrix provides a metric for the spreading of the estimate w.r.t. its expectation. This tells about the sensitivity of the estimate, but in case of biased estimation it does not inform us about the spreading of the estimate w.r.t. the truth. It is therefore common to consider the *mean square error* or MSE matrix,

$$M(\hat{\mathbf{x}}^+) = E\left((\hat{\mathbf{x}}^+ - \mathbf{x})(\hat{\mathbf{x}}^+ - \mathbf{x})^T\right) = D(\hat{\mathbf{x}}^+) + \mathbf{b}_{\hat{\mathbf{x}}^+}\mathbf{b}^T_{\hat{\mathbf{x}}^+}.$$

The MSE matrix is likely more informative, but its practical computation would require knowledge of the estimation bias (which we don't have).

Very often, the estimate is formulated as

$$\hat{\mathbf{x}}_{\alpha}^{+} = \left(\mathbf{A}^T\mathbf{P}\mathbf{A} + \alpha^2\mathbf{R}\right)^{-1}\mathbf{A}^T\mathbf{P}\mathbf{y}$$

with $\mathbf{R}$ given, and α^2 to be determined though some kind of optimization procedure. Numerous papers have been written on this subject. A good first guess may be $\alpha^2 = \frac{\text{trace}(\mathbf{A}^T\mathbf{P}\mathbf{A})}{\text{trace}\mathbf{R}}$. More sophisticated methods are the L-curve method, the Generalized Cross-Validation, and the Variance-Component Estimation method. In statistical literature those kind of problems are called *ridge regression*.

In his original publications, Tikhonov did not consider the discrete case (with a finite number of parameters, as we do here) at all, but the functional-analytic problem, where a certain function is sought that both fits a data function and attains minimum norm. So it is, strictly speaking, incorrect to call the estimate Tikhonov regularization, in particular when no reference is made to the underlying continuous norm.

1.5.1.1 Related Concepts

Obviously, the Tikhonov estimate can be understood as a filtered version of the LS estimate

$$\hat{\mathbf{x}}^{+} = \mathbf{W}\hat{\mathbf{x}}$$

with

$$\mathbf{W} = \left(\mathbf{A}^T\mathbf{P}\mathbf{A} + \mathbf{R}\right)^{-1}\mathbf{A}^T\mathbf{P}\mathbf{A} = \mathbf{I} - \left(\mathbf{A}^T\mathbf{P}\mathbf{A} + \mathbf{R}\right)^{-1}\mathbf{R}\,.$$

Since $\mathbf{R}$ is positive definite, it can be shown that the eigenvalues of $\mathbf{W}$ are smaller than one, and its application reduces the 'length' of the parameter estimate.

In addition, the estimate $\hat{\mathbf{x}}^{+}$ provides the solution to a hybrid norm minimization problem; i.e. it is the minimizer of

$$\Omega = \left(\mathbf{y} - \mathbf{A}\hat{\mathbf{x}}\right)^T\mathbf{P}\left(\mathbf{y} - \mathbf{A}\hat{\mathbf{x}}\right) + \hat{\mathbf{x}}^T\mathbf{R}\hat{\mathbf{x}}\,.$$

In satellite gravity determination problems, this leads to the question under which conditions the matrix norm $||\mathbf{x}||_{\mathbf{R}} = \mathbf{x}^T\mathbf{R}\mathbf{x}$ can be interpreted in a physical sense, i.e. in relation to the gravity field. For example, it is clear that

$$||V||_{L_2(\omega)} = \int_{\omega} V^2(\theta,\lambda)d\omega = \sum_{n=0}^{\infty}\sum_{m=-n}^{n} v_{nm}^2 = \sum_{n=0}^{\infty}\sum_{m=-n}^{n} c_{nm}^2 + s_{nm}^2 = \sum_{n=0}^{\infty} c_n^2$$

with fully (4π-) normalized harmonic coefficients. In other words, Tikhonov regularization with $\mathbf{R} = \mathbf{I}$ can be viewed as involving a discrete approximation

$$\mathbf{x}^T\mathbf{R}\mathbf{x} = \sum_{n=0}^{\bar{n}} \sum_{m=-n}^{n} v_{nm}^2 = \sum_{n=0}^{\bar{n}} c_n^2$$

of the total power (or RMS) of the geopotential averaged over the sphere, into the minimization functional. This is sometimes called zero-order Tikhonov regularization. The estimate seeks to fit the harmonic coefficients to the data but at the same time the averaged square geopotential should be minimized. Likewise, first- and second order TR can be related to minimizing the (surface) gradient or Laplacian of the potential [33].

1.5.1.2 Kaula Regularization

In classical geodesy, the most prominent example is *Kaula regularization*. In this case the regularization matrix becomes

$$\mathbf{R} = \begin{bmatrix} 1 & & & \\ & \cdots & & \\ & & n^4 & \\ & & & \cdots \\ & & & & \bar{n}^4 \end{bmatrix}.$$

Numerous papers ascribe Kaula regularization to *William Kaula* and cite his classical textbook on *Satellite Geodesy*. In fact this is incorrect, this technique is never mentioned or even advocated in this classical work. Kaula regularization is rooted in the observation that the degree variance spectrum of the Earth's gravitational potential, i.e.

$$c_n^2 = \sum_{m=-n}^{n} v_{nm}^2$$

can be, to some extent, approximated by an analytic expression $\bar{c}_n^2 = f(n)$ (a degree-variance model). In the simplest case one would write

$$f(n) = \frac{a}{n^4}.$$

Obviously, Kaula regularization is intended to guarantee that

$$\mathbf{x}^T\mathbf{R}\mathbf{x} = \sum_{n=0}^{\bar{n}} \frac{a}{n^4} n^4 = \bar{n}a$$

is finite. Kaula regularization is usually motivated as (see below) follows: We introduce an a-priori observation of zero for each individual coefficient. Since we know

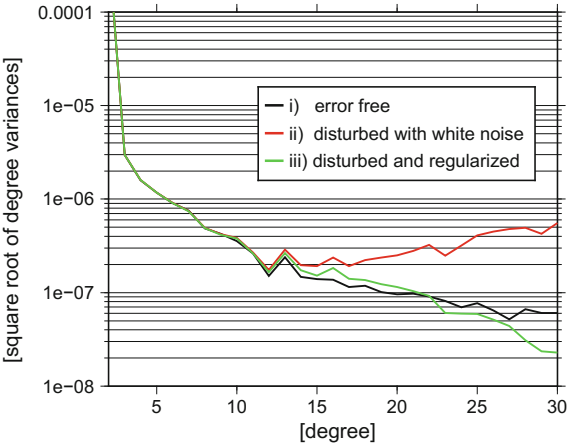

Fig. 1.3 This figure shows the square root of the degree variances of spherical harmonic coeffcients estimated up to degree and order $\bar{n} = 30$ for three different cases: (i) error free simulated gravitational potential (see Eq. (1.4)), (ii) simulated gravitational potential disturbed with random Gaussian noise with zero mean and a standard deviation of 100 $^{m^2}/_{s^2}$, and (iii) disturbed potential and applying Kaula regularization

each individual coefficient has an expected magnitude of the order $\frac{a}{n^4}$, this is assumed to represent the variance of these zero observations.

From this line of reasoning follows, that Kaula regularization can be motivated only if we estimate the full field. Today, we have much better knowledge and we typically estimate a residual field w.r.t. a background mean gravity model. Kaula regularization can thus not be motivated anymore as introducing unbiased prior information and it should be viewed as a biased estimation technique. When estimating time variable gravity fields with GRACE, authors have derived degree-variance models that describe the signal power in the temporal changes and built regularization techniques on this. On yet another subject, it is possible to introduce regularization that constrains the field for some defined spatial region only (polar regions above certain latitude, or land/ocean region), but the price to pay will be a dense matrix $\mathbf{R}$.

Example Spherical harmonic coefficients are estimated (i) from error free simulated gravitational potential, (ii) from simulated gravitational potential disturbed with random Gaussian noise, and (iii) from disturbed potential and applying Kaula regularization. The corresponding square root of the degree variances is shown in Fig. 1.3. In case (ii), the higher degrees are dominated by noise that is amplified due to the downward continuation process (red line). Applying Kaula regularization, in case (iii) the estimated parameters are forced against zero with increasing strength for the higher degrees.

1.5.2 SVD and TSVD

The original GMM $\mathbf{y} + \mathbf{e} = \mathbf{Ax}$ may be transformed to *canonical form* using the SVD of $\mathbf{A}$,

$$\mathbf{A} = \mathbf{UDV}^T$$

with orthogonal $n \times n$ $\mathbf{U}$, orthogonal $m \times m$ $\mathbf{V}$, and rectangular $n \times m$ diagonal $\mathbf{D} = \mathrm{diag}(d_1, \ldots, d_m)$. With this, we can write

$$\mathbf{U}^T\mathbf{y} + \mathbf{U}^T\mathbf{e} = \mathbf{U}^T\mathbf{U}\mathbf{D}\mathbf{V}^T\mathbf{x} = \mathbf{D}\mathbf{V}^T\mathbf{x}$$

or

$$\tilde{\mathbf{y}} + \tilde{\mathbf{e}} = \mathbf{D}\tilde{\mathbf{x}} \,.$$

And the LS estimate of $\mathbf{x}$ can be written, with $m \times m$ $\mathbf{\Lambda} = \mathbf{D}^T\mathbf{D}$ and

$$\mathbf{A}^T\mathbf{A} = \mathbf{V}\mathbf{D}^T\mathbf{U}^T\mathbf{U}\mathbf{D}\mathbf{V}^T = \mathbf{V}\mathbf{D}^T\mathbf{D}\mathbf{V}^T = \mathbf{V}\mathbf{\Lambda}\mathbf{V}^T$$

as

$$\hat{\mathbf{x}} = \left(\mathbf{A}^T\mathbf{A}\right)^{-1}\mathbf{A}^T\mathbf{y} = \mathbf{V}\mathbf{\Lambda}\mathbf{V}^T\mathbf{V}\mathbf{D}\mathbf{U}^T\mathbf{y} = \mathbf{V}\mathbf{\Lambda}\mathbf{D}\tilde{\mathbf{y}} \,.$$

It is easy to see that this can now be written as

$$\hat{\mathbf{x}} = \sum_{i=1}^{m} \mathbf{v}_i \frac{d_i}{d_i^2}(\mathbf{u}_i\mathbf{y}) \,.$$

Let us consider the Tikhonov regularization with $\mathbf{R} = \alpha^2\mathbf{I}$. On realizing that

$$\mathbf{A}^T\mathbf{A} + \alpha^2\mathbf{I} = \mathbf{V}\left(\mathbf{\Lambda}\alpha^2\mathbf{I}\right)\mathbf{V}^T$$

we find that

$$\hat{\mathbf{x}}_\alpha^+ = \sum_{i=1}^{m} \mathbf{v}_i \frac{d_i}{d_i^2 + \alpha^2}(\mathbf{u}_i\mathbf{y}) \,.$$

It appears the singular values are damped (with respect to the least squares estimate) while the singular vectors are maintained. Starting from the SVD representation of the Tikhonov estimate, one can devise other estimates by generalizing the concept. i.e. one prescribes

$$\hat{\mathbf{x}}_\alpha^+ = \sum_{i=1}^{m} \mathbf{v}_i f(d_i)(\mathbf{u}_i\mathbf{y}) \,.$$

The *truncated SVD estimate* (TSVD) has gained popularity similar to the Tikhonov estimator. The TSVD simply reads ($p < m$)

$$\hat{\mathbf{x}}^{(p)} = \sum_{i=1}^{p} \mathbf{v}_i \frac{d_i}{d_i^2}(\mathbf{u}_i\mathbf{y}) \,.$$

1.5.3 Estimation with Prior Information

Finally, a very different view on the problem is as follows. Assuming we do have prior information on the parameter vector, i.e. before we collect measurements.

In reality mostly one has some information. In particular, the Earth's gravity field has been determined numerous times before, from satellite and terrestrial data, and we just aim at improving this. One can think of writing the GMM with the 'new' data as

$$E(\mathbf{y}) = \mathbf{A}\mathbf{x} \qquad \text{and} \qquad D(\mathbf{y}) = \sigma^2 \mathbf{P}^{-1} \,. \tag{1.38}$$

With this, assuming the first data set has been utilized to produce a prior estimate $\mathbf{x}_0$ with covariance

$$E\left(\mathbf{x}_0\right) = \mathbf{x} \qquad \text{and} \qquad D\left(\mathbf{x}_0\right) = \mathbf{R}^{-1}$$

one can write the 'new' or updated estimate utilizing the 'new' data as

$$\hat{\mathbf{x}} = \left(\mathbf{A}^T\mathbf{P}\mathbf{A} + \mathbf{R}\right)^{-1}\left(\mathbf{A}^T\mathbf{P}\mathbf{y} + \mathbf{x}_0\right) \tag{1.39}$$

with

$$D(\hat{\mathbf{x}}) = \left(\mathbf{A}^T\mathbf{P}\mathbf{A} + \mathbf{R}\right)^{-1} \,. \tag{1.40}$$

This, formally, equals to the Tikhonov estimate, and the *estimation with prior information* shares thus the same stabilizing properties. However the covariance of the estimate differs, and the estimate is now unbiased—under the mentioned assumptions.

Estimation with prior information is often identified with Bayesian estimation but this is not true. Bayesian estimation always assumes that one has prior information, but this prior information can be non-informative (i.e. it does not carry information that modifies or 'sharpens' the pdf of the unknowns). On the other hand, non-Bayesian theory does allow prior information to be introduced as well. However, a difference in the concepts exists at a deeper (or more philosophical) level.

In non-Bayesian estimation, specifying prior information on the unknown parameters implicitly requires that we assume this information as the outcome of a—repeatable—random experiment. A prior measurement would be such an experiment that provides us with a covariance matrix, but specifying prior information on high-degree harmonics of the gravity field, or its temporal variation, beyond those that have actually been measured, is difficult to justify on theoretical grounds in non-Bayesian theory. In contrast, Bayesian theory simply assumes that we do have uncertain knowledge, not necessarily related to actual observations, and that we formalize this knowledge (or rather believe) into mathematical form. Of course, our knowledge is always incomplete. Bayesian estimation is not more sensitive toward prior information than conventional estimation is. It rather forces us to formalize our—often vague—knowledge.

1.6 Exercises

Data and files needed for the following exercises are available online at:
http://www.geoq.uni-hannover.de/autumnschool-data
http://extras.springer.com

Purpose of the practical: In this practical the Gauss-Markov-Model (GMM) will be implemented for the computation of spherical harmonic coefficients from given gravitational potential. The error-free gravitational potential is provided along a satellite orbit of one month with a sampling of 60 s. First, the adjustment problem will be solved up to different degrees n_{max}. Then, the influence of noise will be assessed and regularization will be applied.

1: Estimation of spherical harmonic coefficients

(a) Load the file *potential_2007-07.mat*. The four columns contain the orbit locations (longitude [°], latitude [°], height [m]) and the values of the gravitational potential [$^{m^2}/_{s^2}$]. Visualize the data with respect to the reference potential provided in the file *referencePotential.mat* using the function `showData`.

(b) Set up the design matrix A, which relates spherical harmonic coefficients and given gravitational potential, for arbitrary maximum degree n_{max}. Use the function `calculatePnm` for the computation of the Legendre functions. The gravity constant times the Earth's mass amounts to $GM = 3.9860044150 \times 10^{14}$ $^{m^3}/_{s^2}$ and the Earth's radius is $a = 6378137$ m. (The parameter vector should be sorted order-wise and according to cosine and sine components: $c_{0,0}, c_{1,0}, c_{2,0}, c_{3,0}, \ldots, c_{1,1}, c_{2,1}, c_{3,1}, \ldots, c_{n_{max},n_{max}}, s_{1,1}, s_{2,1}, s_{3,1}, \ldots, s_{n_{max},n_{max}}$.)

(c) Compute the normal equation matrix N for $n_{max} = 10$. Visualize the matrix using the function `showN` and discuss its special structure.

(d) Set up the normal equations up to degree and order 10, 20, 30, and 40 and estimate the parameter vector x using cholesky decomposition (`Matlab:chol`). Visualize the estimated parameters using the function `showParameters` and the degree variances of the estimated parameter vector using the function `showSqrtDegreeVariances`. Discuss the results.

(e) Compute the residuals $\hat{\mathbf{e}} = \mathbf{y} - \mathbf{A}\hat{\mathbf{x}}$ for degree and order 10, 20, 30, and 40 and visualize them using the function `showData`.

2: Influence of noise

(a) Perturb the given gravitational potential with random Gaussian noise with zero mean and standard deviations of 10 $^{m^2}/_{s^2}$, 100 $^{m^2}/_{s^2}$, and 1000 $^{m^2}/_{s^2}$ (`Matlab:randn`).

(b) Repeat exercise 1.d for $n_{max} = 40$ with the perturbed observations. Which effect has the noise on estimated parameters of different degree?

3: Regularization

(a) Set up a Tikhonov-type Kaula regularization matrix for arbitrary degree n_{max}.

(b) Apply the regularization matrix for estimating the parameters up to degree n_{max} = 10, 20, 30, and 40 from the gravitational potential perturbed with Gaussian noise ($\sigma = 100\ {}^{m^2}/_{s^2}$). Choose an appropriate scaling factor for the regularization matrix.
(c) Investigate the effects from noise with varying strength and from different scaling of the regularization matrix.

MATLAB functions:

function [Pnm] = calculatePnm(theta, n_{max})	
Calculation of normalized Legendre Functions using stable recursion formulas.	
Input	• theta: co-latitude at which the Legendre Functions are computed. The dimension is 1×1. [rad] • n_{max}: maximum degree up to which the Legendre Functions are computed. The dimension is 1×1.
Output	• Pnm: $n_{max} \times n_{max}$ matrix containing the normalized Legendre functions.

function [c_{nm}, s_{nm}] = sortCoefficients(x, n_{max})	
Divides the parameter vector **x** into two triangular matrix for cosine spherical harmonic coefficients c_{nm} and sine spherical harmonic coefficients s_{nm}.	
Input	• x: $n \times 1$ vector containing the estimated spherical harmonic coefficients sorted order-wise and according to cosine and sine components: $c_{0,0}, c_{1,0}, c_{2,0}, c_{3,0}, \ldots, c_{1,1}, c_{2,1}, c_{3,1}, \ldots, c_{n_{max},n_{max}}$, $s_{1,1}, s_{2,1}, s_{3,1}, s_{4,1}, \ldots\ldots, s_{n_{max},n_{max}}$. The dimension n is the number of the parameters. • n_{max}: maximum degree up to which the spherical harmonic coefficients are given. The dimension is 1×1.
Output	• c_{nm}: $n_{max} \times n_{max}$ matrix containing the cosine spherical harmonic coefficients. • s_{nm}: $n_{max} \times n_{max}$ matrix containing the sine spherical harmonic coefficients.

Functions for visualization:

function showData(data, longitude, latitude, titleString)
Visualization of (global) data along a satellite's orbit. All values are given in a column vector **data**. The longitude and latitude values corresponding to the orbit positions are given in the vectors **longitude** and **latitude**.

Input	• `data`: $n \times 1$ vector containing the data values. • `longitude`: $n \times 1$ vector containing the longitude values of the orbit positions. [degree] • `latitude`: $n \times 1$ vector containing the latitude values of the orbit positions. [degree]
Output	• 2D-plot of the values along the satellite's orbit.

function showN(N,titleString)	
Visualization of the normal equation matrix.	
Input	• N: $n \times n$ normal equation matrix. The dimension n is the number of the parameters.
Output	• 2D-plot of the normal equation matrix.

function showParameters(x,n_{max},titleString)	
Visualization of the estimated parameters in a triangular plot.	
Input	• x: $n \times 1$ vector containing the estimated spherical harmonic coefficients sorted order-wise and according to cosine and sine components: $c_{0,0}, c_{1,0}, c_{2,0}, c_{3,0}, \ldots, c_{1,1}, c_{2,1}, c_{3,1}, \ldots, c_{n_{max},n_{max}}$, $s_{1,1}, s_{2,1}, s_{3,1}, s_{4,1}, \ldots\ldots, s_{n_{max},n_{max}}$. The dimension n is the number of the parameters. • n_{max}: maximum degree up to which the parameters are estimated. The dimension is 1×1.
Output	• 2D-plot of the spherical harmonic coefficients.

function showSqrtDegreeVariances(x,n_{max},titleString)
Computation and visualization of the square root of the degree variances from degree 3 to degree n_{max}. The square root of the degree variances of degree n are computed according to $v_n = \sqrt{\sum_{m=0}^{n}(c_{nm}^2 + s_{nm}^2)}$.

Input	• x: $n \times 1$ vector containing the estimated spherical harmonic coefficients sorted order-wise and according to cosine and sine components: $c_{0,0}$, $c_{1,0}$, $c_{2,0}$, $c_{3,0}$, ..., $c_{1,1}$, $c_{2,1}$, $c_{3,1}$, ..., $c_{n_{max},n_{max}}$, $s_{1,1}$, $s_{2,1}$, $s_{3,1}$, $s_{4,1}$, ..., $s_{n_{max},n_{max}}$. The dimension n is the number of the parameters. • $\mathrm{n_{max}}$: maximum degree up to which the parameters are estimated. The dimension is 1×1.
Output	• 1D-plot of the square root of the degree variances using a logarithmic scale and starting at degree 3.

Chapter 2
Precise Orbit Determination

Adrian Jäggi and Daniel Arnold

Abstract Precise Orbit Determination (POD) is an integral part for analyzing measurements from space geodetic techniques such as Satellite Laser Ranging (SLR) and Global Navigation Satellite Systems (GNSS) such as the Global Positioning System (GPS). In the last two decades, POD based on GPS data has furthermore been established as one of the standard techniques to derive trajectories of satellites in the low Earth orbit (LEO) with highest accuracy. Since the launch of dedicated gravity missions, GPS sensors are not only used as a key tracking system for LEO POD, but also for extracting the long wavelength part of the Earth's gravity field (together with SLR to spherical satellites). This chapter introduces SLR and GNSS measurements collected by the terrestrial networks of the International Laser Ranging Service (ILRS) and the International GNSS Service (IGS) as the observational basis for the realization of a terrestrial reference frame from satellite data. On this foundation, the basic equations and mathematical methods of orbit determination are introduced and extensively discussed. Pseudo-stochastic orbit modeling techniques are eventually presented as a general and efficient concept to determine satellite trajectories of highest quality even in presence of deficient force models, covering the full range between dynamic and purely kinematic solutions. Selected results from the application of the discussed orbit determination techniques are highlighted for GPS LEO data. Special emphasis is also put to present orbit determination in the context of more general orbit determination problems, where satellite trajectories are simultaneously determined with other parameters encompassing (at maximum) all pillars of geodesy, i.e., the shape, rotation, and gravity field of the Earth.

A. Jäggi (✉) · D. Arnold
Astronomical Institute, University of Bern, Bern, Switzerland
e-mail: adrian.jaeggi@aiub.unibe.ch

D. Arnold
e-mail: daniel.arnold@aiub.unibe.ch

M. Naeimi and J. Flury (eds.), *Global Gravity Field Modeling from Satellite-to-Satellite Tracking Data*, Lecture Notes in Earth System Sciences,
DOI 10.1007/978-3-319-49941-3_2

2.1 Precise Tracking Data

Precise orbit determination of artificial satellites requires precise measurements which are related to the position or velocity of the satellites. These data are today collected by satellite tracking systems which measure the properties of the propagation of electromagnetic waves between the transmitter and receiver. In this chapter we focus on precise tracking data collected from Global Navigation Satellite Systems (GNSS), Satellite Laser Ranging (SLR), and inter-satellite ranging. For an overview of various (other) tracking systems the reader is referred to, e.g., [104].

2.1.1 Global Positioning System

Over the past four decades, the Global Positioning System (GPS) has evolved from a predominantly military navigation system into an indispensable tool not only for society at large, but also for geodetic research and global monitoring of the Earth [106]. Over the past two decades, GPS has also become a unique tool for deriving very precise orbits of satellites in the Low Earth Orbit (LEO). Equipped with onboard GPS receivers, uninterrupted three-dimensional GPS tracking makes it possible to perform LEO orbit determination with unprecedented accuracy by combining the strength of dense GPS measurements with the strength of the dynamic laws, e.g., [64]. Over the past decade, the world of satellite navigation has experienced further dramatic changes: with the Russian GLONASS, a second GNSS has achieved full operational status, GPS is introducing modernized civil navigation signals, and a variety of new navigation constellations are being built up in Asia and Europe [106]. Most of these recent developments are not yet available in current spaceborne receivers, which still rely uniquely on GPS at the time of writing these lecture notes.

The GPS satellites are arranged in six orbital planes which are inclined by about 55° with respect to the Earth's equator and equally separated by 60° on the equator. The satellite orbits are close to circular, with a semi-major axis of about 26 600 km. The orbital revolution period is about 11 h 58 min, which is half a sidereal day. The full constellation of 24 active satellites (currently 32) guarantees that at least four satellites are simultaneously visible at any time and any location on and in the vicinity of the Earth's surface. All GPS satellites are equipped with an ensemble of atomic clocks to generate coherent carriers in the L-band, e.g., the L_1 and L_2 carriers with wavelengths of $\lambda_1 \approx 19.0\,\text{cm}$ and $\lambda_2 \approx 24.4\,\text{cm}$. Pseudo-random noise codes are generated and modulated on these carriers by the phase modulation technique. For a more detailed description, the reader is referred to, e.g., [60].

2.1.1.1 International GNSS Service

By the late 1980s, many organizations had recognized the potential of GPS for geodesy and geodynamics. A test campaign, conducted in summer of 1992, involved the deployment and operation of a global GPS tracking network, the rapid acquisition of observational data and transfer to global data centers (DCs), and the regular data analysis by several analysis centers (ACs). Thanks to the successful operation and to the continuing effort of the large majority of participating organizations, the International GNSS Service (IGS) became an official service of the International Association of Geodesy (IAG) on January 1, 1994 [9]. Since then, more than 200 organizations, agencies, and universities have shared their resources to define international standards and to establish an independent ground segment, which generates high-accuracy products on a best efforts basis with reliability through redundancy. About ten ACs produce precise ephemerides and clocks of all active GPS satellites, Earth rotation parameters (ERP's), coordinates, velocities and clock corrections to GPS time, global ionosphere maps, and station troposphere zenith path delays for the IGS tracking sites. In order to respond to the ongoing modernization of the GPS and to make use of the newly emerging GNSS, the IGS has initiated the Multi-GNSS-EXperiment (MGEX) [106].

2.1.1.2 GNSS Observation Equations

GPS receivers collect several types of GPS code observations, e.g., the C/A-, P_1-, and P_2-code observations, and carrier phase observations, denoted as L_A, L_1, and L_2. The code observation (or pseudo-range) of the satellite k at time T^k and registered by the receiver i at time T_i, is defined as

$$P_i^k \doteq c\ (T_i - T^k)\ , \tag{2.1}$$

where P_i^k is expressed in units of length, c is the speed of light, T_i is the arrival (or observation) time of the signal, as measured by the clock of receiver i, and T^k is the transmission time of the signal, as measured by the clock of satellite k.

GPS positioning is thus primarily based on one-way measurements of the signal traveling time. Therefore, a common reference time, the so-called GPS system time [123], has been defined, which is aligned to the international atomic time (TAI) with a constant offset of $-19\,\mathrm{s}$. Although the GPS satellites are equipped with atomic clocks, their clocks have a time-varying offset to GPS time. The same holds for GPS receivers, which are usually not equipped with ultra-stable oscillators. Due to the lack of synchronization between transmitter and receiver clocks, one cannot directly derive ranges from the code measurements, which therefore are called pseudo-ranges. Most receivers usually keep their clocks synchronized with respect to GPS time, but there are also receivers with internal clocks, which are not steered to integer seconds of GPS time. As GPS satellite and receiver clocks are usually affected by a drift, both, transmitter and receiver clock offsets, are only valid for a certain epoch.

The pseudo-range P_i^k may be related to the slant range ρ_i^k, i.e., to the geometric distance between the receiver i at signal reception, expressed in GPS time t_i, and the satellite k at signal transmission, expressed in GPS time t^k, as well, and to the delays due to the Earth's atmosphere as

$$P_i^k = \rho_i^k - c \cdot \Delta t^k + c \cdot \Delta t_i + \Delta\rho_{i,trop}^k + \Delta\rho_{i,ion}^k + \varepsilon_{Pi}^k \,, \tag{2.2}$$

where $\Delta t^k = T^k - t^k$ is the clock offset of the satellite k w.r.t. the GPS system time, $\Delta t_i = T_i - t_i$ is the clock offset of the receiver i w.r.t. the GPS system time, $\Delta\rho_{i,trop}^k$ and $\Delta\rho_{i,ion}^k$ are the signal delays due to the troposphere and ionosphere, expressed in units of length, and ε_{Pi}^k is the residual. Further terms such as relativistic corrections have to be included in the term ρ_i^k to ensure a correct modeling.

The carrier phase observation L_A, L_1, or L_2 corresponding to the code observation is defined as

$$L_i^k \doteq \lambda \, (\phi_i - \phi^k + N_i^k) \,, \tag{2.3}$$

where L_i^k is the accumulated carrier phase observation, expressed in units of length, λ is the corresponding wavelength, ϕ_i is the carrier phase of the reference signal generated by the receiver i at arrival time T_i, ϕ^k is the carrier phase of the transmitted signal at transmission time T^k, and N_i^k is the initial carrier phase ambiguity, expressed in an integer number of cycles of λ. The carrier phase observation equation may be formulated in analogy to the code observation equation (2.2) as

$$L_i^k = \rho_i^k - c \cdot \Delta t^k + c \cdot \Delta t_i + \Delta\rho_{i,trop}^k - \Delta\rho_{i,ion}^k + \lambda \cdot B_i^k + \varepsilon_{Li}^k \,, \tag{2.4}$$

where B_i^k denotes a constant bias related to the initial carrier phase ambiguity, expressed in cycles. The major difference to the code observation equation (2.2) is the bias term B_i^k, which consists of the integer-valued initial carrier phase ambiguity N_i^k, the real-valued non-zero phase difference between ϕ_i and ϕ^k at any common epoch, and the real-valued satellite and receiver specific hardware delays. If the receiver loses lock of the signal, an additional bias term has to be set up due to the discontinuity (cycle slip) in the accumulated carrier phase observations. An additional difference to the code observation equation (2.2) is the opposite sign of the ionospheric refraction term $\Delta\rho_{i,ion}^k$ due to a phase advance instead of a group delay.

In summary, the observation equations provided by a dual-frequency GPS receiver at a certain observation t_i may be written as

$$\begin{aligned} P_{i,1}^k &= \tilde{\rho}_i^k + I_i^k + \varepsilon_{P_1 i}^k \\ P_{i,2}^k &= \tilde{\rho}_i^k + \xi \cdot I_i^k + \varepsilon_{P_2 i}^k \\ L_{i,1}^k &= \tilde{\rho}_i^k - I_i^k + \lambda_1 \cdot B_{i,1}^k + \varepsilon_{L_1 i}^k \\ L_{i,2}^k &= \tilde{\rho}_i^k - \xi \cdot I_i^k + \lambda_2 \cdot B_{i,2}^k + \varepsilon_{L_2 i}^k \,, \end{aligned} \tag{2.5}$$

where $P_{i,1}^k$, $P_{i,2}^k$ are the code observations on both frequencies, $L_{i,1}^k$, $L_{i,2}^k$ are the accumulated carrier phase observations on both frequencies, and where $\tilde{\rho}_i^k$ is the geometric distance between the receiver i and the satellite k including the clock offsets and the tropospheric refraction. $B_{i,1}^k$, $B_{i,2}^k$ are the carrier phase bias parameters on both frequencies, and $\varepsilon_{P_1 i}^k$, $\varepsilon_{P_2 i}^k$, $\varepsilon_{L_1 i}^k$, $\varepsilon_{L_2 i}^k$ the residuals of all measurements. The ionosphere is a dispersive medium for the L-band carrier waves broadcasted by the GPS satellites and the ionospheric refraction is thus proportional to $1/\nu^2$ in first-order approximation of the carrier frequency ν. The signal delays $\Delta\rho_{i,ion}^k$ on both frequencies may therefore be expressed as a function of the L_1-related ionospheric refraction I_i^k. The L_2-related ionospheric refraction then follows by a simple multiplication of I_i^k by the conversion factor $\xi = \nu_1^2/\nu_2^2 \approx 1.6469$.

Because the code observations are two to three orders of magnitude less precise than the carrier phase observations, which exhibit a thermal noise at the level of mm only, the carrier phase observables are primarily used for high-precision geodetic applications. In order to minimize or eliminate specific error sources, such as ionospheric refraction on the right-hand sides of Eq. (2.5), it is common practice to form differences between the original measurements with GPS observations from other receivers (single or double-differences), or to form linear combinations of the original dual-frequency measurements, e.g., the ionosphere-free linear combination, or to combine both techniques. It is, however, also possible to directly process the original (undifferenced) observations from Eq. (2.5) by estimating epoch-wise ionosphere delays, e.g., [163]. For a general discussion and thorough derivation of the GPS observation equations and their linear combinations, e.g., in the context of ambiguity resolution, the reader is referred to [143].

2.1.2 Satellite Laser Ranging

The first SLR measurements to a satellite equipped with laser reflectors were collected on 31 October, 1964 at the NASA Goddard Geophysical and Astronomical Observatory, only four years after the first laser was constructed [131]. Since then the SLR technique has evolved to one of the most important space-geodetic techniques for the determination of the terrestrial reference frame, the determination of the Earth's gravity field, and the validation of results from the other space-geodetic techniques such as GNSS and Very Long Baseline Interferometry (VLBI). For a summary of the current achievements of SLR, the reader is referred to, e.g., [137].

SLR measures the round-trip time of flight Δt_i^k of the ultra-short and highly energetic laser pulses transmitted by a ground station i through a telescope and reflected by special corner cubes onboard of a satellite k back to the telescope. The two-way time of flight may be transformed into a distance by multiplying the time of flight by the speed of light. Similar to other space-geodetic techniques, a number of corrections need to be made, e.g., due to atmospheric delays, relativistic effects, satellite center-of-mass corrections, laser system offsets, etc. Because the

same electronic time interval counter is used at a ground station to register the emission time of a laser pulse and the reception time of the pulse, the SLR two-way measurements are virtually free of synchronization errors. Focusing on the geometric part and omitting all other terms, the fundamental SLR observation equation reads as

$$\Delta t_i^k = \tau_{i,up}^k + \tau_{i,down}^k = \frac{1}{c}\left(|\mathbf{r}_i(t_{sat} - \tau_{i,up}^k) - \mathbf{r}^k(t_{sat})| + |\mathbf{r}_i(t_{sat} + \tau_{i,down}^k) - \mathbf{r}^k(t_{sat})|\right) , \tag{2.6}$$

where Δt_i^k is the sum of the uplink and downlink time of flight of the laser pulse, $\mathbf{r}_i$ is the inertial position of the laser station i at emission time $t_{sat} - \tau_{i,up}^k$ and reception time $t_{sat} + \tau_{i,down}^k$, respectively, and $\mathbf{r}^k$ is the inertial position of the optical phase center at the satellite k at the reflection time t_{sat}. Assuming $\tau_{i,up}^k \approx \tau_{i,down}^k \approx \frac{1}{2}\,\Delta t_i^k$ the inertial position of the laser station may be approximated as

$$\mathbf{r}_i(t_{sat} \pm \frac{1}{2}\,\Delta t_i^k) \approx \mathbf{r}_i(t_{sat}) \pm \frac{1}{2}\,\Delta t_i^k \cdot \dot{\mathbf{r}}_i(t_{sat}) \, . \tag{2.7}$$

Neglecting higher-order terms, the observation equation (2.6) may then be simplified to

$$\Delta t_i^k = \frac{2}{c}\,|\mathbf{r}_i(t_{sat}) - \mathbf{r}^k(t_{sat})| \, , \tag{2.8}$$

where the inertial positions $\mathbf{r}_i$ and $\mathbf{r}^k$ of the laser station i and of the satellite k both refer to the pulse reflection time t_{sat} at the satellite. The approximation is sufficient for terrestrial laser ranging up to the altitude of GNSS satellites. For time of flight measurements to distant targets, e.g., for Lunar Laser Ranging (LLR), the observation equation (2.6) has to be used.

2.2 Orbit Representation

The slant range ρ_i^k contains the necessary geometric information to perform orbit determination of the satellites tracked by the respective tracking data. When determining a LEO orbit from undifferenced GNSS tracking data, the observation equation (2.5) or their ionosphere-free linear combinations have to be used. The relevant geometric term reads as

$$\rho_{leo}^k = |\mathbf{r}_{leo}(t_{leo}) - \mathbf{r}^k(t_{leo} - \tau_{leo}^k)| \, , \tag{2.9}$$

where $\mathbf{r}_{leo}$ is the inertial position of the LEO antenna phase center at GPS time t_{leo}, $\mathbf{r}^k$ is the inertial position of the antenna phase center of GPS satellite k at GPS time $t_{leo} - \tau_{leo}^k$, where τ_{leo}^k is the signal traveling time between the two phase centers.

As Earth orbiting satellites are usually extended objects of considerable size, any of its instruments normally is not located at the satellite's center of mass. The motion

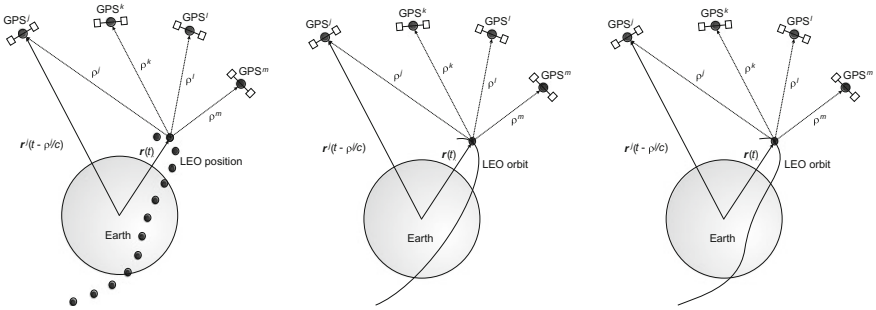

Fig. 2.1 Kinematic (*left*), dynamic (*middle*), and reduced-dynamic (*right*) orbit representation

of the phase center position of an onboard GNSS antenna or an SLR reflector in inertial space thus comprises the satellite's center of mass motion around the Earth, and the rotation of the satellite body around its center of mass. The orientation of a satellite-fixed coordinate system in inertial space is called the attitude of the satellite. In order to relate the phase center to the center of mass of the LEO spacecraft in inertial space at time t_{leo}, the location of the antenna phase center position in the satellite-fixed coordinate system and the attitude of the satellite, e.g., as measured by onboard star cameras, have to be known. If both are fulfilled, the LEO center of mass position in Eq. (2.9) may be modeled either by a kinematic, a dynamic, or a reduced-dynamic orbit. The three orbit types are illustrated by Fig. 2.1 for LEO orbit determination from GNSS tracking data and are described in more detail in the following subsections.

2.2.1 Kinematic Orbit Representation

Kinematic orbit determination describes the satellite's orbital motion by three Cartesian coordinates, estimated from the tracking data for each measurement epoch. The kinematic representation is not limited to satellite orbits, but can be used for all kinds of moving objects, e.g., cars, ships, aircrafts. The inertial phase center position $\mathbf{r}_{leo}$ of the onboard antenna is related to the satellite's center of mass by

$$\mathbf{r}_{leo}(t_{leo}) = \mathbf{R}(t_{leo}) \cdot \mathbf{r}_{leo,e,0}(t_{leo}; x_1, y_1, z_1, ..., x_n, y_n, z_n) + \delta\mathbf{r}_{leo,ant}(t_{leo}) \ , \quad (2.10)$$

where $\mathbf{R}$ is the transformation matrix from the Earth-fixed to the inertial frame, $\mathbf{r}_{leo,e,0}$ is the position vector of the LEO center of mass in the Earth-fixed frame, $x_1, y_1, z_1, ..., x_n, y_n, z_n$ are the epoch-wise kinematic coordinates, and $\delta\mathbf{r}_{leo,ant}$ is the antenna phase center offset in the inertial frame.

$\delta\mathbf{r}_{leo,ant}$ is assumed to be known, and is obtained in the inertial frame from given antenna phase center offsets (and variations), and the LEO attitude. The epoch-wise

kinematic coordinates, either of the center of mass or of the phase center of the antenna, are the unknown parameters of the orbit determination and often directly set-up in the Earth-fixed system. Kinematic positions of the antenna phase center may be estimated from the tracking data without the knowledge of the phase center offsets $\delta \mathbf{r}_{leo,ant}$ and the satellite attitude, which is not possible for the center of mass.

Figure 2.1 (left) shows that a kinematic LEO orbit is a satellite ephemerides provided at the (discrete) measurement epochs of the onboard GNSS receiver. Kinematic positions are derived by geometric means only by a precise point positioning (PPP) approach [167], implying that no position information can be derived for between measurement epochs. No velocity or acceleration information can be directly derived from a kinematic trajectory. This is relevant for gravity field determination from kinematic positions when using the acceleration approach or the energy balance as discussed in Chaps. 4 and 5. Numerical differentiation schemes are inevitable and a proper selection of the associated parameters (filter length, filter degree) is crucial, e.g., [6].

Figure 2.2 shows an extract of a 1-s ephemerides of the GOCE kinematic positions in the SP3 format [122], which provides satellite positions (in km) in the International Terrestrial Reference Frame [1]. Because kinematic positions are always referring to the actual measurement epochs (expressed in Fig. 2.2 in GPS time), they cannot be provided on a completely regular 1 s grid. Also the time tags do not necessarily need to coincide with integer seconds. This is obvious for the GOCE onboard receivers, for which the internal clocks were not steered to integer seconds. If more digits are required for the time tags, clock corrections may be provided in the last column of Fig. 2.2 (expressed in μs) to compute the time tags by subtracting the clock corrections from the nominal epochs.

```
*  2009 11  2  0  0  0.80678020
PL15   -390.612059   6623.987679     73.104149 193219.797196
*  2009 11  2  0  0  1.80678020
PL15   -389.240315   6624.166512     65.402457 193219.799413
*  2009 11  2  0  0  2.80678020
PL15   -387.868014   6624.336133     57.700679 193219.801634
*  2009 11  2  0  0  3.80678020
PL15   -386.495163   6624.496541     49.998817 193219.803855
*  2009 11  2  0  0  4.80678019
PL15   -385.121760   6624.647724     42.296889 193219.806059
*  2009 11  2  0  0  5.80678019
PL15   -383.747819   6624.789703     34.594896 193219.808280
*  2009 11  2  0  0  6.80678019
PL15   -382.373332   6624.922464     26.892861 193219.810495
*  2009 11  2  0  0  7.80678019
PL15   -380.998306   6625.046003     19.190792 193219.812692
*  2009 11  2  0  0  8.80678019
PL15   -379.622745   6625.160329     11.488692 193219.814899
*  2009 11  2  0  0  9.80678018
PL15   -378.246651   6625.265448      3.786580 193219.817123
```

Fig. 2.2 Extract of kinematic GOCE positions at begin of 2 Nov, 2009

Kinematic LEO positions are derived without using any information on the LEO dynamics [151]. Kinematic positions therefore may be used for gravity field determination as pseudo-observations for both alternative (energy balance approach, acceleration approach) and classical gravity field recovery methods (variational equations approach). Reference [46] used for the first time kinematic CHAMP positions and demonstrated that gravity field determination is feasible using the energy balance method [113]. The use of precise kinematic positions stimulated several research groups working on gravity field recovery in the first decade of the 21st century due to the less demanding computational resources than in the case of classical numerical integration techniques, e.g., [149]. For groups using the classical approach, e.g., [11], kinematic positions are attractive, as well, thanks to a much simplified handling of the pseudo-observations compared to the original GNSS tracking data.

Kinematic positions are referred to as pseudo-observations, because they are not original observations but derived from GPS data. Due to the presence of the ambiguity parameters in the GPS carrier phase observation equation (2.4), kinematic positions derived from GPS carrier phase data are furthermore not independent but correlated. Figure 2.3 (left) shows a zoom on 700 epochs of the correlation matrix of the Earth-fixed z-component of GRACE-B kinematic positions. Off-diagonal elements are shown over 200 epochs, which corresponds to slightly more than one revolution period (exactly 100 min due to a 30 s position sampling). As expected, the correlations are decreasing on average for increasing epoch differences. Spots of higher correlations may be recognized, as well, which are related to the satellite crossings of the Earth's equator and are thus occurring twice-per-revolution. The better tracking geometry in these regions ensures a better connection of the GPS carrier phase observations (smaller number of interruptions due to multiple ambiguities) and leads to more correlated kinematic positions. On average the correlations drop on this example day to 51 % after one epoch of 30 s, to 40 % after twenty epochs, to 26 % after forty epochs, and to below 10 % after one hundred epochs. During periods of high correlations, however, values of more than 80 % may still be observed after forty epochs, and even after one hundred epochs correlations may still be as high as 45 %.

Figure 2.3 (right) shows for one example day the residuals for distances between the two GRACE satellites as derived from different GPS-based orbit determinations and biased ranges, which are directly observed by the ultra-precise K-Band ranging system. The best performance (smallest residuals) is obtained for the solution 'PHASE', where the original GPS carrier phase data are directly used as observations for a reduced-dynamic orbit determination (see Sect. 2.2.3 for more details on reduced-dynamic orbit determination). For solution 'KIN-EPO', where the same reduced-dynamic orbit parameters are solved from kinematic positions used as pseudo-observations with only epoch-wise covariance information taken into account for the observation weighting in the least-squares adjustment, a significant degradation is obtained. It is obviously not sufficient to only take into account an epoch-wise weighting in the least-squares adjustment, because long-period variations of the kinematic positions are then erroneously fitted by the parameters of the reduced-dynamic orbit model instead of being interpreted as a pure consequence of

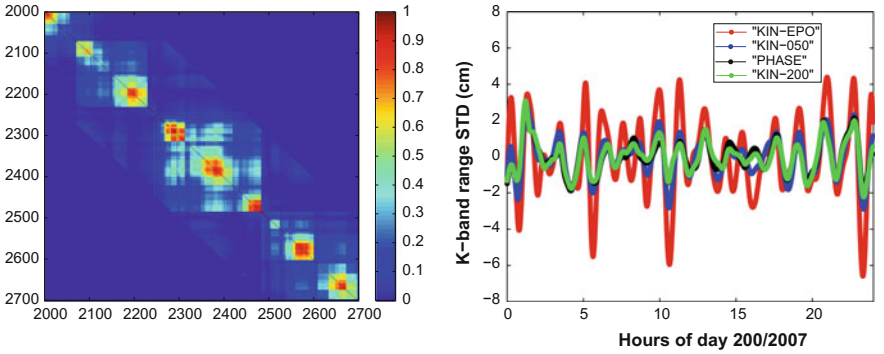

Fig. 2.3 Extract of correlation matrices of the Earth-fixed z-component of GRACE-B kinematic positions for one example day (*left*) and K-band range residuals for distances between reduced-dynamic GRACE-A and -B orbits stemming from different observation handling (*right*). Figures from [70]

the ambiguity-induced correlations in time. For solutions 'KIN-50' and 'KIN-200', where covariances over 50 and 200 epochs are taken into account for the observation weighting, respectively, a considerable improvement of the orbit quality is achieved. Solution 'KIN-200' shows in essence the same quality as the 'PHASE' solution. It has to be emphasized that it is necessary to take into account the rather large number of 200 off-diagonal blocks to achieve a close equivalence to the 'PHASE' solution.

Similar to orbit determination, covariance information from the kinematic positioning has also to be taken into account to obtain equivalent results for gravity field recovery as from original GPS carrier phase data [70]. To further exploit kinematic positions for gravity field recovery, empirically derived covariance information is sometimes taken into account in addition [163].

2.2.2 Dynamic Orbit Representation

Dynamic orbit determination describes the motion of the satellite's center of mass as a particular solution of an equation of motion. As real satellite trajectories are always particular solutions of an equation of motion, a dynamic orbit representation is certainly the most natural choice for modeling orbital motion. In dynamic orbit determination, the phase center of the onboard antenna is related to the satellite's center of mass as

$$\mathbf{r}_{leo}(t_{leo}) = \mathbf{r}_{leo,0}(t_{leo}; a, e, i, \Omega, \omega, u_0; Q_1, ..., Q_d) + \delta\mathbf{r}_{leo,ant}(t_{leo}) \,, \qquad (2.11)$$

where $\mathbf{r}_{leo,0}$ is the LEO center of mass position in the inertial frame, $a, e, i, \Omega, \omega, u_0$ are six LEO orbital elements, $Q_1, ..., Q_d$ are additional LEO dynamical orbit para-

meters, and $\delta\mathbf{r}_{leo,ant}$ is the antenna phase center offset with respect to the center of mass in the inertial frame.

In analogy to Eq. (2.10), $\delta\mathbf{r}_{leo,ant}$ is considered as known. The unknown parameters are the LEO initial osculating orbital elements O_j, $j = 1, ..., 6$, and additional dynamical orbit parameters $Q_1, ..., Q_d$. The latter may be scaling factors of analytically or numerically known accelerations, e.g., derived from a model of the Earth's gravity field, or non-gravitational accelerations as measured by an on-board accelerometer.

In a dynamic orbit representation the LEO center of mass position $\mathbf{r}_{leo,0}$ is modeled as a particular solution of an equation of motion. Dynamic force models are used to describe the equation of motion and to propagate the satellite's center of mass position and velocity over time by numerical integration techniques. Figure 2.1 (middle) shows that a dynamic LEO orbit derived from GNSS tracking data therefore provides a satellite ephemerides, which may be evaluated at any epoch within the orbital arc. By construction, the orbital trajectory is fully dependent on the underlying force models. The equation of motion of an Earth-orbiting satellite including all perturbations reads

$$\ddot{\mathbf{r}} = -GM\frac{\mathbf{r}}{r^3} + \mathbf{f}_p(t, \mathbf{r}, \dot{\mathbf{r}}, Q_1, ..., Q_d) \doteq \mathbf{f} \tag{2.12}$$

with the initial conditions

$$\mathbf{r}(t_0) = \mathbf{r}(a, e, i, \Omega, \omega, u_0; t_0) \quad \text{and} \quad \dot{\mathbf{r}}(t_0) = \dot{\mathbf{r}}(a, e, i, \Omega, \omega, u_0; t_0)\ , \tag{2.13}$$

where GM is the gravity constant times the mass of the Earth, $\mathbf{r}$ the geocentric position of the satellite in the inertial frame, $\mathbf{f}_p$ the perturbing acceleration acting on the satellite in the inertial frame, and $\mathbf{f}$ the total acceleration. The acceleration $\mathbf{f}_p$ comprises all modeled gravitational and non-gravitational perturbations. The force models used may explicitly depend on the time t, or implicitly through the position vector $\mathbf{r}$ and the velocity vector $\dot{\mathbf{r}}$ of the satellite, as well as on additional force model parameters $Q_1, ..., Q_d$ that need to be adjusted.

At least one set of initial conditions (initial osculating elements) is estimated from the tracking data in a dynamic orbit determination procedure. Figure 2.4 illustrates the orbit represented by the six initial osculating elements (Keplerian elements) a, e, i, Ω, ω, and u_0 at time t_0. The semi-major axis a and the numerical eccentricity e describe the orbit's size and shape, the inclination i and the right ascension Ω of the ascending node describe the orbital plane with respect to the Earth's equator, the argument ω of the perigee Π describes the orbit's orientation, and the argument of latitude u_0 describes the satellite's position at time t_0. These six initial osculating elements are equivalent to the coordinates of the initial position and velocity vectors (state vector) at time t_0 as indicated by Eq. (2.13). The formulas of the two-body problem are conventionally used to relate one set of osculating orbital elements to the state vector and vice versa [7].

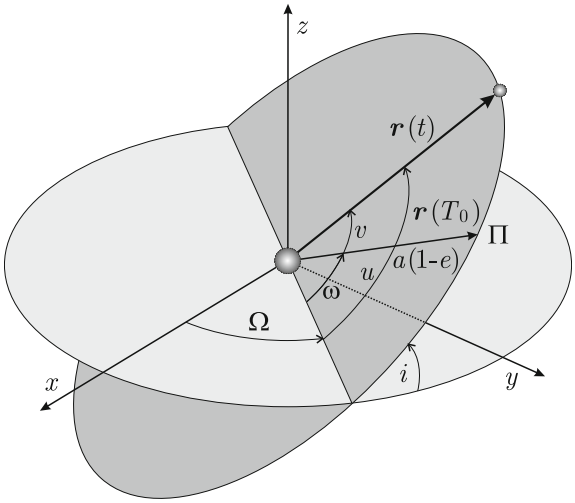

Fig. 2.4 Initial osculating elements a, e, i, Ω, ω, and the argument of latitude u. Figure from [7]

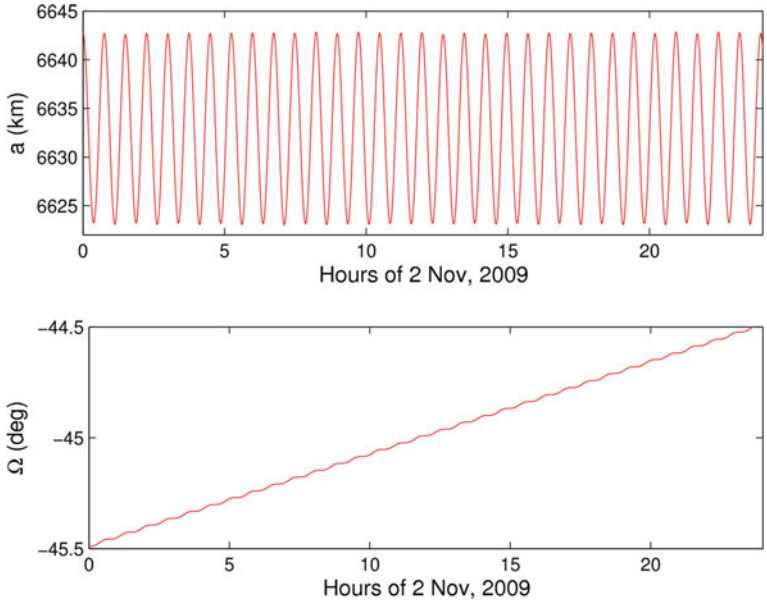

Fig. 2.5 Osculating semi-major axis (*top*) and right ascension of ascending node of the GOCE orbit on 2 Nov, 2009

Figure 2.5 illustrates the time evolution of the osculating semi-major axis a (top) and the right ascension Ω (bottom) of the ascending node of the GOCE orbit. The full force field was used to propagate the GOCE orbit by numerical integration over

one day and to compute osculating elements from the obtained position and velocity vectors. The observed variations are mainly due to the oblateness of the Earth [8]. Figure 2.5 (top) shows twice-per-revolution periodic variations with an amplitude of about 10 km around a mean semi-major axis of 6632.9 km, which corresponds to a mean GOCE orbital altitude of 254.9 km. Apart from small twice-per-revolution periodic variations, Fig. 2.5 (bottom) shows a pronounced linear drift of $\approx 1°$/day (360°/365 days). The node advances, because the inclination of the GOCE orbit is about $96° > 90°$, which in turn is required to maintain the sun-synchronous GOCE orbit. Both effects shown in Fig. 2.5 are mainly due to the oblateness of the Earth and can be explained by solving the Gaussian perturbation equations by first order perturbation theory, see e.g., [7].

2.2.3 Reduced-Dynamic Orbit Representation

The real-world dynamics of LEO satellites is not known to the precision required by highly precise tracking data such as GPS or K-band observations. Therefore, the concept of reduced-dynamic orbit determination has already been introduced several decades ago to better exploit precise tracking data such as GPS carrier phase measurements, [161, 162]. Reduced-dynamic orbits are accomplished by complementing the deterministic orbit model by additional stochastic parameters, which are adjusted together with the deterministic orbit parameters.

Pseudo-stochastic orbit modeling as presented in this chapter may be considered as a particular realization of the reduced-dynamic orbit determination technique and is discussed according to [64]. It makes use of both the geometric strength of GNSS observations and that satellite trajectories are particular solutions of a deterministic equation of motion. The attribute 'pseudo' distinguishes this method from stochastic orbit modeling where a satellite trajectory is modeled as a solution of a stochastic differential equation [73]. Pseudo-stochastic orbit modeling, in contrast, introduces additional empirical parameters $P_1, ..., P_s$, subsequently referred to as pseudo-stochastic orbit parameters, to the deterministic equation of motion (2.12), which then reads as

$$\ddot{\mathbf{r}} = -GM\frac{\mathbf{r}}{r^3} + \mathbf{f}_p(t, \mathbf{r}, \dot{\mathbf{r}}, Q_1, ..., Q_d, P_1, ..., P_s) \doteq \mathbf{f} \,. \tag{2.14}$$

The attribute 'stochastic' arises from the practice to optionally characterize these additional parameters by a priori known statistical properties like, e.g., expectation values and a priori weights, which constrain the estimated parameters to user-specified expectation values.

Figure 2.1 (middle, right) shows that a (reduced-) dynamic LEO orbit is a satellite ephemerides, which may be evaluated at any epoch within the orbital arc. Consequently reduced-dynamic positions can be provided on a regular grid as requested by the SP3 format and illustrated in Fig. 2.6, which shows an extract of a 10 s

```
*  2009 11  2  0  0  0.00000000
PL15   -391.718353   6623.836682     79.317661 999999.999999
VL15  13710.157683   1908.731015 -77015.601314 999999.999999
*  2009 11  2  0  0 10.00000000
PL15   -377.980705   6625.284690      2.298385 999999.999999
VL15  13764.602016    987.250587 -77021.193676 999999.999999
*  2009 11  2  0  0 20.00000000
PL15   -364.190222   6625.811136    -74.721213 999999.999999
VL15  13815.825127     65.631014 -77016.232293 999999.999999
*  2009 11  2  0  0 30.00000000
PL15   -350.350131   6625.415949   -151.730567 999999.999999
VL15  13863.820409   -855.995477 -77000.719734 999999.999999
*  2009 11  2  0  0 40.00000000
PL15   -336.463660   6624.099187   -228.719134 999999.999999
VL15  13908.581905  -1777.497047 -76974.660058 999999.999999
*  2009 11  2  0  0 50.00000000
PL15   -322.534047   6621.861041   -305.676371 999999.999999
VL15  13950.104280  -2698.741871 -76938.058807 999999.999999
*  2009 11  2  0  1  0.00000000
PL15   -308.564533   6618.701833   -382.591743 999999.999999
VL15  13988.382807  -3619.598277 -76890.923043 999999.999999
```

Fig. 2.6 Extract of reduced-dynamic GOCE positions at begin of 2 Nov, 2009

ephemerides of GOCE reduced-dynamic positions and velocities (expressed in dm/s). Opposed to a purely dynamic orbit, the reduced-dynamic solution is more data-driven due to the empirical parameters and to a certain extent allowed to follow 'excursions' which otherwise are not described by the force models. Consequently, the highly accurate tracking data may be better fitted and reduced-dynamic approaches are therefore potentially well suited to compute LEO orbits of highest quality also in the presence of deficient force models. The empirical parameters may compensate unmodeled non-gravitational forces and even cope with rapidly changing accelerations as subsequently illustrated. Depending on the actual parametrization, the orbital trajectories nevertheless still heavily depend of the underlying force models. Reduced-dynamic positions are therefore not recommended to, e.g., serve as pseudo-observations for a subsequent and independent recovery of the Earth's gravity field [65].

Figure 2.7 shows the estimated empirical parameters of a reduced-dynamic orbit determination of the GOCE satellite in the commissioning phase on 7 May, 2009. The empirical parameters are set up as piecewise constant accelerations over 6 min (see Sect. 2.3.2.2) and mainly compensate the not explicitly modeled atmospheric drag experienced by the satellite. The changes in the signature of the estimated along-track accelerations in the middle of the day are related to the commissioning of the ion propulsion assembly of the GOCE satellite. Due to the unexpectedly low drag during the commissioning phase in spring 2009, GOCE was switched into the science mode on this day. Two thrust biases of 4 mN at maximum and follow-up biases of about 2–2.5 mN brought the satellite into the first drag-free flight ever. Figure 2.7 (middle) illustrates that the along-track drag is compensated to a large extent during this first

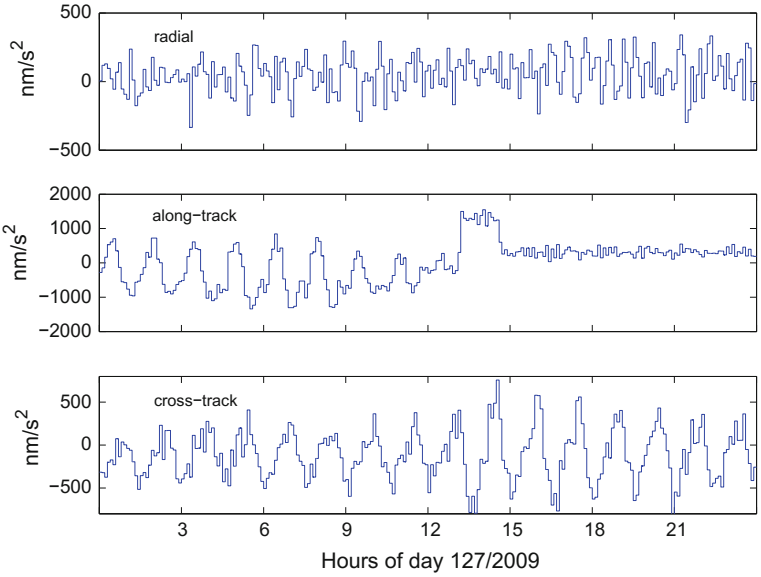

Fig. 2.7 Piecewise constant accelerations of a reduced-dynamic GOCE trajectory during the commissioning phase. Figure from [68]

drag-free flight. Remaining variations were reduced to a magnitude similar to the accelerations experienced in the radial direction. However, due to the extremely low atmospheric density at that time and altitude, a closed-loop drag-free flight was not yet feasible for a longer period than a couple of days. A next, slightly longer test was again started 26 May, 2009, at an altitude of about 272.5 km, but only after having reached the final orbital altitude of 259.56 km (mean spherical altitude, 254.9 km when referring to the mean semi-major axis), the GOCE satellite was eventually brought in the closed-loop drag-free flight on 14 September, 2009, e.g., [68].

2.2.4 Orbit Comparison

The characteristics of kinematic and reduced-dynamic orbits may be further illustrated by forming differences between them. This is a widely used technique to internally assess the consistency between the two types of orbits, e.g., [18, 145]. Although the differences do not give direct information about the orbit accuracy, they are a good indicator for the GPS data quality, e.g., in terms of noise and data outages, because kinematic positions are particularly sensitive to these issues.

Figure 2.8 shows the differences between GOCE kinematic positions and a reduced-dynamic GOCE ephemerides for a 30 h arc in the early phase of the mission as an example. The differences can only be computed at the discrete epochs of the

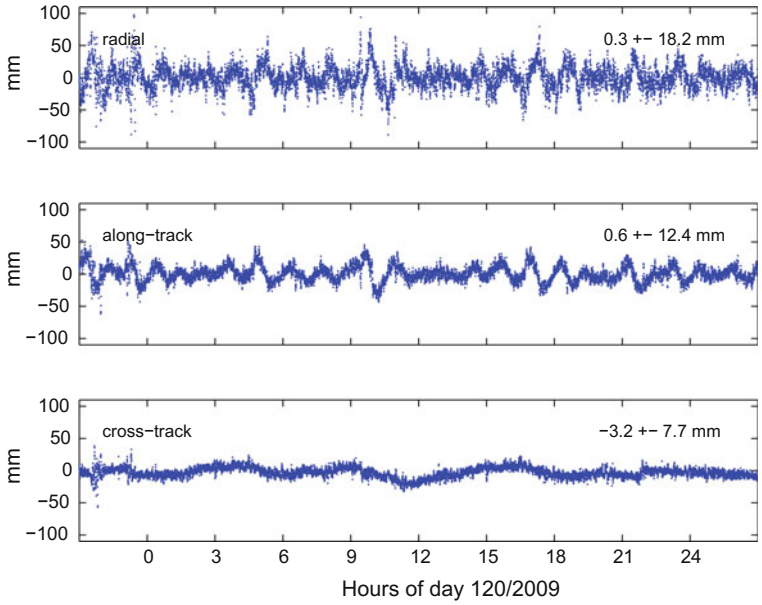

Fig. 2.8 Differences of GOCE kinematic positions with respect to a reduced-dynamic trajectory

kinematic positions, and are then transformed into the radial, along-track and cross-track directions as derived from the reduced-dynamic trajectory. Figure 2.8 shows that the two GOCE orbits agree on a level of a few centimeters. The scatter in the differences is due to the kinematic positions, which are derived without any smoothing or constraints between subsequent epochs. The high-frequency position noise is thus mainly given by the GPS carrier phase noise. It is largest in the radial ('height') direction due to the simultaneous estimation of kinematic positions and receiver clock corrections at every measurement epoch. The low-frequency variations seen in Fig. 2.8 may be caused by both types of orbits. Possible reasons are systematic carrier phase errors, e.g., receiver antenna phase center variations (PCVs), which are affecting kinematic and reduced-dynamic orbits differently [66], dynamic model errors which may not be fully compensated by the adopted empirical parametrization of the reduced-dynamic orbit [48], or colored noise of the kinematic positions [70]. The mean offsets between the kinematic and reduced-dynamic orbits are very small, which is due to the particular parametrization adopted to the reduced-dynamic orbit, where constant empirical accelerations acting over the entire orbital arc are estimated [66].

It should be emphasized that each additional (empirical) parameter introduced into the reduced-dynamic orbit determination weakens the solution for the other (non-empirical) parameters. Thanks to continuously improving models describing the gravitational, but in particular also the non-gravitational forces acting on LEO satellites, e.g., due to better descriptions via macro-models or direct measurements

of the surface forces by onboard accelerometers, purely empirical parameters can be estimated with tighter constraints (see Sect. 2.3.3) to yield a better dynamic stiffness of the reduced-dynamic trajectories while still providing high quality orbits [41, 49, 146]. In the case of the GOCE mission, the excellent quality of the onboard accelerometers even allowed to completely avoid any empirical parameters and to perform purely dynamic orbit determination on a very good quality level [148].

2.3 Orbit Determination

Kinematic positioning can be used for a wide range of applications because no conditions are imposed on the receiver motion. Kinematic positions are, however, very sensitive to bad measurements, unfavorable viewing geometry, and data outages. Kinematic positioning is therefore essentially restricted to LEO orbit determination based on spaceborne GNSS tracking data, or to GNSS orbit determination using tracking data of the terrestrial IGS ground network [151]. Dynamic and reduced-dynamic orbit determination, in contrast, make use of physical models of the satellite motion. The underlying orbit determination techniques are therefore also applicable to tracking systems which only sparsely cover an orbital arc with measurements, e.g., as in case of SLR [138]. In the case of GNSS-based LEO orbit determination the dynamic and reduced-dynamic approaches allow for some kind of 'averaging' the large number of measurements from different epochs, which makes the resulting position estimates much less prone to bad measurements and data outages. Satellite trajectories can therefore be reasonably well propagated across data gaps, especially if good dynamic models are available. This section has the focus on technical aspects of dynamic and reduced-dynamic orbit determination, introduces the primary equations, the variational equations, and the parameter estimation methods needed for the mathematical description of dynamic and reduced-dynamic orbit determination.

2.3.1 Primary Equations

According to Sects. 2.2.2 and 2.2.3 satellite motion is described as a particular solution of an equation of motion when using a dynamic or reduced-dynamic orbit representation. Equations (2.12) and (2.14) are often referred to as the primary equations of the underlying orbit determination problem. The acceleration $\mathbf{f}_p$ encompasses all gravitational and non-gravitational perturbations. Often, the perturbation model consists of a known part with accelerations given by analytical models, and of a part which includes force model parameters to be adjusted in the course of orbit determination. An overview of models typically taken into account for high-precision dynamic orbit determination is given in [8].

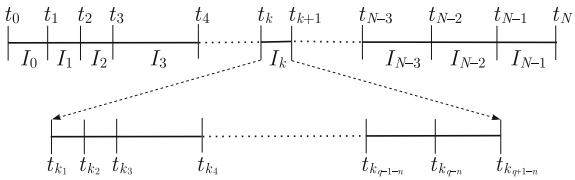

Fig. 2.9 Subdivision of the integration interval I_k for collocation algorithm. Figure from [7]

2.3.1.1 Numerical Integration

The high accuracy required for precise orbit determination may only be achieved by using numerical integration methods for the solutions of the primary (and the variational) equations. A variety of methods exists, among them well known methods such as Runge-Kutta, multi-step, and extrapolation methods, which have been successfully applied to orbit determination problems. For a detailed overview, we refer to original textbooks and articles published on the subject, e.g., [24, 132], or on textbooks providing overviews and detailed comparisons of methods, e.g., [7, 104].

In this section we give a short overview of the collocation methods as they are used in the Bernese GNSS Software [29] for the numerical integration of satellite orbits [7]. They approximate the initial value problems (2.12) and (2.14) by a polynomial of degree q, which is substantially higher than the order $n = 2$ of the underlying differential equation systems (for $q = n$ the method reduces to the algorithm already developed by Leonhard Euler in 1768, often referred to as the Euler method). The polynomial degree q is called the order of the method. Orders up to about 10 to 14 typically make sense in a double precision floating point environment. The interval subdivision (see Fig. 2.9) and the definition of the initial value problems at the left interval boundaries are the same as in the Euler method, except that the collocation method of order q of the previous interval is used to define the new initial values.

The initial value problem referring to the interval I_k, $k = 0, ..., N-1$ may be written as

$$\ddot{\mathbf{r}}_k = \mathbf{f}(t, \mathbf{r}_k, \dot{\mathbf{r}}_k) \tag{2.15}$$

with the initial conditions

$$\mathbf{r}_k(t_k) \doteq \mathbf{r}_{k0} \quad \text{and} \quad \dot{\mathbf{r}}_k(t_k) \doteq \dot{\mathbf{r}}_{k0}\,, \tag{2.16}$$

where the initial values are defined for $i = 0, 1$ as

$$\mathbf{r}_{k0}^{(i)} = \begin{cases} \mathbf{r}_0^{(i)} & ; k = 0 \\ \mathbf{r}_{k-1}^{(i)}(t_k) & ; k > 0 \end{cases}\,. \tag{2.17}$$

The collocation algorithm of order q approximates the initial value problem (2.15) in the interval $I_k = [t_k, t_{k+1}]$ by a polynomial of degree q as

$$\mathbf{r}_k(t) \doteq \sum_{l=0}^{q} \frac{1}{l!}(t - t_k)^l \, \mathbf{r}_{k0}^{(l)} \,, \tag{2.18}$$

where the coefficients $\mathbf{r}_{k0}^{(l)}$, $l = 0, ..., q$ are obtained by requesting that the numerical solution assumes the initial values (2.17) and that the numerical solution solves the differential equation system at exactly $q - 1$ different epochs t_{k_j}, $j = 1, ..., q - 1$, within the interval I_k (see Fig. 2.9 for $n = 2$).

Whereas the first conditions are automatically met by the definition of Eq. (2.18), the second conditions are obtained by replacing $\mathbf{r}_k(t)$ (and its time derivatives) in the differential equation system (2.15) by Eq. (2.18) for the epochs t_{k_j}, which yields

$$\sum_{l=2}^{q} \frac{(t_{k_j} - t_k)^{l-2}}{(l-2)!} \mathbf{r}_{k0}^{(l)} = \mathbf{f}(t_{k_j}, \mathbf{r}_k(t_{k_j}), \dot{\mathbf{r}}_k(t_{k_j})) \quad , \qquad j = 1, ..., q - 1 \,. \tag{2.19}$$

The above mentioned condition equations are algebraic and in general non-linear in the unknowns $\mathbf{r}_{k0}^{(l)}$, $l = 2, ..., q$, because they also implicitly show-up on the right-hand sides of Eq. (2.19), where the terms $\mathbf{r}_k^{(i)}(t_{k_j})$ must be replaced by the right-hand sides of Eq. (2.18). The number of unknowns is equal to the number of condition equations. An efficient solution strategy based on an iterative approach may be found in [7].

Whereas the above mentioned integration technique may be used without any difficulty to represent orbital arcs with much better precision than required by 'classical' tracking data such as GPS carrier phase measurements or SLR data, it is not trivial to generate solutions of the initial value problem (2.15) from which inter-satellite distances may be derived with an accuracy of about 1 µm for arcs as long as one day. In order to guarantee accuracies of better than 1 µm for inter-satellite distances as requested for K-band inter-satellite ranging, the collocation procedures need to be modified to represent the initial state vectors associated with the subintervals with better than double precision when keeping the arclength of one day. For details the reader is referred to [11].

In view of the prospect that the micrometer-precise K-band ranging instrument onboard the future GRACE Follow-On mission will be supplemented by a 50–100 nm precise precise laser interferometer [133], it is clear that future gravity missions relying on ultra-precise inter-satellite ranging observables will pose even higher demands on the numerical integration techniques used to represent the satellite trajectories. A recent study based on a full-scale closed-loop simulation for a GRACE Follow-On type pair of satellites using inter-satellite laser ranging underlined that a standard processing with double precision may indeed be a limiting factor for exploiting the nm precision of a laser interferometer to its full extent and proposed a scheme with enhanced precision that uses both double and quadruple precision in different parts of the processing chain [31].

2.3.1.2 Orbit Improvement

Let us assume that an a priori orbit $\mathbf{r}_0(t)$ is available, which is represented by the (a priori) parameter values $P_{0,i}$. Such an orbit may be realized, e.g., by a dynamical fit of LEO positions obtained from a kinematic solution using GPS code measurements, or from an extrapolation of an orbit trajectory covering the previous day. Orbit determination discussed in this chapter is therefore understood as an orbit improvement process, where the actual orbit $\mathbf{r}(t)$ is expressed as a truncated Taylor series with respect to the unknown orbit parameters P_i about the a priori orbit as

$$\mathbf{r}(t) = \mathbf{r}_0(t) + \sum_{i=1}^{n} \frac{\partial \mathbf{r}_0}{\partial P_i}(t) \cdot (P_i - P_{0,i}) \,, \tag{2.20}$$

where $n = 6 + d$ denotes the total number of orbit parameters and $\frac{\partial \mathbf{r}_0}{\partial P_i}(t)$ describes the orbital change due to a change in the parameter P_i. Provided that the orbit parameter corrections $p_i = P_i - P_{0,i}$, e.g., derived from a least-squares adjustment of spacecraft tracking data as discussed in Sect. 2.3.3, and the partial derivatives of the a priori orbit with respect to the orbit parameters are known, Eq. (2.20) allows it to improve the a priori orbit. The trajectory (2.20) should be called the 'linearized' solution of the original (non-linear) orbit determination problem. Alternatively, it is possible to use the dynamic models together with the improved dynamical parameters to propagate the improved initial state vector by numerical integration. Strictly speaking, however, the latter approach is not fully consistent to the improved orbit parameters.

2.3.2 Variational Equations

Knowledge of the partial derivatives of the a priori orbit with respect to the estimated parameters as a function of time is required for orbit improvement. Let us assume that P_i is one of the parameters defining the initial conditions or the dynamics in the equation of motion (2.12), and that the partial derivative of the a priori orbit $\mathbf{r}_0(t)$ with respect to this parameter is designated by the function

$$\mathbf{z}_{P_i}(t) \doteq \frac{\partial \mathbf{r}_0}{\partial P_i}(t) \,. \tag{2.21}$$

The initial value problem associated with the partial derivatives (2.21) is obtained by taking the partial derivative of the equation of motion (2.12). The result is subsequently referred to as the variational equation of parameter P_i, which is obtained by adopting the 'chain rule' and reads as

$$\ddot{\mathbf{z}}_{P_i} = \mathbf{A}_0 \cdot \mathbf{z}_{P_i} + \mathbf{A}_1 \cdot \dot{\mathbf{z}}_{P_i} + \frac{\partial \mathbf{f}_p}{\partial P_i} , \tag{2.22}$$

with the 3×3 (Jacobian) matrices defined by

$$A_{0[i;k]} \doteq \frac{\partial f_i}{\partial r_{0,k}} \quad \text{and} \quad A_{1[i;k]} \doteq \frac{\partial f_i}{\partial \dot{r}_{0,k}} , \tag{2.23}$$

where f_i denotes the component i of the total acceleration $\mathbf{f}$ from (2.12) and $r_{0,k}$ denotes the component k of the geocentric position from (2.12).

For $P_i \in \{a, e, i, \Omega, \omega, u_0\}$ the variational equations (2.22) are a linear, homogeneous differential equation system of second order in time with initial values $\mathbf{z}_{P_i}(t_0) \neq \mathbf{0}$ and $\dot{\mathbf{z}}_{P_i}(t_0) \neq \mathbf{0}$. For $P_i \in \{Q_1, ..., Q_d\}$ (2.22) are inhomogeneous, but have zero initial values because the initial satellite state does not depend on the force model parameters. It is important that the homogeneous part of (2.22) is the same for dynamical parameters and for parameters defining the initial conditions, which allows for an efficient solution process.

2.3.2.1 General Solution

Let us assume that the functions $\mathbf{z}_{O_j}(t)$, $j = 1, ..., 6$ are the partial derivatives of the a priori orbit $\mathbf{r}_0(t)$ with respect to the six parameters O_j, $j = 1, ..., 6$ defining the initial conditions at time t_0. The ensemble of these six functions forms one complete system of solutions of the homogeneous part of the variational equation (2.22), which allows us to obtain the solution of the inhomogeneous system by the method of 'variation of constants'. The solution and its first time derivative may thus be written as a function of the homogeneous solutions $\mathbf{z}_{O_j}(t)$ as

$$\mathbf{z}_{P_i}^{(k)}(t) = \sum_{j=1}^{6} \alpha_{O_j P_i}(t) \cdot \mathbf{z}_{O_j}^{(k)}(t) ; \quad k = 0, 1 , \tag{2.24}$$

with the coefficient functions defined by

$$\boldsymbol{\alpha}_{P_i}(t) \doteq \int_{t_0}^{t} \mathbf{Z}^{-1}(t') \cdot \mathbf{h}_{P_i}(t') \cdot dt' , \tag{2.25}$$

where $\boldsymbol{\alpha}_{P_i}$ denotes the column array $(\alpha_{O_1 P_i}, ..., \alpha_{O_6 P_i})^T$, $\mathbf{Z}$ denotes the 6×6 matrix defined by $\mathbf{Z}_{[1,...,3;j]} \doteq \mathbf{z}_{O_j}$, $\mathbf{Z}_{[4,...,6;j]} \doteq \dot{\mathbf{z}}_{O_j}$, and $\mathbf{h}_{P_i}$ denotes the column array $(\mathbf{0}^T, \partial \mathbf{f}_p^T / \partial P_i)^T$.

The solution $\mathbf{z}_{P_i}(t)$ of the variational equation (2.22) and its first time derivative may be expressed with the same functions $\alpha_{O_j P_i}(t)$ as a linear combination with the homogeneous solutions $\mathbf{z}_{O_j}(t)$ and $\dot{\mathbf{z}}_{O_j}(t)$, respectively. Due to this representation, only the six initial value problems associated with the initial conditions have to be

actually treated as differential equation systems. All variational equations related to dynamical orbit parameters, however, may be reduced to definite integrals, which can be efficiently solved numerically, e.g., with a Gaussian quadrature technique [7].

2.3.2.2 Piecewise Constant Accelerations

Let us now develop the mathematical background for estimating m constant accelerations A_i in the predetermined direction $\mathbf{e}(t)$ for $t_{i-1} \le t < t_i, i = 1, ..., m$. The contribution of this parameter $P_i = A_i$ to $\mathbf{f}_p$ in (2.14) is of the form $A_i \cdot \mathbf{e}(t)$ for $t_{i-1} \le t < t_i$. The corresponding variational equation reads as

$$\ddot{\mathbf{z}}_{A_i} = \mathbf{A}_0 \cdot \mathbf{z}_{A_i} + \mathbf{A}_1 \cdot \dot{\mathbf{z}}_{A_i} + \begin{cases} \mathbf{e}(t) \; ; \; t_{i-1} \le t < t_i \\ \mathbf{0} \quad ; \quad \text{otherwise} \end{cases} . \tag{2.26}$$

The variational equation (2.26) may be easily solved thanks to the general mathematical properties of variational equations as developed in Sect. 2.3.2.1. Equation (2.25) reads for the special case of a piecewise constant acceleration as

$$\boldsymbol{\alpha}_{A_i}(t) \doteq \int_{t_0}^{t} \mathbf{Z}^{-1}(t') \cdot \mathbf{h}_{A_i}(t') \cdot dt' = \int_{t_{i-1}}^{t^*} \mathbf{Z}^{-1}(t') \cdot \mathbf{h}_{A_i}(t') \cdot dt' \, , \tag{2.27}$$

where the upper integration limit is given by

$$t^* \doteq \begin{cases} t_{i-1} \; ; \; t < t_{i-1} \\ t \quad\;\; ; \; t_{i-1} \le t < t_i \\ t_i \quad\;\; ; \; t \ge t_i \end{cases} . \tag{2.28}$$

The solution $\mathbf{z}_{A_i}(t)$ and its first time derivative for the parameter A_i follow from (2.24), and may be written as

$$\mathbf{z}^{(k)}_{A_i}(t) = \begin{cases} \mathbf{0} & ; \; t < t_{i-1} \\ \sum_{j=1}^{6} \alpha_{O_j A_i}(t) \cdot \mathbf{z}^{(k)}_{O_j}(t) & ; \; t_{i-1} \le t < t_i \\ \sum_{j=1}^{6} \alpha_{O_j A_i}(t_i) \cdot \mathbf{z}^{(k)}_{O_j}(t) & ; \; t \ge t_i \end{cases} . \tag{2.29}$$

Note that $\mathbf{z}_{A_i}(t)$ is a once (continuously) differentiable function of time for the entire arc. The non-zero coefficients $\alpha_{O_j A_i}(t)$ are constant in time for the case $t \ge t_i$. This implies that a change in the parameter A_i does not only affect the orbit in the interval $[t_{i-1}, t_i)$ where it is active, but it affects all positions (and velocities) for $t \ge t_{i-1}$ as well. For a detailed discussion of an efficient solution strategy, the reader is referred to [64].

2.3.2.3 Pulses

Let us briefly mention the special case of instantaneous velocity changes V_i at times t_i in predetermined directions $\mathbf{e}(t_i)$, and outline how it fits into the formalism presented so far. The contribution of this parameter $P_i = V_i$ to $\mathbf{f}_p$ in (2.14) may formally be written as $V_i \cdot \delta(t - t_i) \cdot \mathbf{e}(t)$, where $\delta(t)$ represents Dirac's delta function. The corresponding variational equation reads as

$$\ddot{\mathbf{z}}_{V_i} = \mathbf{A}_0 \cdot \mathbf{z}_{V_i} + \mathbf{A}_1 \cdot \dot{\mathbf{z}}_{V_i} + \delta(t - t_i) \cdot \mathbf{e}(t) \; . \tag{2.30}$$

Using the notation from Sect. 2.3.2.1, but identifying $\mathbf{h}_{V_i}$ with $\mathbf{h}_{A_i}$ in (2.27), the definite integral (2.27) may be simplified for $t \geq t_i$ as

$$\boldsymbol{\alpha}_{V_i}(t) \doteq \int_{t_0}^{t} \delta(t' - t_i) \cdot \mathbf{Z}^{-1}(t') \cdot \mathbf{h}_{V_i}(t') \cdot dt' = \mathbf{Z}^{-1}(t_i) \cdot \mathbf{h}_{V_i}(t_i) \doteq \boldsymbol{\beta}_{V_i} \; . \tag{2.31}$$

Obviously, $\alpha_{O_j V_i}(t)$ is zero for $t < t_i$ and non-zero but constant for $t \geq t_i$. Therefore, the partial derivatives $\mathbf{z}_{V_i}(t)$ may be written as a linear combination of only the six partial derivatives $\mathbf{z}_{O_j}(t)$ of the a priori orbit w.r.t. the parameters defining the initial conditions at time t_0. The parametrization yields a continuous position vector $\mathbf{r}(t)$ but, as opposed to the parametrization from Sect. 2.3.2.2, a discontinuous velocity vector $\dot{\mathbf{r}}(t)$ of the improved orbit at the pulse epoch t_i. This parametrization may be viewed as a special case of the short-arc representation (see Sect. 2.3.2.5) of the entire arc, where the individual short-arcs are forced to be continuous at the arc boundaries.

2.3.2.4 Comparison Between Different Empirical Parametrizations

Fig. 2.10 shows a zoom of along-track differences between a 6 min pulse-based orbit with respect to an orbit which is based on 6 min piecewise constant accelerations. In

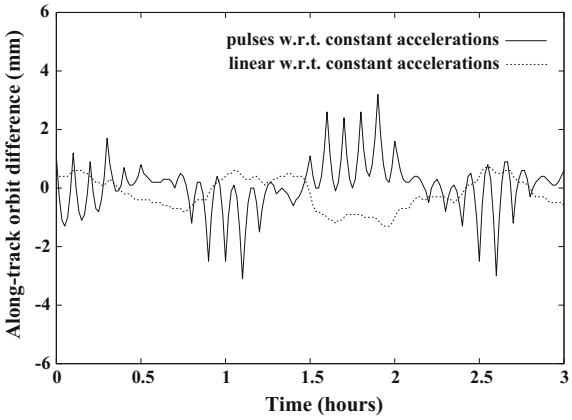

Fig. 2.10 Along-track differences between a CHAMP orbit based on piecewise constant accelerations and orbits based on pulses and piecewise linear accelerations, respectively. Figure from [64]

addition, the differences between an orbit based on 6 min piecewise linear accelerations and the orbit based on 6 min piecewise constant accelerations is shown. The scale of Fig. 2.10 indicates that the differences induced by the different kinds of pseudo-stochastic orbit models are very small, provided that the subinterval length of the underlying parameters are not too long and that the a priori standard deviations are chosen appropriately. Figure 2.10 illustrates that from the point of view of orbit (position) modeling there is no significant gain to be expected when using more refined pseudo-stochastic parameters, e.g., piecewise linear accelerations instead of piecewise constant accelerations. Even the differences between the pulse and the acceleration solution are very small, although the effect of the instantaneous velocity changes can be well observed as sharp peaks at the pulse epochs every 6 min. Figure 2.10 gives one important reason for selecting piecewise constant accelerations as empirical parameters: they avoid obviously 'unphysical' phenomena in the orbits, but are easier to use than more sophisticated parametrizations such as piecewise linear accelerations.

2.3.2.5 Relation to Alternative Parametrizations

The short-arc parametrization represents the solution within each subinterval by a new set of six initial osculating elements, or, alternatively, by two boundary-value positions [97]. The resulting trajectory is thus characterized by a discontinuous velocity vector and a discontinuous position vector as well. It is not only possible to obtain such a trajectory by splitting the original orbital arc into several short-arcs by setting up new initial conditions at the beginning of each short-arc, but in the context of the methods discussed here to solve for one set of initial osculating elements and for instantaneous velocity changes V_i (see Sect. 2.3.2.3) in conjunction with instantaneous position changes X_i at times t_i in predetermined directions $\mathbf{e}(t_i)$. Using the notation from Sect. 2.3.2.2, but identifying $\mathbf{h}_{X_i}$ with $(\mathbf{e}^T(t_i),\ \mathbf{0}^T)$, the coefficients of the partial derivatives $\mathbf{z}_{X_i}(t)$ may be obtained in close analogy to Sect. 2.3.2.3 by

$$\boldsymbol{\alpha}_{X_i}(t) \doteq \int_{t_0}^{t} \delta(t' - t_i) \cdot \mathbf{Z}^{-1}(t') \cdot \mathbf{h}_{X_i}(t') \cdot dt' = \mathbf{Z}^{-1}(t_i) \cdot \mathbf{h}_{X_i}(t_i) \doteq \boldsymbol{\beta}_{X_i} \qquad (2.32)$$

for $t \geq t_i$.

For the sake of completeness and clarity, the two linear systems of algebraic equations to be solved for the coefficients $\alpha_{O_jX_i}(t_i)$ and $\alpha_{O_jV_i}(t_i)$ of the partial derivatives $\mathbf{z}_{X_i}(t)$ and $\mathbf{z}_{V_i}(t)$, respectively, may be explicitly written as

$$\begin{aligned}
\sum_{j=1}^{6} \beta_{O_j X_i} \cdot \mathbf{z}_{O_j}(t_i) &= \mathbf{e}(t_i) \\
\sum_{j=1}^{6} \beta_{O_j X_i} \cdot \dot{\mathbf{z}}_{O_j}(t_i) &= \mathbf{0} \\
&\quad , \\
\sum_{j=1}^{6} \beta_{O_j V_i} \cdot \mathbf{z}_{O_j}(t_i) &= \mathbf{0} \\
\sum_{j=1}^{6} \beta_{O_j V_i} \cdot \dot{\mathbf{z}}_{O_j}(t_i) &= \mathbf{e}(t_i)
\end{aligned} \tag{2.33}$$

which shows that the parameter X_i is 'allowed' to change only the orbital position at time t_i in direction $\mathbf{e}(t_i)$, but not the orbital velocity at time t_i. The opposite statement is valid for the parameter V_i.

The advantage of this alternative formulation is that the original arclength remains formally unchanged, i.e., it is easily possible to solve for deterministic orbit parameters still referring to the original arclength. This might matter if the deterministic orbit parameters are identified with geopotential coefficients. Instead of saving many (large) normal equation systems referring to the short arclength, a reduced number of normal equation systems may be generated, e.g., on a daily basis. For a discussion of further generalizations, e.g., to piecewise once-per-revolution periodic accelerations as they are also widely used for orbit determination, e.g., in the context of the lunar gravity mission GRAIL [92], we refer to [64].

2.3.3 Parameter Estimation

Classical least-squares adjustment (batch least-squares adjustment) is the mathematical method used in this chapter to outline precise orbit determination using precise satellite tracking data. A short overview of the most important formulas is therefore provided in the following subsection. We refer to Chap. 1 for a detailed introduction to parameter estimation techniques. For a discussion of other parameter estimation algorithms in the context of orbit determination, e.g., sequential estimators, we refer to, e.g., [141].

2.3.3.1 Recapitulation of Least-Squares Adjustment

Let us assume that each observation may be expressed as a function of the parameters of a given mathematical model. Based on the model function $\mathbf{F}$, we may write the system of observation equations in the presence of observation errors as

$$\mathbf{L}' + \boldsymbol{\varepsilon} = \mathbf{F}(\mathbf{X}) \; . \tag{2.34}$$

If $\mathbf{F}$ is a non-linear function of the parameters, it is linearized by

$$\mathbf{L}' + \boldsymbol{\varepsilon} = \mathbf{F}(\mathbf{X}_0) + \mathbf{A}\,\mathbf{x}\,, \tag{2.35}$$

with the column arrays $\mathbf{L}'$ of the actual observations, $\boldsymbol{\varepsilon}$ of the observation corrections (or residuals). $\bar{\mathbf{L}} = \mathbf{L}' + \boldsymbol{\varepsilon}$ is the array of the adjusted observations, $\mathbf{X} = \mathbf{X}_0 + \mathbf{x}$ the array of the adjusted model parameters, $\mathbf{X}_0$ the array of the approximate (or a priori) model parameters, $\mathbf{x}$ the array of the model parameter corrections w.r.t. $\mathbf{X}_0$ (solution vector), and $\mathbf{A}$, which denotes the first design (or Jacobian) matrix. The first design matrix is defined by

$$\mathbf{A} \doteq \left.\frac{\partial \mathbf{F}(\mathbf{X})}{\partial \mathbf{X}}\right|_{\mathbf{X}=\mathbf{X}_0} \tag{2.36}$$

Rearranging the linearized observation equations yields

$$\boldsymbol{\varepsilon} = \mathbf{A}\,\mathbf{x} - \left(\mathbf{L}' - \mathbf{F}(\mathbf{X}_0)\right) = \mathbf{A}\,\mathbf{x} - \mathbf{l}\,, \tag{2.37}$$

where the term $\mathbf{l} \doteq \mathbf{L}' - \mathbf{F}(\mathbf{X}_0)$ is often referred to as 'observed-minus-computed' (O–C).

The observation errors are characterized by a stochastic model, which in turn is described by the weight matrix of the observations

$$\mathbf{P} = {\mathbf{Q}_{\mathbf{ll}}}^{-1} = \sigma_0^2\ {\mathbf{C}_{\mathbf{ll}}}^{-1}\,, \tag{2.38}$$

where $\mathbf{Q}_{\mathbf{ll}}$ is the cofactor matrix of the observations, σ_0 is the a priori standard deviation of unit weight, and $\mathbf{C}_{\mathbf{ll}}$ is the covariance matrix of the observations. Note that the weight matrix $\mathbf{P}$ is diagonal, if the observations are uncorrelated. In this case, the diagonal elements are given by $P_{ll} = \sigma_0^2/\sigma_l^2$, where σ_l^2 is the a priori variance of the corresponding observation.

In least-squares adjustment the solution of the observation equations (2.37) is obtained by minimizing the quadratic form $\boldsymbol{\varepsilon}^T\,\mathbf{P}\,\boldsymbol{\varepsilon}$. The underlying variation problem can be solved by Lagrange multipliers, which yield the normal equation system

$$\left(\mathbf{A}^T\,\mathbf{P}\,\mathbf{A}\right)\,\mathbf{x} - \mathbf{A}^T\,\mathbf{P}\,\mathbf{l} = \mathbf{N}\,\mathbf{x} - \mathbf{b} = \mathbf{0}\,, \tag{2.39}$$

where $\mathbf{N} \doteq \mathbf{A}^T\,\mathbf{P}\,\mathbf{A}$ is the normal equation matrix and $\mathbf{b} \doteq \mathbf{A}^T\,\mathbf{P}\,\mathbf{l}$ is the right-hand side of the normal equation system. $\mathbf{N}$ is by definition a quadratic and symmetric matrix. If it is regular, the solution vector follows as

$$\mathbf{x} = \left(\mathbf{A}^T\,\mathbf{P}\,\mathbf{A}\right)^{-1}\,\mathbf{A}^T\,\mathbf{P}\,\mathbf{l} = \mathbf{N}^{-1}\,\mathbf{b}\,, \tag{2.40}$$

where $\mathbf{N}^{-1}$ is the inverse normal equation matrix. The estimated (a posteriori) standard deviation of unit weight is computed as

$$m_0 = \sqrt{\frac{\boldsymbol{\varepsilon}^T \mathbf{P}\, \boldsymbol{\varepsilon}}{f}} \tag{2.41}$$

for $f > 0$, where $f \doteq n - u$ is the degree of freedom of the least-squares adjustment, n is the number of observations, and u is the number of adjusted model parameters. Note that the quadratic form (sum of the weighted residual squares) may be computed either using (2.37), which makes it necessary to evaluate the first design matrix $\mathbf{A}$, or, alternatively, by the more efficient but numerically less stable formula

$$\boldsymbol{\varepsilon}^T \mathbf{P}\, \boldsymbol{\varepsilon} = \mathbf{l}^T \mathbf{P}\, \mathbf{l} - \mathbf{x}^T \mathbf{b} \,. \tag{2.42}$$

The covariance matrix of the adjusted model parameters is given by

$$\mathbf{C_{xx}} = m_0^2\, \mathbf{Q_{xx}} = m_0^2\, \mathbf{N}^{-1} \,, \tag{2.43}$$

where $\mathbf{Q_{xx}}$ is the cofactor matrix of the adjusted model parameters. The (a posteriori) standard deviations of the adjusted model parameters are given by

$$m_x = \sqrt{C_{xx}} = m_0 \sqrt{Q_{xx}} \,, \tag{2.44}$$

where C_{xx} and Q_{xx} are diagonal elements of the covariance and cofactor matrices, respectively.

Parameter Pre-elimination

The parameter pre-elimination technique is useful to handle a large number of model parameters efficiently, e.g., epoch-specific receiver clock offsets in case of GNSS data processing. Let us subdivide the system of normal equations (2.39) into two parts

$$\begin{bmatrix} \mathbf{N}_{11} & \mathbf{N}_{12} \\ \mathbf{N}_{21} & \mathbf{N}_{22} \end{bmatrix} \cdot \begin{bmatrix} \mathbf{x}_1 \\ \mathbf{x}_2 \end{bmatrix} = \begin{bmatrix} \mathbf{b}_1 \\ \mathbf{b}_2 \end{bmatrix} \tag{2.45}$$

and assume that we are not interested in the actual values of the solution sub-vector $\mathbf{x}_2$. In this case, we may reduce the normal equation system (2.45) by pre-eliminating the model parameters $\mathbf{x}_2$, which yields the modified system of normal equations as

$$\mathbf{N}_{11}^* \, \mathbf{x}_1 = \mathbf{b}_1^* \,, \tag{2.46}$$

where $\mathbf{N}_{11}^* = \mathbf{N}_{11} - \mathbf{N}_{12}\, \mathbf{N}_{22}^{-1}\, \mathbf{N}_{21}$ is the normal equation matrix of the model parameters $\mathbf{x}_1$ and $\mathbf{b}_1^* = \mathbf{b}_1 - \mathbf{N}_{12}\, \mathbf{N}_{22}^{-1}\, \mathbf{b}_2$ is the corresponding right-hand side of the normal equation system. The pre-eliminated model parameters $\mathbf{x}_2$ are correctly taken into account in the normal equation system (2.46) although their estimates are (without a dedicated back-substitution process) not available. One must be aware, however, that the parameter pre-elimination step cannot be performed at any arbitrary time;

it can be performed only if additional observations do no longer contribute directly to the elements related to the solution sub-vector $\mathbf{x}_2$ of the normal equation system (2.45).

Parameter Constraining

It is common practice to constrain selected model parameters to their a priori values ('absolute constraints') or to other parameters ('relative constraints'). This may be done to suppress large excursions of weakly determined model parameters from their a priori values or from neighboring parameter values. The technique is often applied to pseudo-stochastic orbit parameters in the context of LEO orbit determination. One must be aware, however, that a priori information is introduced into the system of normal equations through this process, which may or may not be desired for certain applications. Alternatively, parameters may be truly constrained to zero also in an iterative least-squares adjustment, which requires a transformation of the a priori parameter values. For an overview of advanced parameter modifications techniques on the normal equation level, we refer to [21]. Here, we just mention absolute constraining as the simplest and most often applied form of parameter constraining.

Parameter constraints may be introduced by artificial observations with a user-specified variance σ^2_{abs}. These observations have to be appended to the system of observation equations (2.35). If the change with respect to the a priori value is used as the actual parameter in the artificial observation equation, the weight

$$W = \frac{\sigma_0^2}{\sigma^2_{abs}} \tag{2.47}$$

has to be only added to the corresponding diagonal element of the normal equation matrix $\boldsymbol{N}$, because the value O–C is zero in this special case. Observe that the degree of freedom has to be incremented by 1, as well.

2.3.3.2 Partial Derivatives W.r.t. Orbit Parameters

In order to compute the partial derivatives (2.36) related to the r-th observation and the orbit parameter P_i it is advantageous to express the elements of the first design matrix (2.36) with the functions $\mathbf{z}_{P_i}$ defined by (2.21)

$$\frac{\partial F_r(\mathbf{X})}{\partial P_i} = (\nabla F_r(\mathbf{X}))^T \cdot \mathbf{z}_{P_i} \,, \tag{2.48}$$

where F_r denotes the r-th component of the model function $\mathbf{F}$. Its gradient is given by

$$(\nabla F_r(\mathbf{X}))^T = \left(\frac{\partial F_r(\mathbf{X})}{\partial r_{0,1}} \;\; \frac{\partial F_r(\mathbf{X})}{\partial r_{0,2}} \;\; \frac{\partial F_r(\mathbf{X})}{\partial r_{0,3}} \right) . \tag{2.49}$$

Slightly more complicated relations (2.48) result if the observations depend not only on the geocentric position vector, but also on the velocity vector, or if they refer to more than one epoch. Equation (2.48) shows that only the gradient depends on the type of the observations. The functions $\mathbf{z}_{P_i}$, however, are independent of the observation type, which nicely separates the observation-specific (geometric) part from the dynamic part.

2.3.3.3 Structure of Normal Equations Related to Orbit Parameters

The structure of the orbit-related parts in the normal equation system may be exploited for setting-up an efficient solution strategy and to highlight the close relation of pseudo-stochastic orbit modeling techniques with filter strategies. Subsequently we derive the structure of a simplified orbit determination problem with initial conditions and pulses as the only parameters. More complicated scenarios are detailed in [64].

The observation equation (2.37) of observation number r of this orbit determination problem reads as

$$\varepsilon_r = \sum_{k=1}^{6} \frac{\partial F_r}{\partial O_k} \cdot o_k + \sum_{m=1}^{i} \sum_{j=1}^{3} \frac{\partial F_r}{\partial V_{m,j}} \cdot v_{m,j} - l_r \ , \tag{2.50}$$

where o_k, $k = 1, ..., 6$ and $v_{i,j}$, $j = 1, ..., 3$ denote the corrections to the six initial conditions and the three pulses at each epoch t_i, $i = 1, ..., n-1$, respectively; it is assumed that the observation time t_l is part of the subinterval $[t_i, t_{i+1})$. The relations (2.48) and (2.24) with the constant coefficients $\beta_{O_k V_{m,j}}$ for pulses yield

$$\frac{\partial F_r}{\partial V_{m,j}} = (\nabla F_r)^T \cdot \mathbf{z}_{V_{m,j}} = (\nabla F_r)^T \cdot \sum_{k=1}^{6} \beta_{O_k V_{m,j}} \cdot \mathbf{z}_{O_k}(t) \ , \tag{2.51}$$

which is why the observation equation (2.50) can be rearranged as follows:

$$\varepsilon_r = \sum_{k=1}^{6} (\nabla F_r)^T \cdot \mathbf{z}_{O_k} \cdot \left(o_k + \sum_{m=1}^{i} \sum_{j=1}^{3} \beta_{O_k V_{m,j}} \cdot v_{m,j} \right) - l_r \ . \tag{2.52}$$

The term in parentheses has an important meaning. It does not represent the 'initially' solved for correction to the osculating element O_k at t_0, which would fully characterize the solution of this particular orbit determination problem in the subinterval $[t_0, t_1)$. Because a change in the initial osculating element O_k induced by a change in the pulse $V_{i,j}$ can be computed as

$$\Delta O_k = \frac{\partial O_k}{\partial V_{i,j}} \cdot \Delta V_{i,j} = \beta_{O_k V_{i,j}} \cdot \Delta V_{i,j} \ , \tag{2.53}$$

the term in in Eq. (2.52) represents the correction $o_{i,k}$ to a different initial osculating element $O_{i,k}$ at t_0 which fully characterizes the solution in the subinterval $[t_i, t_{i+1})$ after the occurrence of the first $3\,i$ pulses. Equation (2.52) illustrates that orbit determination based on pulses may also be understood as a special case of the short-arc parametrization from Sect. 2.3.2.5 when asking for continuity at the short-arc boundaries. The properties of the newly defined osculating elements $O_{i,k}$ at t_0 will be exploited in Sect. 2.3.3.4. As the pulse epochs divide the orbital arc into n subintervals, it is advisable to write all n_{o_i} observation equations of the subinterval $I_i = [t_i, t_{i+1})$ in a matrix notation

$$\boldsymbol{\varepsilon}_i = \mathbf{A}_i\,\mathbf{o} + \mathbf{A}_i \sum_{m=1}^{i} \mathbf{B}_m\,\mathbf{v}_m - \mathbf{l}_i\ , \tag{2.54}$$

with the column arrays $\boldsymbol{\varepsilon}_i$ of the residuals of subinterval I_i, $\mathbf{l}_i$ of the terms O–C of subinterval I_i, $\mathbf{o}$ of the corrections to the initial osculating elements, and $\mathbf{v}_i$ of the pulse corrections at epoch t_i. The matrix $\mathbf{A}_i$ denotes the $n_{o_i} \times 6$ first design matrix of the subinterval I_i related to the six initial osculating elements and $\mathbf{B}_m$ denotes the 6×3 coefficient matrix defined by $B_{m[k;j]} \doteq \beta_{O_k V_{m,j}}$.

Taking the observation equations of all subintervals I_i, $i = 0, ..., n-1$ into account, the complete system of normal equations (2.39) reads in the above matrix notation as

$$\begin{bmatrix} \mathbf{N} & \sum\limits_{i=1}^{n-1} \mathbf{N}_i\,\mathbf{B}_1 & \cdots & \sum\limits_{i=n-1}^{n-1} \mathbf{N}_i\,\mathbf{B}_{n-1} \\ . & \mathbf{B}_1^T \sum\limits_{i=1}^{n-1} \mathbf{N}_i\,\mathbf{B}_1 & \cdots & \mathbf{B}_1^T \sum\limits_{i=n-1}^{n-1} \mathbf{N}_i\,\mathbf{B}_{n-1} \\ . & . & \ddots & \vdots \\ . & . & . & \mathbf{B}_{n-1}^T \sum\limits_{i=n-1}^{n-1} \mathbf{N}_i\,\mathbf{B}_{n-1} \end{bmatrix} \cdot \begin{bmatrix} \mathbf{o} \\ \mathbf{v}_1 \\ \vdots \\ \mathbf{v}_{n-1} \end{bmatrix} = \begin{bmatrix} \mathbf{A}^T\,\mathbf{P}\,\mathbf{l} \\ \mathbf{B}_1^T \sum\limits_{i=1}^{n-1} \mathbf{A}_i^T\,\mathbf{P}_i\,\mathbf{l}_i \\ \vdots \\ \mathbf{B}_{n-1}^T \sum\limits_{i=n-1}^{n-1} \mathbf{A}_i^T\,\mathbf{P}_i\,\mathbf{l}_i \end{bmatrix}, \tag{2.55}$$

where $\mathbf{N}_i \doteq \mathbf{A}_i^T\,\mathbf{P}_i\,\mathbf{A}_i$ is the part associated with the observation interval I_i of the normal equation matrix related to the six initial osculating elements. In analogy, $\mathbf{A}_i^T\,\mathbf{P}_i\,\mathbf{l}_i$ is the contribution of the same subinterval to the right-hand side of the normal equation system related to the six initial osculating elements. The abbreviations

$$\mathbf{N} = \sum_{i=0}^{n-1} \mathbf{A}_i^T\,\mathbf{P}_i\,\mathbf{A}_i \qquad \text{and} \qquad \mathbf{A}^T\,\mathbf{P}\,\mathbf{l} = \sum_{i=0}^{n-1} \mathbf{A}_i^T\,\mathbf{P}_i\,\mathbf{l}_i \tag{2.56}$$

are the normal equation matrix and the right-hand side of the normal equation system of the deterministic problem without any pulses, respectively. Obviously, the contributions $\mathbf{N}_i$ and $\mathbf{A}_i^T\,\mathbf{P}_i\,\mathbf{l}_i$, $i = 0, ..., n-1$ do not only form the complete system of normal equations for dynamic POD according to Eq. (2.56), they are together with

the matrices $\mathbf{B}_i$ also the building blocks of the complete system of normal equations (2.55) for reduced-dynamic POD based on pulses.

Equation (2.55) shows that the normal equation matrix has a simple structure. Unfortunately, it is not possible to apply the parameter pre-elimination technique (see Sect. 2.3.3.1) to any of the pseudo-stochastic parameters before the very last observation is incorporated into the system of normal equations. This can be seen from the upper summation limits in (2.55), which all include all subintervals up to the very last one. An efficient solution strategy, which is closely related to filter algorithms, may, however, be found and will be outlined in the next section.

2.3.3.4 Relation to Filter Solutions

Equation (2.52) implicitly introduced the transformation

$$\mathbf{o}_i \doteq \mathbf{o} + \sum_{m=1}^{i} \mathbf{B}_m \, \mathbf{v}_m \tag{2.57}$$

between the 'initially' solved for corrections $\mathbf{o}$ to the a priori values of the initial osculating elements $\mathbf{O}$ at t_0 (subsequently denoted as $\mathbf{o}_0$) and the corrections $\mathbf{o}_i$ to the a priori values of the initial osculating elements $\mathbf{O}_i$ at t_0 which define the solution in the subinterval $[t_i, t_{i+1})$. For the following deliberations, it is convenient to define the transformation (2.57) recursively, and in reverse order as

$$\begin{aligned} \mathbf{o}_0 \quad &\doteq \mathbf{o} && ; \, i = 0 \\ \mathbf{o}_{i-1} &\doteq \mathbf{o}_i - \mathbf{B}_i \, \mathbf{v}_i = (\mathbf{I}_6 \;\; -\mathbf{B}_i) \cdot \begin{bmatrix} \mathbf{o}_i \\ \mathbf{v}_i \end{bmatrix} && ; \, i \geq 1 \end{aligned} \;, \tag{2.58}$$

where $\mathbf{I}_6$ denotes the identity matrix of dimension 6.

First, we consider the system of normal equations in the presence of initial conditions and pulses in its initial stages during the collection of the GPS observations. Let us assume that we already have incorporated all observations for times $t_l \leq t_i$ and that the system may be written in a reduced form as

$$\overline{\mathbf{N}}_{i-1} \, \mathbf{o}_{i-1} = \overline{\mathbf{b}}_{i-1} \; . \tag{2.59}$$

The normal equation matrix $\overline{\mathbf{N}}_{i-1}$ and the right-hand side $\overline{\mathbf{b}}_{i-1}$ of the normal equation system (2.59) may be computed from the contributions to the normal equation system of the deterministic problem for the observation times $t_l \leq t_i$, i.e., from $\mathbf{N}_l$ and $\mathbf{b}_l$, $l = 0, ..., i-1$, as

$$\begin{aligned} \overline{\mathbf{N}}_0 &\doteq \mathbf{N}_0 \\ \overline{\mathbf{b}}_0 &\doteq \mathbf{b}_0 \end{aligned} \quad ; \; i = 1$$

$$\begin{aligned} \overline{\mathbf{N}}_{i-1} &\doteq \overline{\mathbf{N}}^*_{i-2} + \mathbf{N}_{i-1} \\ \overline{\mathbf{b}}_{i-1} &\doteq \overline{\mathbf{b}}^*_{i-2} + \mathbf{b}_{i-1} \end{aligned} \quad ; \; i \geq 2 \tag{2.60}$$

with $\overline{\mathbf{N}}^*_{i-2}$ and $\overline{\mathbf{b}}^*_{i-2}$ to be defined later by (2.63).

The normal equation system (2.59) may be expanded into a system in the unknowns $\mathbf{o}_i$ and $\mathbf{v}_i$ by replacing $\mathbf{o}_{i-1}$ on the left-hand side with the transformation (2.58), and by multiplying both sides of the normal equation system (2.59) from the left with the matrix $(\mathbf{I}_6 \;\; -\mathbf{B}_i)^T$:

$$\begin{bmatrix} \overline{\mathbf{N}}_{i-1} & -\overline{\mathbf{N}}_{i-1}\,\mathbf{B}_i \\ -\mathbf{B}_i^T\,\overline{\mathbf{N}}_{i-1} & \mathbf{B}_i^T\,\overline{\mathbf{N}}_{i-1}\,\mathbf{B}_i \end{bmatrix} \cdot \begin{bmatrix} \mathbf{o}_i \\ \mathbf{v}_i \end{bmatrix} = \begin{bmatrix} \overline{\mathbf{b}}_{i-1} \\ -\mathbf{B}_i^T\,\overline{\mathbf{b}}_{i-1} \end{bmatrix} . \tag{2.61}$$

The system (2.61) is the key to a most efficient solution of the orbit determination problem. According to the observation equation (2.52), the observations contained in the subintervals I_i, I_{i+1}, ..., I_{n-1} do not depend on the terms $\mathbf{v}_i$ explicitly as their influence is already taken into account by the osculating elements $\mathbf{o}_i$. It is thus possible to apply the parameter pre-elimination technique (see Sect. 2.3.3.1) to the pseudo-stochastic parameters. The normal equation system reads after the pre-elimination as

$$\overline{\mathbf{N}}^*_{i-1}\,\mathbf{o}_i = \overline{\mathbf{b}}^*_{i-1} \tag{2.62}$$

with

$$\begin{aligned} \overline{\mathbf{N}}^*_{i-1} &\doteq \overline{\mathbf{N}}_{i-1} - \overline{\mathbf{N}}_{i-1}\,\mathbf{B}_i \left(\mathbf{B}_i^T\,\overline{\mathbf{N}}_{i-1}\,\mathbf{B}_i\right)^{-1} \mathbf{B}_i^T\,\overline{\mathbf{N}}_{i-1} \\ \overline{\mathbf{b}}^*_{i-1} &\doteq \overline{\mathbf{b}}_{i-1} - \overline{\mathbf{N}}_{i-1}\,\mathbf{B}_i \left(\mathbf{B}_i^T\,\overline{\mathbf{N}}_{i-1}\,\mathbf{B}_i\right)^{-1} \mathbf{B}_i^T\,\overline{\mathbf{b}}_{i-1} \end{aligned} . \tag{2.63}$$

A priori weights of the pseudo-stochastic parameters (see Sect. 2.3.3.1), e.g., in the form of absolute constraints given by an identical weight matrix

$$\mathbf{W} = \sigma_0^2\;{\mathbf{C}_{\mathbf{vv}}}^{-1} \tag{2.64}$$

for all pulse epochs, have to be added prior to the pre-elimination to the sub-matrix $\mathbf{B}_i^T\,\overline{\mathbf{N}}_{i-1}\,\mathbf{B}_i$ of the normal equation matrix in (2.61).

The procedure outlined by the Eqs. (2.59), (2.61), (2.62), and (2.60) has to be repeated until the very last observation of the subinterval I_{n-1} is incorporated into the reduced normal equation system. After completion of data collection, we may solve for the initial osculating element corrections $\mathbf{o}_{n-1}$ of the last subinterval I_{n-1} by

$$\mathbf{o}_{n-1} = \overline{\mathbf{N}}^{-1}_{n-1}\,\overline{\mathbf{b}}_{n-1} = \mathbf{Q}_{o_{n-1}o_{n-1}}\,\overline{\mathbf{b}}_{n-1} \;, \tag{2.65}$$

where $\mathbf{Q}_{o_{n-1}o_{n-1}}$ is the cofactor matrix of the solved for corrections $\mathbf{o}_{n-1}$. Details of the algorithm, including the back-substitution process, are available in [64].

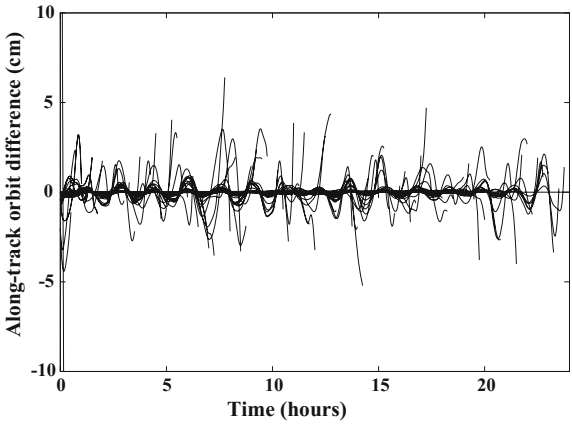

Fig. 2.11 Along-track orbit differences between filter and least-squares reduced-dynamic solutions for CHAMP. Figure from [64]

The solution (2.65) shows that in principle there is no need to compute the 'intermediary' corrections $\mathbf{o}_{i-1}$, $i = 1, ..., n-1$ during data collection. They would actually represent the filter solutions based on all observations of the interval $[t_0, t_i)$ and could be easily made available. It must be mentioned, however, that our definition of a 'filter' solution differs slightly from the usual terminology in the literature: it represents the least-squares solution of the considered orbit determination problem based on all observations from the very first epoch to the actually processed epoch. This implies that the orbit trajectory is still represented by pseudo-stochastic parameters, e.g., set up every n-th minute. A new filter solution is thus provided only every n-th minute as well, and not after each newly incorporated observation epoch. Only in the special case of pseudo-stochastic parameters set up at the observation sampling rate, the above algorithm will provide the same solutions as 'classical' filter solutions, where stochastic parameters are set up at every measurement epoch and the confidence in the dynamical modeling is controlled by process noise [105].

Figure 2.11 shows the along-track orbit differences between the least-squares solution for an orbit determination based on piecewise constant accelerations estimated over 15 min and different filter solutions. The filter trajectories were computed whenever a batch of 15 min of data had been collected, whereas the least-squares solution (last filter solution) was computed after data collection in the back-substitution process. It can be seen that large differences occur for the first 15 min which may be attributed to a weak determination of the orbit parameters from 15 min data only (filter initialization). The consistency between the individual filter solutions and the final least-squares solutions dramatically improves if longer data batches are processed, e.g., sub-millimeter differences at the beginning of the orbital arc are reached for a batch of 8 h. Figure 2.11 also shows, however, that the orbit solution is not very well constrained by the tracking data at the boundaries of the processed time span, which can be seen in this experiment at the right-ends of the individual filter solutions. The orbit consistency may be severely degraded by several centimeters. For this reason longer arcs are often processed than actually needed. When generating the GOCE precise science orbits in the frame of the GOCE High-level processing facility, 30 h

arcs of GPS carrier phase data were analyzed each day for orbit determination to minimize a degraded orbit quality at the boundaries of the central 24 h provided to the user community [16].

2.3.4 Quality of GPS-Based LEO Orbit Determination

A large number of LEO satellites with stringent accuracy requirements on orbit determination were equipped with high-quality dual-frequency GPS receivers in the last two decades. Examples are the altimetry satellites TOPEX/Poseidon, Jason-1 and -2 [44, 91, 101], the gravity missions CHAMP, GRACE, and GOCE [37, 121, 142], the Synthetic Aperture Radar (SAR) satellites TerraSAR-X and TanDEM-X [24, 88], the magnetic field mission Swarm [43], and the currently launched Sentinel satellites serving various purposes of Earth observation. For all these missions high-quality orbit solutions were/are generated by many research teams. Selected results and the associated publications are highlighted in the subsequent sections. For an overview of methodologies for orbit determination based on single-frequency GPS data, we refer to, e.g., [14].

The core products from the IGS [36], such as highly accurate GPS ephemerides, Earth rotation parameters, and GPS satellite clock corrections, are the backbone for precise orbit determination of LEO satellites. Especially GPS satellite clock corrections are indispensable for precise orbit determination when using undifferenced GPS data. Alternatively, double differences may be formed between two spaceborne receivers of formation flying satellites, or between a spaceborne and terrestrial receivers of the IGS ground tracking network to allow for a relative positioning of the LEO satellites [64]. Subsequently, however, we highlight results from GRACE and GOCE orbit determination which are based on undifferenced GPS data and the orbit and clock products from the Center for Orbit Determination in Europe (CODE), one of the global analysis centers of the IGS [28]. In view of the available sampling rates of usually 0.1–1 Hz of the GPS observations from spaceborne receivers, high-rate clock corrections are of crucial importance to avoid the interpolation errors of GPS satellite clock corrections over long intervals and to guarantee the best possible results for orbit determination [15].

2.3.4.1 SLR Validation

For LEO satellites equipped with a laser retro reflector array, independent SLR measurements collected by the tracking network of the International Laser Ranging Service (ILRS, [114]) may be used to compare the observed SLR ranges to the satellites with the computed ranges derived from the GPS-based reduced-dynamic or kinematic ephemerides. This allows for an absolute validation of the line-of-sight directions between the SLR tracking stations and the LEO satellites, i.e., it allows to directly assess the one-dimensional orbit accuracies in these directions. For high

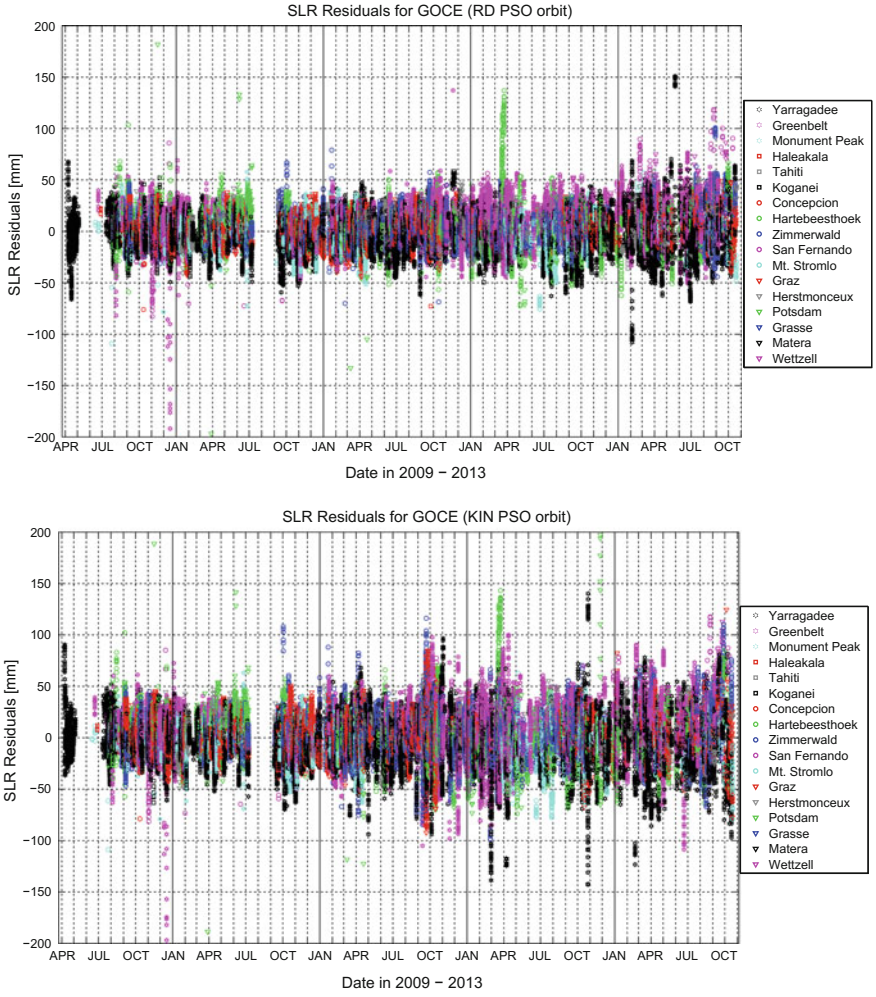

Fig. 2.12 SLR validation of reduced-dynamic (*top*) and kinematic (*bottom*) GOCE precise science orbits. Figure from [18]

elevation passes the line-of-sight direction mainly corresponds to the radial direction of the co-rotating orbital frame. SLR data collected at low elevations, however, may also be used to recover along-track and cross-track orbital errors if the satellites are orbiting the Earth at sufficiently low altitudes. This became obvious for the extremely low orbital altitude of the GOCE satellite, where systematic orbital shifts in the cross-track direction, caused by unmodeled GPS antenna phase center variations, could be directly confirmed by SLR [17, 68]. Recently, systematic cross-track biases were quantified from SLR residuals data as a function of high-fidelity dynamic orbit models used for the TerraSAR-X satellite orbiting the Earth at a higher orbital altitude [48].

Figure 2.12 shows the SLR residuals of the reduced-dynamic and the kinematic orbits of the GOCE precise science orbits over the entire mission [18]. In order not to deteriorate the validation by single outliers, SLR residuals larger than 20 cm are excluded. The overall SLR RMS error of the reduced-dynamic orbits is 1.84 cm and impressively shows the quality of pseudo-stochastic orbit modeling techniques. A slightly worse but still excellent validation is obtained for the kinematic orbits with 2.42 cm. This is expected, because kinematic orbits are more sensitive to GPS data problems. Due to the large number of 12 channels of the GOCE onboard GPS receiver, the quality of the kinematic positions is outstanding. Current LEO satellites such as those from the Swarm mission, which are all equipped with 8-channel receivers, do not allow to generate kinematic orbits of the same quality [72]. Figure 2.12 shows, however, that the accuracy of both types of GOCE orbits is degrading towards the end of the mission. This is unexpected and was found to be related to problems in the GOCE GPS data [18, 71].

2.3.4.2 K-Band Validation

For the GRACE twin satellites which are following each other on the same orbit in a distance of about 200 km, an additional independent validation of the orbit quality may be performed. K-band measurements may be used to compare the orbit-derived distances between the two GRACE satellites with the biased ranges which are directly observed by the ultra-precise K-band ranging system [36]. Figure 2.13 (left) shows the daily K-band range standard deviation obtained from distances computed every 5 s between reduced-dynamic GRACE-A and -B orbit positions derived from zero-difference or double-difference GPS carrier phase data with empirical receiver antenna phase center variations (PCVs) taken into account or not. Figure 2.13 (left)

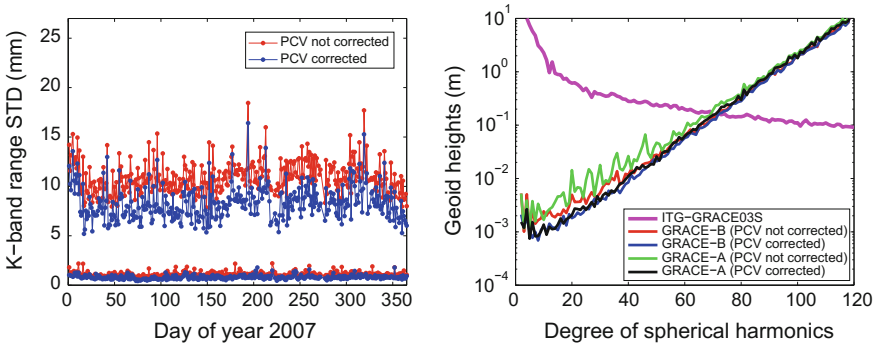

Fig. 2.13 Impact of PCV modeling on daily standard deviations of K-band range residuals for distances between reduced-dynamic GRACE-A and GRACE-B orbits using undifferenced (*left*, *top curves*) or doubly-differenced GPS data with resolved carrier phase ambiguities (*left*, *bottom curves*) and on difference degree amplitudes of gravity field recoveries based on one year of kinematic GRACE orbits (*right*). Figures from [67]

shows that the relative orbit precision of GRACE reduced-dynamic orbit determination is about 1 cm when using zero-difference GPS carrier phase observations and about 1 mm when using double-difference GPS carrier phase observations with ambiguities fixed to their integer values [64]. In both cases the reduction of systematic carrier phase measurement errors, e.g., by empirical modeling of antenna phase center variations, is of crucial relevance to derive trajectories of highest quality [66]. The same statement holds for kinematic orbits, which are particularly sensitive to systematic carrier phase errors. Figure 2.13 (right) shows that unmodeled receiver PCVs may even propagate into gravity field solutions derived from kinematic GRACE positions in the frame of a generalized orbit determination problem (see next section). Further systematic carrier phase errors were identified in the frame of the GOCE and the Swarm missions and suspected to be related to the modeling of higher order ionosphere correction terms [18, 145]. They propagate via orbits into the gravity field estimation, as well [71, 72].

2.3.5 Generalized Orbit Determination

Based on a given a priori orbit $\mathbf{r}_0(t)$ orbit improvement as introduced in Sect. 2.3.1.2 may be generalized by including a variety of different types of other than just arc-specific orbit parameters. Gravity field recovery may in particular be understood and treated as a generalized orbit improvement problem relying on the analysis of a large number of orbital arcs. In analogy to Sect. 2.3.1.2 the actual orbit $\mathbf{r}(t)$ of an involved satellite may be expressed for each orbital arc as a truncated Taylor series with respect to the unknown orbit parameters O_i (arc-specific parameters) and, e.g., the unknown coefficients of the Earth's gravity field Q_i (global parameters) about the a priori orbit, which is represented by the a priori parameter values O_{0i} and Q_{0i}:

$$\mathbf{r}(t) = \mathbf{r}_0(t) + \sum_{i=1}^{n_O} \frac{\partial \mathbf{r}_0(t)}{\partial O_i} \cdot o_i + \sum_{i=1}^{d} \frac{\partial \mathbf{r}_0(t)}{\partial Q_i} \cdot q_i \ , \tag{2.66}$$

where $o_i \doteq O_i - O_{0,i}$ denote the n_O corrections to be estimated for the arc-specific orbit parameters and $q_i \doteq Q_i - Q_{0,i}$ the d corrections to the global coefficients of the Earth's gravity field.

Analogously, gravity field recovery from inter-satellite measurements, e.g., from K-band ranging between the two GRACE satellites, may be understood and treated as a generalized differential orbit improvement process, as well. The actual orbit difference $\mathbf{r}_a(t) - \mathbf{r}_b(t)$ may be expressed as a truncated Taylor series with respect to the unknown parameters about the a priori orbit difference. The distinction needs to be made between n_{aO} parameters O_{ai} and n_{bO} parameters O_{bi}, which are specific to the orbital arcs of GRACE-A and -B, respectively, and d global parameters Q_i, which are common to both GRACE satellites such as the coefficients of the Earth's gravity field. The truncated Taylor series then reads as

$$\begin{aligned}\mathbf{r}_a(t) - \mathbf{r}_b(t) = \quad & \mathbf{r}_{a0}(t) - \mathbf{r}_{b0}(t) \\ & + \sum_{i=1}^{n_{aO}} \frac{\partial \mathbf{r}_{a0}(t)}{\partial O_{ai}} \cdot o_{ai} \\ & - \sum_{i=1}^{n_{bO}} \frac{\partial \mathbf{r}_{b0}(t)}{\partial O_{bi}} \cdot o_{bi} \\ & + \sum_{i=1}^{d} \left(\frac{\partial \mathbf{r}_{a0}(t)}{\partial Q_i} - \frac{\partial \mathbf{r}_{b0}(t)}{\partial Q_i} \right) \cdot q_i \end{aligned} \quad . \tag{2.67}$$

The partial derivatives in Eqs. (2.66) and (2.67) are obtained by solving the corresponding variational equations as outlined in Sect. 2.3.2.1. Note that Eqs. (2.24) and (2.25) from Sect. 2.3.2.1 are valid for any orbit parameters, in particular for gravity field coefficients. The solution of the variational equations corresponding to gravity field parameters is thus reduced to numerical quadrature.

In order to set-up the observation equations, the partial derivatives of the a priori orbits need to be related to the observables, e.g., according to Sect. 2.3.3.2 for GPS data or by projecting the respective terms in Eq. (2.67) to the line-of-sight between GRACE-A and -B in the case of K-Band biased range observations. Special care is needed to not lose numerical precision related to orbit parameters in case of ultra-precise biased range observations and the resulting, very similar partials for the close formation of both satellites. The problem can be substantially mitigated by transforming the original orbital parameters of both satellites to the sum and the differences of the original orbital parameters [11]. In case of GPS data or kinematic positions used as pseudo-observations for a satellite trajectory, the observation equations may be written in matrix notation as

$$\boldsymbol{\varepsilon} = \mathbf{A}_o\, \mathbf{o} + \mathbf{A}_q\, \mathbf{q} - \mathbf{l}\,, \tag{2.68}$$

where $\mathbf{o}$ contains all parameters defining the initial conditions, all satellite- and arc-specific dynamic parameters, and all pseudo-stochastic parameters, $\mathbf{q}$ contains all common dynamic parameters such as the gravity field coefficients, and $\mathbf{A}_o$ and $\mathbf{A}_q$ are the first design matrices corresponding to the parameter arrays $\mathbf{o}$ and $\mathbf{q}$. According to Eq. (2.39) the system of normal equations reads as

$$\begin{bmatrix} \mathbf{N}_{oo} & \mathbf{N}_{oq} \\ \mathbf{N}_{oq}^T & \mathbf{N}_{qq} \end{bmatrix} \cdot \begin{bmatrix} \mathbf{o} \\ \mathbf{q} \end{bmatrix} = \begin{bmatrix} \mathbf{b}_o \\ \mathbf{b}_q \end{bmatrix} \tag{2.69}$$

with $\mathbf{N}_{oo} = \mathbf{A}_o^T\, \mathbf{P}\, \mathbf{A}_o$, $\mathbf{N}_{oq} = \mathbf{A}_o^T\, \mathbf{P}\, \mathbf{A}_q$, $\mathbf{N}_{qq} = \mathbf{A}_q^T\, \mathbf{P}\, \mathbf{A}_q$, and $\mathbf{b}_o = \mathbf{A}_o^T\, \mathbf{P}\, \mathbf{l}$, $\mathbf{b}_q = \mathbf{A}_q^T\, \mathbf{P}\, \mathbf{l}$. Similar NEQs may be also set-up for other observables such as K-Band, where orbital parameters of both satellites have to be included, however, in $\mathbf{o}$. The underlying normal equation matrices are therefore singular when trying to solve them from K-band data alone without the normal equation contributions from GPS. The normal equation contributions stemming from each observable may be superimposed for each orbital arc by adopting measurement-specific weight factors, see

[10, 11]. Furthermore, the arc-specific parameters can be pre-eliminated according to Eq. (2.46), which yields the reduced system

$$(\mathbf{N}_{qq} - \mathbf{N}_{oq}^T \, \mathbf{N}_{oo}^{-1} \, \mathbf{N}_{oq}) \, \mathbf{q} = \mathbf{b}_q - \mathbf{N}_{oq}^T \, (\mathbf{N}_{oo}^{-1} \, \mathbf{b}_o) \tag{2.70}$$

The dimension of the resulting normal equation system is reduced by the number of arc-specific parameters $\mathbf{o}$, while the impact of these parameters is correctly taken into account when solving for the gravity field coefficients. To solve for these coefficients up to the desired resolution, normal equation systems stemming from a large number of arcs have to be accumulated to achieve the needed spatial coverage before the corrections to the a priori parameter values can be obtained by inversion of the accumulated normal equation system according to Eq. (2.40).

2.3.5.1 Gravity Field Determination from Kinematic Positions

Figure 2.14 shows the typical performance of static gravity field recoveries derived from different sets of kinematic positions of LEO satellites used as pseudo-observations to solve a generalized orbit determination problem as outlined above. Shown are square-roots of the degree difference variances of the GPS-only gravity field recoveries with respect to superior gravity field models based on dedicated measurements such as GRACE K-Band and GOCE gradiometer observations [98, 99]. The GPS-only solutions shown in Fig. 2.14 (left) are all based on different amounts of data. Only the solutions based on GOCE and GRACE-B kinematic positions are based on a rather similar time span such that a comparable quality may be expected for the low degree SH coefficients. For the determination of the higher degree coefficients, however, GOCE GPS data is significantly better suited than GRACE GPS data due to the lower orbital altitude, which is reflected by the smallest slope in Fig. 2.14

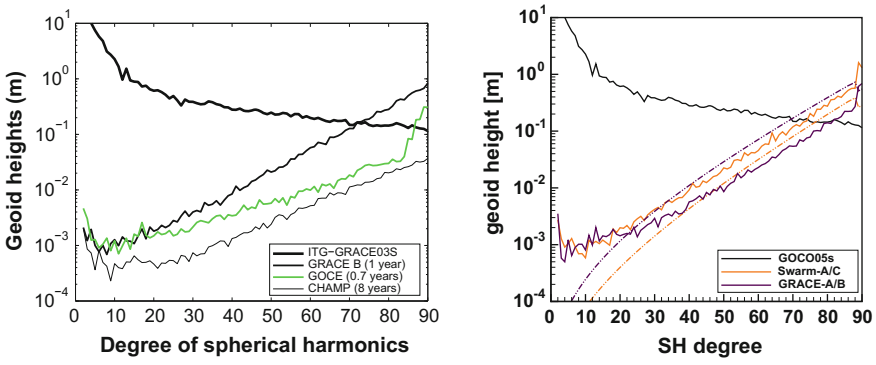

Fig. 2.14 Square-roots of degree difference variances of gravity field recoveries from kinematic positions of GRACE-B, GOCE, and CHAMP (*left*) and GRACE-A, -B and Swarm-A, -C (*right*). Figures from [69, 72]

(left). The CHAMP solution is based on a significantly larger amount of data and therefore superior to the other solutions. Figure 2.14 (right) shows more recent and better comparable recoveries based on one year of GRACE-A and -B and Swarm-A and -C kinematic positions, respectively. Again Swarm is equally well suited to derive the long wavelength part of the Earth's gravity field as it is possible from GRACE GPS data. This is of relevance to bridge a potential gap between the GRACE mission and the GRACE Follow-On mission to continue the monitoring of the (long wavelength part) of the Earth's time-variable gravity field [40]. Encouraging results based on CHAMP, GRACE, GOCE, and Swarm GPS data have been reported by [71, 72, 158, 163]. For degrees above 20 in Fig. 2.14 (right), however, the GRACE solution outperforms the Swarm solution. This is only to a minor extent related to the higher orbital altitude of the Swarm satellites, as indicated by only a slightly larger slope of the Swarm formal errors, but mostly related to a more problematic quality of the Swarm GPS data [72].

2.3.5.2 Separation of Orbit and Gravity Field Determination

For didactic reasons we abandon in this section the processing scheme described in the previous section and fix the arc-specific parameters to previously determined values, while estimating the corrections to the gravity field parameters. This may be done by explicitly solving for the arc-specific parameters using the a priori force model and by consequently deleting them from the NEQ-system, instead of following the implicit and correct solution described by Eq. (2.70). This procedure implies that the sub-system

$$\mathbf{N}_{oo}\,\mathbf{o}' = \mathbf{b}_o \tag{2.71}$$

is solved independently from the remaining parts of Eq. (2.69) and that the parameters $\mathbf{o}'$ are introduced in the following gravity recovery step as known. The remaining normal equation system

$$\mathbf{N}_{qq}\,\mathbf{q}' = \mathbf{b}_q - \mathbf{N}_{oq}^T\,\mathbf{o}' = \mathbf{b}_g - \mathbf{N}_{oq}^T\,(\mathbf{N}_{oo}^{-1}\,\mathbf{b}_o) \tag{2.72}$$

inevitably leads to solutions $\mathbf{q}'$ for the gravity model parameters different from the solutions $\mathbf{q}$ in Eq. (2.70). In the case of a separate solution of orbit and gravity field coefficients the orbit parameters $\mathbf{o}'$ fully depend on the a priori gravity model and the correlations between orbit and gravity field parameters are ignored. As a consequence the estimated gravity field parameters $\mathbf{q}'$ are biased, as well, towards the a priori gravity field. For details concerning the consequences of this approach, we refer to [103], where the impact on gravity field recovery is studied and where it is shown that the conditions $\mathbf{N}_{oq}\,\mathbf{q} = \mathbf{0}$ used to separate orbit and gravity field determination (compare Eqs. (2.70) and (2.72)) are actually equivalent to a special regularization imposed on the gravity field coefficients resulting in recoveries biased towards the a priori gravity field.

2.3.5.3 Relation to the Acceleration Approach

Let us assume that the second derivatives of the position vector have been observed (in practice derived by numerical differentiation from kinematic positions). The observation equations for the accelerations referring to one particular epoch t_r follow from Eq. (2.68) by identifying the observations with kinematic positions and by taking the second time derivative as

$$\varepsilon_r = \sum_{k=1}^{n_0} \frac{\partial \ddot{\mathbf{r}}(t_r)}{\partial O_k} \cdot o_k + \sum_{k=1}^{d} \frac{\partial \ddot{\mathbf{r}}(t_r)}{\partial Q_k} \cdot q_k - \Delta\ddot{\mathbf{r}}_r \ , \tag{2.73}$$

where $\Delta\ddot{\mathbf{r}}_r$ represents the observed minus the computed acceleration. The partial derivatives in the second sum may be replaced by the right-hand sides of the variational equations (2.22) as

$$\frac{\partial \ddot{\mathbf{r}}(t_r)}{\partial Q_k} = \frac{\partial \mathbf{f}(t_r)}{\partial \mathbf{r}(t_r)} \cdot \frac{\partial \mathbf{r}(t_r)}{\partial Q_k} + \frac{\partial \mathbf{f}(t_r)}{\partial \dot{\mathbf{r}}(t_r)} \cdot \frac{\partial \dot{\mathbf{r}}(t_r)}{\partial Q_k} + \frac{\partial \mathbf{f}(t_r)}{\partial Q_k} \ , \tag{2.74}$$

where use was made of Eq. (2.23). The observation equations used in the acceleration approach, e.g., [6], simply read as

$$\varepsilon_r = \sum_{k=1}^{d} \frac{\partial \mathbf{f}(t_r)}{\partial Q_k} \cdot q_k - \Delta\ddot{\mathbf{r}}_r \ . \tag{2.75}$$

From the point of view of orbit determination this implies that the following approximation was made:

$$\sum_{k=1}^{n_0} \frac{\partial \ddot{\mathbf{r}}(t_r)}{\partial O_k} \cdot o_k + \sum_{k=1}^{d} \left(\frac{\partial \mathbf{f}(t_r)}{\partial \mathbf{r}(t_r)} \cdot \frac{\partial \mathbf{r}(t_r)}{\partial Q_k} + \frac{\partial \mathbf{f}(t_r)}{\partial \dot{\mathbf{r}}(t_r)} \cdot \frac{\partial \dot{\mathbf{r}}(t_r)}{\partial Q_k} \right) = \mathbf{0} \ . \tag{2.76}$$

The acceleration method thus assumes that the changes in the second derivatives of the orbit caused by the estimated gravity field parameters q_k are counterbalanced by changes of the second derivatives of the orbit due to the changes in the arc-specific parameters o_k. The assumption is obviously met if the a priori orbit used to compute $\Delta\ddot{\mathbf{r}}_r$ in the acceleration approach equals the estimated a posteriori orbit resulting from classical orbit determination. If this is not the case, the assumption cannot be met precisely. For further discussions and comparisons of the outlined orbit determination strategies with other approaches such as the short-arc approach, the reader is referred to [11].

2.4 Exercises

Data and files needed for the following exercises are available online at:
http://aiuws.unibe.ch/WEHeraeusAS2015/Chapter2-OrbitDetermination.zip

1: Orbit determination using a least-squares solution and a filter solution

In this exercise a true orbit in the two-body problem is used, from which a number of pseudo-observations is created. Your main task is then to perform an orbit determination using a conventional least-squares solution and a filter solution. You will perform the task by completing the MATLAB skeleton file **`ex1.m`**. In this file, incomplete lines are commented out (by the character %) and marked with 'TO BE COMPLETED'. The following MATLAB functions are available and can be used:

- **`[x v] = ephem(GM,ele,tOsc,t)`**: This function takes the gravity constant **`GM`**, a 6-element array **`ele`** containing the six Keplerian orbital elements,
  - **`ele`**(1): semi-major axis, a
  - **`ele`**(2): numerical eccentricity, e
  - **`ele`**(3): inclination, i
  - **`ele`**(4): right ascension of ascending node, Ω
  - **`ele`**(5): argument of perigee, ω
  - **`ele`**(6): argument of latitude at osculating epoch, u_0,

  the osculating epoch **`tOsc`** (set to zero in all exercises), and an arbitrary epoch **`t`**. It returns the vectors **`x`** and **`v`**, which contain the position and the velocity of the satellite (in the geocentric inertial frame) at epoch **`t`**. The formulas of the two-body problem are used for the orbit propagation.
- **`ele = xyzele(GM,x,v,tOsc,t)`**: This function is the inverse of the function **`ephem`**, i.e., it takes **`GM`**, an osculating epoch **`tOsc`** (set to zero in all exercises), an epoch **`t`** and the vectors **`x`** and **`v`**, containing position and velocity of the satellite at epoch **`t`**, and returns the array **`ele`** with the above six orbital elements.
- **`[drdele dvdele] = rvpder(ini,GM,t,tOsc,ele)`**: This function computes the partial derivatives of positions and velocities of a Keplerian orbit w.r.t. the Keplerian elements. It takes **`GM`**, the epoch **`t`** at which the partials shall be computed, the osculating epoch **`tOsc`** (set to zero in all exercises) and the Keplerian elements **`ele`**. The first argument **`ini`** is set to 1 in order to initialize the computation (on first call). The function returns the 3×6 matrices **`drdele`** and **`dvdele`** which contain the partial derivatives.

At the beginning of the MATLAB skeleton file **`ex1.m`** the six Keplerian elements of an orbit of a two-body problem are defined (osculating epoch is 0):

- $a = 6800\,\text{km}$
- $e = 0.05$
- $i = 89°$
- $\Omega = 130°$

- $\omega = 30°$
- $u_0 = 30°$

These elements define the true orbit which shall be determined during this exercise. Using the function **ephem**, every 30 s the position vector of the satellite is computed (for a full day). A normally distributed noise is added to the positions, which are then stored in the matrix **psdObs** (rows: components, columns: epochs). These positions serve as pseudo-observations for the following orbit determination.

(a) For a first crude initial orbit determination, take the first **nObsIni = 10** observations of the day and fit a polynomial of degree **polDeg = 4** through each component separately by using the MATLAB command **polyfit**.[1] Use $t - t_{Avg}$ as time argument of the polynomials, where t_{Avg} is the center of the initial observation period. Use these polynomials to compute the position and velocity vector of the satellite at time t_{Avg}. Use the function **kyzele** to find the corresponding orbital elements from these vectors. What are their values? These elements shall serve as a priori orbital elements for the orbit determination.[2]

(b) Compute and plot the differences of the a priori orbit (obtained from the a priori orbital elements computed in exercise 1a and the true orbit for all epochs of the day in the geocentric (x,y,z) and in the local orbital (radial R, along-track S, cross-track C) frame. In which component is the difference largest? Why?

(c) Perform a conventional least-squares solution of the orbit determination problem, i.e., solve for the six orbital elements. Use the pseudo-observations in **psdObs** with equal weighting and introduce the orbital elements computed in exercise 1a as a priori values. Perform the following steps:

- Loop over all epochs. For each epoch:
  - Compute the satellite position using the function **ephem** and the a priori orbital elements.
  - Compute the 'observed minus computed' term.
  - Compute the first design matrix using the function **rvpder**.
  - Accumulate the normal equation system.
- Solve the normal equation system[3] and compute the a posteriori standard deviation of unit weight.
- Update the orbital elements.
  What are the values of the updated orbital elements?

---

[1] Usage: **p = polyfit(x,y,n)**, where **p** are the coefficients of a polynomial p(x) of degree **n**, that is a best fit (in a least-squares sense) for the data in **y**. The coefficients in **p** are in descending powers, and the length of the array **p** is **n + 1**.

[2] Please notice that this way of initial orbit determination is not what is usually done; there are much more elaborate approaches which lead to more accurate initial orbits.

[3] You can solve the normal equation system by inverting the normal equation matrix (using the MATLAB command **inv**) and multiplying by the right hand side of the normal equation system. However, a faster and more robust way to solve a linear system is by using the command **mldivide** (matrix left division): **x = mldivide(A,b)** solves the linear system **A*x = b**. The abbreviation for **mldivide** is the backslash operator: **x = A\b**.

(d) Compute the residuals in two ways:

- Consider the linearized problem of the least-squares adjustment and calculate the residuals as they appear in the linearized observation equations.
- Take the updated orbital elements and propagate the orbit using the function **`ephem`**. For each epoch compute the differences between the propagated orbit and the observations.

Plot the z-component of the two kinds of residuals. Why are they different?

(e) Perform a filter solution of the orbit determination problem using the recursive filter formulas (see the online data) for the inverted normal equations. Use the pseudo-observations in **`psd0bs`** with equal weighting and introduce the orbital elements computed in exercise 1a as a priori values. Perform the following steps:

- Loop over the first two epochs and initialize the filter:
  - Compute the satellite position using the function **`ephem`** and the a priori orbital elements.
  - Compute the 'observed minus computed' term.
  - Compute the first design matrix using the function **`rvpder`**.
  - Accumulate the normal equation system.
- Solve the normal equation system of the initialization.
- Loop over the remaining epochs and perform the filter steps:
  - Compute the satellite position using the function **`ephem`** and the a priori orbital elements.
  - Compute the 'observed minus computed' term.
  - Compute the first design matrix using the function **`rvpder`**.
  - Compute the resubstitution term as shown in the lecture slides (see the online data).
  - Compute the gain matrix as shown in the lecture slides (see the online data).
  - Update the solution vector. Store the solution vector at each filter step.

Plot the determined semi-major axis a for all filter steps. When does it converge? Plot the x-component of the resubstitution term for each filter step.

(f) Implement the conventional least-squares adjustment into an iteration loop, where, at each step, you use the updated orbital elements from the previous step as a priori elements. Think about a reasonable stop criterion for the iteration loop. Compute and plot the linearized and true residuals after the last iteration.

2: Orbit determination with pseudo-stochastic pulses

Here, we use a 'true' orbit which was obtained by not only using the equations of motion of the two-body problem, but by additionally applying along-track (perturbation) accelerations in a numerical integration. From this orbit a number of pseudo-observations are created. Your main task is then to use these pseudo-observations to perform the orbit determination in the frame of the two-body problem, but by additionally solving for pseudo-stochastic pulses, which shall compensate the perturbing accelerations. You will again carry out a conventional least-squares adjustment and a filter approach.

You will perform the task by completing the MATLAB skeleton file **ex2.m.** The same MATLAB functions as in exercise 1 are used. At the beginning of the MATLAB skeleton file **ex2.m** the same six Keplerian elements as in exercise 1 are defined. Starting from the initial conditions defined by these elements, a perturbed orbit was created beforehand by numerical integration of the equations of motion by taking the 10 s piecewise constant along-track accelerations in the file **GRCA.ACC** into account. The positions and velocities resulting from the numerical integration were written in a 30 s sampling into the file **STOCH_ORB** (column 1: time, columns 2-4: positions in geocentric inertial frame, columns 5-7: velocities). This file is read (using the MATLAB command **load**). Using the function **xyzele**, for each 30 s epoch a set of osculating orbital elements is computed. Finally, a normally distributed noise is added to the positions, which are then stored in the matrix **psdObs**. These positions serve as pseudo-observations for the following orbit determination. You will only process the first two hours of observations.

(a) Perform a conventional least-squares solution of the orbit determination problem. Solve for the orbital elements and additionally for pulses in the velocity direction at every measurement epoch. Use the pseudo-observations in **psdObs** with equal weighting and introduce the orbital elements of the unperturbed orbit (defined at the beginning of **ex2.m**) as a priori elements. Perform the following steps:

- Loop over all epochs. For each epoch:
  - Compute the satellite position of the a priori orbit using the function **ephem** and the a priori orbital elements (propagation in the two-body problem).
  - Compute the partial derivatives of the positions and velocities of the a priori orbit w.r.t. the orbital elements (using the function **rvpder**).
  - Compute the (constant) coefficients β_k, $k = 1, ..., 6$, which allow to express the partial derivatives of the orbit w.r.t. the pulses as a linear combination of the partials w.r.t. the six orbital elements.
  - Compute the 'observed minus computed' term and the first design matrix.
- Set up the normal equation system.
- Add the weights on the normal equation system to constrain the pulses towards zero.
- Solve the normal equation system.

How many parameters do you solve for? How big is the normal equation matrix? What is the estimated value for the first pulse?

(b) Plot the estimated pulses when using different a priori standard deviations **sig0** for the pseudo-observations (e.g., **sig0** = 1 and **sig0** = 10^{-7}). Read in the accelerations in the file **GRCA.ACC** and transform them into velocity changes. Plot these together with the estimated pulses. What changes if you change **sig0**?

(c) Compute and plot the orbit residuals and the differences of the improved orbit w.r.t. the true orbit for all epochs in the geocentric (x,y,z) frame. Here you cannot compute the 'true' residuals by taking the updated orbital elements and propagating the new orbit (as you did in the second part of exercise 1d), since for the propagation you would need a numerical integration that takes the acceler-

ations in **GRCA.ACC** and the estimated pulses into account. Hence, compute the residuals of the linearized problem. Likewise, for the orbit difference add the (linearized) orbit corrections (computed by using the solution of exercise 2a to the a priori orbit (obtained by propagating the elements **eleTru** using the function **ephem**) and compare these positions with the true positions in the file **STOCH_ORBIT**. Make again experiments with different values of **sig0**.

(d) At each epoch the pseudo-stochastic pulse induces a change in the initial conditions (defined at the initial epoch). Compute and plot the difference of the epoch-specific semi-major axis w.r.t. the a priori value. Compare this difference with the difference of the true osculating semi-major axis w.r.t. the a priori value (in **difOsc**). Do this for different values of **sig0**.

(e) Perform a filter solution of the orbit determination problem with only six unknowns by pre-eliminating the pulses every epoch. Initially, this is is not possible, since for each new epoch all pulses up to this epoch will contribute to the observation equation. The pre-elimination becomes, however, possible when conducting a parameter transformation discussed in Sects. 2.3.3.3 and 2.3.3.4. Use the pseudo-observations in **psdObs** with equal weighting and introduce the orbital elements in **eleTru** as a priori values. In a loop over all epochs, perform the following steps:

- Compute the satellite position using the function **ephem** and the a priori orbital elements.
- Compute the first design matrix using the function **rvpder**.
- Compute the 'observed minus computed' term.
- Update the normal equation system with the observation equations of the current epoch.
- Perform the parameter transformation, add the pseudo-observation for the pulse (with the corresponding weight) and pre-eliminate the pulse.
- Generate and save the solution for the orbital elements, the residuals and the orbit difference w.r.t. the true orbit.

What are the estimated values of the orbital elements after the 5th filter step?

(f) Compute and plot the real-time semi-major axis, the orbit residuals and the differences w.r.t. the true orbit in the geocentric (x,y,z) frame for each filter step.

Chapter 3
The Classical Variational Approach

Srinivas Bettadpur and Christopher McCullough

3.1 Differential Corrections

While the fundamental theory behind the differential correction process is more than a century old, its cutting edge applications utilize high fidelity modeling, advanced numerical techniques, and observations with unprecedented precision/accuracy. This chapter will cover the basic mathematical formulation and then comment on the specialization of the process to the estimation of gravity field parameters from the Gravity Recovery and Climate Experiment (GRACE).

3.1.1 Orbital Motion

The equations of motion governing satellite orbits are given as,

$$\begin{aligned} \ddot{\mathbf{r}} &= -\frac{\mu}{r^2}\hat{\mathbf{e}}_r + \mathbf{f_p}\left(\mathbf{r}, \dot{\mathbf{r}}, \alpha\right) \\ &= \mathbf{g}\left(\mathbf{r}, \dot{\mathbf{r}}, \mu, \alpha\right), \\ \mathbf{r}\left(t_0\right) &= \mathbf{r_0}, \\ \dot{\mathbf{r}}\left(t_0\right) &= \mathbf{v_0} \end{aligned} \tag{3.1}$$

S. Bettadpur (✉) · C. McCullough
Center for Space Research (CSR), The University of Texas at Austin, Austin, USA
e-mail: srinivas@csr.utexas.edu

C. McCullough
e-mail: mcculloughchris@utexas.edu

M. Naeimi and J. Flury (eds.), *Global Gravity Field Modeling from Satellite-to-Satellite Tracking Data*, Lecture Notes in Earth System Sciences,
DOI 10.1007/978-3-319-49941-3_3

where,

$\mathbf{r}$ = 3×1 vector of the satellite's position,
$\dot{\mathbf{r}}$ = 3×1 vector of the satellite's velocity,
$\ddot{\mathbf{r}}$ = 3×1 vector of the satellite's acceleration,
μ = gravitational parameter of the central body,
r = satellite's distance form the center of mass of the central body,
$\hat{\mathbf{e}}_{\mathbf{r}}$ = a unit vector directed along the vector from the central body's center of mass to the center of mass of the satellite,
$\mathbf{f_p}$ = perturbative accelerations,
α = parameters of the force model,
$\mathbf{r_0}$ = 3×1 vector of the satellite's initial position,
$\mathbf{v_0}$ = 3×1 vector of the satellite's initial velocity.

Formally integrating Eq. (3.1) yields,

$$\dot{\mathbf{r}}(t) = \dot{\mathbf{r}}_0 + \int_{t_0}^{t} \mathbf{g}\left(\mathbf{r}(\tau), \dot{\mathbf{r}}(\tau), \mu, \mathbf{f_p}(\tau)\right) d\tau \tag{3.2}$$

And integrating again yields,

$$\mathbf{r}(t) = \mathbf{r_0} + \dot{\mathbf{r}}_0 (t - t_0) + \int_{t_0}^{t} \int_{t_0}^{s} \mathbf{g}\left(\mathbf{r}(\tau), \dot{\mathbf{r}}(\tau), \mu, \mathbf{f_p}(\tau)\right) d\tau ds \tag{3.3}$$

Therefore, in order to arrive at the correct position with the correct velocity, we have to

1. Start with the correct initial conditions (IC): $\mathbf{r_0}$, $\dot{\mathbf{r}}_0$.
2. And know the integrand (exact force model parameters) for all intermediate points.

The solution for the position and velocity at any time is realized, in practice, by numerical integration of the differential equations of motion, resulting in the satellite ephemerides.

3.1.2 Observations

How do we know if the satellite ephemerides are wrong? If we have an instrument system that gives us an observation (generally a nonlinear function) of satellite position and velocity

$$Y = G(\mathbf{r}(t), \dot{\mathbf{r}}(t), \ldots) \tag{3.4}$$

and we have a mathematical model for that observation, then we see a non-zero residual between the measurement Y_0 and the predicted value of the measurement

$$y(t) = Y_0 - G(\mathbf{r}(t), \dot{\mathbf{r}}(t), \ldots) \tag{3.5}$$

How can we use a sequence of these observations to "correct the orbit?" Unlike the standard point Parameter Estimation problem, we attempt to correct the trajectory. One option is to take the so-called kinematic approach, where the trajectory at observation epoch is independently corrected based on observations at that epoch, and a sequence of such corrections are used to infer the corrections needed to the force model. Alternatively, the force model parameter errors and initial condition errors are estimated by mapping them to the epoch of the observations using variational equations. We discuss only the latter approach in the following sections.

3.1.3 Formalism

Recall the equations of motion for a satellite,

$$\ddot{\mathbf{r}} = -\frac{\mu}{r^2}\hat{\mathbf{e}}_{\mathbf{r}} + \mathbf{f}_{\mathbf{p}}(\mathbf{r}, \dot{\mathbf{r}}, \alpha) \tag{3.6}$$

where α represents the parameterized force model (e.g. drag, gravity, etc.). The state of the satellite may be defined as,

$$\mathbf{X}(t) = \begin{bmatrix} \mathbf{r}(t) \\ \dot{\mathbf{r}}(t) \end{bmatrix} \tag{3.7}$$

Then,

$$\begin{aligned} \dot{\mathbf{X}}(t) &= \begin{bmatrix} \dot{\mathbf{r}}(t) \\ \ddot{\mathbf{r}}(t) \end{bmatrix} = \begin{bmatrix} \dot{\mathbf{r}}(t) \\ \mathbf{f}_{\mathbf{p}}(\mathbf{r}, \dot{\mathbf{r}}, \alpha) \end{bmatrix} = \mathbf{F}(\mathbf{X}, \alpha) \\ \mathbf{X}(t_0) &= \begin{bmatrix} \mathbf{r_0} \\ \dot{\mathbf{r}}_0 \end{bmatrix} \end{aligned} \tag{3.8}$$

Observations are typically some non-linear function of the orbital position/velocity and other parameters.

$$Y(t) = G(\mathbf{r}(t), \dot{\mathbf{r}}(t), \beta) \tag{3.9}$$

where β is the set of observation model parameters. For example, the range from a ground station to a satellite is given by,

$$\begin{aligned} \rho(t) &= \mathbf{r}_{\mathbf{SAT}}(t) - \mathbf{r}_{\mathbf{STA}}(t) \\ \rho(t) &= \left\| \mathbf{r}_{\mathbf{SAT}}(t) - \mathbf{r}_{\mathbf{STA}}(t) \right\| \end{aligned} \tag{3.10}$$

where,

$\rho(t)$ = 3×1 vector of the relative distance between the ground station and the satellite,
$\mathbf{r}_{\mathbf{SAT}}(t)$ = 3×1 vector of the satellite's position,
$\mathbf{r}_{\mathbf{STA}}(t)$ = 3×1 vector of the ground station's position,
$\rho(t)$ = scalar line of sight distance between the ground station and the satellite.

We can represent our best a priori knowledge of the initial condition and force model parameters (in jargon, referred to as the "Background Model") by a superscript "*" on $\mathbf{r}(t)$ and $\dot{\mathbf{r}}(t)$, so that

$$C = G\left(\mathbf{r}^*(t), \dot{\mathbf{r}}^*(t), \beta^*\right) \tag{3.11}$$

where,

$\mathbf{r}^*(t)$ = best knowledge of the satellite's position
$\dot{\mathbf{r}}^*(t)$ = best knowledge of the satellite's velocity,
β^* = best known observational parameters, such as $\mathbf{r}_{\mathbf{STA}}$ in Eq. (3.10),
G = mathematical observation model, such as that given by Eq. (3.10), which is assumed "complete."

So,

$$\begin{aligned} y(t) &= O - C \\ O &: O\left(\mathbf{r}(t), \dot{\mathbf{r}}(t), \beta\right) \end{aligned} \tag{3.12}$$

where the numerical value of O is the known observation; however, $\mathbf{r}(t)$, $\dot{\mathbf{r}}(t)$, and β are unknown. How can we use $y(t)$?

$$y(t) = O\left(\mathbf{r}(t), \dot{\mathbf{r}}(t), \beta\right) - C\left(\mathbf{r}^*(t), \dot{\mathbf{r}}^*(t), \beta^*\right) \tag{3.13}$$

Let,

$$\begin{aligned} \mathbf{r}(t) &= \mathbf{r}^*(t) + \boldsymbol{\delta}\mathbf{r}(t) \\ \dot{\mathbf{r}}(t) &= \dot{\mathbf{r}}^*(t) + \boldsymbol{\delta}\dot{\mathbf{r}}(t) \\ \beta &= \beta^* + \boldsymbol{\delta}\beta \end{aligned} \tag{3.14}$$

Then,

$$\begin{aligned} y(t) &= G\left(\mathbf{r}^*(t) + \boldsymbol{\delta}\mathbf{r}(t), \dot{\mathbf{r}}^*(t) + \boldsymbol{\delta}\dot{\mathbf{r}}(t), \beta + \boldsymbol{\delta}\beta\right) - G\left(\mathbf{r}^*(t), \dot{\mathbf{r}}^*(t), \beta^*\right) \\ &= \frac{\partial G}{\partial \mathbf{r}}\boldsymbol{\delta}\mathbf{r}(t) + \frac{\partial G}{\partial \dot{\mathbf{r}}}\boldsymbol{\delta}\dot{\mathbf{r}}(t) + \frac{\partial G}{\partial \beta}\boldsymbol{\delta}\beta \end{aligned} \tag{3.15}$$

where the partial derivatives are evaluated on the nominal, or *, values. So,

$$\begin{aligned} y(t_1) &= \tilde{\mathbf{H}}_{\mathbf{r}_1^*}\delta\mathbf{r}(t_1) + \tilde{\mathbf{H}}_{\dot{\mathbf{r}}_1^*}\delta\dot{\mathbf{r}}(t_1) + \tilde{\mathbf{H}}_{\beta^*}\delta\beta^* \\ &\vdots \\ y(t_k) &= \tilde{\mathbf{H}}_{\mathbf{r}_k^*}\delta\mathbf{r}(t_k) + \tilde{\mathbf{H}}_{\dot{\mathbf{r}}_k^*}\delta\dot{\mathbf{r}}(t_k) + \tilde{\mathbf{H}}_{\beta^*}\delta\beta^* \\ &\vdots \\ y(t_m) &= \tilde{\mathbf{H}}_{\mathbf{r}_m^*}\delta\mathbf{r}(t_m) + \tilde{\mathbf{H}}_{\dot{\mathbf{r}}_m^*}\delta\dot{\mathbf{r}}(t_m) + \tilde{\mathbf{H}}_{\beta^*}\delta\beta^* \end{aligned} \tag{3.16}$$

At this point, there are 2 things that must be addressed

1. Typically, $dim(y) < dim(\boldsymbol{\delta}\mathbf{r}$ or $\boldsymbol{\delta}\dot{\mathbf{r}}$ or $\beta)$. So we must reduce the sequence $\{\boldsymbol{\delta}\mathbf{r}(t_k), \boldsymbol{\delta}\dot{\mathbf{r}}(t_k)\}k = 1, \ldots, m\}$ to fewer parameters.
2. We must make the dependence of the observations on α explicit.

To achieve these goals in the variational approach, we insist that $\boldsymbol{\delta}\mathbf{r}(t_k)$ and $\boldsymbol{\delta}\dot{\mathbf{r}}(t_k)$ are, for all t_k, not arbitrary, but result in a dynamically consistent fashion from variations in the parameters of the problem, that is, the initial conditions and the force model parameters. Therefore,

$$\begin{aligned} \boldsymbol{\delta}\mathbf{r}(t_k) &= \frac{\partial\mathbf{r}(t_k)}{\partial\mathbf{r_0}}\boldsymbol{\delta}\mathbf{r_0} + \frac{\mathbf{r}(t_k)}{\boldsymbol{\delta}\dot{\mathbf{r}}_\mathbf{0}}\boldsymbol{\delta}\dot{\mathbf{r}}_\mathbf{0} + \frac{\partial\mathbf{r}(t_k)}{\partial\alpha}\boldsymbol{\delta}\alpha \\ \boldsymbol{\delta}\dot{\mathbf{r}}(t_k) &= \frac{\partial\dot{\mathbf{r}}(t_k)}{\partial\mathbf{r_0}}\boldsymbol{\delta}\mathbf{r_0} + \frac{\dot{\mathbf{r}}(t_k)}{\boldsymbol{\delta}}\dot{\mathbf{r}}_\mathbf{0}\boldsymbol{\delta}\dot{\mathbf{r}}_\mathbf{0} + \frac{\partial\dot{\mathbf{r}}(t_k)}{\partial\alpha}\boldsymbol{\delta}\alpha \\ \begin{bmatrix}\boldsymbol{\delta}\mathbf{r}(t_k)\\ \boldsymbol{\delta}\dot{\mathbf{r}}(t_k)\end{bmatrix} &= \begin{bmatrix}\frac{\partial\mathbf{r}(t_k)}{\partial\mathbf{r_0}} & \frac{\partial\mathbf{r}(t_k)}{\dot{\mathbf{r}}_\mathbf{0}} & \frac{\partial\mathbf{r}(t_k)}{\partial\alpha} \\ \frac{\partial\dot{\mathbf{r}}(t_k)}{\partial\mathbf{r_0}} & \frac{\partial\dot{\mathbf{r}}(t_k)}{\dot{\mathbf{r}}_\mathbf{0}} & \frac{\partial\dot{\mathbf{r}}(t_k)}{\partial\alpha}\end{bmatrix} \begin{bmatrix}\boldsymbol{\delta}\mathbf{r_0}\\ \boldsymbol{\delta}\dot{\mathbf{r}}_\mathbf{0}\\ \boldsymbol{\delta}\alpha\end{bmatrix} \end{aligned} \tag{3.17}$$

Equation (3.17) is the explicit form of the so-called State Transition Matrix $\boldsymbol{\Phi}$ (STM). If the state $\dot{\boldsymbol{X}}$ of a system is governed by the equations of motion

$$\dot{\boldsymbol{X}} = \boldsymbol{F}(\boldsymbol{X}) \tag{3.18}$$

then the variations $\mathbf{x}$ of $\mathbf{X}$ with

$$\dot{\mathbf{X}}^* + \dot{\mathbf{x}} = \mathbf{F}\left(\mathbf{X}^* + \mathbf{x}\right) = \mathbf{F}\left(\mathbf{X}^*\right) + \left.\frac{\partial\mathbf{F}}{\partial\mathbf{X}}\right|_{\mathbf{X}^*}\mathbf{x}(t) + H.O.T. \tag{3.19}$$

are governed by

$$\dot{\mathbf{x}}(t) = \mathbf{A}(t)\,\mathbf{x}(t) \tag{3.20}$$

where

$$\mathbf{A}(t) = \left.\frac{\partial\mathbf{F}}{\partial\mathbf{X}}\right|_{\mathbf{X}^*} \tag{3.21}$$

Combining Eqs. (3.17)–(3.20),

$$\begin{aligned}\mathbf{x}(t) &= \boldsymbol{\Phi}(t,t_0)\,\mathbf{x}(t_0)\\ \dot{\mathbf{x}}(t) &= \dot{\boldsymbol{\Phi}}(t,t_0)\,\mathbf{x}(t_0)\\ &= \mathbf{A}(t)\,\mathbf{x}(t) = \mathbf{A}(t)\,\boldsymbol{\Phi}(t,t_0)\,\mathbf{x}(t_0)\end{aligned} \tag{3.22}$$

$$\dot{\boldsymbol{\Phi}}(t,t_0) = \mathbf{A}(t)\,\boldsymbol{\Phi}(t,t_0), \qquad \boldsymbol{\Phi}(t_0,t_0) = \mathbf{I}$$

Now, let us examine the components of the STM in detail.

$$\begin{aligned}\frac{\partial \mathbf{r}(t)}{\partial \mathbf{r_0}} &= \boldsymbol{\Phi}_{rr_0}\\ \dot{\boldsymbol{\Phi}}_{rr_0}(t,t_0) = \frac{d}{dt}\left[\frac{\partial \mathbf{r}(t)}{\partial \mathbf{r_0}}\right] &= \frac{\partial}{\partial \mathbf{r_0}}\frac{d}{dt}[\mathbf{r}(t)]\\ &= \frac{\partial \dot{\mathbf{r}}(t)}{\partial \mathbf{r_0}} = \boldsymbol{\Phi}_{vr_0}(t,t_0)\end{aligned} \tag{3.23}$$

$$\begin{aligned}\frac{\partial \mathbf{r}(t)}{\partial \mathbf{v_0}} &= \boldsymbol{\Phi}_{rv_0}(t,t_0)\\ \frac{d}{dt}\left[\frac{\partial \mathbf{r}(t)}{\partial \mathbf{v_0}}\right] = \frac{\partial}{\partial \mathbf{v_0}}\left[\frac{d\mathbf{r}}{dt}\right] &= \frac{\partial \mathbf{v}(t)}{\partial \mathbf{v_0}} = \boldsymbol{\Phi}_{vv_0}\end{aligned} \tag{3.24}$$

$$\begin{aligned}\frac{\partial \mathbf{r}(t)}{\partial \alpha} &= \boldsymbol{\Phi}_{r\alpha}(t,t_0)\\ \frac{d}{dt}\left[\frac{\partial \mathbf{r}(t)}{\partial \alpha}\right] = \frac{\partial}{\partial \alpha}\left[\frac{d\mathbf{r}}{dt}\right] &= \frac{\partial \mathbf{v}(t)}{\partial \alpha} = \boldsymbol{\Phi}_{v\alpha}\end{aligned} \tag{3.25}$$

$$\begin{aligned}\frac{\dot{\mathbf{r}}(t)}{\partial \mathbf{r_0}} &= \boldsymbol{\Phi}_{vr_0}(t,t_0)\\ \frac{d}{dt}\left[\frac{\partial \dot{\mathbf{r}}(t)}{\partial \mathbf{r_0}}\right] = \frac{\partial}{\partial \mathbf{r_0}}\left[-\frac{\mu}{r^2}\hat{\mathbf{e}}_{\mathbf{r}} + \mathbf{f}_{\mathbf{p}}\right] &= \frac{\partial}{\partial \mathbf{r_0}}[\mathbf{f}(\mathbf{r},\dot{\mathbf{r}},\alpha)]\\ &= \frac{\partial \mathbf{f}}{\partial \mathbf{r}(t)}\frac{\partial \mathbf{r}(t)}{\partial \mathbf{r_0}} + \frac{\partial \mathbf{f}}{\partial \mathbf{v}(t)} + \frac{\partial \mathbf{v}(t)}{\partial \mathbf{r_0}}\\ &= \frac{\partial \mathbf{f}}{\partial \mathbf{r}}\boldsymbol{\Phi}_{rr_0} + \frac{\partial \mathbf{f}}{\partial \mathbf{v}}\boldsymbol{\Phi}_{vr_0}\end{aligned} \tag{3.26}$$

$$\begin{aligned} \frac{\partial \dot{\mathbf{r}}}{\partial \dot{\mathbf{r}}_{\mathbf{0}}} &= \boldsymbol{\Phi}_{vv_0} \\ \frac{d}{dt}\left[\frac{\partial \dot{\mathbf{r}}}{\partial \dot{\mathbf{r}}_{\mathbf{0}}}\right] &= \frac{\partial \mathbf{f}}{\partial \mathbf{r}}\boldsymbol{\Phi}_{rv_0} + \frac{\partial \mathbf{f}}{\partial \mathbf{v}}\boldsymbol{\Phi}_{vv_0} \end{aligned} \tag{3.27}$$

$$\begin{aligned} \frac{\partial \dot{\mathbf{r}}\,(t)}{\partial \alpha} &= \boldsymbol{\Phi}_{v\alpha}\,(t, t_0) \\ \frac{d}{dt}\left[\frac{\partial \dot{\mathbf{r}}\,(t)}{\partial \alpha}\right] &= \frac{\partial}{\partial \alpha}\left[\frac{d\dot{\mathbf{r}}}{dt}\right] \\ &= \frac{\partial \mathbf{f}}{\partial \alpha} = \frac{\partial \mathbf{f}}{\partial \mathbf{r}}\boldsymbol{\Phi}_{r\alpha} + \frac{\partial \mathbf{f}}{\partial \mathbf{v}}\boldsymbol{\Phi}_{v\alpha} + \frac{\partial \mathbf{f}}{\partial \alpha} \end{aligned} \tag{3.28}$$

Combining these all together yields,

$$\begin{aligned} \frac{d}{dt}\begin{bmatrix} \boldsymbol{\Phi}_{rr_0} & \boldsymbol{\Phi}_{rv_0} & \boldsymbol{\Phi}_{r\alpha} \\ \boldsymbol{\Phi}_{vr_0} & \boldsymbol{\Phi}_{vv_0} & \boldsymbol{\Phi}_{v\alpha} \end{bmatrix} &= \begin{bmatrix} \mathbf{0} & \mathbf{I} \\ \frac{\partial \mathbf{f}}{\partial \mathbf{r}} & \frac{\partial \mathbf{f}}{\partial \mathbf{v}} \end{bmatrix}\begin{bmatrix} \boldsymbol{\Phi}_{rr_0} & \boldsymbol{\Phi}_{rv_0} & \boldsymbol{\Phi}_{r\alpha} \\ \boldsymbol{\Phi}_{vr_0} & \boldsymbol{\Phi}_{vv_0} & \boldsymbol{\Phi}_{v\alpha} \end{bmatrix} \\ &\quad + \begin{bmatrix} \mathbf{0}\,\mathbf{0} & \mathbf{0} \\ \mathbf{0}\,\mathbf{0} & \frac{\partial \mathbf{f}}{\partial \alpha} \end{bmatrix} \end{aligned} \tag{3.29}$$

3.1.4 Simple State Transition Matrix Example

Consider the Kepler ellipse, given by the orbital elements (a, e, I, ω, Ω, and M), and a variation Δa_0. In this case, only two coordinates are affected.

$$\begin{aligned} \Delta a\,(t) &= \Delta a_0 \\ \Delta M\,(t) &= -\frac{3n^*}{2a^*}\Delta a_0, \qquad \text{where} \quad n^* = \sqrt{\frac{\mu}{a^{*3}}} \end{aligned} \tag{3.30}$$

$$\begin{bmatrix} \Delta a\,(t) \\ \Delta e\,(t) \\ \Delta I\,(t) \\ \Delta \omega\,(t) \\ \Delta \Omega\,(t) \\ \Delta M\,(t) \end{bmatrix} = \begin{bmatrix} 1 & 0\,0\,0\,0\,0 \\ 0 & 1\,0\,0\,0\,0 \\ 0 & 0\,1\,0\,0\,0 \\ 0 & 0\,0\,1\,0\,0 \\ 0 & 0\,0\,0\,1\,0 \\ -\frac{3n^*}{2a^*}\Delta t & 0\,0\,0\,0\,1 \end{bmatrix}\begin{bmatrix} \Delta a_0 \\ \Delta e_0 \\ \Delta I_0 \\ \Delta \omega_0 \\ \Delta \Omega_0 \\ \Delta M_0 \end{bmatrix} \tag{3.31}$$

3.1.5 Summary

1. The time-sequence of $\boldsymbol{\delta}\mathbf{r}\,(t_k)$ have a defined relationship (the variational equations) to the force parameters, α. Therefore, the observation residuals, y_k, have

a defined relationship to the force parameters. It is in this sense that we say that "...the orbit is the observable...".

2. Given any sequence of $\boldsymbol{\delta}\mathbf{r}(t_k)$ and $\boldsymbol{\delta}\dot{\mathbf{r}}(t_k)$, one can set $\boldsymbol{\delta}\alpha = 0$ and find some $(\boldsymbol{\delta}\mathbf{r_0}, \boldsymbol{\delta}\dot{\mathbf{r}}_\mathbf{0})$ that satisfy the variational equations. For each t_k, the derived $(\boldsymbol{\delta}\mathbf{r_0}, \boldsymbol{\delta}\dot{\mathbf{r}}_\mathbf{0})$ will be different. Lesser the duration between t_k and t_0, and lesser the error in the force models or the initial conditions, the better this approximation becomes. Conversely we can set $(\boldsymbol{\delta}\mathbf{r_0}, \boldsymbol{\delta}\dot{\mathbf{r}}_\mathbf{0}) = 0$ and correct only $\boldsymbol{\delta}\alpha$. This duality of similar signal changes in $\boldsymbol{\delta}\mathbf{r}$ due to errors in $\boldsymbol{\delta}\mathbf{r_0}$, $\boldsymbol{\delta}\dot{\mathbf{r}}_\mathbf{0}$ or $\boldsymbol{\delta}\alpha$ (particularly at low frequencies) can lead to difficulties in the orbit and gravity estimation problem. This thread is further explored in the series of exercises.
3. The concept of an "arc":
   - An arc is defined as the duration over which a single set of initial conditions are adjusted.
   - Epoch of an arc can be anywhere—it need not be at the epoch of the first observation.

3.2 Least Squares Adjustment and Spectrum of Perturbations

Now we look at the details of the variational formulation for the specific needs of estimation of the gravity field parameters using the GRACE mission data.

3.2.1 Modeling Satellite Motion

Recalling the mathematical model describing the motion of a satellite,

$$\ddot{\mathbf{r}} = -\frac{\mu}{r^2}\hat{\mathbf{e}}_\mathbf{r} + \mathbf{f_p} \tag{3.32}$$

where the perturbing acceleration, denoted by $\mathbf{f_p}$, is given by a combination of non-gravitational forces, gravitational forces, and empirical accelerations.

3.2.1.1 Non-gravitational Forces

The non-gravitational forces are measured using an accelerometer. The accelerometer provides a (possibly) biased and scaled value of the true non-gravitational accelerations. Tabular acceleration inputs are therefore provided to the orbit propagator, in a form that allows for the adjustment of the accelerometer bias and scale parameters. While the user may not choose to estimate every bias/scale parameter together with the orbit initial conditions and the gravity field model parameters, the model may be represented as,

$$\begin{aligned}\mathbf{f}_{NG}^{ACC} &= b_x + s_x f_x^{ACC} \\ &+ b_y + s_y f_y^{ACC} \\ &+ b_z + s_z f_z^{ACC}\end{aligned} \tag{3.33}$$

In this case, b_i and s_i become components of α, which are dynamical parameters.

3.2.1.2 Gravitational Forces

The gravitational forces, in an Earth centered Earth fixed (ECEF) coordinate system or an Earth centered inertial (ECI) coordinate system, can be modeled as

$$\begin{aligned}\mathbf{f}_G^{ECEF} &= \nabla U, \\ U &= \sum_{l=2}^{N_{MAX}} \left(\frac{a_e}{r}\right)^l \sum_{m=0}^{l} P_{lm}(\sin\phi)\left[\left(\langle C_{lm}\rangle + \delta C_{lm}(t)\right)\cos m\lambda\right. \\ &\quad \left. + \left(\langle S_{lm}\rangle + \delta S_{lm}(t)\right)\sin m\lambda\right] \\ \mathbf{f}_G^{ECI} &= \mathbf{M}_{ECEF}^{ECI}\nabla U\end{aligned} \tag{3.34}$$

where $\langle\cdot\rangle$ denotes time average. The only exception to this formulation are third body and solid Earth tide accelerations, which are calculated from Luni-Solar ephemerides. In typical GRACE analyses, the background gravity model, represented as above, reflects our current best knowledge of the Earth gravity field variations. The Earth processes for which do not yet have good models—such as due to land water cycle variations, ice-sheet variations, non-tidal ocean dynamics, etc., and that are to be estimated from the GRACE data—are parametrized as piece-wise constant corrections to $\delta C_{lm}(t)$ and $\delta S_{lm}(t)$. However, the use of spherical harmonic formulation is not a strict requirement as there are well developed theories for other parameterizations of the gravitational accelerations.

3.2.1.3 Empirical Parameters

It has been known for a very long time that mean and 1-cpr (cycle per revolution) accelerations have special effects on the orbit. We can illustrate this using a set of non-singular coordinates defined in terms of the typical Keplerian orbital elements [37, 38], with "i" the unit imaginary, and the argument of latitude $u = \omega + M$

$$\begin{aligned}\Delta U(t) &= \frac{\Delta a}{\bar{a}} + i\left(\Delta u + \Delta\Omega\cos\bar{I}\right) \\ \Delta P(t) &= (\Delta e - i\,\Delta\omega)\,e^{-i\bar{\omega}} \\ \Delta Q(t) &= \Delta I - i\,\Delta\Omega\sin\bar{I}\end{aligned} \tag{3.35}$$

where quantities with a bar are averaged quantities. The averaged (longer than 1 orbital period) equations of motion are,

$$\begin{aligned}
\Delta\dot{U} + i\left[\frac{3\bar{n}}{2} - \dot{\bar{\mu}}_a\right]\Delta U_r - i\dot{\bar{\mu}}_I \Delta Q_r &= \frac{2}{\bar{a}\bar{n}}\left(\bar{T} - i\bar{R}\right) \\
\Delta\dot{P} + i\bar{\omega}\Delta P &= \frac{2}{\bar{a}\bar{n}}\left[\left(T_c + \frac{1}{2}R_s\right) - i\left(T_s - \frac{1}{2}R_c\right)\right] \\
\Delta\dot{Q} - i\dot{\bar{\nu}}_i \Delta Q_r - i\dot{\bar{\nu}}_a \Delta U_r &= \frac{1}{2\bar{a}\bar{n}}\left[N_c - iN_s\right]
\end{aligned} \tag{3.36}$$

in case the perturbing accelerations are given by,

$$\begin{aligned}
f_r &= \bar{R} + R_c\cos\bar{u} + R_s\sin\bar{u} \\
f_\tau &= \bar{T} + T_c\cos\bar{u} + T_s\sin\bar{u} \\
f_\nu &= \bar{N} + N_c\cos\bar{u} + N_s\sin\bar{u}
\end{aligned} \tag{3.37}$$

with $\dot{\bar{\mu}}_a$, $\dot{\bar{\mu}}_I$, $\dot{\bar{\nu}}_a$, and $\dot{\bar{\nu}}_I$ being coupling constants of the order J_2, and subscript r indicating the real part of the complex quantity [37, 38]. Also, note that the variations in the radial (r), transverse (τ), and normal (ν) coordinates of the satellite are given by,

$$\begin{aligned}
\Delta z &= \Delta r + i\Delta\tau = \bar{a}\Delta U + \frac{1}{2}\bar{a}\left[\Delta P e^{i\bar{u}} - 3\Delta P^* e^{-i\bar{u}}\right] \\
\Delta\nu &= \bar{a}\Re\{-i\Delta Q e^{i\bar{u}}\}
\end{aligned} \tag{3.38}$$

In orbit and gravity field adjustment process, it is common practice to estimate the mean accelerations, and/or the amplitudes of the once-per-revolution acceleration amplitudes simultaneously with the initial conditions or the gravity field parametrs. These equations help us understand the effect of the simultaneous estimation of these so-called "empirical acceleration" parameters. The equations show, in summary, that,

$\bar{R}$	adjusts to a mean offset in a and/or linear drift in ΔM,
$\bar{T}$	adjusts to a linear drift in a and/or quadratic drift along track,
R_C, T_C, R_S, T_S	adjust to slow variations in (e, ω) or to once-per-revolution variations in the orbit plane $(\Delta r, \Delta\tau)$,
N_C, N_S	adjust to slow variations in (I, Ω) or to once-per-revolution variations in the normal direction $\Delta\nu$.

Commonly, several such piece-wise constant parameters will be solved within one arc—a practice known in the jargon as "sub-arcing". In all such cases, we are able to fit slow variations in orbital elements by piecewise constants. So why does all of this matter?

1. Every signal/noise with an influence on the orbit dynamics leads to slow/near-1 cpr perturbations, in addition to a perturbation at its natural time scale. This is

mathematically explainable by the observation that the particular integral of the variational differential equations include the homogeneous solutions.
2. The estimation process cannot discriminate whether these slow drifts arose from the geophysical signals of interest, or from instrument or system effects when the mission data is entering the orbit integration process, such as from the accelerometer or the star camera.

3.2.1.4 Observation Empiricals

The environment on the spacecraft also changes as the satellites flies through the near Earth environment, or as the solar illumination changes the energy input to the system. These effects also potentially impose slow and 1-cpr data variations in the measurements such as the inter-satellite ranging signal in GRACE. These effects are inseparable, during the estimation process, from the effects of the geophysical signals discussed above. Mitigation to some extent is attempted by introducing observation empirical parameters in the form:

$$\delta\dot{\rho} = A + Bt + Ct^2 + E\cos nt + F\sin nt \tag{3.39}$$

$A - E$ or some subset thereof are included in the β parameters.

3.2.2 Reassembling the Variational Problem

Reassembling the variational problem for one arc yields,

$$\begin{bmatrix} y_1 \\ y_2 \\ \vdots \\ y_m \end{bmatrix} = \begin{bmatrix} \mathbf{H}_{\mathbf{r}_1} & \mathbf{H}_{\dot{\mathbf{r}}_1} & \mathbf{H}_\alpha & \mathbf{H}_\beta \\ \mathbf{H}_{\mathbf{r}_2} & \mathbf{H}_{\dot{\mathbf{r}}_2} & \mathbf{H}_\alpha & \mathbf{H}_\beta \\ \vdots & \vdots & \vdots & \vdots \\ \mathbf{H}_{\mathbf{r}_m} & \mathbf{H}_{\dot{\mathbf{r}}_m} & \mathbf{H}_\alpha & \mathbf{H}_\beta \end{bmatrix} \begin{bmatrix} \boldsymbol{\Delta} r_0 \\ \boldsymbol{\Delta}\dot{r}_0 \\ \boldsymbol{\Delta}\alpha \\ \boldsymbol{\Delta}\beta \end{bmatrix} \tag{3.40}$$

where,

$$\mathbf{H}_{\mathbf{r}_k} = \tilde{\mathbf{H}}_{\mathbf{r}_k} \boldsymbol{\Phi}_{rr_0}(t_k, t_0), \qquad \text{etc.} \tag{3.41}$$

Information equations from a collection of such arcs are assembled together to solve simultaneously for initial conditions for each arc as well as the gravity field parameters $\boldsymbol{\Delta\beta}$. The methods for solving such a system of equations are discussed in other chapters.

Interested readers are also referred to [141] for more details.

3.3 Exercises

Data and files needed for the following exercises are available online at:
http://www.geoq.uni-hannover.de/autumnschool-data
http://extras.springer.com

Important Note: The usage of all the functions is given by reading the comments at the top of each function or typing, 'help function_name' in the MATLAB command window.

1: Adjustment of Initial Conditions

Run the program *Exercise_1*. This program does a variety of things:

(a) Reads in 2 separately computed GRACE orbit solutions (each trajectory is read by the get_traj subroutine). These trajectories are perturbed by gravitational forces, third bodies, time variable gravity, non-gravitational forces, etc. One of these trajectories is the red curve in the plots that arise when you run *Exercise_1*.
(b) For each trajectory, the osculating orbit (orbit forced only by the two-body, central forcing term) can be computed at each step and numerically integrated back in time to the initial epoch (for each arc). These are the black curves in the plots that arise when you run Exercise_1. Note their scatter. The average initial condition of the black curves is output from Homogenous IC.
(c) The difference in the initial conditions, computed from each GRACE orbit solution, provide an estimate (in the absence of a full orbit solution) for the error between each trajectory, as the initial conditions are adjusted. This difference is output in the MATLAB command window.

The case you ran in *Exercise_1* adjusted the initial conditions once every day (arc length of 86400.0). Repeat this for smaller arc lengths (say 6 h and once per satellite revolution 5660.0 s).

Note the change in the difference as the arc length is shortened. The error should reduce with shorter arc length.

Implications: Trajectories can be fit with arbitrary forces, to some extent, by adjusting the initial conditions more frequently. Therefore, if the initial conditions are adjusted too frequently, they may have a detrimental effect on the gravity field.

2: Removal of the Homogeneous Solution (remodel)

Run the program *Exercise_2*. This program computes an inter-satellite range and range-rate residual (O-C). The residual is formed as follows:

(a) The observed inter-satellite range/range-rate are computed by propagating GRACE-like orbits under the influence of a two body, central forcing term and a 200 gigatonne point mass placed along the ground track of satellites.

(b) The computed inter-satellite range/range-rate are computed by propagating GRACE-like orbits under the influence of only a two body, central forcing term.
(c) The difference between these trajectories shows the effect of the point mass, with contributions from the homogeneous portion of the solution (secular and 1 cycle per revolution effects) and the transient effect of the point mass flyovers.

The output from *Exercise_2* displays 4 figures: the range residual, the range-rate residual, the range residual after a poorly executed attempt to remove the homogeneous solution effects, and the range-rate residual after a poorly executed attempt to remove the homogeneous solution effects. The homogeneous solution is removed with the subroutine remodel. Typing, help remodel will show you a message describing what remodel does (it is designed to mimic the inter-satellite tracking empirical parameters estimated during GRACE gravity field estimation).

Adjust the remodel parameters (lines 64 and 65 in *Exercise_2*) to more adequately remove the homogeneous portion of the residual and reveal the range-rate features caused by the flyovers of the point mass. Note: the orbit period is 5668.0 seconds.

Once this is completed add white noise accelerations to the observed trajectory (change the white noise sigma value-variable sig on line 11 of *Exercise_2*—a reasonable level is around $2.0 \times 10^{10}\,{}^{\mathrm{m}}/_{\mathrm{s}^2}$). How does the white noise affect the output from remodel? What happens as you increase the white noise?

Implications: The dominant affect of orbital perturbations come from the homogeneous solution of the differential equations (secular and 1 cycle per revolution effects). These contaminate/hide the higher frequency effects that GRACE is sensitive to. Their appropriate treatment is important to accurate gravity field recovery. The addition of white noise adds additional signal at all frequencies, further contaminating the residual.

3: State Transition Matrix (STM)

Run the program *Exercise_3*. This program numerically computes the state transition matrix in order to map perturbations in the orbital elements (and other parameters) at the initial epoch to later epochs. This allows for the efficient computation of arbitrary perturbations from the nominal trajectory. In this case, the nominal trajectory is a GRACE-like orbit under the influence of the two body, central forcing term, J2, a simple drag model, and tangential/normal 1 cycle per revolution accelerations.

In the initial run of *Exercise_3*, the effect of a perturbation in semi-major axis is shown. Similarly, you should individually add a perturbation to the other parameters and observe their effect on the orbital elements. Note: The parameters in the STM are ordered as follows:

- Semi-major axis (meters)—Suggested perturbation: 1 mm
- Eccentricity—Suggested perturbation: 1.0×10^{-4}
- Inclination (radians)—Suggested perturbation: 1 arc minute
- Argument of perigee (radians)—Suggested perturbation: 1 arc minute
- Ascending node (radians)—Suggested perturbation: 1 arc minute
- Mean Anomaly (radians)—Suggested perturbation: 1 arc minute
- J2 (C20)—Suggested perturbation: 1.0×10^{-8}

- Ballistic coefficient (Scaled drag coefficient)—Suggested perturbation: 1.0×10^{-3}
- Empirical 1 cycle per revolution acceleration amplitudes—Suggested perturbation: $1.0 \times 10^{-7}\,{}^{\mathrm{m}}/_{\mathrm{s}^2}$ —These include the last 4 parameters.

Run the program *Exercise_3v2*. This will show the effect of the predefined perturbations (shown in lines 75–86 of *Exercise_3v2*) under the influence of different force models. Observe these figures and note the effect various force models have on the orbital elements.

Implications: The STM allows the computation of the effect of arbitrary perturbations at any point on the orbit. This is vital to the least squares solution process because it allows for a simple mapping between the adjusted parameters (solution from the least squares-initial conditions, gravity field coefficients, etc.) and their effect on the orbit/observations. Finally, note the different effects of each force model in the presence of perturbations, when you run *Exercise_3v2*:

(a) Two body force—The orbital elements exhibit a constant offset equivalent to the input perturbation. This is the definition of the two body problem.
(b) Two body force + J2—The orbital elements now have sinusoidal variations and the well known secular trend in the ascending node due to the inclusion of the Earth's oblateness.
(c) Two body force + J2 + Drag—Note the downward trend in semi-major axis and eccentricity, due to the reduction in altitude and circularization of the orbit due to the inclusion of drag.
(d) Two body force + J2 + Drag + 1 cycle per revolution empirical accelerations—Note the apparent trends in eccentricity and inclination, as well as an increased secular drift in the ascending node, due to the inclusion of the 1 cpr empirical accelerations.

4: Spatial Resolution (simplified to 1 dimension)

Run the program *Exercise_4*. In addition read the comments in the subroutine FitLegendre to determine the function usage and outputs. This program computes a set of Legendre polynomials up to the user specified degree n_{max} and creates a transient spatial signal of user specified width. The scaling parameters, as shown below, are then best fit to the transient signal.

$$y = \sum_{n=0}^{n_{max}} a_k P_n(x)$$

This simulates, in a very simplified sense, the effect of attempting to fit high-resolution spatial features with a limited set of spherical harmonics.

Running *Exercise_4* displays 3 figures:

(a) Signal Comparison—This figure shows the spatial extent of the highest degree (highest spatial resolution) Legendre polynomial relative to the transient signal. Note: the difference in spatial resolution.

(b) Transient Signal versus Fit Signal—This figure shows the Legendre polynomial fit and the transient signal. It is a visual representation of how well the Legendre polynomials can fit the transient signal.
(c) Signal Residual—This figure shows the difference between the Legendre polynomial fit and the transient signal. This is another visual representation of how well the Legendre polynomials fit the transient signal.

Experiment with different sized spatial signals and observe how well the Legendre polynomial fit matches the transient signal.

Rerun the *FitLegendre* function for a variety of spatial sizes and plot the evolution of the percentage peak error (per_err) versus transient signal size. Adjust the spatial scale from 1.0°–20.0° and note how well each fits the peak amplitude.

Implications: Note that these examples are highly simplified (only 1 dimensional and the link between satellite observations at altitude to the Earth's surface is missing), but they show some effects of representing high-resolution spatial features with a truncated set of spherical harmonics.

Chapter 4
The Acceleration Approach

Matthias Weigelt

Abstract The Gravity Recovery and Climate Experiment (GRACE) mission is a key instrument to monitor and understand variations in the mass distribution of the Earth. The primary observable is the (biased) range between the two satellites which is a geometric observation. The task is therefore to connect this kind of observation to the physically meaningful gravity field of the Earth or in other words connecting the kinematic observation to a force. Various approaches exist. Here, the focus is on the so-called acceleration approach which conceptually tries to avoid the solution of the variational equations by linking observed range accelerations to the gradient of the gravitational potential. Practically, it requires the observation of range accelerations, the attitude and their changes with matching precision in all three dimensions which are currently not available for GRACE. Three possible solutions are presented: (1) an approximate solution neglecting terms with low precision observations by reducing the basic equation to residual quantities, (2) a stringent solution by considering the term of low precision as unknown and solving it via the variational equations and (3) an alternative description using rotational quantities. Only the second approach yields solutions at the same level of precision as other approaches but offers no conceptual or computational advantage due to the need for solving the variational equations. The first kind of solution results primarily in a mis-modeling of long-wavelength signal but may still serve well for local or regional solutions. The third kind of solution is currently not feasible since the required precision in the attitude information is far from being available. However, it offers interesting insight into the observation system. It allows to describe GRACE as a two-dimensional observation system and explain mathematically the poor East-West sensitivity yielding the striping artifact in today's GRACE solutions.

M. Weigelt (✉)
Institut für Erdmessung, Leibniz Universität Hannover, Hannover, Germany
e-mail: weigelt@ife.uni-hannover.de

M. Naeimi and J. Flury (eds.), *Global Gravity Field Modeling from Satellite-to-Satellite Tracking Data*, Lecture Notes in Earth System Sciences,
DOI 10.1007/978-3-319-49941-3_4

4.1 Introduction

The Gravity Recovery And Climate Experiment (GRACE) mission [140] enabled the determination of the Earth's gravity field and its temporal variations with unprecedented precision. The key instrument is the highly precise microwave-based K-Band ranging system which constantly tracks the relative motion of the two satellites, i.e. the distance between the spacecrafts (*range*) ρ in the direction of the line-of-sight (LOS). Range rate $\dot{\rho}$ and the range acceleration $\ddot{\rho}$ are numerically derived, c.f. [85], and frequently used as the primary observation whereas correlations due to the differentiation scheme are often neglected. For a successful recovery of the gravity field these kinematic quantities need to be connected to the gravitational potential V or any of their functionals, e.g. gravity (first derivatives of V) or gravity gradients (second derivatives of V). The acceleration approach is one such method.

Generally, various approaches exist and have been implemented with varying success. The most notable ones are based on the solution of the classical variational equations [119, 140] and are implemented by the Center for Space Research (CSR) at the University of Texas at Austin, the German Research Center for Geosciences (GFZ) and the NASA's Jet Propulsion Laboratory (JPL). They are used to produce the official releases of monthly and static gravity fields. Variants of the variational equation approach are the Celestial Mechanics Approach (CMA) [10, 11] developed by the Astronomical Institute of the University Bern and the short-arc method by [95].

Alternatively, there exist methods which may be summarized as *in-situ observation* approaches. These methods aim at avoiding an integration of the variational equations by forming (pseudo-) observations and connecting these directly and pointwise to a gravity field quantity. The energy integral approach links range-rate observations $\dot{\rho}$ to potential differences [74]. The acceleration approach discussed here utilizes range accelerations which are connected to the gradient of the gravitational potential ∇V (Sect. 4.2.1). Several variants of this approach exist, e.g. the differential gravimetry approach [93] and the inter-satellite range interpolation approach [165]. One conceptually very interesting variant is known as the line-of-sight gradiometry approach [82] which forms pseudo-observation by dividing the range-accelerations through the range and relating them to the tensor components of the gravitational potential V_{ij} projected on the LOS.

Both kind of approaches, i.e. those based on the variational equations and the in-situ observations, have their particular advantages and disadvantages. From a theoretical point of view, all approaches yield the same quality of solution as they are all based on Newton's equation of motion, see also Sect. 4.1.1. Differences occur due to different error characteristics of the primary observation quantity or derived pseudo-observations and the propagation of these errors through the processing chain, but it is beyond the scope of this section to compare their performance. Generally, it can be stated that methods based on variational equations need sophisticated orbit integration methods whereas in-situ observations need augmentation with additional observations, e.g. GPS. This kind of combination often poses the main culprit in the

derivation of gravity field solutions and therefore the approaches based on variational equations seem to perform at the current stage slightly better.

After introducing basics about Newton's equation of motion in Sect. 4.1.1 and the difference of kinematic and dynamic quantities in Sect. 4.1.2, the geometry of the GRACE system in Sect. 4.2 will form the basis for the *rigorous solution* of the acceleration approach in Sect. 4.2.1. This type of solution still requires the solution of the variational equations which leads ultimately to the development of an *approximate solution* valid under specific assumptions as the name already implies. Section 4.2.2 will discuss this often implemented solution and shows the limitations of this approach. Last but not least an alternative approach is developed in Sect. 4.2.3 which is based on rotational quantities, namely rotation-rates and changes in rotation-rates. It forms a theoretical framework to better understand and exploit low-low satellite-to-satellite tracking systems under the condition that the rotational quantities can be observed with the precision required to match the inter-satellite observations which is nowadays not the case.

4.1.1 Newton's Equation of Motion

For the acceleration approach two fundamental equations are needed. First the Newton's second law of motion:

$$\mathbf{F} = m\,\mathbf{a}, \tag{4.1}$$

where $\mathbf{F}$ is the force, m the mass of a body and $\mathbf{a}$ the acceleration. Equation (4.1) is already written in the form introduced by Leonard Euler. Newton wrote his version originally in the form of impulses on the right-hand side [111]. It is important to note the difference between the left-hand, i.e. the force, and the right-hand side (here acceleration) of Eq. (4.1). The left-hand side contains dynamical quantities, whereas the right-hand side denote kinematic quantities. Although the difference seems trivial it is fundamental to space geodesy and the subsequent discussions. The difference in the handling of these two quantities will become more evident in Sect. 4.1.2. Finally, an equation of motion is formed by equalizing kinematic and dynamic quantities as done in case of Eq. (4.1).

For satellite motions the second important equation is Newton's universal law of gravitation:

$$\mathbf{F}_{12} = -G\frac{m_1\,m_2}{r_{12}^2}\mathbf{e}_{12}, \tag{4.2}$$

where $\mathbf{F}_{12}$ is the force vector acting on the connecting line $\mathbf{e}_{12}$ between two bodies of mass m_1 and m_2 separated by the distance r_{12}. G is the gravitational constant which happens to be the least well known fundamental physical constant of modern physics. Equation (4.2) states that the force between two attracting bodies is proportional to the individual masses and inversely proportional to the square ot the distance. Obviously $\mathbf{F}_{12} = -\mathbf{F}_{21}$ holds. Note that the law is only valid for point-masses or equivalently homogeneous spheres or shells.

For satellite applications it is convenient to work per unit mass, i.e. $m_1 = M$ and $m_2 = 1$ is assumed. Forming the equation of motion for satellite applications by combining Eqs. (4.1) and (4.2) yields:

$$\mathbf{F}_{12} = -\frac{GM}{r_{12}^3}\mathbf{r}_{12} = \mathbf{a} = \ddot{\mathbf{r}}, \tag{4.3}$$

which is the fundamental equation for the so-called two-body problem. Obviously the acceleration is equal to the second derivative of the position vector $\mathbf{r}$ resulting in a second-order differential equation. The solution can be either achieved analytically or numerically. The analytical solution is best described by the Keplerian solution and the six integration constants of the second-order differential equation are the Keplerian elements. Generally, analytical solutions can only be derived for simple cases whereas solutions for satellites evolving around inhomogeneous bodies like the Earth are only achieved numerically. It is therefore better to denote the integration constants *initial conditions* since they are normally expressed as the initial position and initial velocity of the satellite. Practically, Eq. (4.3) in conjunction with some given initial conditions allows to uniquely define the orbit of a satellite. Vice-versa by observing the position of a satellite one can infer the initial conditions and the underlying force(s). Both cases occur in practical applications depending if one is interested in the position of a satellite or in the forces governing its motion. The acceleration approach is an application of the latter case.

So far we only considered the force of a homogeneous point-mass. The superposition principle allows to extend the left-hand side of Eq. (4.3) by considering all kinds of forces acting on the satellite. Typically these forces are:

- the inhomogeneous part of the Earth's gravity field $\mathbf{f}_{\mathrm{E}}$,
- third-body attractions of the Sun $\mathbf{f}_{\mathrm{S}}$ and the Moon $\mathbf{f}_{\mathrm{M}}$,
- tidal effects $\mathbf{f}_{\mathrm{T}}$,
- atmospheric drag $\mathbf{f}_{\mathrm{D}}$,
- solar radiation pressure $\mathbf{f}_{\mathrm{SP}}$,
- Earth's albedo $\mathbf{f}_{\mathrm{A}}$,
- relativistic effects $\mathbf{f}_{\mathrm{R}}$,
- third-body attractions of other planets and bodies $\mathbf{f}_{\mathrm{P}}$,
- ...

For a detailed discussion on the strength and impact of these forces the reader is referred to the extensive literature, e.g. [104] among many others.

4.1.2 Kinematic Versus Dynamic Quantities

Before being able to formulate the acceleration approach for the low-low satellite-to-satellite tracking case the behavior of kinematic quantities (the right-hand side

of Eq. (4.1)), in a moving frame needs to be reconsidered, especially in the point of view of differentiation. Suppose we have the following relation given:

$$\mathbf{r}_{\mathrm{I}} = R_{\mathrm{I}}^{\mathrm{E}} \mathbf{r}_{\mathrm{E}}. \tag{4.4}$$

$\mathbf{r}_{\mathrm{I}}$ describes the position of a body or satellite in the inertial frame which is equal to a position in a moving frame E rotated by the rotation matrix $R_{\mathrm{I}}^{\mathrm{E}}$. For convenience and an easier understanding the moving frame is here denoted by E following the Earth-fixed frame but the derivations are valid for any moving frame related to the inertial frame in the form of Eq. (4.4). For differentiation it has to be taken into account that the rotation matrix is not time-invariant and thus the temporal derivative $\dot{R}_{\mathrm{I}}^{\mathrm{E}}$ is not zero. Applying the multiplication rule and solving for the velocity in the moving frame yields:

$$\dot{\mathbf{r}}_{\mathrm{E}} = R_{\mathrm{E}}^{\mathrm{I}} \dot{\mathbf{r}}_{\mathrm{I}} - R_{\mathrm{E}}^{\mathrm{I}} \dot{R}_{\mathrm{I}}^{\mathrm{E}} \mathbf{r}_{\mathrm{E}} \tag{4.5}$$

Introducing the Cartan matrix $\Omega = R_{\mathrm{E}}^{\mathrm{I}} \dot{R}_{\mathrm{I}}^{\mathrm{E}}$ and the rotation vector ω Eq. (4.5) can be rewritten as:

$$\dot{\mathbf{r}}_{\mathrm{E}} = R_{\mathrm{E}}^{\mathrm{I}} \dot{\mathbf{r}}_{\mathrm{I}} - \Omega \mathbf{r}_{\mathrm{E}} = R_{\mathrm{E}}^{\mathrm{I}} \dot{\mathbf{r}}_{\mathrm{I}} - \omega \times \mathbf{r}_{\mathrm{E}} \tag{4.6}$$

The derivation of acceleration in a moving frame results from another differentiation:

$$\ddot{\mathbf{r}}_{\mathrm{E}} = R_{\mathrm{E}}^{\mathrm{I}} \ddot{\mathbf{r}}_{\mathrm{I}} - 2\omega \times \dot{\mathbf{r}}_{\mathrm{E}} - \omega \times (\omega \times \mathbf{r}_{\mathrm{E}}) - \dot{\omega} \times \mathbf{r}_{\mathrm{E}}, \tag{4.7}$$

where the second term on the right-hand side is generally known as the Coriolis acceleration, the third term as the centrifugal acceleration and the last term as the Euler acceleration.

An equation of motion is then formed identically as in the case of inertial quantities by equalizing kinematic and dynamic quantities, i.e.:

$$\ddot{\mathbf{r}}_{\mathrm{E}} + 2\omega \times \dot{\mathbf{r}}_{\mathrm{E}} + \omega \times (\omega \times \mathbf{r}_{\mathrm{E}}) + \dot{\omega} \times \mathbf{r}_{\mathrm{E}} = R_{\mathrm{E}}^{\mathrm{I}} \mathbf{F}_{\mathrm{I}} \tag{4.8}$$

Confer to Eq. (4.3) and note the different handling of kinematic and dynamical quantities. Dynamics or forces only change their orientation according to the motion of the body whereas for kinematic quantities the so-called apparent accelerations need to be considered which in-turn depend on the motion of the frame.

4.2 Mathematical Description of the Acceleration Approach

Before going into the detailed derivation of the approach it is mandatory to understand the geometry of the GRACE system. Figure 4.1 visualizes the general setup.

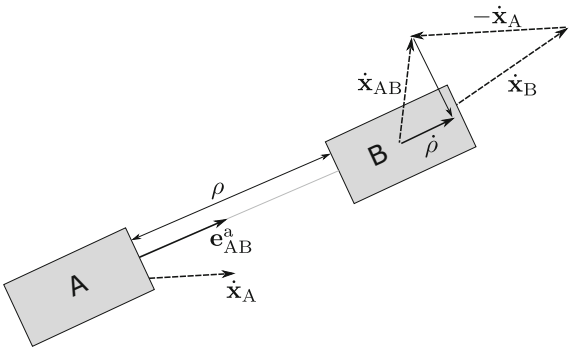

Fig. 4.1 Geometry of the GRACE system adapted from [127]

The range ρ is observed which is the distance between two satellites A and B. It is equivalent to the relative position $\mathbf{x}_{AB}$ projected on the LOS expressed by the unit vector $\mathbf{e}^a_{AB}$ along the connecting line from satellite A to B.

$$\rho = \mathbf{x}_{AB} \cdot \mathbf{e}^a_{AB} = (\mathbf{x}_B - \mathbf{x}_A) \cdot \mathbf{e}^a_{AB}. \tag{4.9}$$

Similarly, the relative velocity vector $\dot{\mathbf{x}}_{AB}$ is formed by taking the difference between the two velocity vectors $\dot{\mathbf{x}}_A$ and $\dot{\mathbf{x}}_B$ of the two satellites. This resulting vector is nearly perpendicular to the LOS vector and thus the projection of the range-rate $\dot{\rho}$ results in relatively small numbers:

$$\dot{\rho} = \dot{\mathbf{x}}_{AB} \cdot \mathbf{e}^a_{AB} = (\dot{\mathbf{x}}_B - \dot{\mathbf{x}}_A) \cdot \mathbf{e}^a_{AB}. \tag{4.10}$$

From a theoretical point of view it would therefore be much better to fly two satellites in a radial separation but obviously the satellites will drift apart due to their different orbital velocity. This concept was actually discussed in [127] but practically only an along-track separation is feasible.

For the derivation of the acceleration approach Eq. (4.9) is rearranged in order to express the inertial relative position vector $\mathbf{x}_{AB}$ as the (scalar) range times the LOS unit vector. Applying differentiation twice yields expressions containing the relative velocity vector $\dot{\mathbf{x}}_{AB}$ and the relative acceleration vector $\ddot{\mathbf{x}}_{AB}$ on the left-hand side and combinations of inter-satellite quantities on the right-hand side.

$$\mathbf{x}_{AB} = \rho\, \mathbf{e}^a_{AB} \tag{4.11a}$$

$$\dot{\mathbf{x}}_{AB} = \dot{\rho}\, \mathbf{e}^a_{AB} + \rho\, \dot{\mathbf{e}}^a_{AB} \tag{4.11b}$$

$$\ddot{\mathbf{x}}_{AB} = \ddot{\rho}\, \mathbf{e}^a_{AB} + 2\, \dot{\rho}\, \dot{\mathbf{e}}^a_{AB} + \rho\, \ddot{\mathbf{e}}^a_{AB}. \tag{4.11c}$$

Equation (4.10) can be derived by multiplying both sides of (4.11b) with $\mathbf{e}^a_{AB}$. Since $\mathbf{e}^a_{AB}$ and $\dot{\mathbf{e}}^a_{AB}$ are perpendicular to each other the last term on the right-hand side of Eq. (4.11b) will cancel. The LOS-vector $\mathbf{e}^a_{AB}$ is part of a right-handed reference frame moving with the satellite system and is denoted here as the *instantaneous relative*

reference frame (IRRF). One convenient choice to complete the reference frame is calculated according to:

$$\mathbf{e}^{\mathrm{a}}_{\mathrm{AB}} = \frac{\mathbf{x}_{\mathrm{AB}}}{|\mathbf{x}_{\mathrm{AB}}|} \tag{4.12a}$$

$$\mathbf{e}^{\mathrm{v}}_{\mathrm{AB}} = \frac{\dot{\mathbf{x}}_{\mathrm{AB}}}{|\dot{\mathbf{x}}_{\mathrm{AB}}|} \tag{4.12b}$$

$$\mathbf{e}^{\mathrm{c}}_{\mathrm{AB}} = \frac{\mathbf{e}^{\mathrm{v}}_{\mathrm{AB}} \times \mathbf{e}^{\mathrm{a}}_{\mathrm{AB}}}{|\mathbf{e}^{\mathrm{v}}_{\mathrm{AB}} \times \mathbf{e}^{\mathrm{a}}_{\mathrm{AB}}|} \tag{4.12c}$$

$$\mathbf{e}^{\mathrm{r}}_{\mathrm{AB}} = \frac{\mathbf{e}^{\mathrm{a}}_{\mathrm{AB}} \times \mathbf{e}^{\mathrm{c}}_{\mathrm{AB}}}{|\mathbf{e}^{\mathrm{a}}_{\mathrm{AB}} \times \mathbf{e}^{\mathrm{c}}_{\mathrm{AB}}|} \tag{4.12d}$$

In Eq. (4.12) the unit vector formed by the relative velocity vector in Eq. (4.12b) is an intermediate quantity which is aligned with the relative velocity vector but not perpendicular to the LOS-vector. Nevertheless, $\mathbf{e}^{\mathrm{a}}_{\mathrm{AB}}$ and $\mathbf{e}^{\mathrm{v}}_{\mathrm{AB}}$ form a plane that contains the desired unit vector perpendicular to the LOS-vector. This vector will form the radial direction as it is in the orbital plane spanned by the two aforementioned unit vectors and directed outward, i.e. away from the Earth's surface. Note that this vector is significantly different from the radial unit vectors of each individual satellite. For its derivation the cross-track unit vector $\mathbf{e}^{\mathrm{c}}_{\mathrm{AB}}$ is first derived by forming the cross product of $\mathbf{e}^{\mathrm{a}}_{\mathrm{AB}}$ and $\mathbf{e}^{\mathrm{v}}_{\mathrm{AB}}$ which is pointing outside the plane formed by the LOS- and the unit vector of the relative velocity. Using the cross product one more time and applying it to the along-track and cross-track unit vectors $\mathbf{e}^{\mathrm{a}}_{\mathrm{AB}}$ and $\mathbf{e}^{\mathrm{c}}_{\mathrm{AB}}$, respectively, the searched-for radial unit vector $\mathbf{e}^{\mathrm{r}}_{\mathrm{AB}}$ can be derived. The IRRF will also play an important role if the acceleration approach is expressed with rotational quantities, c.f. also Sect. 4.2.3.

Multiplying Eq. (4.11c) with these three unit vectors rotates the inertial relative acceleration into the IRRF yielding after the consideration of orthogonalities:

$$\ddot{\mathbf{x}}_{\mathrm{AB}} \cdot \mathbf{e}^{\mathrm{a}}_{\mathrm{AB}} = \ddot{\rho} + 0 + \rho\, \ddot{\mathbf{e}}^{\mathrm{a}}_{\mathrm{AB}} \cdot \mathbf{e}^{\mathrm{a}}_{\mathrm{AB}} \tag{4.13a}$$

$$\ddot{\mathbf{x}}_{\mathrm{AB}} \cdot \mathbf{e}^{\mathrm{c}}_{\mathrm{AB}} = 0 + 0 + \rho\, \ddot{\mathbf{e}}^{\mathrm{a}}_{\mathrm{AB}} \cdot \mathbf{e}^{\mathrm{c}}_{\mathrm{AB}} \tag{4.13b}$$

$$\ddot{\mathbf{x}}_{\mathrm{AB}} \cdot \mathbf{e}^{\mathrm{r}}_{\mathrm{AB}} = 0 + 2\,\dot{\rho}\,|\dot{\mathbf{e}}^{\mathrm{a}}_{\mathrm{AB}}| + \rho\, \ddot{\mathbf{e}}^{\mathrm{a}}_{\mathrm{AB}} \cdot \mathbf{e}^{\mathrm{r}}_{\mathrm{AB}}. \tag{4.13c}$$

For the GRACE scenario the applicable equation is (4.13a) but the reader should keep in mind that the acceleration approach is generally a three-dimensional approach. The full exploitation of the approach however requires the observation of the unit vector(s) and its derivatives with the same precision as the inter-satellite observations which is not possible with GPS. Only Eq. (4.13a) can be solved for the range acceleration yielding an observation on the left-hand side which solely comes from the K-Band system. For the last term in (4.13a) the following relations hold which make the connection to the relative velocity vector and thus the influence by GPS clear:

$$\rho\, \ddot{\mathbf{e}}^{\mathrm{a}}_{\mathrm{AB}} \cdot \mathbf{e}^{\mathrm{a}}_{\mathrm{AB}} = \mathbf{x}_{\mathrm{AB}} \cdot \ddot{\mathbf{e}}^{\mathrm{a}}_{\mathrm{AB}} = \dot{\mathbf{x}}_{\mathrm{AB}} \cdot \dot{\mathbf{e}}^{\mathrm{a}}_{\mathrm{AB}}$$
$$= -\rho\, |\dot{\mathbf{e}}^{\mathrm{a}}_{\mathrm{AB}}|^2 = -\frac{1}{\rho} \left(\dot{\mathbf{x}}_{\mathrm{AB}} \cdot \dot{\mathbf{x}}_{\mathrm{AB}} - \dot{\rho}^2 \right). \tag{4.14}$$

The reader is advised to reproduce these relations in order to fully understand the relation between the various components.

So far this section dealt only with the geometry and kinematic quantities. By considering Newton's second law and forming the relation between the relative acceleration vector and the relative gradient of the gravitational field

$$\ddot{\mathbf{x}}_{\mathrm{AB}} = \ddot{\mathbf{x}}_{\mathrm{B}} - \ddot{\mathbf{x}}_{\mathrm{A}} = \nabla V_B - \nabla V_A = \nabla V_{AB},$$

an equation of motion for the case of GRACE can be derived:

$$\nabla V_{AB} \cdot \mathbf{e}^{\mathrm{a}}_{\mathrm{AB}} = \ddot{\rho} - \frac{1}{\rho} \left(\dot{\mathbf{x}}_{\mathrm{AB}} \cdot \dot{\mathbf{x}}_{\mathrm{AB}} - \dot{\rho}^2 \right) \tag{4.15}$$

Equation (4.15) is known as the basic equation of the acceleration approach connecting the range acceleration to the gradient of the gravitational field. It is also immediately evident that no integration is necessary if the relative velocity vector $\dot{\mathbf{x}}_{\mathrm{AB}}$ is observed. Obviously it has to be observed with a matching precision on the level of the range acceleration in order to take full advantage of the highly-precise inter-satellite observation. Practically this is not fulfilled in the case of GRACE. The range-quantities are observed with the K-band microwave system with a precision of $\approx 1\,\mu\mathrm{m}$ for the range, $\approx 0.1\ {}^{\mu\mathrm{m}}/_{\mathrm{s}}$ for the range-rate or $\approx 10\ {}^{\mathrm{nm}}/_{\mathrm{s}^2}$ for the range accelerations whereas the relative velocity vector can only be observed with GPS on a precision level of $\approx 0.1\ {}^{\mathrm{mm}}/_{\mathrm{s}}$.

Figure 4.2 shows an example of the impact of GPS errors on the gravity field recovery for a GRACE scenario. The blue solution assumes the relative velocity vector to be error-free and is only limited by errors in the range acceleration which have been simulated as white noise with zero mean and a standard deviation of $\approx 10\ {}^{\mathrm{nm}}/_{\mathrm{s}^2}$. In case of the red solution the simulated GPS observations have also been contaminated with white noise with zero mean and a standard deviation of $\approx 0.1\ {}^{\mathrm{mm}}/_{\mathrm{s}}$. The quality of the gravity field solution consequently reduces by approximately one order of magnitude. For real data this corresponds to solutions based on CHAMP data which are approximately one order of magnitude worse than state-of-the-art gravity field solutions from GRACE. In order to take full advantage of the precision of the K-band observations using the acceleration approach as is, the precision of the relative velocity vector needs to be reduced by two to three orders of magnitude which is unrealistic considering the current knowledge and limitations of GPS observations. Therefore the relative velocity vector has to be considered as unknown which will be discussed in the subsequent section and will be coined the *rigorous solution*. The careful reader will realize that considering the relative velocity vector as unknown will still require the solution of the variational equations as there is no linear relation between any of the functionals of the gravitational field and the velocity of a satel-

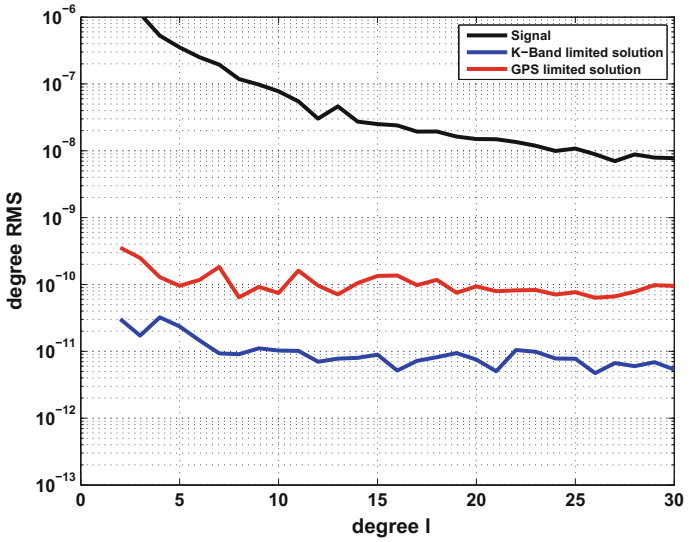

Fig. 4.2 Gravity field recovery from simulated GRACE observations till degree and order 30: signal curve in *black*; K-band limited solution in *blue*; GPS-limited solution in *red*

lite. Strictly speaking the rigorous solution does therefore not belong to the class of in-situ observations but to the class of solutions based on the variational equations. Nevertheless it is important to first present the complete solution before simplifications and assumptions are introduced that allow the solution to be real in-situ. This solution will be called the *approximate solution* and is introduced in Sect. 4.2.2.

4.2.1 Rigorous Solution

GRACE quantities like the relative velocity vector $\dot{\mathbf{x}}_{\mathrm{AB}}$ cannot be observed with the same precision as the K-band system-derived quantities and have to be considered unknown. The mathematical model of the acceleration approach for the low-low satellite-to-satellite tracking (ll-SST) case is therefore given as:

$$\begin{aligned}\ddot{\rho} &= \ddot{\mathbf{x}}_{\mathrm{AB}} \cdot \mathbf{e}^{\mathrm{a}}_{\mathrm{AB}} + \frac{1}{\rho}\dot{\mathbf{x}}_{\mathrm{AB}} \cdot \dot{\mathbf{x}}_{\mathrm{AB}} - \frac{\dot{\rho}^2}{\rho} \\ &= (\nabla V_B - \nabla V_A) \cdot \mathbf{e}^{\mathrm{a}}_{\mathrm{AB}} + \frac{1}{\rho}\dot{\mathbf{x}}_{\mathrm{AB}} \cdot \dot{\mathbf{x}}_{\mathrm{AB}} - \frac{\dot{\rho}^2}{\rho} \\ &= f + g_1 + g_2\end{aligned} \tag{4.16}$$

For convenience the abbreviations:

$$\begin{aligned} f = &\quad (\nabla V_B - \nabla V_A) \cdot \mathbf{e}^{\mathrm{a}}_{\mathrm{AB}}, \\ g_1 = &\quad \frac{1}{\rho}\dot{\mathbf{x}}_{\mathrm{AB}} \cdot \dot{\mathbf{x}}_{\mathrm{AB}} \quad \text{and} \\ g_2 = &-\frac{\dot{\rho}^2}{\rho} \end{aligned}$$

are introduced. Note that f actually consists of two parts: (1) the relative gradient and (2) the LOS-vector. The latter is dependent on the position of the satellites and thus on the gravity field. Therefore it will be necessary to split f in Sect. 4.2.1.3 into two components f_1 and f_2 as well. The solution of the variational equations requires the linearisation of the mathematical model. The first step is therefore to introduce a priori observations and reduce the equation system to residual quantities for which a subsequent linearisation holds:

$$\begin{aligned} \ddot{\rho} - \ddot{\rho}^0 = &(\nabla V_B - \nabla V_A) \cdot \mathbf{e}^{\mathrm{a}}_{\mathrm{AB}} + \frac{1}{\rho}\left(\dot{\mathbf{x}}_{\mathrm{AB}} \cdot \dot{\mathbf{x}}_{\mathrm{AB}} - \dot{\rho}^2\right) \\ &- \left(\nabla V^0_B - \nabla V^0_A\right) \cdot \mathbf{e}^{\mathrm{a},0}_{\mathrm{AB}} - \frac{1}{\rho^0}\left(\dot{\mathbf{x}}^0_{\mathrm{AB}} \cdot \dot{\mathbf{x}}^0_{\mathrm{AB}} - \left(\dot{\rho}^0\right)^2\right) \end{aligned} \tag{4.17}$$

Practically it means that some kind of 'observed' orbit is needed to fit and approximate a dynamic orbit. 'Observed' in this context means that it is normally coming from a kinematic or (reduced-)dynamic orbit determination. For GRACE, the GNV1B product or one of the available kinematic orbits may be used. If such an orbit is not available, an initial orbit determination process needs to be included which will multiply the efforts. Linearisation of the right-hand side yields:

$$\ddot{\rho} - \ddot{\rho}^0 \approx \sum_i \frac{\partial f}{\partial p_i}\Delta p_i + \sum_i \frac{\partial g_1}{\partial p_i}\Delta p_i + \sum_i \frac{\partial g_2}{\partial p_i}\Delta p_i \tag{4.18}$$

with

$$\begin{aligned} (\nabla V_B - \nabla V_A) \cdot \mathbf{e}^{\mathrm{a}}_{\mathrm{AB}} - \left(\nabla V^0_B - \nabla V^0_A\right) \cdot \mathbf{e}^{\mathrm{a},0}_{\mathrm{AB}} &= \sum_i \frac{\partial f}{\partial p_i}\Delta p_i + \hbar^2 \\ \frac{1}{\rho}\dot{\mathbf{x}}_{\mathrm{AB}} \cdot \dot{\mathbf{x}}_{\mathrm{AB}} - \frac{1}{\rho^0}\dot{\mathbf{x}}^0_{\mathrm{AB}} \cdot \dot{\mathbf{x}}^0_{\mathrm{AB}} &= \sum_i \frac{\partial g_1}{\partial p_i}\Delta p_i + \hbar^2 \\ -\frac{\dot{\rho}^2}{\rho} + \frac{\left(\dot{\rho}^0\right)^2}{\rho^0} &= \sum_i \frac{\partial g_2}{\partial p_i}\Delta p_i + \hbar^2, \end{aligned}$$

where $\hbar^2$ denotes neglected terms of second order or higher. The parameter p_i represent all unknown parameters that are to be estimated in a least-squares adjustment. These are specifically:

1. six initial conditions $x\,(t_0) \ldots \dot{z}\,(t_0)$ for each of the two satellites,
2. spherical harmonic coefficients $\overline{C}_{lm}$ and $\overline{S}_{lm}$,
3. accelerometer calibration parameters such as bias, drift and scaling,
4. empirical constant or linear accelerations and
5. any possible other parameter of interest ...

After linearisation the acceleration approach can be solved in its rigorous form by solving the variational equations. Most frequently two approaches are used: (1) the classical approach by setting up differential equations for each unknown and (2) the variation of constant approach, e.g. [64]. The second approach is normally faster in the implementation and is followed here.

4.2.1.1 Variational Equations for the Initial Conditions (Homogeneous Solution)

The solution of the variational equations by the method of the variation of constant is a two-step approach. First a homogeneous solution is derived which resembles here the partial derivatives towards the initial conditions of the satellite and subsequently the inhomogeneous solution includes all other parameters of interest. The homogeneous solution yields the partial derivatives of the position $\mathbf{x} = (x, y, z)$ and the velocity $\dot{\mathbf{x}} = (\dot{x}, \dot{y}, \dot{z})$ towards the initial conditions $\mathbf{x}_0 = (x_0, y_0, z_0)$ and $\dot{\mathbf{x}}_0 = (\dot{x}_0, \dot{y}_0, \dot{z}_0)$ which are determined by setting up a system of differential equations and solving them simultaneously with the orbit approximation of the 'observed' orbit by a purely dynamic orbit integration:

$$\frac{d}{dt^2}\Phi = F(\mathbf{x}, \dot{\mathbf{x}}) \cdot \Phi, \tag{4.19}$$

where F is the change in the force function. Theoretically, this tensor has to be set up for all forces included in the orbit integration but practically it is normally sufficient to only consider the gravitational tensor. Φ contains the partial derivative of the position towards the initial conditions, i.e. for every time point the matrix has the dimension $[3 \times 6]$

$$\frac{d}{dt^2}\begin{bmatrix} \frac{\partial x}{\partial x_0} & \frac{\partial x}{\partial y_0} & \cdots & \frac{\partial x}{\partial \dot{z}_0} \\ \frac{\partial y}{\partial x_0} & \frac{\partial y}{\partial y_0} & \cdots & \frac{\partial y}{\partial \dot{z}_0} \\ \frac{\partial z}{\partial x_0} & \frac{\partial z}{\partial y_0} & \cdots & \frac{\partial z}{\partial \dot{z}_0} \end{bmatrix} = \begin{bmatrix} \frac{\partial^2 V}{\partial x^2} & \frac{\partial^2 V}{\partial x \partial y} & \frac{\partial^2 V}{\partial x \partial z} \\ \frac{\partial^2 V}{\partial y \partial x} & \frac{\partial^2 V}{\partial y^2} & \frac{\partial^2 V}{\partial y \partial z} \\ \frac{\partial^2 V}{\partial z \partial x} & \frac{\partial^2 V}{\partial z \partial y} & \frac{\partial^2 V}{\partial z^2} \end{bmatrix} \cdot \begin{bmatrix} \frac{\partial x}{\partial x_0} & \frac{\partial x}{\partial y_0} & \cdots & \frac{\partial x}{\partial \dot{z}_0} \\ \frac{\partial y}{\partial x_0} & \frac{\partial y}{\partial y_0} & \cdots & \frac{\partial y}{\partial \dot{z}_0} \\ \frac{\partial z}{\partial x_0} & \frac{\partial z}{\partial y_0} & \cdots & \frac{\partial z}{\partial \dot{z}_0} \end{bmatrix}$$

Instead of integrating the equation twice, every second order differential equation can be rewritten as a set of first order differential equations:

$$\frac{d}{dt}\begin{pmatrix}\Phi\\ \dot{\Phi}\end{pmatrix}=\begin{pmatrix}\dot{\Phi}\\ F(\mathbf{x},\dot{\mathbf{x}})\cdot\Phi\end{pmatrix} \tag{4.20}$$

The solution will then yield the partial derivatives of position and velocity:

$$\frac{d}{dt}\begin{bmatrix}\frac{\partial x}{\partial x_0} & \frac{\partial x}{\partial y_0} & \cdots & \frac{\partial x}{\partial \dot{x}_0} & \frac{\partial x}{\partial \dot{z}_0}\\ \frac{\partial y}{\partial x_0} & \frac{\partial y}{\partial y_0} & \cdots & \frac{\partial y}{\partial \dot{x}_0} & \frac{\partial y}{\partial \dot{z}_0}\\ \frac{\partial z}{\partial x_0} & \frac{\partial z}{\partial y_0} & \cdots & \frac{\partial z}{\partial \dot{x}_0} & \frac{\partial z}{\partial \dot{z}_0}\\ \frac{\partial \dot{x}}{\partial x_0} & \frac{\partial \dot{x}}{\partial y_0} & \cdots & \frac{\partial \dot{x}}{\partial \dot{x}_0} & \frac{\partial \dot{x}}{\partial \dot{z}_0}\\ \frac{\partial \dot{y}}{\partial x_0} & \frac{\partial \dot{y}}{\partial y_0} & \cdots & \frac{\partial \dot{y}}{\partial \dot{x}_0} & \frac{\partial \dot{y}}{\partial \dot{z}_0}\\ \frac{\partial \dot{z}}{\partial x_0} & \frac{\partial \dot{z}}{\partial y_0} & \cdots & \frac{\partial \dot{z}}{\partial \dot{x}_0} & \frac{\partial \dot{z}}{\partial \dot{z}_0}\end{bmatrix}=\begin{bmatrix}0 & 0 & 0 & 1 & 0 & 0\\ 0 & 0 & 0 & 0 & 1 & 0\\ 0 & 0 & 0 & 0 & 0 & 1\\ \frac{\partial^2 V}{\partial x^2} & \frac{\partial^2 V}{\partial x \partial y} & \frac{\partial^2 V}{\partial x \partial z} & 0 & 0 & 0\\ \frac{\partial^2 V}{\partial y \partial x} & \frac{\partial^2 V}{\partial y^2} & \frac{\partial^2 V}{\partial y \partial z} & 0 & 0 & 0\\ \frac{\partial^2 V}{\partial z \partial x} & \frac{\partial^2 V}{\partial z \partial y} & \frac{\partial^2 V}{\partial z^2} & 0 & 0 & 0\end{bmatrix}\cdot\begin{bmatrix}\frac{\partial x}{\partial x_0} & \frac{\partial x}{\partial y_0} & \cdots & \frac{\partial x}{\partial \dot{x}_0} & \frac{\partial x}{\partial \dot{z}_0}\\ \frac{\partial y}{\partial x_0} & \frac{\partial y}{\partial y_0} & \cdots & \frac{\partial y}{\partial \dot{x}_0} & \frac{\partial y}{\partial \dot{z}_0}\\ \frac{\partial z}{\partial x_0} & \frac{\partial z}{\partial y_0} & \cdots & \frac{\partial z}{\partial \dot{x}_0} & \frac{\partial z}{\partial \dot{z}_0}\\ \frac{\partial \dot{x}}{\partial x_0} & \frac{\partial \dot{x}}{\partial y_0} & \cdots & \frac{\partial \dot{x}}{\partial \dot{x}_0} & \frac{\partial \dot{x}}{\partial \dot{z}_0}\\ \frac{\partial \dot{y}}{\partial x_0} & \frac{\partial \dot{y}}{\partial y_0} & \cdots & \frac{\partial \dot{y}}{\partial \dot{x}_0} & \frac{\partial \dot{y}}{\partial \dot{z}_0}\\ \frac{\partial \dot{z}}{\partial x_0} & \frac{\partial \dot{z}}{\partial y_0} & \cdots & \frac{\partial \dot{z}}{\partial \dot{x}_0} & \frac{\partial \dot{z}}{\partial \dot{z}_0}\end{bmatrix}$$

The equation is integrated along with orbit and yields a $[6\times 6]$ matrix $\Phi(t)$ with the partial derivatives of the position and velocity w.r.t. the initial conditions at each time point t. For completeness the shape and structure of Φ is given:

$$\Phi=\begin{bmatrix}\frac{\partial x}{\partial x_0} & \frac{\partial x}{\partial y_0} & \frac{\partial x}{\partial z_0} & \frac{\partial x}{\partial \dot{x}_0} & \frac{\partial x}{\partial \dot{y}_0} & \frac{\partial x}{\partial \dot{z}_0}\\ \frac{\partial y}{\partial x_0} & \frac{\partial y}{\partial y_0} & \frac{\partial y}{\partial z_0} & \frac{\partial y}{\partial \dot{x}_0} & \frac{\partial y}{\partial \dot{y}_0} & \frac{\partial y}{\partial \dot{z}_0}\\ \frac{\partial z}{\partial x_0} & \frac{\partial z}{\partial y_0} & \frac{\partial z}{\partial z_0} & \frac{\partial z}{\partial \dot{x}_0} & \frac{\partial z}{\partial \dot{y}_0} & \frac{\partial z}{\partial \dot{z}_0}\\ \frac{\partial \dot{x}}{\partial x_0} & \frac{\partial \dot{x}}{\partial y_0} & \frac{\partial \dot{x}}{\partial z_0} & \frac{\partial \dot{x}}{\partial \dot{x}_0} & \frac{\partial \dot{x}}{\partial \dot{y}_0} & \frac{\partial \dot{x}}{\partial \dot{z}_0}\\ \frac{\partial \dot{y}}{\partial x_0} & \frac{\partial \dot{y}}{\partial y_0} & \frac{\partial \dot{y}}{\partial z_0} & \frac{\partial \dot{y}}{\partial \dot{x}_0} & \frac{\partial \dot{y}}{\partial \dot{y}_0} & \frac{\partial \dot{y}}{\partial \dot{z}_0}\\ \frac{\partial \dot{z}}{\partial x_0} & \frac{\partial \dot{z}}{\partial y_0} & \frac{\partial \dot{z}}{\partial z_0} & \frac{\partial \dot{z}}{\partial \dot{x}_0} & \frac{\partial \dot{z}}{\partial \dot{y}_0} & \frac{\partial \dot{z}}{\partial \dot{z}_0}\end{bmatrix}$$

It is convenient to store the elements of the matrix in one single line for one particular epoch. The initial epoch matrix is set equal to the unit matrix. One such matrix is needed for each GRACE satellite.

4.2.1.2 Variation of Constants (Inhomogeneous Solution)

Once the homogeneous solution is derived, the inhomogeneous solution can be derived by the method of the variation of constants where the inhomogeneous solution is formed by a linear combination of the homogeneous solution. The general concept is given as:

$$\boldsymbol{\alpha}_{p_i}(t)=\int_{t_0}^{t}\Phi^{-1}(\tau)\cdot\frac{\partial\mathbf{h}(\tau)}{\partial p_i}d\tau \tag{4.21}$$

$$\boldsymbol{\phi}_{p_i}(t)=\sum_{n=1}^{6}\boldsymbol{\alpha}_{n,p_i}(t)\cdot\Phi_n(t)\,. \tag{4.22}$$

For each unknown parameter, the partial derivative of the force function $\mathbf{h}$ towards the unknown parameter p_i is needed. Details for the considered parameters are listed below. Here this vector is of dimension $[3 \times 1]$ and needs to be augmented by zeros to comply with the shape of Φ, i.e. the partial derivative has the shape:

$$\frac{\partial \mathbf{h}(\tau)}{\partial p_i} = \begin{bmatrix} 0 \\ 0 \\ 0 \\ \partial h_x/\partial p_i \\ \partial h_y/\partial p_i \\ \partial h_z/\partial p_i \end{bmatrix}$$

The vector is multiplied with the inverse of the matrix Φ at time τ and the vectorial weighting factor $\boldsymbol{\alpha}_{p_i}$ for a particular time point t is derived by integrating the product to the time of interest t. t_0 corresponds to the initial epoch, i.e. the time point when the satellite has the coordinates $\mathbf{x}_0 = (x_0, y_0, z_0)$ and $\dot{\mathbf{x}}_0 = (\dot{x}_0, \dot{y}_0, \dot{z}_0)$. Finally, the linear combination is formed by multiplying the columns of Φ with the weighting factor $\boldsymbol{\alpha}_{p_i}$. For each time point t a $[6 \times 1]$ vector containing the partial derivatives of position and velocity towards the desired unknown parameter p_i is the result, i.e.:

$$\boldsymbol{\phi}_{p_i} = \left[\partial x/\partial p_i \;\; \partial y/\partial p_i \;\; \partial z/\partial p_i \;\; \partial \dot{x}/\partial p_i \;\; \partial \dot{y}/\partial p_i \;\; \partial \dot{z}/\partial p_i \right]^T,$$

or in other words $\boldsymbol{\phi}_{p_i}$ describes the change of the orbit in response to a change in the parameter p_i. With the homogeneous solution and the concept for inhomogeneous solution all necessary ingredients to derive the partial derivatives of f, g_1 and g_2 in Sects. 4.2.1.3–4.2.1.5 are available. The last step within this section is to provide the partial derivatives $\frac{\partial \boldsymbol{h}}{\partial p_i}$ for spherical harmonic coefficients, accelerometer parameters such as bias, drift and scaling factors and empirical constant or linear accelerations. The derivation of other parameters of interest is left up to the reader.

Spherical Harmonic Coefficients

The force function due to the gravity field of the Earth is the gradient of the gravitation potential V. The gradient of V at a specific location (λ, ϕ, r) is best calculated using non-singular expressions, e.g. [95]:

$$\nabla V(\lambda, \phi, r) = \begin{bmatrix} \partial V/\partial x_E \\ \partial V/\partial y_E \\ \partial V/\partial z_E \end{bmatrix} = \tag{4.23}$$

$$\frac{GM}{2R^2} \sum_{l=0}^{\infty} \left(\frac{R}{r}\right)^{l+2} \sqrt{\frac{2l+1}{2l+3}} \sum_{m=0}^{l} \overline{C}_{lm} \begin{bmatrix} \overline{R}_{l+1,m-1} - \overline{R}_{l+1,m+1} \\ -\overline{Q}_{l+1,m-1} - \overline{Q}_{l+1,m+1} \\ -2\overline{R}_{l+1,m} \end{bmatrix} + \tag{4.24}$$

$$\overline{S}_{lm} \begin{bmatrix} \overline{Q}_{l+1,m-1} - \overline{Q}_{l+1,m+1} \\ \overline{R}_{l+1,m-1} + \overline{R}_{l+1,m+1} \\ -2\overline{Q}_{l+1,m} \end{bmatrix}$$

with the following definitions:

$$
\begin{aligned}
\overline{R}_{l+1,m+1} &= \overline{P}_{l+1,m+1}\,(\sin\phi)\;\cos\left((m+1)\,\lambda\right) && \sqrt{(l+m+1)\,(l+m+2)\left(1+\delta_{0,m}\right)}\\
\overline{R}_{l+1,m} &= \overline{P}_{l+1,m}\;\;\;(\sin\phi)\;\cos\left(m\lambda\right) && \sqrt{(l-m+1)\,(l+m+1)}\\
\overline{R}_{l+1,m-1} &= \overline{P}_{l+1,m-1}\,(\sin\phi)\;\cos\left((m-1)\,\lambda\right) && \sqrt{(l-m+1)\,(l-m+2)\left(1+\delta_{1,m}\right)}\\
&= 0 \quad \forall\, m \leq 0 &&\\
\overline{Q}_{l+1,m+1} &= \overline{P}_{l+1,m+1}\,(\sin\phi)\;\sin\left((m+1)\,\lambda\right) && \sqrt{(l+m+1)\,(l+m+2)\left(1+\delta_{0,m}\right)}\\
\overline{Q}_{l+1,m} &= \overline{P}_{l+1,m}\;\;\;(\sin\phi)\;\sin\left(m\lambda\right) && \sqrt{(l-m+1)\,(l+m+1)}\\
&= 0 \quad \forall\, m \leq 0 &&\\
\overline{Q}_{l+1,m-1} &= \overline{P}_{l+1,m-1}\,(\sin\phi)\;\sin\left((m-1)\,\lambda\right) && \sqrt{(l-m+1)\,(l-m+2)\left(1+\delta_{1,m}\right)}\\
&= 0 \quad \forall\;\; m \leq 1 &&
\end{aligned}
$$

Using these equations the resulting gradient is given in the Earth-fixed frame, i.e. the equation system yields the partial derivatives of V towards Cartesian Earth-fixed coordinates x_E, y_E and z_E although λ, ϕ and r have been used for the calculation. Taking the derivative towards $\overline{C}_{lm}$ yields:

$$
\begin{aligned}
\frac{\partial \boldsymbol{h}\,(\tau)}{\partial \overline{C}_{lm}} &= \begin{bmatrix} 0\\0\\0\\ \partial h_x/\partial\overline{C}_{lm}\\ \partial h_y/\partial\overline{C}_{lm}\\ \partial h_z/\partial\overline{C}_{lm}\end{bmatrix} = \begin{bmatrix} 0\\0\\0\\ \partial(\partial V/\partial x)/\partial\overline{C}_{lm}\\ \partial(\partial V/\partial y)/\partial\overline{C}_{lm}\\ \partial(\partial V/\partial z)/\partial\overline{C}_{lm}\end{bmatrix} = \\
&= \frac{GM}{2R^2}\left(\frac{R}{r}\right)^{l+2}\sqrt{\frac{2l+1}{2l+3}}\begin{bmatrix} 0\\0\\0\\ R_{\mathrm{I}}^{\mathrm{E}}\begin{pmatrix}\overline{R}_{l+1,m-1}-\overline{R}_{l+1,m+1}\\ -\overline{Q}_{l+1,m-1}-\overline{Q}_{l+1,m+1}\\ -2\overline{R}_{l+1,m}\end{pmatrix}\end{bmatrix}
\end{aligned}
\tag{4.25}
$$

where $R_{\mathrm{I}}^{\mathrm{E}}$ is the rotation matrix from the Earth-fixed to the inertial frame. The solution according to Eqs. (4.21) and (4.22) yields

$$
\boldsymbol{\phi}_{\overline{C}_{lm}} = \left[\,\partial x/\partial\overline{C}_{lm}\;\;\partial y/\partial\overline{C}_{lm}\;\;\partial z/\partial\overline{C}_{lm}\;\;\partial\dot{x}/\partial\overline{C}_{lm}\;\;\partial\dot{y}/\partial\overline{C}_{lm}\;\;\partial\dot{z}/\partial\overline{C}_{lm}\,\right]^T
$$

Analogously the derivative towards the $\overline{S}_{lm}$ is derived:

$$
\frac{\partial \boldsymbol{h}\,(\tau)}{\partial \overline{S}_{lm}} = \begin{bmatrix} 0\\0\\0\\ \partial h_x/\partial\overline{S}_{lm}\\ \partial h_y/\partial\overline{S}_{lm}\\ \partial h_z/\partial\overline{S}_{lm}\end{bmatrix} = \begin{bmatrix} 0\\0\\0\\ \partial(\partial V/\partial x)/\partial\overline{S}_{lm}\\ \partial(\partial V/\partial y)/\partial\overline{S}_{lm}\\ \partial(\partial V/\partial z)/\partial\overline{S}_{lm}\end{bmatrix} = \tag{4.26}
$$

$$= \frac{GM}{2R^2}\left(\frac{R}{r}\right)^{l+2}\sqrt{\frac{2l+1}{2l+3}}\begin{bmatrix} 0 \\ 0 \\ 0 \\ R_{\mathrm{I}}^{\mathrm{E}}\begin{pmatrix} \overline{Q}_{l+1,m-1} - \overline{Q}_{l+1,m+1} \\ \overline{R}_{l+1,m-1} + \overline{R}_{l+1,m+1} \\ -2\overline{Q}_{l+1,m} \end{pmatrix} \end{bmatrix}$$

yielding

$$\boldsymbol{\phi}_{\overline{S}_{lm}} = \left[\, \partial x/\partial \overline{S}_{lm} \;\; \partial y/\partial \overline{S}_{lm} \;\; \partial z/\partial \overline{S}_{lm} \;\; \partial \dot{x}/\partial \overline{S}_{lm} \;\; \partial \dot{y}/\partial \overline{S}_{lm} \;\; \partial \dot{z}/\partial \overline{S}_{lm} \,\right]^T$$

Accelerometer Calibration Parameters (Bias, Drift and Scaling)

The force model for the accelerometer calibration parameters is given as:

$$\mathbf{h}\,(t) = R_I^{SBF}\,(t)\left(S\mathbf{f}^{\mathrm{obs}}\,(t) + \mathbf{b} + \mathbf{d}\,(t - t_0)\right) \tag{4.27}$$

where R_I^{SBF} is the rotation matrix from the space-body to the inertial frame, S a diagonal matrix with scaling parameters, b bias parameters and d drift parameters. In the following the element in the i^{th}-row and j^{th}-column of the rotation matrix will be abbreviated as R_{ij}. The partial derivatives towards the unknown parameters are then given as:

$$\frac{\partial \boldsymbol{h}}{\partial s_x} = \begin{bmatrix} R_{11}\cdot f_x^{\mathrm{obs}} \\ R_{21}\cdot f_y^{\mathrm{obs}} \\ R_{31}\cdot f_z^{\mathrm{obs}} \end{bmatrix} \quad \frac{\partial \boldsymbol{h}}{\partial s_y} = \begin{bmatrix} R_{12}\cdot f_x^{\mathrm{obs}} \\ R_{22}\cdot f_y^{\mathrm{obs}} \\ R_{32}\cdot f_z^{\mathrm{obs}} \end{bmatrix} \quad \frac{\partial \boldsymbol{h}}{\partial s_z} = \begin{bmatrix} R_{13}\cdot f_x^{\mathrm{obs}} \\ R_{23}\cdot f_y^{\mathrm{obs}} \\ R_{33}\cdot f_z^{\mathrm{obs}} \end{bmatrix}$$

$$\frac{\partial \boldsymbol{h}}{\partial b_x} = \begin{bmatrix} R_{11} \\ R_{21} \\ R_{31} \end{bmatrix} \quad \frac{\partial \boldsymbol{h}}{\partial b_y} = \begin{bmatrix} R_{12} \\ R_{22} \\ R_{32} \end{bmatrix} \quad \frac{\partial \boldsymbol{h}}{\partial b_z} = \begin{bmatrix} R_{13} \\ R_{23} \\ R_{33} \end{bmatrix}$$

$$\frac{\partial \boldsymbol{h}}{\partial d_x} = \begin{bmatrix} R_{11}\,(t-t_0) \\ R_{21}\,(t-t_0) \\ R_{31}\,(t-t_0) \end{bmatrix} \quad \frac{\partial \boldsymbol{h}}{\partial d_y} = \begin{bmatrix} R_{12}\,(t-t_0) \\ R_{22}\,(t-t_0) \\ R_{32}\,(t-t_0) \end{bmatrix} \quad \frac{\partial \boldsymbol{h}}{\partial d_z} = \begin{bmatrix} R_{13}\,(t-t_0) \\ R_{23}\,(t-t_0) \\ R_{33}\,(t-t_0) \end{bmatrix}$$

Solving by variation of the constant yields for each time point t:

$$\begin{aligned}
\boldsymbol{\phi}_{s_x} &= [\,\partial x/\partial s_x \;\; \partial y/\partial s_x \;\; \partial z/\partial s_x \;\; \partial \dot{x}/\partial s_x \;\; \partial \dot{y}/\partial s_x \;\; \partial \dot{z}/\partial s_x \;\;]^T \\
\boldsymbol{\phi}_{s_y} &= [\,\partial x/\partial s_y \;\; \partial y/\partial s_y \;\; \partial z/\partial s_y \;\; \partial \dot{x}/\partial s_y \;\; \partial \dot{y}/\partial s_y \;\; \partial \dot{z}/\partial s_y \;\;]^T \\
\boldsymbol{\phi}_{s_z} &= [\,\partial x/\partial s_z \;\; \partial y/\partial s_z \;\; \partial z/\partial s_z \;\; \partial \dot{x}/\partial s_z \;\; \partial \dot{y}/\partial s_y \;\; \partial \dot{z}/\partial s_z \;\;]^T \\
\boldsymbol{\phi}_{b_x} &= [\,\partial x/\partial b_x \;\; \partial y/\partial b_x \;\; \partial z/\partial b_x \;\; \partial \dot{x}/\partial b_x \;\; \partial \dot{y}/\partial b_x \;\; \partial \dot{z}/\partial b_x]^T \\
\boldsymbol{\phi}_{b_y} &= [\,\partial x/\partial b_y \;\; \partial y/\partial b_y \;\; \partial z/\partial b_y \;\; \partial \dot{x}/\partial b_y \;\; \partial \dot{y}/\partial b_y \;\; \partial \dot{z}/\partial b_y]^T \\
\boldsymbol{\phi}_{b_z} &= [\,\partial x/\partial b_z \;\; \partial y/\partial b_z \;\; \partial z/\partial b_z \;\; \partial \dot{x}/\partial b_z \;\; \partial \dot{y}/\partial b_y \;\; \partial \dot{z}/\partial b_z \;\;]^T \\
\boldsymbol{\phi}_{d_x} &= [\,\partial x/\partial d_x \;\; \partial y/\partial d_x \;\; \partial z/\partial d_x \;\; \partial \dot{x}/\partial d_x \;\; \partial \dot{y}/\partial d_x \;\; \partial \dot{z}/\partial d_x]^T \\
\boldsymbol{\phi}_{d_y} &= [\,\partial x/\partial d_y \;\; \partial y/\partial d_y \;\; \partial z/\partial d_y \;\; \partial \dot{x}/\partial d_y \;\; \partial \dot{y}/\partial d_y \;\; \partial \dot{z}/\partial d_y]^T \\
\boldsymbol{\phi}_{d_z} &= [\,\partial x/\partial d_z \;\; \partial y/\partial d_z \;\; \partial z/\partial d_z \;\; \partial \dot{x}/\partial d_z \;\; \partial \dot{y}/\partial d_y \;\; \partial \dot{z}/\partial d_z \;\;]^T\,.
\end{aligned}$$

Piecewise Constant Accelerations

For the orbit-fit empirical accelerations are needed as not all forces can be modeled or observed well. One possible model is to apply piecewise constant accelerations in the orbit frame defined by the three unit vectors:

$$\mathbf{e}_{\mathrm{r}} = \frac{\mathbf{x}}{|\mathbf{x}|} \qquad \mathbf{e}_{\mathrm{c}} = \frac{\mathbf{x} \times \dot{\mathbf{x}}}{|\mathbf{x} \times \dot{\mathbf{x}}|} \qquad \mathbf{e}_{\mathrm{a}} = \frac{\mathbf{e}_{\mathrm{c}} \times \mathbf{e}_{\mathrm{r}}}{|\mathbf{e}_{\mathrm{c}} \times \mathbf{e}_{\mathrm{r}}|} \tag{4.28}$$

designating the radial, along- and cross-track direction. These unit vectors are given in the inertial frame and thus no rotation matrix will be needed as in case of the accelerometer calibration. Note that they differ from the unit vectors of the IRRF as the unit vectors here are specific for each of the satellite whereas the IRRF unit vectors are based on the LOS-vector. The force model is given as:

$$\boldsymbol{h}\,(t) = a_r \cdot \boldsymbol{e}_r\,(t) + a_c \cdot \boldsymbol{e}_c\,(t) + a_a \cdot \boldsymbol{e}_a\,(t)\,. \tag{4.29}$$

The corresponding partial derivatives towards the unknown parameters a_r, a_c and a_a are then easily derived as:

$$\frac{\partial \boldsymbol{h}}{\partial a_r} = \boldsymbol{e}_r \qquad \frac{\partial \boldsymbol{h}}{\partial a_c} = \boldsymbol{e}_c \qquad \frac{\partial \boldsymbol{h}}{\partial a_a} = \boldsymbol{e}_a$$

For the practical implementation the A-matrix requires special treatment if several piecewise constant accelerations in one direction are estimated per arc at the same time. The last entry $\boldsymbol{\phi}_{s_i}\,(t_{end})$ for one particular acceleration needs to be repeated in all subsequent rows, i.e. for all subsequently estimated accelerations the accelerations of previous pieces remain constant. Solving by variation of the constant yields for each piecewise linear arc:

$$\begin{aligned}
\boldsymbol{\phi}_{a_{r_i}} &= [\,\partial x/\partial a_{r_i}\ \partial y/\partial a_{r_i}\ \partial z/\partial a_{r_i}\ \partial \dot{x}/\partial a_{r_i}\ \partial \dot{y}/\partial a_{r_i}\ \partial \dot{z}/\partial a_{r_i}\,]^T \\
\boldsymbol{\phi}_{a_{c_i}} &= [\,\partial x/\partial a_{c_i}\ \partial y/\partial a_{c_i}\ \partial z/\partial a_{c_i}\ \partial \dot{x}/\partial a_{c_i}\ \partial \dot{y}/\partial a_{c_i}\ \partial \dot{z}/\partial a_{c_i}\,]^T \\
\boldsymbol{\phi}_{a_{a_i}} &= [\,\partial x/\partial a_{a_i}\ \partial y/\partial a_{a_i}\ \partial z/\partial a_{a_i}\ \partial \dot{x}/\partial a_{a_i}\ \partial \dot{y}/\partial a_{a_i}\ \partial \dot{z}/\partial a_{a_i}]^T
\end{aligned}$$

Piecewise linear accelerations

Piecewise constant accelerations can easily be extended to piecewise linear accelerations by considering a trend in the force model.

$$\begin{aligned}
\mathbf{h}\,(t) = {} & a_{r_i} \cdot \frac{t - t_{i-1}}{t_i - t_{i-1}} \cdot \mathbf{e}_{\mathrm{r}}\,(t) + a_{r_{i-1}} \cdot \frac{t_i - t}{t_i - t_{i-1}} \cdot \mathbf{e}_{\mathrm{r}}\,(t) \\
& + a_{c_i} \cdot \frac{t - t_{i-1}}{t_i - t_{i-1}} \cdot \mathbf{e}_{\mathrm{c}}\,(t) + a_{c_{i-1}} \cdot \frac{t_i - t}{t_i - t_{i-1}} \cdot \mathbf{e}_{\mathrm{c}}\,(t) \\
& + a_{a_i} \cdot \frac{t - t_{i-1}}{t_i - t_{i-1}} \cdot \mathbf{e}_{\mathrm{a}}\,(t) + a_{a_{i-1}} \cdot \frac{t_i - t}{t_i - t_{i-1}} \cdot \mathbf{e}_{\mathrm{a}}\,(t)\,.
\end{aligned} \tag{4.30}$$

The corresponding partial derivatives towards the unknown parameters a_r, a_c and a_a are then easily derived as:

$$\frac{\partial \mathbf{h}}{\partial a_{r_i}} = \frac{t - t_{i-1}}{t_i - t_{i-1}} \cdot \mathbf{e}_{\mathrm{r}} \qquad \frac{\partial \mathbf{h}}{\partial a_{c_i}} = \frac{t - t_{i-1}}{t_i - t_{i-1}} \cdot \mathbf{e}_{\mathrm{c}} \qquad \frac{\partial \mathbf{h}}{\partial a_{a_i}} = \frac{t - t_{i-1}}{t_i - t_{i-1}} \cdot \mathbf{e}_{\mathrm{a}}$$
$$\frac{\partial \mathbf{h}}{\partial a_{r_{i-1}}} = \frac{t_i - t}{t_i - t_{i-1}} \cdot \mathbf{e}_{\mathrm{r}} \qquad \frac{\partial \mathbf{h}}{\partial a_{c_{i-1}}} = \frac{t_i - t}{t_i - t_{i-1}} \cdot \mathbf{e}_{\mathrm{c}} \qquad \frac{\partial \mathbf{h}}{\partial a_{a_{i-1}}} = \frac{t_i - t}{t_i - t_{i-1}} \cdot \mathbf{e}_{\mathrm{a}}$$

As aforementioned the last entry $\boldsymbol{\phi}_{s_i}(t_{end})$ for one particular acceleration needs to be repeated in all subsequent rows if more than one empirical acceleration is estimated per arc. Solving by the variation of the constant yields:

$$\begin{aligned}
\boldsymbol{\phi}_{a_{r_i}} &= [\,\partial x/\partial a_{r_i}\ \partial y/\partial a_{r_i}\ \partial z/\partial a_{r_i}\ \partial \dot{x}/\partial a_{r_i}\ \partial \dot{y}/\partial a_{r_i}\ \partial \dot{z}/\partial a_{r_i}\ ]^T \\
\boldsymbol{\phi}_{a_{c_i}} &= [\,\partial x/\partial a_{c_i}\ \partial y/\partial a_{c_i}\ \partial z/\partial a_{c_i}\ \partial \dot{x}/\partial a_{c_i}\ \partial \dot{y}/\partial a_{c_i}\ \partial \dot{z}/\partial a_{c_i}\ ]^T \\
\boldsymbol{\phi}_{a_{a_i}} &= [\,\partial x/\partial a_{a_i}\ \partial y/\partial a_{a_i}\ \partial z/\partial a_{a_i}\ \partial \dot{x}/\partial a_{a_i}\ \partial \dot{y}/\partial a_{a_i}\ \partial \dot{z}/\partial a_{a_i}]^T\,.
\end{aligned}$$

After deriving the partial derivatives of the coordinates towards all parameters of interest the final step is to connect these partial derivatives to the linearized mathematical model in Eq. (4.18) by applying the chain-rule.

4.2.1.3 Partial Derivatives for f

The term f is the relative gravity vector $(\nabla V_B - \nabla V_A)$ projected on the LOS-vector $\mathbf{e}^{\mathrm{a}}_{\mathrm{AB}}$. As mentioned before the term needs to be split into two parts as both the relative gravity vector as well as the LOS-vector depend on the gravity field.

$$f = (\nabla V_B - \nabla V_A) \cdot \mathbf{e}^{\mathrm{a}}_{\mathrm{AB}} \tag{4.31}$$

The line-of-sight vector $\mathbf{e}^{\mathrm{a}}_{\mathrm{AB}}$ is given as:

$$\mathbf{e}^{\mathrm{a}}_{\mathrm{AB}} = \frac{\mathbf{x}_{\mathrm{AB}}}{|\mathbf{x}_{\mathrm{AB}}|} = \frac{1}{\sqrt{(x_B - x_A)^2 + (y_B - y_A)^2 + (z_B - z_A)^2}} \begin{bmatrix} x_B - x_A \\ y_B - y_A \\ z_B - z_A \end{bmatrix} \tag{4.32}$$

Applying the chain rule yields:

$$\begin{aligned}
\frac{\partial f}{\partial p_i} &= \frac{\partial}{\partial p_i} (\nabla V_B - \nabla V_A) \cdot \mathbf{e}^{\mathrm{a}}_{\mathrm{AB}} + (\nabla V_B - \nabla V_A) \cdot \frac{\partial \mathbf{e}^{\mathrm{a}}_{\mathrm{AB}}}{\partial p_i} \\
\frac{\partial f}{\partial p_i} &= \frac{\partial f_1}{\partial p_i} + \frac{\partial f_2}{\partial p_i}
\end{aligned} \tag{4.33}$$

For most of the unknown parameters of interest their partial derivatives derived in Sects. 4.2.1.1 and 4.2.1.2 are linked via applying the chain-rule and substitution to

Eq. (4.34). The partial derivatives of the relative gravity vector w.r.t. the spherical harmonic coefficients are the only exception as they can be derived analytically.

Partial Derivatives Towards $\overline{C}_{lm}$ and $\overline{S}_{lm}$

The partial derivatives of f towards the spherical harmonics consist of two terms: (1) the derivative of the relative gravity vector and (2) the derivative of the line-of-sight vector. Thus the chain rule needs to be applied. The relation is given as:

$$\begin{aligned}\frac{\partial f_1}{\partial \overline{C}_{lm}} = & \frac{\partial(\partial V_B/\partial x_E)}{\partial \overline{C}_{lm}} \cdot e^0_{AB,x_E} + \frac{\partial(\partial V_B/\partial y_E)}{\partial \overline{C}_{lm}} \cdot e^0_{AB,y_E} + \frac{\partial(\partial V_B/\partial z_E)}{\partial \overline{C}_{lm}} \cdot e^0_{AB,z_E} \\ & - \frac{\partial(\partial V_A/\partial x_E)}{\partial \overline{C}_{lm}} \cdot e^0_{AB,x_E} - \frac{\partial(\partial V_A/\partial y_E)}{\partial \overline{C}_{lm}} \cdot e^0_{AB,y_E} - \frac{\partial(\partial V_A/\partial z_E)}{\partial \overline{C}_{lm}} \cdot e^0_{AB,z_E}\end{aligned} \tag{4.34}$$

$$\begin{aligned}\frac{\partial f_2}{\partial \overline{C}_{lm}} = & \frac{1}{\left(\rho^0\right)^3} \cdot \left(\nabla V^0_B - \nabla V^0_A\right) \cdot \begin{bmatrix} \left(x^0_B - x^0_A\right)^2 - \left(\rho^0\right)^2 \\ \left(x^0_B - x^0_A\right)\left(y^0_B - y^0_A\right) \\ \left(x^0_B - x^0_A\right)\left(z^0_B - z^0_A\right) \end{bmatrix} \cdot \left(\frac{\partial x_A}{\partial \overline{C}_{lm}} - \frac{\partial x_B}{\partial \overline{C}_{lm}}\right) \\ & + \frac{1}{\left(\rho^0\right)^3} \cdot \left(\nabla V^0_B - \nabla V^0_A\right) \cdot \begin{bmatrix} \left(x^0_B - x^0_A\right)\left(y^0_B - y^0_A\right) \\ \left(y^0_B - y^0_A\right)^2 - \left(\rho^0\right)^2 \\ \left(y^0_B - y^0_A\right)\left(z^0_B - z^0_A\right) \end{bmatrix} \cdot \left(\frac{\partial y_A}{\partial \overline{C}_{lm}} - \frac{\partial y_B}{\partial \overline{C}_{lm}}\right) \\ & + \frac{1}{\left(\rho^0\right)^3} \cdot \left(\nabla V^0_B - \nabla V^0_A\right) \cdot \begin{bmatrix} \left(x^0_B - x^0_A\right)\left(z^0_B - z^0_A\right) \\ \left(y^0_B - y^0_A\right)\left(z^0_B - z^0_A\right) \\ \left(z^0_B - z^0_A\right)^2 - \left(\rho^0\right)^2 \end{bmatrix} \cdot \left(\frac{\partial z_A}{\partial \overline{C}_{lm}} - \frac{\partial z_B}{\partial \overline{C}_{lm}}\right)\end{aligned} \tag{4.35}$$

The Taylor-point of the linearisation is the a priori orbit. For convenience the partial derivatives of the relative gravity vector are best determined in the Earth-fixed frame and the partial derivatives are given in Eq. (4.25). Being in the Earth-fixed frame, the Earth-fixed LOS-vector needs to be derived by rotation. For partial derivatives related to $\mathbf{e}^{\mathrm{a}}_{\mathrm{AB}}$ the gravity vector needs to be determined in the inertial frame. Remember that the gravity vector is a force, i.e. dynamical quantity, and the Earth-fixed gravity vector can therefore be rotated to the inertial frame by using the rotation matrix from the Earth-fixed to the inertial frame $R^{\mathrm{E}}_{\mathrm{I}}$, c.f. Sect. 4.1.2.

Analogously the derivative towards $\overline{S}_{lm}$ can be determined.

$$\begin{aligned}\frac{\partial f_1}{\partial \overline{S}_{lm}} = & \frac{\partial(\partial V_B/\partial x_E)}{\partial \overline{S}_{lm}} \cdot e^0_{AB,x_E} + \frac{\partial(\partial V_B/\partial y_E)}{\partial \overline{S}_{lm}} \cdot e^0_{AB,y_E} + \frac{\partial(\partial V_B/\partial z_E)}{\partial \overline{S}_{lm}} \cdot e^0_{AB,z_E} \\ & - \frac{\partial(\partial V_A/\partial x_E)}{\partial \overline{S}_{lm}} \cdot e^0_{AB,x_E} - \frac{\partial(\partial V_A/\partial y_E)}{\partial \overline{S}_{lm}} \cdot e^0_{AB,y_E} - \frac{\partial(\partial V_A/\partial z_E)}{\partial \overline{S}_{lm}} \cdot e^0_{AB,z_E}\end{aligned} \tag{4.36}$$

$$\frac{\partial f_2}{\partial \overline{S}_{lm}} = \frac{1}{\left(\rho^0\right)^3} \cdot \left(\nabla V_B^0 - \nabla V_A^0\right) \cdot \begin{bmatrix} \left(x_B^0 - x_A^0\right)^2 - \left(\rho^0\right)^2 \\ \left(x_B^0 - x_A^0\right)\left(y_B^0 - y_A^0\right) \\ \left(x_B^0 - x_A^0\right)\left(z_B^0 - z_A^0\right) \end{bmatrix} \cdot \left(\frac{\partial x_A}{\partial \overline{S}_{lm}} - \frac{\partial x_B}{\partial \overline{S}_{lm}}\right) \tag{4.37}$$

$$+ \frac{1}{\left(\rho^0\right)^3} \cdot \left(\nabla V_B^0 - \nabla V_A^0\right) \cdot \begin{bmatrix} \left(x_B^0 - x_A^0\right)\left(y_B^0 - y_A^0\right) \\ \left(y_B^0 - y_A^0\right)^2 - \left(\rho^0\right)^2 \\ \left(y_B^0 - y_A^0\right)\left(z_B^0 - z_A^0\right) \end{bmatrix} \cdot \left(\frac{\partial y_A}{\partial \overline{S}_{lm}} - \frac{\partial y_B}{\partial \overline{S}_{lm}}\right)$$

$$+ \frac{1}{\left(\rho^0\right)^3} \cdot \left(\nabla V_B^0 - \nabla V_A^0\right) \cdot \begin{bmatrix} \left(x_B^0 - x_A^0\right)\left(z_B^0 - z_A^0\right) \\ \left(y_B^0 - y_A^0\right)\left(z_B^0 - z_A^0\right) \\ \left(z_B^0 - z_A^0\right)^2 - \left(\rho^0\right)^2 \end{bmatrix} \cdot \left(\frac{\partial z_A}{\partial \overline{S}_{lm}} - \frac{\partial z_B}{\partial \overline{S}_{lm}}\right)$$

Partial Derivatives Towards All Other Unknown Parameters

The partial derivatives of f towards all other parameters resemble the same structure. Introducing the elements of the gravity tensor V_{jj}^{i} in the inertial frame, rotating the line-of-sight vector to the inertial frame $\mathbf{e}_{\mathrm{AB}}^{\mathrm{a}}$ and applying the chain rule yields for GRACE A:

$$\begin{aligned} \frac{\partial f_1}{\partial p_{i_A}} = &- \left[V_{\mathrm{xx,A}}^{\mathrm{i},0} e_{\mathrm{AB,x}}^{\mathrm{i},0} + V_{\mathrm{xy,A}}^{\mathrm{i},0} e_{\mathrm{AB,y}}^{\mathrm{i},0} + V_{\mathrm{xz,A}}^{\mathrm{i},0} e_{\mathrm{AB,z}}^{\mathrm{i},0}\right] \cdot \frac{\partial x_A}{\partial p_{i_A}} \\ &- \left[V_{\mathrm{yx,A}}^{\mathrm{i},0} e_{\mathrm{AB,x}}^{\mathrm{i},0} + V_{\mathrm{yy,A}}^{\mathrm{i},0} e_{\mathrm{AB,y}}^{\mathrm{i},0} + V_{\mathrm{yz,A}}^{\mathrm{i},0} e_{\mathrm{AB,z}}^{\mathrm{i},0}\right] \cdot \frac{\partial y_A}{\partial p_{i_A}} \\ &- \left[V_{\mathrm{zx,A}}^{\mathrm{i},0} e_{\mathrm{AB,x}}^{\mathrm{i},0} + V_{\mathrm{zy,A}}^{\mathrm{i},0} e_{\mathrm{AB,y}}^{\mathrm{i},0} + V_{\mathrm{zz,A}}^{\mathrm{i},0} e_{\mathrm{AB,z}}^{\mathrm{i},0}\right] \cdot \frac{\partial z_A}{\partial p_{i_A}} \end{aligned} \tag{4.38}$$

$$\begin{aligned} \frac{\partial f_2}{\partial p_{i_A}} = &\frac{1}{\left(\rho^0\right)^3} \cdot \left(\nabla V_B^0 - \nabla V_A^0\right) \cdot \begin{bmatrix} \left(x_B^0 - x_A^0\right)^2 - \left(\rho^0\right)^2 \\ \left(x_B^0 - x_A^0\right)\left(y_B^0 - y_A^0\right) \\ \left(x_B^0 - x_A^0\right)\left(z_B^0 - z_A^0\right) \end{bmatrix} \cdot \frac{\partial x_A}{\partial p_{i_A}} \\ &+ \frac{1}{\left(\rho^0\right)^3} \cdot \left(\nabla V_B^0 - \nabla V_A^0\right) \cdot \begin{bmatrix} \left(x_B^0 - x_A^0\right)\left(y_B^0 - y_A^0\right) \\ \left(y_B^0 - y_A^0\right)^2 - \left(\rho^0\right)^2 \\ \left(y_B^0 - y_A^0\right)\left(z_B^0 - z_A^0\right) \end{bmatrix} \cdot \frac{\partial y_A}{\partial p_{i_A}} \\ &+ \frac{1}{\left(\rho^0\right)^3} \cdot \left(\nabla V_B^0 - \nabla V_A^0\right) \cdot \begin{bmatrix} \left(x_B^0 - x_A^0\right)\left(z_B^0 - z_A^0\right) \\ \left(y_B^0 - y_A^0\right)\left(z_B^0 - z_A^0\right) \\ \left(z_B^0 - z_A^0\right)^2 - \left(\rho^0\right)^2 \end{bmatrix} \cdot \frac{\partial z_A}{\partial p_{i_A}} \end{aligned} \tag{4.39}$$

Analogously for GRACE B:

$$\begin{aligned}\frac{\partial f_1}{\partial p_{i_B}} = &\left[V^{\mathrm{i},0}_{\mathrm{xx,B}} e^{\mathrm{i},0}_{\mathrm{AB,x}} + V^{\mathrm{i},0}_{\mathrm{xy,B}} e^{\mathrm{i},0}_{\mathrm{AB,y}} + V^{\mathrm{i},0}_{\mathrm{xz,B}} e^{\mathrm{i},0}_{\mathrm{AB,z}}\right] \cdot \frac{\partial x_B}{\partial p_{i_B}} \\ &+ \left[V^{\mathrm{i},0}_{\mathrm{yx,B}} e^{\mathrm{i},0}_{\mathrm{AB,x}} + V^{\mathrm{i},0}_{\mathrm{yy,B}} e^{\mathrm{i},0}_{\mathrm{AB,y}} + V^{\mathrm{i},0}_{\mathrm{yz,B}} e^{\mathrm{i},0}_{\mathrm{AB,z}}\right] \cdot \frac{\partial y_B}{\partial p_{i_B}} \\ &+ \left[V^{\mathrm{i},0}_{\mathrm{zx,B}} e^{\mathrm{i},0}_{\mathrm{AB,x}} + V^{\mathrm{i},0}_{\mathrm{zy,B}} e^{\mathrm{i},0}_{\mathrm{AB,y}} + V^{\mathrm{i},0}_{\mathrm{zz,B}} e^{\mathrm{i},0}_{\mathrm{AB,z}}\right] \cdot \frac{\partial z_B}{\partial p_{i_B}}\end{aligned} \tag{4.40}$$

$$\begin{aligned}\frac{\partial f_2}{\partial p_{i_B}} = &- \frac{1}{\left(\rho^0\right)^3} \cdot \left(\nabla V_B^0 - \nabla V_A^0\right) \cdot \begin{bmatrix} \left(x_B^0 - x_A^0\right)^2 - \left(\rho^0\right)^2 \\ \left(x_B^0 - x_A^0\right)\left(y_B^0 - y_A^0\right) \\ \left(x_B^0 - x_A^0\right)\left(z_B^0 - z_A^0\right) \end{bmatrix} \cdot \frac{\partial x_B}{\partial p_{i_B}} \\ &- \frac{1}{\left(\rho^0\right)^3} \cdot \left(\nabla V_B^0 - \nabla V_A^0\right) \cdot \begin{bmatrix} \left(x_B^0 - x_A^0\right)\left(y_B^0 - y_A^0\right) \\ \left(y_B^0 - y_A^0\right)^2 - \left(\rho^0\right)^2 \\ \left(y_B^0 - y_A^0\right)\left(z_B^0 - z_A^0\right) \end{bmatrix} \cdot \frac{\partial y_B}{\partial p_{i_B}} \\ &- \frac{1}{\left(\rho^0\right)^3} \cdot \left(\nabla V_B^0 - \nabla V_A^0\right) \cdot \begin{bmatrix} \left(x_B^0 - x_A^0\right)\left(z_B^0 - z_A^0\right) \\ \left(y_B^0 - y_A^0\right)\left(z_B^0 - z_A^0\right) \\ \left(z_B^0 - z_A^0\right)^2 - \left(\rho^0\right)^2 \end{bmatrix} \cdot \frac{\partial z_B}{\partial p_{i_B}}\end{aligned} \tag{4.41}$$

p_{i_A} and p_{i_B} need to be replaced depending on the unknown of interest according to the following scheme:

initial conditions: $x_0, y_0, z_0, \dot{x}_0, \dot{y}_0, \dot{z}_0$
accelerometer parameter: $s_x, s_y, s_z, b_x, b_y, b_z, d_x, d_y, d_z$
empirical accelerations: a_r, a_c, a_a

4.2.1.4 Partial Derivatives for g_1

The term g_1 consists of the square of the length of the relative velocity vector divided by the range:

$$g_1 = \frac{1}{\rho} \dot{\mathbf{x}}_{\mathrm{AB}} \cdot \dot{\mathbf{x}}_{\mathrm{AB}} \tag{4.42}$$

with

$$\begin{aligned}\dot{\mathbf{x}}_{\mathrm{AB}} \cdot \dot{\mathbf{x}}_{\mathrm{AB}} &= (\dot{x}_B - \dot{x}_A)^2 + (\dot{y}_B - \dot{y}_A)^2 + (\dot{z}_B - \dot{z}_A)^2 \\ \rho &= \sqrt{(x_B - x_A)^2 + (y_B - y_A)^2 + (z_B - z_A)^2}\end{aligned}$$

Remember that the relative velocity vector can only be observed by GPS currently and cannot be determined with sufficient precision in order to take full advantage of the K-band observations. The range itself is observed but with an integer ambiguity (phase observation) and can therefore also be seen as an unknown.

The partial derivatives towards all unknowns (including the spherical harmonic coefficients) are derived according to the same scheme by forming chains of partial derivatives and linking them to the partial derivatives of the position and velocity of each satellite.

GRACE A:

$$\begin{aligned}\frac{\partial g_1}{\partial p_{i_A}} = &\frac{x_B^0 - x_A^0}{\left(\rho^0\right)^3}\left(\dot{\mathbf{x}}_{\mathrm{AB}}^0 \cdot \dot{\mathbf{x}}_{\mathrm{AB}}^0\right)\frac{\partial x_A}{\partial p_{i_A}} + \frac{y_B^0 - y_A^0}{\left(\rho^0\right)^3}\left(\dot{\mathbf{x}}_{\mathrm{AB}}^0 \cdot \dot{\mathbf{x}}_{\mathrm{AB}}^0\right)\frac{\partial y_A}{\partial p_{i_A}} \\ &+ \frac{z_B^0 - z_A^0}{\left(\rho^0\right)^3}\left(\dot{\mathbf{x}}_{\mathrm{AB}}^0 \cdot \dot{\mathbf{x}}_{\mathrm{AB}}^0\right)\frac{\partial z_A}{\partial p_{i_A}} \\ &- \frac{2}{\rho^0}\left(\dot{x}_B^0 - \dot{x}_A^0\right)\frac{\partial \dot{x}_A}{\partial p_{i_A}} - \frac{2}{\rho^0}\left(\dot{y}_B^0 - \dot{y}_A^0\right)\frac{\partial \dot{y}_A}{\partial p_{i_A}} - \frac{2}{\rho^0}\left(\dot{z}_B^0 - \dot{z}_A^0\right)\frac{\partial \dot{z}_A}{\partial p_{i_A}} \end{aligned} \tag{4.43}$$

GRACE B:

$$\begin{aligned}\frac{\partial g_1}{\partial p_{i_B}} = &-\frac{x_B^0 - x_A^0}{\left(\rho^0\right)^3}\left(\dot{\mathbf{x}}_{\mathrm{AB}}^0 \cdot \dot{\mathbf{x}}_{\mathrm{AB}}^0\right)\frac{\partial x_B}{\partial p_{i_B}} - \frac{y_B^0 - y_A^0}{\left(\rho^0\right)^3}\left(\dot{\mathbf{x}}_{\mathrm{AB}}^0 \cdot \dot{\mathbf{x}}_{\mathrm{AB}}^0\right)\frac{\partial y_B}{\partial p_{i_B}} \\ &- \frac{z_B^0 - z_A^0}{\left(\rho^0\right)^3}\left(\dot{\mathbf{x}}_{\mathrm{AB}}^0 \cdot \dot{\mathbf{x}}_{\mathrm{AB}}^0\right)\frac{\partial z_B}{\partial p_{i_B}} \\ &+ \frac{2}{\rho^0}\left(\dot{x}_B^0 - \dot{x}_A^0\right)\frac{\partial \dot{x}_B}{\partial p_{i_B}} + \frac{2}{\rho^0}\left(\dot{y}_B^0 - \dot{y}_A^0\right)\frac{\partial \dot{y}_B}{\partial p_{i_B}} + \frac{2}{\rho^0}\left(\dot{z}_B^0 - \dot{z}_A^0\right)\frac{\partial \dot{z}_B}{\partial p_{i_B}} \end{aligned} \tag{4.44}$$

p_{i_A} and p_{i_B} need again to be replaced depending on the unknown of interest according to the following scheme:

spherical harmonic coefficients: $\overline{C}_{lm}, \overline{S}_{lm}$
initial conditions: $x_0, y_0, z_0, \dot{x}_0, \dot{y}_0, \dot{z}_0$
accelerometer parameter: $s_x, s_y, s_z, b_x, b_y, b_z, d_x, d_y, d_z$
empirical accelerations: a_r, a_c, a_a

4.2.1.5 Partial Derivatives for g_2

The term g_2 consists of the square of the range rate divided by the range:

$$g_2 = -\frac{\dot{\rho}^2}{\rho} = -\frac{\left[\left(\dot{x}_B - \dot{x}_A\right)\left(x_B - x_A\right) + \left(\dot{y}_B - \dot{y}_A\right)\left(y_B - y_A\right) + \left(\dot{z}_B - \dot{z}_A\right)\left(z_B - z_A\right)\right]^2}{\left[\left(x_B - x_A\right) + \left(y_B - y_A\right) + \left(z_B - z_A\right)\right]^{3/2}} \tag{4.45}$$

Again all partial derivatives are derived according to the same scheme, i.e. by forming chains of partial derivatives and linking to the partial derivatives of the position and velocity of each satellite towards the unknown of interest.

GRACE A:

$$\begin{aligned}\frac{\partial g_2}{\partial p_{i_A}} = & \left[2\frac{\dot\rho^0}{\left(\rho^0\right)^5}\left(\dot x_B^0-\dot x_A^0\right)-\frac{3\left(\dot\rho^0\right)^2}{2\left(\rho^0\right)^3}\right]\frac{\partial x_A}{\partial p_{i_A}} \\ & +\left[2\frac{\dot\rho^0}{\left(\rho^0\right)^5}\left(\dot y_B^0-\dot y_A^0\right)-\frac{3\left(\dot\rho^0\right)^2}{2\left(\rho^0\right)^3}\right]\frac{\partial y_A}{\partial p_{i_A}} \\ & +\left[2\frac{\dot\rho^0}{\left(\rho^0\right)^5}\left(\dot z_B^0-\dot z_A^0\right)-\frac{3\left(\dot\rho^0\right)^2}{2\left(\rho^0\right)^3}\right]\frac{\partial z_A}{\partial p_{i_A}} \\ & +2\frac{\dot\rho^0}{\left(\rho^0\right)^2}\left(x_B^0-x_A^0\right)\frac{\partial \dot x_A}{\partial p_{i_A}}+2\frac{\dot\rho^0}{\left(\rho^0\right)^2}\left(y_B^0-y_A^0\right)\frac{\partial \dot y_A}{\partial p_{i_A}}+2\frac{\dot\rho^0}{\left(\rho^0\right)^2}\left(z_B^0-z_A^0\right)\frac{\partial \dot z_A}{\partial s_{i_A}}\end{aligned} \tag{4.46}$$

GRACE B:

$$\begin{aligned}\frac{\partial g_2}{\partial p_{i_B}} = & -\left[2\frac{\dot\rho^0}{\left(\rho^0\right)^5}\left(\dot x_B^0-\dot x_A^0\right)-\frac{3\left(\dot\rho^0\right)^2}{2\left(\rho^0\right)^3}\right]\frac{\partial x_B}{\partial p_{i_B}} \\ & -\left[2\frac{\dot\rho^0}{\left(\rho^0\right)^5}\left(\dot y_B^0-\dot y_A^0\right)-\frac{3\left(\dot\rho^0\right)^2}{2\left(\rho^0\right)^3}\right]\frac{\partial y_B}{\partial p_{i_B}} \\ & -\left[2\frac{\dot\rho^0}{\left(\rho^0\right)^5}\left(\dot z_B^0-\dot z_A^0\right)-\frac{3\left(\dot\rho^0\right)^2}{2\left(\rho^0\right)^3}\right]\frac{\partial z_B}{\partial p_{i_B}} \\ & -2\frac{\dot\rho^0}{\left(\rho^0\right)^2}\left(x_B^0-x_A^0\right)\frac{\partial \dot x_B}{\partial p_{i_B}}-2\frac{\dot\rho^0}{\left(\rho^0\right)^2}\left(y_B^0-y_A^0\right)\frac{\partial \dot y_B}{\partial p_{i_B}}-2\frac{\dot\rho^0}{\left(\rho^0\right)^2}\left(z_B^0-z_A^0\right)\frac{\partial \dot z_B}{\partial p_{i_B}}\end{aligned} \tag{4.47}$$

s_{i_A} and s_{i_B} need again to be replaced depending on the unknown of interest according to the following scheme:

spherical harmonic coefficients: $\overline{C}_{lm}, \overline{S}_{lm}$
initial conditions: $x_0, y_0, z_0, \dot x_0, \dot y_0, \dot z_0$
accelerometer parameter: $s_x, s_y, s_z, b_x, b_y, b_z, d_x, d_y, d_z$
empirical accelerations: a_r, a_c, a_a

This summarizes the derivation of the rigorous solution. For the implementation the sum of all parameters towards all unknowns of interest has to be developed which is a cumbersome task. Moreover, the rigorous solution is another implementation of the variational equations which in-fact is more tedious than considering range or range-rate measurements as primary observation quantities due to the additional terms g_1 and g_2.

4.2.2 The Approximate Solution

One of the primary goals of the acceleration approach is to derive a linear relation between range-accelerations and the relative gradient of the gravitational potential. This may be achieved by two steps:

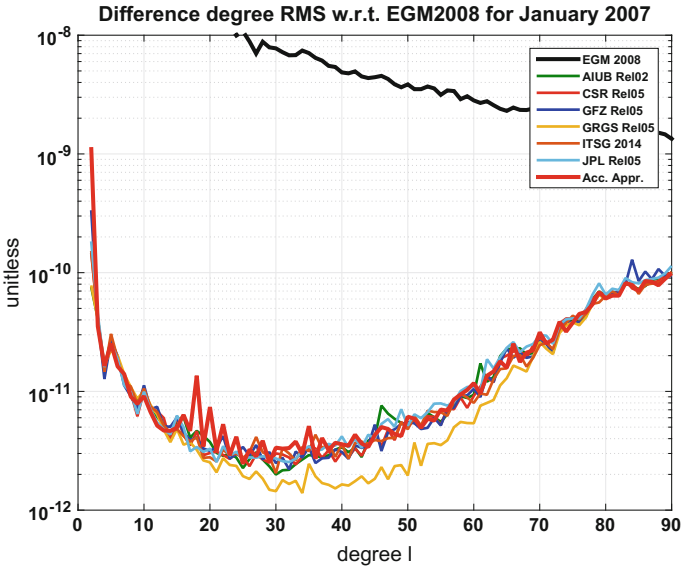

Fig. 4.3 Difference degree RMS w.r.t. EGM2008 of monthly solutions for January 2007 provided by different processing centers and in comparison the solution based on the acceleration approach (Acc. Appr.)

1. reduction to residual quantities and
2. assuming that the residual terms $g_1 - g_1^0$ and $g_2 - g_2^0$ can be neglected.

The mathematical model of Eq. (4.17) reduces then to:

$$\ddot{\rho} - \ddot{\rho}^0 \approx (\nabla V_B - \nabla V_A) \cdot \mathbf{e}_{\mathrm{AB}}^{\mathrm{a}} - \left(\nabla V_B^0 - \nabla V_A^0\right) \cdot \mathbf{e}_{\mathrm{AB}}^{\mathrm{a},0} \tag{4.48}$$

The relation is linear and no integration of the variational equations is necessary anymore. This is the most used version of the acceleration approach as it is easy to understand and implement. The only remaining difficulty lies in the determination of an a priori orbit with sufficient precision.

The quality of the solution depends however directly on the aforementioned assumptions. For early solutions, these assumptions were fulfilled but with nowadays gradually increasing precision of gravity field solutions based on other approaches the assumptions limit the quality of a solution based on the acceleration approach.

Figure 4.3 shows difference degree RMS values for monthly solutions (January 2007) provided by several processing centers and in red a solution based on the acceleration approach. Note that the solutions primarily show the deficiencies of EGM2008 indicated by the lumping of all monthly solutions although it is known that they are of different quality. Nevertheless it becomes obvious that the assumptions in the acceleration approach degrades the solution to an extend larger than the difference between the monthly solutions and EGM2008. Errors primarily occur at degree 2

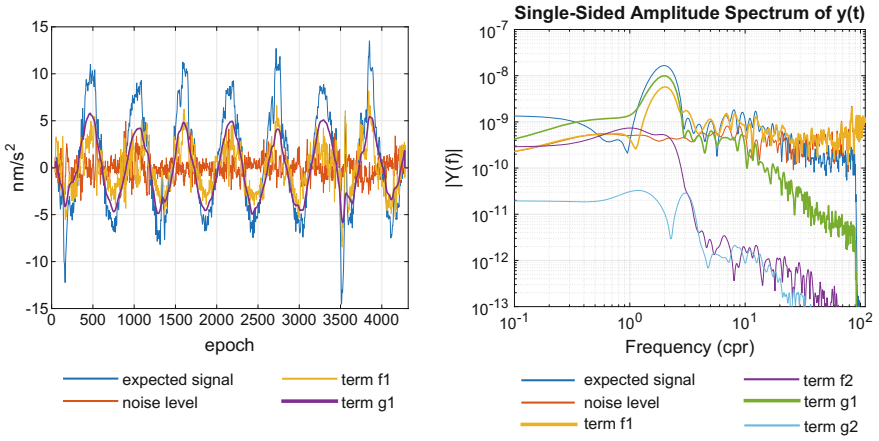

Fig. 4.4 *Left panel*: time domain representation of simulated range-acceleration compared to the expected signal and a white noise level of $1\,{}^{\mathrm{nm}}/_{\mathrm{s}^2}$; *right panel* amplitude spectrum of the components of the acceleration approach

and around degree 16 which is close to the number of revolutions per day of the GRACE system (repeat period).

The approximation can be further visualized in the time and spectral domain using simulated data. For the following test, the gravity field model GOCO05s [96] was used to simulate the true world and the gravity field model EGM2008 [114] was used to create a priori values. Both model have been developed to degree and order 100. All quantities are subsequently reduced to residual level.

Figure 4.4 shows on the left panel the expected signal in blue which is the difference between the two vectors projected on the LOS along the orbit. The red curve represents a white-noise level of $1\,{}^{\mathrm{nm}}/_{\mathrm{s}^2}$. The orange curve represents the term f_1 of Eq. (4.34) which is equivalent to the approximation in Eq. (4.48). Obviously, a significant part of the signal is missing. The signal lost due to the approximation is represented mostly by the term g_1 of Eq. (4.42). Both f_1 and g_1 will sum nearly to the expected signal. The findings are confirmed in the spectral domain shown in the right panel of Fig. 4.4. The curves for the terms f_1 and g_1 will sum to the expected signal. More importantly, it becomes evident that g_1 resembles a smooth signal and thus primarily affects the low degrees of the gravity field solution as previously observed. From approximately 10 cpr onwards g_1 is quickly decaying, i.e. it does not significantly contribute to approximately degree 10 and higher. Besides terms f_1 and g_1, the terms f_2 and g_2 are also shown which play a minor role in the case of GRACE. For future gravity field missions based on the concept of low-low satellite-to-satellite tracking the noise level (red curve) will drop and they will become important in due time.

In conclusion, the approximated solution is not applicable for global solutions nowadays anymore. Due to the quick decay of the term g_1 in the spectral domain, the approximate solution of the acceleration approach is nevertheless very much

suitable for local applications. The reader should keep in mind that for a consistent local processing first a global solution needs to be recovered which can only be achieved by the rigorous approach of Sect. 4.2.1. Using any other global gravity field model may result in long-wavelength aliasing to the local solution.

4.2.3 A Derivation Based on Rotational Quantities

The lack of precision in the GPS observation currently prevents the direct implementation of the acceleration approach without further measures. Thus, an alternative to GPS and the rigorous implementation is needed. SLR observations are of limited use due to their availability and only slightly better precision. The only other observation system on-board the satellites are the star cameras which are used to determine the orientation of the satellites but may also be used to derive rotation rates. Therefore the acceleration approach needs to be reformulated in terms of rotations.

4.2.3.1 General Representation in Terms of Rotations

The basis are again the three unit vectors $\mathbf{e}^{\mathrm{a}}_{\mathrm{AB}}$, $\mathbf{e}^{\mathrm{c}}_{\mathrm{AB}}$ and $\mathbf{e}^{\mathrm{r}}_{\mathrm{AB}}$ forming the instantaneous relative reference frame (IRRF). The name has already been introduced in Sect. 4.2 but here the definition and choice of this frame is discussed in more detail. The name has been chosen because first it is based on the relative position of the two satellites and secondly its orientation and its origin is constantly changing with the LOS-vector, i.e. the frame is instantaneous and moving with the satellites. Consequently, the observation equation needs to be reformulated for a moving frame and the rotation rates around the three axes of the IRRF need to be derived. For this, the three unit vectors are arranged into a rotation matrix $R^{\mathrm{I}}_{\mathrm{F}}$ which describes the rotation from the inertial frame I to the IRRF denoted by F:

$$R^{\mathrm{I}}_{\mathrm{F}} = \begin{bmatrix} \left(\mathbf{e}^{\mathrm{a}}_{\mathrm{AB}}\right)^T \\ \left(\mathbf{e}^{\mathrm{c}}_{\mathrm{AB}}\right)^T \\ \left(\mathbf{e}^{\mathrm{r}}_{\mathrm{AB}}\right)^T \end{bmatrix}. \tag{4.49}$$

The multiplication of this matrix with the transpose of its derivative forms the Cartan-Matrix Ω which contains the rotation rates ω^i around the three axes formed by the unit vector:

$$\Omega = R^{\mathrm{I}}_{\mathrm{F}} \left(\dot{R}^{\mathrm{I}}_{\mathrm{F}}\right)^T = \begin{bmatrix} 0 & -\omega^{\mathrm{r}} & \omega^{\mathrm{c}} \\ \omega^{\mathrm{r}} & 0 & -\omega^{\mathrm{a}} \\ -\omega^{\mathrm{c}} & \omega^{\mathrm{a}} & 0 \end{bmatrix}. \tag{4.50}$$

By means of the rotation rates, the inertial unit-vector related quantities of Eq. (4.13) can be transformed:

$$R_{\mathrm{F}}^{\mathrm{I}}\mathbf{e}_{\mathrm{AB}}^{\mathrm{a,c,r}} = \mathbf{e}_{\mathrm{AB,F}}^{\mathrm{a,c,r}} \tag{4.51a}$$

$$R_{\mathrm{F}}^{\mathrm{I}}\dot{\mathbf{e}}_{\mathrm{AB}}^{\mathrm{a}} = \dot{\mathbf{e}}_{\mathrm{AB,F}}^{\mathrm{a}} + \boldsymbol{\omega} \times \mathbf{e}_{\mathrm{AB,F}}^{\mathrm{a}} \tag{4.51b}$$

$$R_{\mathrm{F}}^{\mathrm{I}}\ddot{\mathbf{e}}_{AB}^{a} = \ddot{\mathbf{e}}_{\mathrm{AB,F}}^{\mathrm{a}} + 2\boldsymbol{\omega} \times \dot{\mathbf{e}}_{\mathrm{AB,F}}^{\mathrm{a}} + \boldsymbol{\omega} \times \left(\boldsymbol{\omega} \times \mathbf{e}_{\mathrm{AB,F}}^{\mathrm{a}}\right) + \dot{\boldsymbol{\omega}} \times \mathbf{e}_{\mathrm{AB,F}}^{\mathrm{a}} \tag{4.51c}$$

Equations (4.51b) and (4.51c) can be significantly simplified since the three unit vectors in the IRRF have the form:

$$\mathbf{e}_{\mathrm{AB,F}}^{\mathrm{a}} = \begin{bmatrix} 1 \\ 0 \\ 0 \end{bmatrix} \quad \mathbf{e}_{\mathrm{AB,F}}^{\mathrm{c}} = \begin{bmatrix} 0 \\ 1 \\ 0 \end{bmatrix} \quad \mathbf{e}_{\mathrm{AB,F}}^{\mathrm{r}} = \begin{bmatrix} 0 \\ 0 \\ 1 \end{bmatrix}, \tag{4.52}$$

and their derivatives are consequently all zero:

$$R_{\mathrm{F}}^{\mathrm{I}}\dot{\mathbf{e}}_{\mathrm{AB}}^{\mathrm{a}} = \boldsymbol{\omega} \times \mathbf{e}_{\mathrm{AB,F}}^{\mathrm{a}} \tag{4.53a}$$

$$R_{\mathrm{F}}^{\mathrm{I}}\ddot{\mathbf{e}}_{\mathrm{AB}}^{\mathrm{a}} = \boldsymbol{\omega} \times \left(\boldsymbol{\omega} \times \mathbf{e}_{\mathrm{AB,F}}^{\mathrm{a}}\right) + \dot{\boldsymbol{\omega}} \times \mathbf{e}_{\mathrm{AB,F}}^{\mathrm{a}} \tag{4.53b}$$

Projecting Eq. (4.11c) to the axes of the IRRF and introducing the relations of Eq. (4.53) yields:

$$\ddot{\mathbf{x}}_{\mathrm{AB,F}} \cdot \mathbf{e}_{\mathrm{AB,F}}^{\mathrm{a}} = \ddot{\rho} - \rho\left((\omega^{\mathrm{c}})^2 + (\omega^{\mathrm{r}})^2\right) \tag{4.54a}$$

$$\ddot{\mathbf{x}}_{\mathrm{AB,F}} \cdot \mathbf{e}_{\mathrm{AB,F}}^{\mathrm{c}} = 2\,\dot{\rho}\,\omega^{\mathrm{r}} - \rho\,\omega^{\mathrm{a}}\omega^{\mathrm{c}} + \rho\,\dot{\omega}^{\mathrm{r}} \tag{4.54b}$$

$$\ddot{\mathbf{x}}_{\mathrm{AB,F}} \cdot \mathbf{e}_{\mathrm{AB,F}}^{\mathrm{r}} = -2\,\dot{\rho}\,\omega^{\mathrm{c}} + \rho\,\omega^{\mathrm{a}}\omega^{\mathrm{r}} - \rho\,\dot{\omega}^{\mathrm{c}} \tag{4.54c}$$

Considering again the equation of motion (4.1), Eq. (4.54) forms a set of three equations connecting the relative acceleration and thus the relative gradient of the gravitational potential to the K-Band observations and rotation rates around the three axes of the IRRF.

So far, the equations imply no restrictions on the choice of the IRRF although the definitions of Sect. 4.2 have been used but the Eq. (4.54) are actually independent of the orientation of the frame and may be used with any setup of low-low satellite-to-satellite tracking. Equation (4.54a) represents again the case of GRACE, i.e. for a successful implementation of the equation in its current formulation the rotation rate around the cross-track as well as the rotation rate around the radial axis needs to be observed with a matching precision. In the subsequent section it will become clear why the choice made in Sect. 4.2 is convenient but it is emphasized that this choice is not the only possible one and better choices may exist.

4.2.3.2 Choosing an IRRF and the Resulting Equation System

So far, the implementation of the IRRF given in Sect. 4.2 has not been discussed in detail. The basis for the IRRF is the LOS-vector or alongtrack direction of the relative observation system which is obviously defined. The radial direction is however

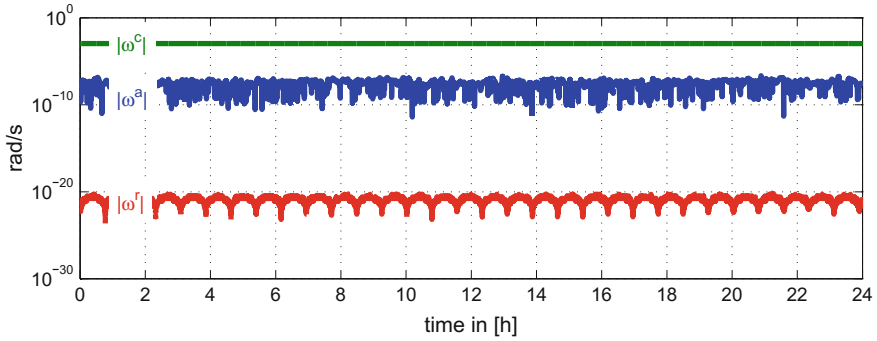

Fig. 4.5 Rotation rates based on the simulated SC7 data

ambiguous. Choices could be the radial direction of (a) GRACE A, (b) GRACE B, (c) the midpoint of the two satellites or (d) any other direction which seems convenient. The cross-track component will complete then the right-handed triad. Besides the definition one may define other constraints on the choice such as e.g. the accessibility, the precision or a physical meaning. At the same time, one may strive for a simplification of Eq. (4.54) and/or to minimize the number of rotations rates to be measured.

The choice of the unit vectors presented in Eq. (4.12) has various such desirable properties: (1) the unit vectors can be derived with sufficient precision from the GPS observations; (2) the rotation rate around the radial direction ω_r becomes zero and the rotation rate around the alongtrack direction ω_a is orders of magnitudes smaller than the rotation rate of the cross-track direction ω_c. The latter is resembling the rotation of the LOS-vector which rotates once per revolution, i.e. its rate is approximately the orbit frequency of the two satellites. Figure 4.5 visualizes the findings using the SC7 data set provided by the University of Bonn (http://www.igg.uni-bonn.de/apmg/index.php?id=satellitenmissionen) simulating a GRACE-like scenario.

Introducing $\omega_\mathrm{r} \approx 0$ into Eq. (4.54) yields a considerable simplification:

$$\nabla V_{AB,F} \cdot \mathbf{e}^{\mathrm{a}}_{\mathrm{AB,F}} = \ddot{\rho} - \rho\,(\omega^{\mathrm{c}})^2 \tag{4.55a}$$

$$\nabla V_{AB,F} \cdot \mathbf{e}^{\mathrm{c}}_{\mathrm{AB,F}} = -\,\rho\,\omega^{\mathrm{a}}\omega^{\mathrm{c}} \tag{4.55b}$$

$$\nabla V_{AB,F} \cdot \mathbf{e}^{\mathrm{r}}_{\mathrm{AB,F}} = -\,2\,\dot{\rho}\,\omega^{\mathrm{c}} - \rho\,\dot{\omega}^{\mathrm{c}}. \tag{4.55c}$$

The case of GRACE is represented by Eq. (4.55a). Only the cross-track component of the rotation rate vector ω^{c} needs to be measured with matching precision. A second direction is within reach if the change of the rotation rate around the cross-track component $\dot{\omega}^{\mathrm{c}}$ is either observed or derived from the rotation rate ω^{c} e.g. by numerical differentiation. Further, the cross-track component of the gravity field (Eq. 4.55b) is nearly zero as the multiplication of the range with the rotation rates around the along-track and the cross-track direction is orders of magnitude smaller than the two other components. Since this cross-track direction is also approximately

oriented in East-West direction of the Earth, Eq. (4.55b) is a mathematical description of the poor East-West observation capability of GRACE which causes the striping effects in the final GRACE products.

The current choice of the IRRF thus has many desirable properties but still may not be the best and future research may reveal a better choice. Note that any possible device to measure the rotation rate will not remove the necessity for GPS observations as they are needed for the left-hand side and the determination of the IRRF itself. The last open question for the application to GRACE is if it is possible to derive the rotation rates with sufficient precision but simple tests showed that besides the insufficient precision of the current star-tracker system of GRACE the motion of the LOS-vector also cannot be separated from the attitude variations of each individual satellite.

4.3 Exercises

Data and files needed for the following exercises are available online at:
http://www.geoq.uni-hannover.de/autumnschool-data
http://extras.springer.com

1: Working with noise-free observations

(a) Create observations of two satellites
Create position, velocity and accelerations for the two satellites. You may use the program `orbitsim` for this. The call for GRACE A is:

```
[time,A_ipos,A_ivel,A_iacc] = orbitsim('GraceA','goco05s')
```

The call integrates for one day an orbit for satellite A using the gravity field model GOCO05s till degree and order 60. The output is the time in a two column format: the first column denotes the modified Julian day, the second column the time of the day. The position is given in the inertial frame and in (m). Likewise velocity and acceleration is given in (m/s) and (m/s^2). Repeat the calculation for GRACE B using:

```
[time,B_ipos,B_ivel,B_iacc] = orbitsim('GraceB','goco05s')
```

(b) Create range, range-rate and range acceleration
Calculate (noise-free) range, range-rate and range-acceleration observations. Determine maximum, minimum and the RMS of the quantities.

(c) A priori quantities
Assume that GOCO05s represents the true world. Repeat steps 1 and 2 for the gravity fields EGM96 and GGM03s. They are used as approximation. Take the difference between the range calculated with GOCO05s and the other two, plot

it and compare the maximum, minimum and the RMS. Repeat the steps for the range-rate and the range-acceleration. What do you observe? Why is there a difference? Which one of the two approximation would you prefer?

(d) Unit vectors
Derive the along-track, cross-track and radial unit vector. Project the relative acceleration (which is in this special case identical to the force) onto the different axes and plot the results. What do you observe? Why don't we use the radial instead of the along-track component then?
Also determine the derivative of the along-track unit vector analytically and numerically (you may use `diff` or a central difference differentiator, see e.g. Wikipedia). Compare the two solutions and discuss if it is feasible to derive the unit vector numerically.

2: Working with noisy observations

(a) White noise
Add white noise (using `randn`) values to the range, the range-rate, the range-acceleration and the position and velocities of the two satellite which have been based on the orbit integration of GOCO05s. You will have to choose a 'reasonable' scaling parameter for your noise. How could you define 'reasonable' here? The resulting vectors and matrices represent now your (pseudo-) observations for the following parts.

(b) Signal-to-noise ratio
Derive the residual pseudo-observations by subtracting the noise-free range and range-rate of EGM96 and GGM03s. Compare the noisy residual range observations with the noise-free residual range using both EGM96 and GGM03s. The difference represents the signal-to-noise ratio (SNR). Plot the difference and take the maximum, minimum and RMS. Obviously the SNR is higher for the EGM96 because the approximation is poorer than for GGM03s. Can you observe signal in GGM03s or is it all hidden in the noise already? Repeat the steps for the range-rate and the range-acceleration.

(c) Unit vectors
Derive the along-track unit vector and its derivative from the noisy observations. Compare the results with the noise-free version and interpret the consequences for the approach. Reduce the noise level (=scaling) for the position and velocity of your observations but leave the range, range-rate and range-acceleration level unchanged. Find the point where the noise-level of the range-quantities will dominate the noise. This means that the noise level is low enough to take full advantage of the range observations and the GPS-observations are not the limiting factor anymore. Note the noise level and discuss if such a level is achievable.

(d) Approximation
Now we focus on the centrifugal/radial term. Test the approximation, i.e. the difference between the noise-free GOCO05s and EGM96. This difference must be as small as possible. Compare it to the noise level of the range acceleration. Repeat the steps for the quantities based on GGM03s. What do you conclude? You may also determine the spectrum using e.g. `pwelch`.

(e) Least-squares adjustment
Solve for the gravity field using the approximate approach and your knowledge from Chap. 1. For testing purposes you can use the difference between the noise-free observations but ultimately you should use the noisy observations as input. You can compare your solution to the difference in the coefficient given in the mat-files (variable `klm`).
Hint: solve only for degree 10 or 20 at most. This results in high-frequency aliasing but you have no other choice since you have only one day of data available. For degree 60 (input field of integration) you need at least 5–10 days of data. You may repeat the exercise with an input field of degree 10 or 20 for which you have to adapt the input fields.

Chapter 5
The Energy Balance Approach

Christopher Jekeli

Abstract The energy balance approach to geopotential modeling from satellite-to-satellite tracking offers the advantage of emulating an in-situ measurement system, analogous to satellite-borne gravity gradiometry, but in terms of differences in potential. Although the theoretical background is well known, based on the conservation of energy in celestial mechanics, its application to geopotential determination from satellite tracking had to await the capability for accurate, independent, kinematic orbit determination. This is now possible with Global Navigation Satellite Systems (GNSS), such as GPS. The precision tracking between two co-orbiting satellites brings additional short-wavelength information to the in-situ measurement. These tutorial notes derive the exact relationships between the gravitational potential and the orbital state vectors from the energy balance perspective, both in the inertial frame and in the Earth-fixed frame. Also derived are the equations that specifically incorporate the range-rate between co-orbiting satellites. Particular attention is given to the rotation potential and the temporal dependence of the potential due to various sources, including tidal variations, Earth's orientation and deformation, and terrestrial mass fluxes. A detailed analysis of magnitudes then leads to possibly acceptable approximations. It also shows for a satellite configuration such as GRACE (Gravity Recovery and Climate Experiment) that the radial component of the relative velocity between two co-orbiting satellites is as important in magnitude as the along-track component. Thus, the measured inter-satellite range-rate, for example, cannot be used alone to determine the potential difference. However, it is also shown that the short-wavelength content of the potential resides more in the along-track component than in the radial component, which demonstrates the significance of the range-rate measurement. A simple error analysis of the system identifies the requirements for state-vector accuracies (both for position and velocity) in relation to the range-rate accuracy. The observational equations for satellite-to-satellite tracking are derived

C. Jekeli (✉)
School of Earth Sciences, The Ohio State University, Columbus, USA
e-mail: jekeli.1@osu.edu

M. Naeimi and J. Flury (eds.), *Global Gravity Field Modeling from Satellite-to-Satellite Tracking Data*, Lecture Notes in Earth System Sciences,
DOI 10.1007/978-3-319-49941-3_5

and related to both global and regional geopotential modeling. The discussion concludes with a sample of published case studies that have demonstrated the energy balance approach and achieved tangible results in large-scale hydrological mass flux monitoring.

5.1 Introduction

5.1.1 Theoretical Perspectives

The duality in geodesy between Earth's gravity field and its overall geometric shape as defined by the geoid is well known. Fundamentally it derives from Newton's law of gravitation and leads eventually to Bruns's equation that expresses the geoid height as proportional to the disturbing potential. Conversely, geometric measurements (distances) are needed to infer gravitational acceleration. Galileo's law of falling bodies is at the heart of absolute gravimetry, which, expressed in Newton's theory, also allows determination of the global gravity field by tracking satellites orbiting (falling around) the Earth. Another example is the determination of the geopotential difference between points on Earth's surface according to a line integral of gravity, more commonly known as geometric leveling with gravity reduction. Somewhat analogously, satellite-to-satellite tracking between two low co-orbiting satellites also yields a potential difference, which is the topic of this lecture.

5.1.2 Background

Although satellite tracking since the early 1960s has been fundamental to global gravitational field modeling, one of the more limiting aspects was the irregular and sparse distribution of tracking stations. This problem now is almost eliminated as Global Navigation Satellite Systems (GNSS), such as the Global Positioning System (GPS), provide continual and accurate tracking of any low-Earth-orbiting satellite. Still, it is not the same as having an on-board instrument that senses the field directly as the Earth rotates under the orbit. A significant seed toward such an ideal scenario was OKeefe's [113] proposal in 1957 to use measurements of a satellite's velocity to determine its kinetic energy that with the law of conservation of energy then leads to a direct measurement of gravitational potential (up to a constant) in what may be called the energy balance approach. This idea was an adaptation of Jacobi's integral [30] which solves a specialized three-body problem in celestial mechanics, namely the motion of a small body of insignificant mass (a satellite in our case) near two massive bodies that together by their mutual orbital motion represent a time-varying gravitational field. Bjerhammar [12] elaborated on this idea, but the same problem of irregular tracking remained.

It was Wolff [160] who in 1969 proposed to use two satellites following in similar orbits that by tracking each other and on the basis of the energy principles would create a virtual in-situ measurement system of potential differences. Absolute tracking was still needed but deemed secondary to the principal sensitivity to gravitational variations between the satellites. The idea was adopted in the 1980s by NASA for its program of a dedicated gravity mapping mission (GRAVSAT, Geopotential Research Mission (GRM) [81]). Numerous simulations and analyses based on Wolff's simplified relationship between the potential difference and satellite-to-satellite tracking (Sect. 5.3) were conducted in preparation for GRAVSAT and GRM (e.g., [32, 77, 152]), and later for proposed high-low satellite-to-satellite tracking [78].
However, the 'in-situ' aspect was never the focus, neither of the simulations nor of the implementation when such a dedicated mission was finally realized in 2001 as GRACE (Gravity Recovery and Climate Experiment) [142]. Rather, the tried and true orbit determination methodology augmented to take advantage of the additional satellite-to-satellite tracking observation (K-band ranging, KBR) formed the basis for global gravity mapping. A second look at Wolff's proposal [74] and the demonstrated kinematic methodology of orbit determination using GPS helped to elevate the energy balance approach as a fundamental alternative that could yield a space-wise distribution of gravitational potential data. Subsequently a series of investigations was launched for both the CHAMP (Challenging Minisatellite Payload, [120] and GRACE missions in terms of theory, simulation, and analysis [52, 54, 61, 117, 149, 157, 164, 155], as well as with successes in producing gravity models from actual data [2, 46, 55, 56, 136]. Significant was the fact that regional solutions were advanced (at least enabled) by the in situ nature of the data. A brief concluding review of these is given in Sect. 5.6.

5.1.3 Summary of Lecture Notes

The main focus of these lecture notes is to derive and analyze the energy balance approach to geopotential modeling. Exact equations are given for the potential in terms of orbital state vectors, the range-rate between satellites, and all temporal variations in the potential due to Earth's rotation, the tidal potential, as well as consequent and additional deformations of the Earth. An analysis of the magnitudes of each term, based on simulations, then determines their significance in relation to the desired geopotential accuracy. A straightforward error analysis identifies key constituents that contribute to the overall error in the computed geopotential difference, where the source of error in the principal terms comes from inaccuracy in the orbital state vectors. Alternative geopotential modeling strategies are illustrated briefly as a prelude to the concluding section that highlights the successes of the energy balance approach to monitoring temporal variations in the geopotential field both globally and regionally.

5.2 Mathematical Formulations

This section derives the exact energy balance equations in detail from first principles in both the inertial and Earth-fixed reference frames. Initial approximations are also indicated, and analyzed and verified numerically in subsequent sections. It concludes with the derivation of the energy balance equation for the potential difference between two satellites that incorporates inter-satellite, range-rate tracking.

In a neoclassical sense, three laws of physics are invoked in the measurement of gravitation. They also form the underpinnings of the relevant energy relations. The first two are Newton's second law of motion and his law of gravitation. Newton's law of motion states that the rate of change of linear momentum of a particle is equal to the totality of forces, $\mathbf{F}$, acting on it. Given more familiarly as $m_i d^2\mathbf{x}/dt^2 = \mathbf{F}$, it involves the inertial mass, m_i, of the particle. Conceptually, the forces, $\mathbf{F}$, should be interpreted in the first place as action forces, like propulsion or friction. On the other hand, the gravitational field, which is part of the space we occupy and is due to the presence of masses like the Earth, Sun, Moon and planets, induces a different kind of force, the gravitational force. This force is proportional to gravitational acceleration, $\mathbf{g}$, through the gravitational mass, m_g, according to the law of gravitation, abbreviated here as: $m_g\mathbf{g} = \mathbf{F}_g$. In the presence of a gravitational field, Newton's law of motion must be modified to include $\boldsymbol{F}_g$ separately; that is, $m_i d^2\mathbf{x}/dt^2 = \overline{\mathbf{F}} + \mathbf{F}_g$, where $\overline{\mathbf{F}}$ is strictly the sum of all the action forces. With the third fundamental law, Einstein's equivalence principle, which states that inertial and gravitational masses are indistinguishable, one finally obtains

$$\frac{d^2\mathbf{x}}{dt^2} = \mathbf{a} + \mathbf{g}, \tag{5.1}$$

where $\mathbf{a}$ is the specific force ($\overline{\mathbf{F}}/m_i$), or also the inertial acceleration, due to action forces. This equation holds in a non-rotating, freely falling frame (that is, an inertial frame) and variants of it can be derived in more complicated frames that rotate or have their own dynamic motion. However, one can always assume the existence of an inertial frame and proceed on that basis. Equation (5.1) is the foundation for all of gravimetry and consequently for all geopotential measurements and modeling.

5.2.1 The Energy Balance Equations

It is easiest to obtain the energy balance equation for a body in motion in the inertial (i-) frame; and, subsequent formulations in a rotating frame, such as an Earth-fixed (e-) frame, may be obtained with appropriate position and velocity transformations. It is assumed that the moving body, viz., the satellite, is rigid. The mechanical energy of such a body is defined by the amount of work it is capable of doing. It is separated into energy due to its motion (velocity), called kinetic energy, and energy due to its location within the gravitational field, called potential energy (other fields, such as

the electro-magnetic field, and rotational motion of the satellite are not considered in the present derivations).
The kinetic energy of a body in translational motion (all parts of the body have the same velocity) is defined as the amount of work needed to bring it from rest, $\mathbf{x}_0^i$, to a velocity, $\dot{\mathbf{x}}^i$, using forces, $\mathbf{F}^i$. The superscript on all vectors and coordinates refers to the frame in which they are expressed, and the over-scripted dots mean differentiation with respect to time in the indicated frame, $\dot{\mathbf{x}}^i \doteq d\mathbf{x}^i/dt$, $\ddot{\mathbf{x}}^i \doteq d^2\mathbf{x}^i/dt^2$, etc. Since work is defined as

$$W = \int_{x_0^i}^{x^i} \mathbf{F}^i \cdot d\mathbf{x}^i, \tag{5.2}$$

and noting from Newton's second law of motion that

$$\mathbf{F}^i \cdot d\mathbf{x}^i = m\ddot{\mathbf{x}}^i \cdot d\mathbf{x}^i = m\dot{\mathbf{x}}^i \cdot d\dot{\mathbf{x}}^i, \tag{5.3}$$

the kinetic energy per unit mass becomes, with $\dot{\mathbf{x}}_0^i = 0$,

$$T(\dot{\mathbf{x}}^i, t) = \frac{1}{2}\dot{\mathbf{x}}^i \cdot \dot{\mathbf{x}}^i, \tag{5.4}$$

where the dependence on time is implicit on the right side.
The potential energy, on the other hand, is the amount of work needed to bring the body from infinity to $\mathbf{x}^i$ in the gravitational field. Per unit mass, it is thus simply the (negative) gravitational potential at $\mathbf{x}^i$, $-V(\mathbf{x}^i, t)$. The sign conforms to geodetic and geophysical convention that defines the potential as positive, implying that the work needed in this case is negative. It is noted that the geopotential in the inertial frame is a function explicitly of time, particularly due to the rotation of the Earth, but also because of the relative motions of the Moon, Sun, and other planets and because of the dynamic character of the Earth's mass. The corresponding gravitational force per unit mass, or gravitational acceleration, is:

$$\mathbf{g}^i = \nabla_{x^i} V, \tag{5.5}$$

where ∇_{x^i} denotes the gradient operator with respect to components of $\mathbf{x}^i$. In general, due to dissipative forces (such as atmospheric drag) the total mechanical energy of the satellite varies in time,

$$E = T - V = E^{(0,i)} + \int_{t_0}^{t} \frac{dE}{dt'} dt', \tag{5.6}$$

where $E^{(0,i)}$ is its energy in the inertial frame at the initial time, t_0. Applying the chain rule for differentiation,

$$\begin{aligned}\frac{dE}{dt'} &= \frac{\partial T}{\partial \dot{\mathbf{x}}^i}\cdot\frac{d\dot{\mathbf{x}}^i}{dt'} - \frac{\partial V}{\partial \mathbf{x}^i}\cdot\frac{d\mathbf{x}^i}{dt'} - \frac{\partial V}{\partial t'} \\ &= \nabla_{\dot{x}^i} T\cdot\ddot{\mathbf{x}}^i - \nabla_{x^i} V\cdot\dot{\mathbf{x}}^i - \frac{\partial V}{\partial t'}\end{aligned} \tag{5.7}$$

where the dots now refer to derivatives with respect to t'. From Eq. (5.4),

$$\nabla_{\dot{x}^i} T = \dot{\mathbf{x}}^i, \tag{5.8}$$

and from Eqs. (5.1) and (5.5),

$$\nabla_{x^i} V = \mathbf{g}^i = \ddot{\mathbf{x}}^i - \mathbf{a}^i. \tag{5.9}$$

The partial derivative, $\partial V/\partial t'$, means differentiation explicitly with respect to time, holding the position and velocity constant. Combining (5.6) through (5.9) results in

$$\begin{aligned}E &= E^{(0,i)} + \int_{t_0}^{t}\left(\dot{\mathbf{x}}^i\cdot\ddot{\mathbf{x}}^i - \left(\ddot{\mathbf{x}}^i - \mathbf{a}^i\right)\cdot\dot{\mathbf{x}}^i - \frac{\partial V}{\partial t'}\right)dt' \\ &= E^{(0,i)} + \int_{t_0}^{t}\mathbf{a}^i\cdot\dot{\mathbf{x}}^i dt' - \int_{t_0}^{t}\frac{\partial V}{\partial t'}dt'\end{aligned} \tag{5.10}$$

With $E = T - V$ and (5.4), Eq. (5.10) yields an expression for the gravitational potential,

$$V(\mathbf{x}^i, t) = \frac{1}{2}|\dot{\mathbf{x}}^i|^2 - \int_{t_0}^{t}\mathbf{a}^i\cdot\dot{\mathbf{x}}^i dt' + \int_{t_0}^{t}\frac{\partial V}{\partial t'}dt' - E^{(0,i)}. \tag{5.11}$$

This represents the *balance in energy* in the most general case and in the inertial frame. If the gravitational potential at a point is time-invariant, i.e., $\partial V/\partial t' = 0$ (e.g., no Earth rotation), and there are no action forces disturbing the satellite ($\mathbf{a}^i = \mathbf{0}$), then $E = E^{(0,i)}$ for all t, which is a manifestation of the law of conservation of mechanical energy. Note, however, even in this situation there is a trade-off within this constant between the kinetic and potential energies as a function of time as the satellite falls in the gravitational field.

The energy balance equation in a rotating frame, such as the terrestrial reference frame fixed to the Earth's crust, may be obtained from Eq. (5.11) with suitable transformations. Let $\mathbf{x}^e = (x_1^e\ x_2^e\ x_3^e)^T$ denote a position vector of the satellite in the Earth-fixed e-frame that is rotating with angular rate, $\omega_{ie}^e = (\omega_1^e\ \omega_2^e\ \omega_3^e)^T$, with respect to the i-frame. By assumption, both frames share the same origin point. The Coriolis Law [75] relates the velocities in the two frames,

$$\mathbf{C}_i^e\dot{\mathbf{x}}^i = \dot{\mathbf{x}}^e + \omega_{ie}^e\times\mathbf{x}^e, \tag{5.12}$$

where $\mathbf{C}_i^e$ is the rotation matrix from the i-frame to the e-frame (e.g.; $\mathbf{x}^e = \mathbf{C}_i^e\mathbf{x}^i$). Again, the dot-notation refers to time-differentiation in the frame specifically des-

ignated by the superscript. Noting the orthogonality of rotation matrices, $\mathbf{C}_e^i = (\mathbf{C}_i^e)^{-1} = (\mathbf{C}_i^e)^T$, the substitution of (5.12) and of $\mathbf{a}^i = \mathbf{C}_e^i \mathbf{a}^e$ into (5.11) yields

$$
\begin{aligned}
&V(\mathbf{x}^e, t) = \\
&\frac{1}{2}|\dot{\mathbf{x}}^e + \omega_{ie}^e \times \mathbf{x}^e|^2 - \int_{t_0}^{t} \mathbf{C}_e^i \mathbf{a}^e \cdot \mathbf{C}_e^i(\dot{\mathbf{x}}^e + \omega_{ie}^e \times \mathbf{x}^e)dt' + \int_{t_0}^{t} \frac{\partial V^i}{\partial t'}dt' - E^{(0,i)} = \\
&\frac{1}{2}|\dot{\mathbf{x}}^e|^2 + \frac{1}{2}|\omega_{ie}^e \times \mathbf{x}^e|^2 + \dot{\mathbf{x}}^e \cdot (\omega_{ie}^e \times \mathbf{x}^e) - \\
&\int_{t_0}^{t} \mathbf{a}^e \cdot \dot{\mathbf{x}}^e dt' - \int_{t_0}^{t} \mathbf{a}^e \cdot (\omega_{ie}^e \times \mathbf{x}^e)dt' + \int_{t_0}^{t} \frac{\partial V^i}{\partial t'}dt' - E^{(0,i)}
\end{aligned}
\tag{5.13}
$$

It is easy to show, by one more time-differentiation of (5.12) and with [75, p. 21]

$$
\dot{\mathbf{C}}_e^i = \mathbf{C}_e^i[\omega_{ie}^e \times], \tag{5.14}
$$

that

$$
\mathbf{a}^e = \ddot{\mathbf{x}}^e - \mathbf{g}^e + 2\omega_{ie}^e \times \dot{\mathbf{x}}^e + \omega_{ie}^e \times (\omega_{ie}^e \times \mathbf{x}^e) + \dot{\omega}_{ie}^e \times \mathbf{x}^e. \tag{5.15}
$$

In (5.14), $[\omega_{ie}^e \times]$ denotes a skew-symmetric matrix whose off-diagonal elements are the components of ω_{ie}^e according to

$$
[\omega_{ie}^e \times] = \begin{bmatrix} 0 & -\omega_3^e & \omega_2^e \\ \omega_3^e & 0 & -\omega_1^e \\ -\omega_2^e & \omega_1^e & 0 \end{bmatrix}. \tag{5.16}
$$

The second integral in (5.13) with (5.15) may be evaluated using some identities. Specifically, since $\omega_{ie}^e \times (\omega_{ie}^e \times \mathbf{x}^e)$ is orthogonal to $\omega_{ie}^e \times \mathbf{x}^e$,

$$
(\omega_{ie}^e \times (\omega_{ie}^e \times \mathbf{x}^e)) \cdot (\omega_{ie}^e \times \mathbf{x}^e) = 0; \tag{5.17}
$$

and similarly, $(\omega_{ie}^e \times \dot{\mathbf{x}}^e) \cdot \dot{\mathbf{x}}^e = 0$. Also,

$$
\frac{d}{dt'}(\omega_{ie}^e \times \mathbf{x}^e) = \dot{\omega}_{ie}^e \times \mathbf{x}^e + \omega_{ie}^e \times \dot{\mathbf{x}^e}. \tag{5.18}
$$

Hence, integrating the following integral by parts yields

$$
\int_{t_0}^{t} (\omega_{ie}^e \times \mathbf{x}^e) \cdot \ddot{\mathbf{x}}^e dt' = (\omega_{ie}^e \times \mathbf{x}^e) \cdot \dot{\mathbf{x}}^e - E_1 - \int_{t_0}^{t} (\dot{\omega}_{ie}^e \times \mathbf{x}^e) \cdot \dot{\mathbf{x}}^e dt'. \tag{5.19}
$$

where E_1 is an integration constant. Again, using (5.18), there is

$$
\begin{aligned}
&2\int_{t_0}^{t}(\omega_{ie}^{e}\times\dot{\mathbf{x}}^{e})\cdot(\omega_{ie}^{e}\times\mathbf{x}^{e})dt' = \\
&\int_{t_0}^{t}\frac{d}{dt'}|\omega_{ie}^{e}\times\mathbf{x}^{e}|^2dt' - 2\int_{t_0}^{t}(\omega_{ie}^{e}\times\mathbf{x}^{e})\cdot(\dot{\omega}_{ie}^{e}\times\mathbf{x}^{e})dt' = \\
&|\omega_{ie}^{e}\times\mathbf{x}^{e}|^2 - E_2 - 2\int_{t_0}^{t}(\omega_{ie}^{e}\times\mathbf{x}^{e})\cdot(\dot{\omega}_{ie}^{e}\times\mathbf{x}^{e})dt'
\end{aligned}
\tag{5.20}
$$

Substituting (5.15), (5.17), (5.19) and (5.20) into the second integral of (5.13) yields

$$
\begin{aligned}
\int_{t_0}^{t}\mathbf{a}^{e}\cdot(\omega_{ie}^{e}\times\mathbf{x}^{e})dt' &= (\omega_{ie}^{e}\times\mathbf{x}^{e})\cdot\dot{\mathbf{x}}^{e}) + |\omega_{ie}^{e}\times\mathbf{x}^{e}|^2 - E_1 - E_2 \\
&- \int_{t_0}^{t}(\dot{\omega}_{ie}^{e}\times\mathbf{x}^{e})\cdot\dot{\mathbf{x}}^{e}dt' - \int_{t_0}^{t}(\mathbf{g}^{e}+\dot{\omega}_{ie}^{e}\times\mathbf{x}^{e})\cdot(\omega_{ie}^{e}\times\mathbf{x}^{e})dt'
\end{aligned}
\tag{5.21}
$$

The gravitational potential in the e-frame, (5.13), then becomes

$$
\begin{aligned}
V(\mathbf{x}^{e},t) = \frac{1}{2}|\dot{\mathbf{x}}^{e}|^2 - \frac{1}{2}|\omega_{ie}^{e}\times\mathbf{x}^{e}|^2 - \int_{t_0}^{t}\mathbf{a}^{e}\cdot\dot{\mathbf{x}}^{e}dt' + \int_{t_0}^{t}(\dot{\omega}_{ie}^{e}\times\mathbf{x}^{e})\cdot\dot{\mathbf{x}}^{e}dt' \\
+ \int_{t_0}^{t}(\omega_{ie}^{e}\times\mathbf{x}^{e})\cdot(\mathbf{g}^{e}+\dot{\omega}_{ie}^{e}\times\mathbf{x}^{e})dt' + \int_{t_0}^{t}\frac{\partial V(x^{e},t')}{\partial t'}dt' - E^{(0,e)}
\end{aligned}
\tag{5.22}
$$

where the constants are combined in $E^{(0,e)}$. The partial derivative of the potential with respect to time in this expression still refers to the potential in the e-frame according to

$$
\frac{\partial V(x^{e},t')}{\partial t'} = \frac{\partial V(\mathbf{C}_{e}^{i}x^{i},t')}{\partial t'} \tag{5.23}
$$

Simplifications of (5.22) ensue by noting that the last integral can be combined in part with the integrals involving $\mathbf{g}^{e}$ and ω_{ie}^{e}, as shown in the next section.

5.2.2 *Separation of the Temporal Variations*

The primary temporal variation of the gravitational potential in the inertial frame is due to Earth rotation, with a small secondary effect caused by its temporal variation as modeled by the Earth orientation parameters, EOP, associated with precession, nutation, and polar motion. These temporal variations are entirely due to the transformation between the e- and i-frames. In addition, the total potential includes the tidal potential that changes with the relative motion of the extraterrestrial bodies. The tidal potential causes corresponding gravitational deformation of the non-rigid Earth body, including ocean tides, Earth tides, and ocean loading on the solid Earth. Even the potential variation due to polar motion changes gravity (by changing the

centrifugal acceleration at the Earth's surface), which causes a deformation of the solid Earth, called the pole tide. Being of longer temporal wavelength, it is generally assumed that polar motion does not affect the oceans. Any deformation in the Earth naturally generates a change in the geopotential. Finally, any other terrestrial mass redistributions, such as atmospheric variations, which also cause a barotropic ocean response, hydrological (including ice mass) variations, and episodic events such as major earthquakes and volcanic eruptions, can cause discernible changes in Earth's gravitational potential.

In view of the deformations and mass redistributions, it is more appropriate to model the total geopotential in the e-frame. It is convenient to separate the various temporal effects from the main, static, gravitational potential, $V^{(E)}$,

$$V = V^{(E)} + V^{(\delta E)}, \tag{5.24}$$

where the residual includes the tidal potential (TP) and effects due to all deformations and mass redistributions,

$$V^{(\delta E)} = V^{(TP)} + V^{(deform)} + V^{(\delta mass)}, \tag{5.25}$$

with

$$V^{(deform)} = V^{(ET)} + V^{(OT)} + V^{(OL)} + V^{(PT)}, \tag{5.26}$$

which further identifies time-varying component potentials due to Earth tides (ET), ocean tides (OT), and the deformations associated with ocean loading (OL) and the pole tide (PT).

Regarding the potential in the i-frame, one may write $V(\mathbf{x}^i, t) = V(C_e^i \mathbf{x}^e, t)$, and note that the explicit derivative with respect to time involves two terms,

$$\frac{\partial V(\mathbf{x}^i, t)}{\partial t} = \nabla_{x^e} V \cdot \frac{\partial}{\partial t}(\mathbf{C}_i^e \mathbf{x}^i) + \frac{\partial V(\mathbf{C}_e^i \mathbf{x}^e, t)}{\partial t}. \tag{5.27}$$

The potential in the second term is written explicitly as a function of $\mathbf{x}^e$ to indicate that the time derivative is in the e-frame and then transformed to the i-frame. Since $V^{(E)}$ at a point in the e-frame does not depend on time by definition, the second term in (5.27) is zero for this part of the potential,

$$\frac{\partial V^{(E)}(\mathbf{C}_e^i \mathbf{x}^e, t)}{\partial t} = 0. \tag{5.28}$$

The first term on the right of (5.27), however, is never zero because the transformation matrix, $\mathbf{C}_e^i$, depends on time. Since the position vector, $\mathbf{x}^i$, is held fixed, this term is given by

$$\begin{aligned}\nabla_{x^e} V \cdot \frac{\partial}{\partial t}(\mathbf{C}_i^e \mathbf{x}^i) &= \nabla_{x^e} V \cdot \dot{\mathbf{C}}_i^e \mathbf{x}^i = \nabla_{x^e} V \cdot \mathbf{C}_i^e [\omega_{ei}^e \times] \mathbf{x}^i \\ &= \mathbf{g}^e \cdot \mathbf{C}_i^e [\omega_{ei}^e \times] \mathbf{C}_e^i \mathbf{C}_i^e \mathbf{x}^i \\ &= -\mathbf{g}^e \cdot (\omega_{ie}^e \times \mathbf{x}^e)\end{aligned} \tag{5.29}$$

noting that $\omega_{ei}^e = -\omega_{ie}^e$, and where (5.14) was used in the first line. Hence

$$\frac{\partial V(\mathbf{x}^i, t)}{\partial t} = \frac{\partial V(\mathbf{x}^e, t)}{\partial t} - \mathbf{g}^e \cdot (\omega_{ie}^e \times \mathbf{x}^e). \tag{5.30}$$

Being the scalar product of two vectors (neither a derivative), the second term in (5.30) is coordinate-frame invariant (rotating each vector using $\mathbf{C}_i^e$ does not change the value of the product),

$$\mathbf{g}^e \cdot (\omega_{ie}^e \times \mathbf{x}^e) = \mathbf{g}^i \cdot (\omega_{ie}^i \times \mathbf{x}^i); \tag{5.31}$$

and thus, from (5.24) and (5.28), one also has the derivative of the potential in the i-frame by co-ordinate transformation,

$$\frac{\partial V(\mathbf{x}^i, t)}{\partial t} = \frac{\partial V^{(\partial E)}(\mathbf{C}_e^i \mathbf{x}^e, t)}{\partial t} - \mathbf{g}^i . (\omega_{ie}^i \times \mathbf{x}^i), \tag{5.32}$$

where the partial derivative on the right side holds $\mathbf{x}^i$ fixed. It is written for the transformed position variable because the models for $V^{(\partial E)}$ typically are given in the e-frame. With (5.32), (5.9), (5.24) and (5.28) the energy balance equation (5.11) in the i-frame becomes

$$\begin{aligned}&V(\mathbf{x}^i, t) = \frac{1}{2}|\dot{\mathbf{x}}^i|^2 - \int_{t_0}^t \mathbf{a}^i \cdot \dot{\mathbf{x}}^i dt' - \int_{t_0}^t (\ddot{\mathbf{x}}^i - \mathbf{a}^i) \cdot (\omega_{ie}^i \times \mathbf{x}^i) dt' + \\ &\int_{t_0}^t \frac{\partial V^{(\partial E)}(\mathbf{C}_e^i \mathbf{x}^e, t')}{\partial t'} dt' - E^{(0,i)} = \\ &\frac{1}{2}|\dot{\mathbf{x}}^i|^2 - \int_{t_0}^t \ddot{\mathbf{x}}^i \cdot (\omega_{ie}^i \times \mathbf{x}^i) dt' - \int_{t_0}^t \mathbf{a}^i \cdot (\dot{\mathbf{x}}^i - \omega_{ie}^i \times \mathbf{x}^i) dt' + \\ &\int_{t_0}^t \frac{\partial V^{(\partial E)}(\mathbf{C}_e^i \mathbf{x}^e, t')}{\partial t'} dt' - E^{(0,i)}\end{aligned} \tag{5.33}$$

Similar to (5.18),

$$\frac{d}{dt'}(\omega_{ie}^i \times \mathbf{x}^i) = \dot{\omega}_{ie}^i \times \mathbf{x}^i + \omega_{ie}^i \times \dot{\mathbf{x}}^i; \tag{5.34}$$

therefore, integrating the first integral in (5.33) by parts,

$$\int_{t_0}^{t} \ddot{\mathbf{x}}^i \cdot (\omega_{ie}^i \times \mathbf{x}^i) dt' = \dot{\mathbf{x}}^i \cdot (\omega_{ie}^i \times \mathbf{x}^i) - E_3 - \int_{t_0}^{t} \dot{\mathbf{x}}^i \cdot (\dot{\omega}_{ie}^i \times \mathbf{x}^i + \omega_{ie}^i \times \dot{\mathbf{x}}^i) dt'$$
$$= \dot{x}^i \cdot (\omega_{ie}^i \times \mathbf{x}^i) - E_3 - \int_{t_0}^{t} \dot{\mathbf{x}}^i \cdot (\dot{\omega}_{ie}^i \times \mathbf{x}^i) dt' \tag{5.35}$$

by the orthogonality of $\dot{\mathbf{x}}^i$ and $\omega_{ie}^i \times \dot{\mathbf{x}}^i$, and where E_3 is a constant. Thus,

$$V(\mathbf{x}^i, t) = \frac{1}{2}|\dot{\mathbf{x}}^i|^2 - \dot{\mathbf{x}}^i \cdot (\omega_{ie}^i \times x^i) - \int_{t_0}^{t} \mathbf{a}^i \cdot (\dot{\mathbf{x}}^i - \omega_{ie}^i \times x^i) dt'$$
$$+ \int_{t_0}^{t} \dot{\mathbf{x}}^i \cdot (\dot{\omega}_{ie}^i \times \dot{\mathbf{x}}^i) dt' + \int_{t_0}^{t} \frac{\partial V^{(\partial E)}(\mathbf{C}_e^i x^e, t')}{\partial t'} dt' - E^{(0,i)} \tag{5.36}$$

where $E^{(0,i)}$ has absorbed the constant, E_3. Similarly, for the e-frame formulation, (5.22), substitution of (5.30) with (5.29) yields

$$V(\mathbf{x}^e, t) = \frac{1}{2}|\dot{\mathbf{x}}^e|^2 - \frac{1}{2}|\omega_{ie}^e \times \mathbf{x}^e|^2 - \int_{t_0}^{t} \mathbf{a}^e \cdot \dot{\mathbf{x}}^e dt' + \int_{t_0}^{t} (\dot{\omega}_{ie}^e \times \mathbf{x}^e) \cdot \dot{\mathbf{x}}^e dt'$$
$$+ \int_{t_0}^{t} (\omega_{ie}^e \times \mathbf{x}^e) \cdot (\dot{\omega}_{ie}^e \times \mathbf{x}^e) dt' + \int_{t_0}^{t} \frac{\partial V^{(\partial E)}(\mathbf{x}^e, t')}{\partial t'} dt' - E^{(0,i)} \tag{5.37}$$

Equations (5.36) and (5.37) are the final, exact forms of the energy balance equations in the i- and e-frames, respectively. Two important aspects of these equations should be noted. First, the integrand, $\partial V/\partial t'$, in the last time-integrals in (5.36) and (5.37) is integrated along the satellite orbit (that is how the integral in (5.6) is defined), but it is the partial derivative of the potential with respect to time for fixed $\mathbf{x}^e$ (respectively, $\mathbf{x}^i$). Second, the potential on the left side of each equation, of course, includes all effects as defined in (5.24) through (5.26). To emphasize the latter and identify the contributions on the right sides of the energy balance equations, one can write generally for either frame,

$$V^{(E)} + V^{(\partial E)} = V^{(K)} - V^{(R)} - V^{(F)} + V^{(TI)} - E^{(0)}, \tag{5.38}$$

where the kinetic energy term is

$$V^{(K,i,e)} = \frac{1}{2}|\dot{\mathbf{x}}^{i,e}|^2; \tag{5.39}$$

and, the rotation potential term is either

$$V^{(R,i)} = \dot{\mathbf{x}}^i \cdot (\omega_{ie}^i \times x^i) - \int_{t_0}^{t} \dot{\mathbf{x}}^i \cdot (\dot{\omega}_{ie}^i \times \mathbf{x}^i) dt', \tag{5.40}$$

or

$$V^{(R,e)} = \frac{1}{2}|\omega_{ie}^e \times \mathbf{x}^e|^2 - \int_{t_0}^t \dot{\mathbf{x}}^e \cdot (\dot{\omega}_{ie}^e \times \mathbf{x}^e)dt' - \int_{t_0}^t (\omega_{ie}^e \times \mathbf{x}^e) \cdot (\dot{\omega}_{ie}^e \times \mathbf{x}^e)dt'. \tag{5.41}$$

All but the first terms on the right sides of (2.37) and (2.38) are shown in the next section to be negligible since $\dot{\omega}_{ie}^i \approx 0$. The *dissipative energy* terms are

$$V^{(F,i)} = \int_{t_0}^t \mathbf{a}^i \cdot (\dot{\mathbf{x}}^i - \omega_{ie}^i \times \mathbf{x}^i)dt', \qquad V^{(F,e)} = \int_{t_0}^t \mathbf{a}^e \cdot \dot{\mathbf{x}}^e dt', \tag{5.42}$$

where the second term in the integral for $V^{(F,i)}$ can be neglected since $|\omega_{ie}^i \times x^i| \ll |\dot{\mathbf{x}}^i|$ for low Earth-orbiting satellites. Finally, the integral of the time-derivative of the potentials that are not constant in the e-frame is denoted

$$V^{(TI,i)} = \int_{t_0}^t \frac{\partial V^{(\partial E)}(\mathbf{C}_e^i x^e, t')}{\partial t'}dt', \quad V^{(TI,e)} = \int_{t_0}^t \frac{\partial V^{(\partial E)}(\mathbf{x}^e, t')}{\partial t'}dt'. \tag{5.43}$$

5.2.3 Earth Orientation Effects

The need to consider Earth Orientation Parameters for the most part is a consequence of the requirement to define *reference* coordinate systems, and since Earth's spin axis varies in both the i- and e-frames. The rotation rate vector, ω_{ie}^i, is dominated by the component along the third axis, represented by the unit vectors, $\mathbf{e}_3^{i,e}$, in either reference frame, and one may write

$$\omega_{ie}^{i,e} = \omega_E \mathbf{e}_3^{i,e} + \delta\omega_{ie}^{i,e}, \tag{5.44}$$

where $\omega_E = 7.292115 \times 10^{-5}$ rad/s is the mean Earth rotation rate and where $\omega_{ie}^e = \mathbf{C}_i^e \omega_{ie}^i$. The transformation between the terrestrial and celestial reference frames is ([116], Chap. 5)

$$\mathbf{C}_i^e = \mathbf{W}^T(x_p, y_p)\mathbf{R}_3(\theta)\mathbf{Q}^T(X, Y), \tag{5.45}$$

where $\mathbf{Q}$ is the precession-nutation matrix in the modern formulation; $\mathbf{R}_3$ is the cardinal rotation matrix for the third Cartesian axis depending on the Earth rotation angle, θ; and $\mathbf{W}$ is the polar motion matrix. The arguments, X, Y, of $\mathbf{Q}$ are coordinates of the Celestial Intermediate Pole (CIP, approximately Earth's spin axis) in the i-frame, and those of $\mathbf{W}$ are the coordinates, x_p, y_p, of the CIP in the e-frame (Fig. 5.1). These EOP are functions of time and are determined accurately from VLBI (Very-Long Baseline Interferometry) and other space techniques [131]. From (5.14) (and, interchanging frames, i and e), the rotation rates in the e- and i-frames are given by

$$[\omega_{ie}^e \times] = \mathbf{C}_i^e \dot{\mathbf{C}}_e^i, \qquad [\omega_{ie}^i \times] = -\mathbf{C}_e^i \dot{\mathbf{C}}_i^e. \tag{5.46}$$

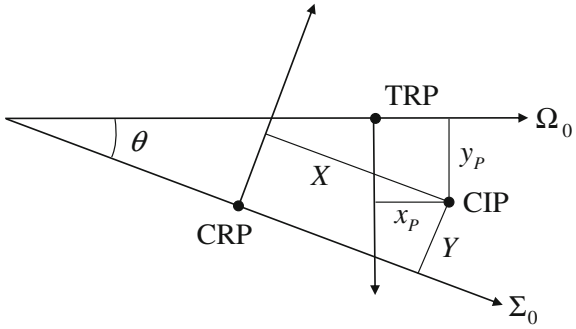

Fig. 5.1 Definition of the polar motion coordinates, x_p,y_p, of the Celestial Intermediate Pole (CIP) relative to the terrestrial reference pole (TRP) and the precession/nutation coordinates, X, Y of the CIP relative to the celestial reference pole (CRP). Σ_0 and Ω_0 are the origins in right ascension and longitude, respectively, in the celestial and terrestrial reference systems. The Earth rotation angle, $\theta = \omega_E t$, formally is an angle about the CIP; it is approximately the angle indicated in the diagram

The residual rotation rate, $\delta\omega_{ie}^{i,e}$, is analyzed in Sect. 5.3, where it is also evident that the rate of $\omega_{ie}^{i,e}$, that is, $\dot{\omega}_{ie}^{i,e}$, is exceedingly small and all corresponding terms in the rotation potentials, (5.40) and (5.41), may be omitted without significant loss in precision. The remaining first terms of the rotation potentials are separated according to the dominant and residual rates,

$$V^{(R,i)} = V^{(R0,i)} + V^{(\delta R,i)} = \dot{\mathbf{x}}^i \cdot (\omega_E e_3^i \times \mathbf{x}^i) + \dot{\mathbf{x}}^i \cdot (\delta\omega_{ie}^i \times \mathbf{x}^i), \tag{5.47}$$

$$V^{(R,e)} = V^{(R0,e)} + V^{(\delta R,e)} = \frac{1}{2}|\omega_E e_3^e \times \mathbf{x}^e|^2 + (\omega_E e_3^e \times \mathbf{x}^e) \cdot (\delta\omega_{ie}^e \times \mathbf{x}^e), \tag{5.48}$$

where second-order terms have been neglected. The dominant terms have the following simplified forms,

$$V^{(R0,i)} = \omega_E (x_1^i \dot{x}_2^i - x_2^i \dot{x}_1^i), \tag{5.49}$$

$$V^{(R0,e)} = \frac{1}{2}\omega_E^2((x_1^e)^2 + (x_2^e)^2). \tag{5.50}$$

$V^{(R0,e)}$ is also recognized in physical geodesy as the *centrifugal potential* that is responsible for the difference between *gravity* (measured on the rotating Earth) and *gravitation* (the mass attraction). And, $V^{(\delta R,e)}$ is known as the *pole tide potential*, which is due to changes in the Earth rotation vector (principally its direction; the reference to 'tide' comes from the association with Earth rotation). Because the pole tide potential varies in time at a fixed point in the *e*-frame, the corresponding change

in gravity causes a deformation in the Earth, which further causes a change in the mass-attraction potential; this is included in $V^{(deform)}$ in (5.26).

5.2.4 Models for the Potential

In a strict sense, (5.36) or (5.37) is a kind of integral equation for the time variable potential, appearing on both sides of the equation. The left sides, of course, contain all mass-attraction potentials as detailed in (5.24) through (5.26); and, the right sides include the integral along the orbit of the explicit time derivative of the time-varying part, $V^{(\delta E)}$. Separating the potentials for particular sources requires the development of corresponding models, which then also facilitates the analysis of their significance on the estimation of any particular component.

For present purposes, only the static and tidal potentials are given, being the most significant. The static part, $V^{(E)}$, is expressed typically in the e-frame as an infinite series of solid spherical harmonics using the usual spherical coordinates, r, ϕ, λ,

$$V^{(E)}(r,\phi,\lambda) = \frac{GM}{a}\sum_{n=0}^{\infty}\sum_{m=-n}^{n}(\frac{a}{r})^{n+1}C^{(E)}_{n,m}\bar{Y}_{n,m}(\phi,\lambda), \tag{5.51}$$

where the coefficients, $C^{(E)}_{n,m}$, are constants, and the surface spherical harmonics are defined by

$$\bar{Y}_{n,m}(\phi,\lambda) = \bar{P}_{n,|m|}(\sin\theta)\begin{cases}\cos m\lambda, m \geq 0\\ \sin|m|\lambda, m < 0\end{cases} \tag{5.52}$$

where the $\bar{P}_{n,m}$ are fully normalized associated Legendre functions [59].

The tidal potential, $V^{(TP)}$, is the potential of the extraterrestrial bodies of the solar system that is associated with the residual gravitational acceleration due to these bodies, relative to the acceleration at Earth's center of mass. Thus, there are no zero- and first-degree harmonics in $V^{(TP)}$ since their gradients would vanish or be constant [144, 153]. Following the formulation of [90], the tidal potential in the e-frame due to a body considered as a point mass, M_B, located at (r_B, ϕ_B, λ_B) is given by the interior potential,

$$V^{(TP)}_B(r,\phi,\lambda,t) = \frac{GM_B}{r_B(t)}\sum_{n=2}^{n_B}\frac{1}{2n+1}(\frac{r}{r_B(t)})^n \sum_{m=0}^{n}\bar{P}_{n,m}(\sin\phi)\bar{P}_{n,m}(\sin\phi_B(t))\cos(mh_B(t)), \tag{5.53}$$

where h_B is the hour angle of the body, given in terms of the Earth rotation angle, θ, between the reference meridians of the e- and i-frames (Fig. 5.1), the longitude, λ, and the right ascension of the body, α_B, by

$$h_B(t) = \theta(t) + \lambda - \alpha_B(t). \tag{5.54}$$

In view of the ratio, r/r_B, the maximum degree typically is $n_B = 2$ or $n_B = 3$, and, usually only the Sun and Moon are considered to generate a significant tidal potential; however, see also [57]. The time argument, t, is international atomic time (which may be converted easily to GPS time in the case of GRACE).
If the Earth were rigid (and without oceans), the only time-varying mass-attraction potential would be the tidal potential, $V^{(TP)}$. Because of Earth's non-rigidity, the time-varying potential due to extra-terrestrial bodies creates indirect effects, $V^{(ET)}$,$V^{(OT)}$, and $V^{(OL)}$, in the potential due to the consequent deformation of the solid (elastic) terrestrial and oceanic masses, known as Earth and ocean tides (ET and OT), and an additional deformation in the solid Earth due to ocean loading (OL). Although the latter three potentials may be viewed as time-varying potentials due to mass redistributions, they are distinguished as being a consequence of the tidal potential (TP), which is well modeled.
Therefore, models for these secondary effects are also readily modeled on the basis of assumed rheological properties of the Earth. For example, considered as a force on the Earth, the tidal acceleration exerted by an extra-terrestrial body deforms the Earth, which under the assumption of elasticity and in a first approximation, behaves according to Hooke's law. In this case, the 'spring constants', appropriately scaled to be dimension-less, are called Love (and Shida) numbers. It is outside the present scope to delve into the details of models for $V^{(ET)}$, $V^{(OT)}$ and $V^{(OL)}$ and deference for these and models for the other components of $V^{(\delta E)}$ is given to more authoritative texts (e.g., [116] Chaps. 6, 7; [47]); and references listed in [139]).

5.2.5 *Energy Balance Equations for Satellite-to-Satellite Tracking*

For two satellites following each other in a similar orbit (Fig. 5.2), whose position and velocity vectors are $\mathbf{x}_1$, $\mathbf{x}_2$, $\dot{\mathbf{x}}_1$, $\dot{\mathbf{x}}_2$, define the differences,

$$\mathbf{x}_{12} = \mathbf{x}_2 - \mathbf{x}_1, \;\; \dot{\mathbf{x}}_{12} = \dot{\mathbf{x}}_2 - \dot{\mathbf{x}}_1, \quad V_{12} = V(\mathbf{x}_2) - V(\mathbf{x}_1). \tag{5.55}$$

To simplify the notation, the time argument in the potential functions is omitted henceforth, as is the frame designation in the state vectors; they are included only when the formulation requires it. Indeed, the following details for the kinetic energy, $V^{(K)} = \frac{1}{2}|\dot{\mathbf{x}}|^2$ (Eq. 5.39), is the same in either frame. In addition to generic tracking of each satellite (ground-based and/or more prevalently GNSS-based), there is precise satellite-to-satellite range tracking, where the range between the satellites is

$$\rho_{12} = |\mathbf{x}_{12}| = \sqrt{\mathbf{x}_{12}^T \mathbf{x}_{12}}. \tag{5.56}$$

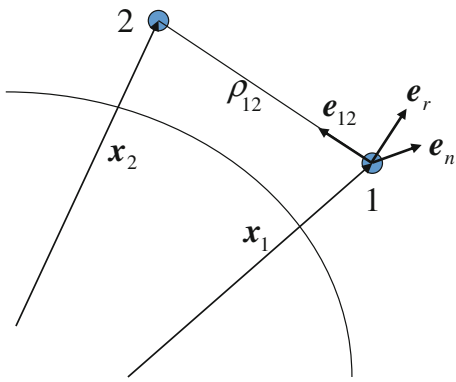

Fig. 5.2 Geometry of low–low satellite-to-satellite tracking

The corresponding principal observable is given as the range-rate, $\dot{\rho}_{12}$. Since $\rho_{12}\dot{\rho}_{12} = \mathbf{x}_{12}^T\mathbf{x}_{12}$, it is the projection of the velocity difference onto the line-of sight between the satellites,

$$\dot{\rho}_{12} = \dot{\mathbf{x}}_{12}^T\mathbf{e}_{12}, \tag{5.57}$$

where $\mathbf{e}_{12}$ is the unit vector from the first to the second satellite,

$$e_{12} = \frac{x_2 - x_1}{|x_2 - x_1|}. \tag{5.58}$$

With some imprecision, it is called here for convenience the *along-track* unit vector. From $|\dot{\mathbf{x}}_2|^2 - |\dot{\mathbf{x}}_1|^2 = (\dot{\mathbf{x}}_2 - \dot{\mathbf{x}}_1)^T(\dot{\mathbf{x}}_2 + \dot{\mathbf{x}}_1)$, the kinetic energy part of the potential difference is

$$V_{12}^{(K)} = \frac{1}{2}(|\dot{\mathbf{x}}_2|^2 - |\dot{\mathbf{x}}_1|^2) = \frac{1}{2}\dot{\mathbf{x}}_{12}^T(\dot{\mathbf{x}}_2 + \dot{\mathbf{x}}_1) \tag{5.59}$$

Let $\mathbf{e}_n$, $\mathbf{e}_r$ be unit vectors that together with $\mathbf{e}_{12}$ form a right-handed mutually orthogonal triad, and decompose $\dot{\mathbf{x}}_{12}$ into components along $\mathbf{e}_{12}$, $\mathbf{e}_n$, and $\mathbf{e}_r$,

$$\dot{\mathbf{x}}_{12} = (\mathbf{e}_{12}^T\dot{\mathbf{x}}_{12})\mathbf{e}_{12} + (\mathbf{e}_n^T\dot{\mathbf{x}}_{12})e_n + (\mathbf{e}_r^T\dot{\mathbf{x}}_{12})\mathbf{e}_r. \tag{5.60}$$

For example, $\mathbf{e}_n$ and $\mathbf{e}_r$ may be computed from

$$\mathbf{e}_n = \frac{\mathbf{x}_1 \times \mathbf{x}_2}{|\mathbf{x}_1 \times \mathbf{x}_2|}, \quad \mathbf{e}_r = \mathbf{e}_{12} \times \mathbf{e}_n. \tag{5.61}$$

The unit vector, $\mathbf{e}_n$, is orthogonal to the plane defined by the instantaneous position vectors of the two satellites; it is called here the cross-track unit vector. The third vector, $\mathbf{e}_r$, is called the radial unit vector, being roughly in that direction. Then, from (5.57), one has

$$V_{12}^{(K)} = \frac{1}{2}(\dot{\rho}_{12}\mathbf{e}_{12}^T + (\mathbf{e}_n^T\dot{\mathbf{x}}_{12})\mathbf{e}_n^T + (\mathbf{e}_r^T\dot{\mathbf{x}}_{12})\mathbf{e}_r^T)(\dot{\mathbf{x}}_1 + \dot{\mathbf{x}}_2), \tag{5.62}$$

which separates the potential difference into a range-rate (along-track) component and two differences, one of the squares of the cross-track velocities and one of the squares of their radial velocities.

$$V_{12}^{(K)} = \frac{1}{2}\dot{\rho}_{12}(\dot{\mathbf{x}}_1 + \dot{\mathbf{x}}_2)^T\mathbf{e}_{12} + \frac{1}{2}(|\mathbf{e}_n^T\dot{\mathbf{x}}_2|^2 - |\mathbf{e}_n^T\dot{\mathbf{x}}_1|^2) + \frac{1}{2}(|\mathbf{e}_r^T\dot{\mathbf{x}}_2|^2 - |\mathbf{e}_r^T\dot{\mathbf{x}}_1|^2). \tag{5.63}$$

As shown in Sect. 5.3 by simulations, the first term is generally the largest, but the last, radial term is nearly as large (and opposite in phase), while the cross-track term is almost negligible by comparison. Furthermore, Sect. 5.5 shows why including the range-rate as an explicit observable enables the determination of high-accuracy potential differences.

The other contributions to the potential difference, such as the rotation potential, $V^{(R)}$, and the other time-varying potentials appearing in $V^{(TI,i,e)}$, may be formulated simply as differences; for example,

$$V_{12}^R = V_2^{(R)} - V_1^{(R)}. \tag{5.64}$$

The nominal part of the rotation potential difference in the i-frame may also be written in terms of position and velocity differences,

$$\begin{aligned} V_{12}^{(R0)} &= \omega_E(\dot{\mathbf{x}}_2 \cdot (\mathbf{e}_3 \times \mathbf{x}_2) - \dot{\mathbf{x}}_1.(\mathbf{e}_3 \times \mathbf{x}_1)) \\ &= \omega_E(\dot{\mathbf{x}}_2 \cdot (\mathbf{e}_3 \times \mathbf{x}_2) - \dot{\mathbf{x}}_1 \cdot (\mathbf{e}_3 \times \mathbf{x}_1) - \dot{\mathbf{x}}_1 \cdot (\mathbf{e}_3 \times \mathbf{x}_2) + \dot{\mathbf{x}}_1 \cdot (\mathbf{e}_3 \times \mathbf{x}_2)) \\ &= \omega_E(\dot{\mathbf{x}}_{12} \cdot (\mathbf{e}_3 \times \mathbf{x}_2) + \mathbf{x}_1 \cdot (\mathbf{e}_3 \times \dot{\mathbf{x}}_1) - \mathbf{x}_2 \cdot (\mathbf{e}_3 \times \dot{\mathbf{x}}_1)) \\ &= \omega_E(\dot{\mathbf{x}}_{12} \cdot (\mathbf{e}_3 \times \mathbf{x}_2) - \mathbf{x}_{12} \cdot (\mathbf{e}_3 \times \dot{\mathbf{x}}_1)) \end{aligned} \tag{5.65}$$

5.3 Magnitudes and Approximations

From purely schematic considerations, the dominant velocity components of the GRACE satellites are along their orbits, hence cross-track (in the inertial frame) and radial components are expected to be relatively small. One might argue that also the differences of these components are small, leaving in (5.63) only the first term as significant. Indeed, recognizing that $\dot{\mathbf{x}}_1 \approx \dot{\mathbf{x}}_2$ and $|\dot{\mathbf{x}}| \approx \dot{\mathbf{x}}^T\mathbf{e}_{12}$, the first-order part of the kinetic energy difference might be roughly approximated as

$$V_{12}^{(K)} \approx |\dot{\mathbf{x}}_1|\dot{\rho}_{12}. \tag{5.66}$$

This was the model originally introduced by Wolff [160]. While this approximation may serve general feasibility studies, practical applications demand a more precise

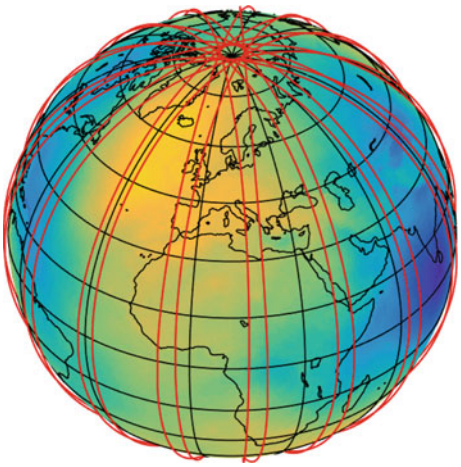

Fig. 5.3 Simulated orbits in the *e*-frame for GRACE-like satellites during one day. The background on the globe is the geoid undulation with maximum values indicated by the *color yellow* and minima by the *color blue*

formulation. On the other hand, the exact form of the energy balance equation given in Sect. 5.2 also contains possibly still negligible terms. In this section, its various components are analyzed to determine which may be neglected and which provide the essential information on the gravitational potential at the resolution and accuracy of interest.

Toward that end GRACE-like orbits are simulated on the basis of a high-resolution geopotential model. Specifically, EGM2008 [114] may be used, but its full degree-and-order complement of harmonics is not needed since current satellite gravitation-mapping missions are limited in resolution by their velocity and system integration time [76]. Here, the maximum degree (and order), $n_{max} = 180$ serves the purpose and is already somewhat larger than the resolution of current GRACE-derived models. A single day of orbits (roughly 15 revolutions of the satellites) also suffices to sample the entire field of the rotating Earth, even though that sample is not uniform (Fig. 5.3). The initial Kepler elements of these orbits are shown in Table 5.1. The orbital state vectors of each satellite are generated by numerically integrating the equations of motion, (5.1), with $\mathbf{a} = \mathbf{0}$. No specific forces acting on the satellites nor time-varying potentials are included in this simulation. Therefore, the corresponding potential difference in the inertial frame is given by

$$V_{12} = V_{12}^{(K)} - V_{12}^{(R0,i)} - E_{12}^{(0,i)}. \tag{5.67}$$

The error in the numerical integration of the equations of motion is determined by comparing the potential difference for the points of the generated orbits with the geopotential model that generated the orbits; the standard deviation of the difference, $5 \times 10^{-7}\,\mathrm{m}^2/\mathrm{s}^2$ is attributable to computational round-off error.

Table 5.1 Initial Keplerian elements for the GRACE-like simulated orbits

	Leading satellite	Trailing satellite	
Semi−major axis	6808140 m	6808140 m	alt ≈ 430 km
Eccentricity	0	0	near circular
Inclination	87°	87°	near polar
Argument of perigee	0°	0°	
Longitude of node	−83°	−83°	
Time of first perigee	0 s	30 s	$\rho 12 \approx 230$ km

5.3.1 Kinetic Energy Term

The values of the along-track, cross-track, and radial constituents of $V_{12}^{(K)}$ in the inertial frame, repeated here,

$$V_{12}^{(K)} = \frac{\mathbf{1}}{\mathbf{2}}\dot{\rho}_{12}(\dot{\mathbf{x}}_1 + \dot{\mathbf{x}}_2)^T e_{12} + \frac{\mathbf{1}}{\mathbf{2}}(|\mathbf{e_n}^T\dot{\mathbf{x}}_2|^2 - |\mathbf{e_n}^T\dot{\mathbf{x}}_1|^2) + \frac{\mathbf{1}}{\mathbf{2}}(|\mathbf{e_r}^T\dot{\mathbf{x}}_2|^2 - |\mathbf{e_r}^T\dot{\mathbf{x}}_1|^2) = V_{12}^{(\dot{\rho})} + V_{12}^{(n)} + V_{12}^{(r)} \tag{5.68}$$

are shown in (Fig. 5.4), purposely drawn on a logarithmic scale to illustrate the disparate magnitudes. Also included is the magnitude of the nominal rotation potential term, $V_{12}^{(R0,i)}$. The difference of cross-track velocity projections are many orders of magnitude smaller than the along-track difference; but, the difference of radial projections is commensurate in magnitude. Figure 5.4 focuses on the first 1.5 revolutions for the latter two constituents, $V_{12}^{(\dot{\rho})}$ and $V_{12}^{(r)}$, showing that they combine with opposite phase to yield a smaller total geopotential difference.

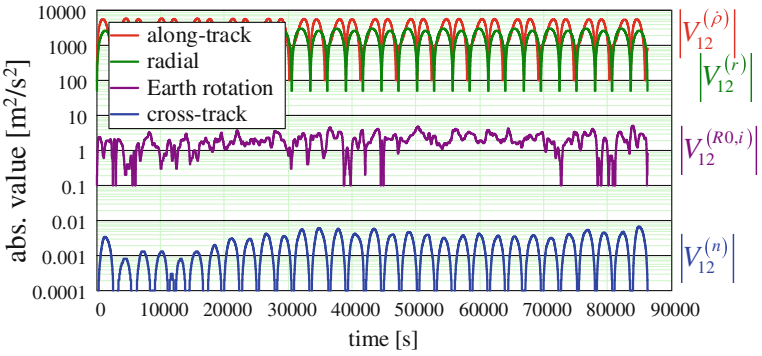

Fig. 5.4 Magnitudes of kinetic energy difference constituents, as well as the principal rotation potential difference in the i-frame

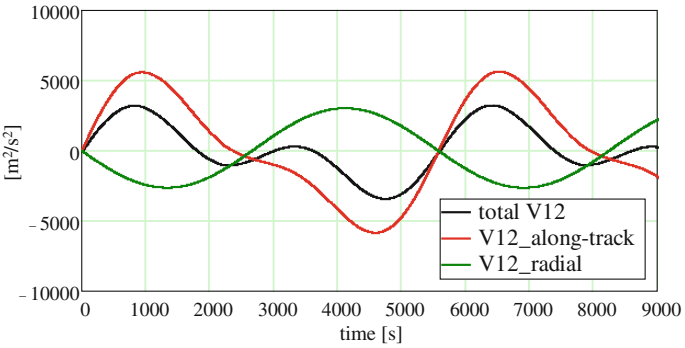

Fig. 5.5 Magnitudes of kinetic energy difference constituents, $V_{12}^{(\dot{\rho})}$ and $V_{12}^{(r)}$, as well as the total difference, $V_{12}^{(i)} = V_{12}^{(K,i)} - V_{12}^{(R0,i)}$

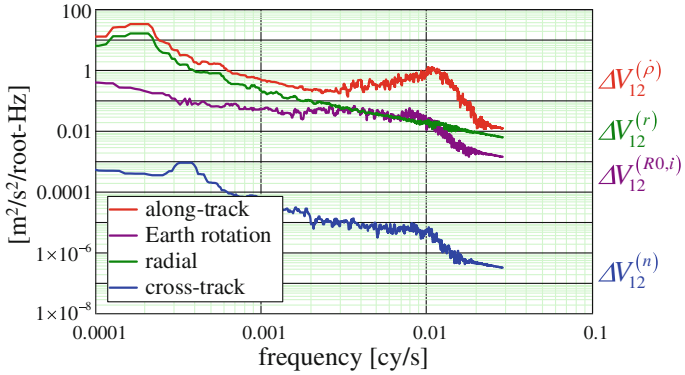

Fig. 5.6 Spectral analysis of the potential difference constituents in the kinetic energy difference, as well as the principal rotation potential difference in the *i*-frame. The analysis is for the entire 1-day orbit and is displayed as the *square root* of the power spectral density, approximated by the median-smoothed periodogram. The spectral peak in $V_{12}^{(\dot{\rho})}$ near $0.01^{\text{cy}}/_{\text{s}}$ corresponds to the maximum degree of the reference model (i.e., theoretically, the residual has no power at lower frequencies)

At first sight one might conclude that satellite-to-satellite tracking could not improve geopotential modeling since, by definition (Eq. 5.61), it does not sense the important radial component (Fig. 5.5). However, a spectral analysis of the components (Fig. 5.6) shows that the radial component is primarily a long-wavelength signal compared to the along-track component. Thus, a long-wavelength reference model would suffice to supplement the SST that then fills in the high-resolution variation of the field.

5.3.2 Earth Rotation Rate Terms

To understand the influence of the Earth Orientation Parameters (EOP) on satellite-to-satellite tracking, one may consider just the first-order approximations of $\mathbf{Q}$ and $\mathbf{W}$ in (5.45). Neglecting second-order terms, one has

$$\mathbf{W} \approx \mathbf{R}_1(y_p)\mathbf{R}_2(x_p), \tag{5.69}$$

$$\mathbf{Q}^T \approx \mathbf{R}_1(-Y)\mathbf{R}_2(X). \tag{5.70}$$

Substituting these into (5.46) and again neglecting all second-order terms, it can be shown that the Earth rotation rate vector may written succinctly as

$$\omega_{i,e}^{i,e} = \omega_E(m_1^{i,e}\mathbf{e}_1^{i,e} + m_2^{i,e}\mathbf{e}_2^{i,e} + (1 + m_3^{i,e})\mathbf{e}_3^{i,e}), \tag{5.71}$$

where $\mathbf{e}_j^{i,e}$ is a unit vector along the j^{th} coordinate axis of the i- or e-frame, and the $m_1^{i,e}$ are functions of the (EOP), listed in Table 5.2 along with typical values. Comparing (5.44) and (5.71), the residual rotation rate is

$$\delta\omega_{i,e}^{i,e} = \omega_E(m_1^{i,e}\mathbf{e}_1^{i,e} + m_2^{i,e}\mathbf{e}_2^{i,e} + m_3^{i,e}\mathbf{e}_3^{i,e}). \tag{5.72}$$

With the nominal values of EOP given in the second column of Table 5.2, it is clear that $m_{1,2}^e$ and $m_{1,2}^i$ are dominated, respectively, by the polar motion and precession coordinates (as noted in the third column); And, since $\Delta\omega_E = O(10^{-12\,\mathrm{rad}/\mathrm{s}})$, the third-axis component, $m_3^{i,e}$, is negligible by comparison. Thus, from (5.47) and (5.48),

Table 5.2 Components of the residual Earth rotation rate due to precession/nutation and polar motion. Typical values are for July 2014

First-order approximation	Typical values	Further approx.
$m_1^i = -X + \frac{\dot{Y} - \dot{x}_p \sin\theta + \dot{y}_p \cos\theta}{\omega_E}$	$X = 1.4 \times 10^{-3}$ rad, $\dot{X}/\omega_E = 4 \times 10^{-8}$	$m_1^i = -X$
$m_2^i = -Y - \frac{\dot{X} - \dot{y}_p \sin\theta - \dot{x}_p \cos\theta}{\omega_E}$	$Y = -2 \times 10^{-6}$ rad, $\dot{Y}/\omega_E = -1 \times 10^{-10}$	$m_2^i = -Y$
$m_3^i = \frac{\Delta\omega_E}{\omega_E}$ [a]	$m_3^i = -5 \times 10^{-9}$	$m_3^i = 0$
$m_1^e = -x_p + \frac{\dot{y}_p - \dot{X}\sin\theta - \dot{Y}\cos\theta}{\omega_E}$	$x_p = 9 \times 10^{-7}$ rad, $\dot{x}_p/\omega_E = 7 \times 10^{-10}$	$m_1^e = -x_p$
$m_2^e = y_p + \frac{\dot{x}_p - \dot{Y}\sin\theta - \dot{X}\cos\theta}{\omega_E}$	$y_p = 2 \times 10^{-6}$ rad, $\dot{y}_p/\omega_E = -1 \times 10^{-9}$	$m_2^e = y_p$
$m_3^e = \frac{\Delta\omega_E}{\omega_E}$	$m_3^i = -5 \times 10^{-9}$	$m_3^e = 0$

[a] $\Delta\omega_E$ is length-of-day variation

$$\begin{aligned} V^{(\delta R,i)} &= \omega_E \dot{\mathbf{x}}^i \cdot (X\mathbf{e}_1^i \times \mathbf{x}^i + Y\mathbf{e}_2^i \times \mathbf{x}^i) \\ &= \omega_E (X(x_2^i \dot{x}_3^i) - \dot{x}_2^i x_3^i) + Y(x_3^i \dot{x}_1^i - \dot{x}_3^i x_1^i)) \end{aligned} \tag{5.73}$$

$$\begin{aligned} V^{(\delta R,e)} &= \omega_E^2 (\mathbf{e}_3^e \times \mathbf{x}^e) \cdot (x_p \mathbf{e}_1^e \times \mathbf{x}^e - y_p \mathbf{e}_2^e \times \mathbf{x}^e) \\ &= \omega_E^2 (y_p x_2^e x_3^e - x_p x_1^e x_3^e) \end{aligned} \tag{5.74}$$

These and the principal rotation potential terms, as well as the omitted terms in (5.47) and (5.48), given by

$$V_{12}^{(\dot{\omega},i)} = \int_{t0}^{t} (\dot{\mathbf{x}}_2^i \cdot (\dot{\omega}_{ie}^i \times \mathbf{x}_2^i) - \dot{\mathbf{x}}_1^i \cdot (\dot{\omega}_{ie}^i \times \mathbf{x}_1^i)) dt', \tag{5.75}$$

$$\begin{aligned} V_{12}^{(\dot{\omega},e)} = \int_{t_0}^{t} [&(\dot{\omega}_{ie}^e \times \mathbf{x}_2^e) \cdot \dot{\mathbf{x}}_2^e + (\omega_{ie}^e \times \mathbf{x}_2^e) \cdot (\dot{\omega}_{ie}^e \times \mathbf{x}_2^e) \\ &- (\dot{\omega}_{ie}^e \times \mathbf{x}_1^e) \cdot \dot{\mathbf{x}}_1^e - (\omega_{ie}^e \times \mathbf{x}_1^e) \cdot (\dot{\omega}_{ie}^e \times \mathbf{x}_1^e)] dt'. \end{aligned} \tag{5.76}$$

are shown in (Fig. 5.7). The omitted terms, indeed, are negligible, since

$$\dot{\omega}_{ie}^i = \dot{\omega}_E \mathbf{e}_3^i + \delta\dot{\omega}_{ie}^i \approx \omega_E \dot{\boldsymbol{m}}_1^i \mathbf{e}_1^i = O(10^{-16\,\mathrm{rad/s^2}}), \tag{5.77}$$

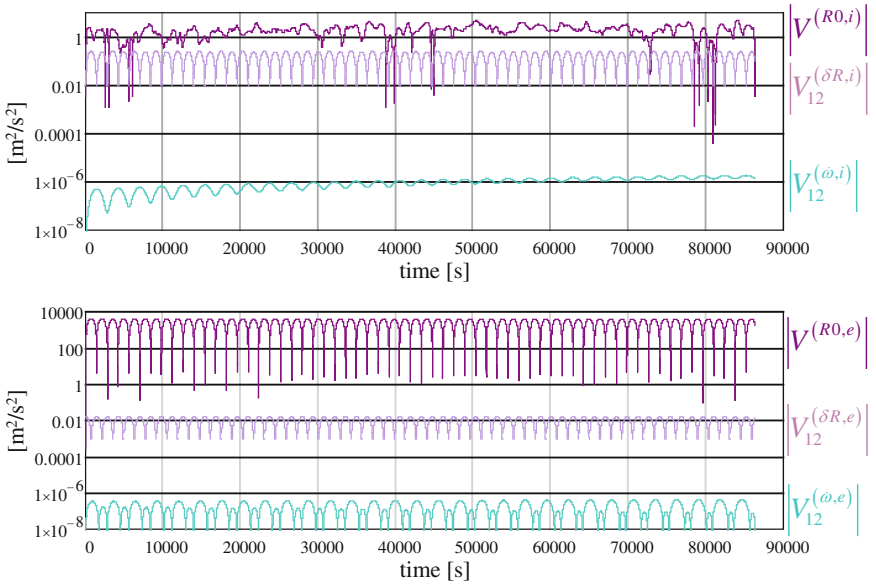

Fig. 5.7 Rotation potential terms in the *i*-frame (*top*) and *e*-frame (*bottom*) based on orbits simulated using EGM2008($n_{max} = 180$)

$$\dot{\omega}_{ie}^{e} = O(10^{-18}\,\mathrm{rad}/\mathrm{s}^2). \tag{5.78}$$

However, the residual rotation rates, especially in the i-frame ($V_{12}^{(\delta R,i)} = O(0.2\,\mathrm{m}^2/\mathrm{s}^2)$) and possibly in the e-frame ($V_{12}^{(\delta R,e)} = O(0.01\,\mathrm{m}^2/\mathrm{s}^2)$, are not negligible. It is also noted that $|V^{(R0,e)}| \gg |V^{(R0,i)}|$; i.e., the nominal rotation potential is far greater in magnitude when expressed in the e-frame.

5.3.3 Dissipative Energy Term

The term on the right side of the energy balance equation due to specific forces acting on the satellite represents the dissipative energy, that which is lost due to friction with the satellite's environment (atmospheric drag, solar radiation pressure, and Earth's albedo radiation), or additive energy due to propulsion (needed to counter the orbit-decaying friction). The environmental effects depend on the particular configuration of the satellite as well as its altitude. For example, the drag is proportional to the area-to-mass ratio of the satellite and to the square of its velocity relative to the drag medium, as well as to the density of the medium [45]. The on-board accelerometers that sense these forces, though precise over a given bandwidth, also suffer large bias and scale factor errors. Thus, instead of simulating the dissipative energy, actual data are shown here to illustrate its magnitude. From Han et al. [56], the term, $V_{12}^{(F,i)}$, is shown in (Fig. 5.8), as a result of careful calibration of systematic errors coming from the inter-satellite microwave ranging system and the accelerometers. The term is relatively small but not negligible.

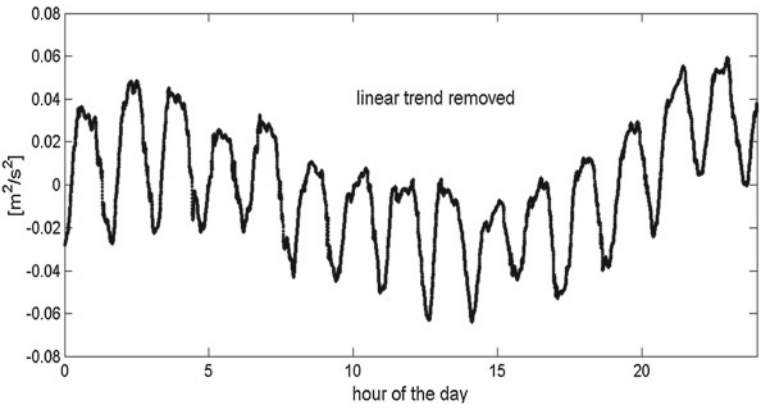

Fig. 5.8 The dissipative energy term, $V_{12}^{(F,i)}$, derived from accelerometer data, orbital and inter-satellite range-rate data, and an a priori geopotential model for a 1-day orbit of the GRACE satellites, copied from [56]

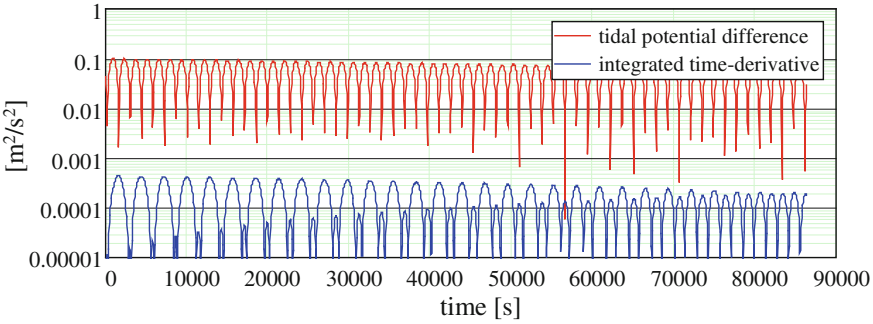

Fig. 5.9 $V_{12}^{(TI)}$ for the tidal potential in comparison to the tidal potential difference, itself, derived for actual GRACE orbits and the potentials of the Sun and Moon on 1 December 2008

5.3.4 *Tidal and Other Model Approximations*

All time-varying potentials including the tidal potential due to extraterrestrial bodies and indirect deformation potentials resulting from Earth tides, ocean tides, and ocean loading, as well other deformation potentials due to atmospheric effects and the pole tide, enter on the right side of the energy balance equation only within the time-integral of their explicit time derivative,

$$V_{12}^{(TI)} = \int_{t_0}^{t} \frac{\partial V_{12}^{(\delta E)}(\mathbf{x}^e, \boldsymbol{t}')}{\partial t'} dt', \tag{5.79}$$

where $V^{(\delta E)}$ is given by (5.24) and (5.25). This is illustrated for the tidal potential by simulation and for some of the other effects by referring to published results.
The effect of the integrated time-derivative of the tidal potential is compared to the tidal potential, itself (which enters only on the left side of the energy balance equation), in (Fig. 5.9). The tidal potential difference, $V_{12}^{(TP)}$, is determined by utilizing (5.53) expressed in the *i*-frame, assuming that latitude and declination are identical and that the hour angle is given in terms of the right ascension of a GRACE satellite by

$$h_{B(t)} = \alpha - \alpha_B(t). \tag{5.80}$$

The bodies are restricted to the Sun and Moon, whose ephemerides are available from NASA (e.g., http://ssd.jpl.nasa.gov/horizons.cgi). The time-derivative is computed numerically using a two point formula and assuming that the radial coordinate of each body is constant. The integration subsequently is also performed numerically.
Similarly, the Earth tide, ocean tide, atmospheric effect, and pole tide are computed using models described by Guo et al. [47], and shown in their Fig. 1 reproduced here in Fig. 5.10. The time-integral effect is largest for the derivative of the ocean tide potential difference, $V_{12}^{(OT)}$, while that of the pole tide deformation potential is negligible.

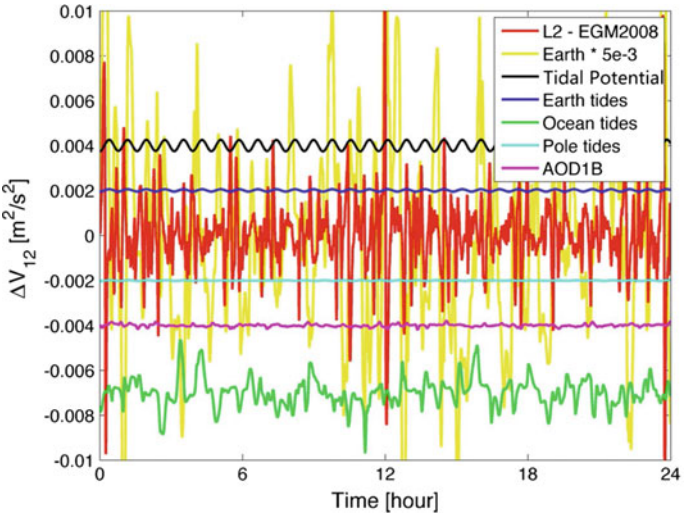

Fig. 5.10 (copied from [47] with permission from Springer) A comparison of the contribution of different sources to the potential rotation term. Random offsets have been added to distinguish the curves. L2-EGM2008—The difference between the gravitational potential differences computed using the EGM2008 and a GRACE level 2 solution randomly chosen (the GFZ L2 data of May, 2006), which represents the level of the 'signal' of gravitational potential variation to be recovered using GRACE data. Earth—Contribution of Earths time-invariable gravitational potential VE, which is scaled by the factor 5×10^{-3}; Tidal potential—Contribution of the tidal generating potential; Earth tides—Contribution of Earth tides; Ocean tides—Contribution of ocean tides; Pole tide—Contribution of pole tide; AOD1B—Contribution of the GRACE AOD1B de-aliasing product. Significance of a contribution should be considered with respect to the curve L2-EGM2008

5.4 Observational Equations

The parts of the potential difference in the inertial frame that depend exclusively on the satellite state vectors, $\mathbf{x}_1, \dot{\mathbf{x}}_1, \mathbf{x}_2, \dot{\mathbf{x}}_2$, presumed to be 'observables' (e.g., derived from kinematic orbit determination), and the observed range-rate, $\dot{\rho}_{12}$, are the kinetic energy and the nominal rotation potential (Eqs. (5.63) and (5.49)),

$$\begin{aligned}\tilde{V}_{12} &= V_{12}^{(K)} - V_{12}^{(R0)} \\ &= \frac{1}{2}\dot{\rho}_{12}(\dot{\mathbf{x}}_1 + \dot{\mathbf{x}}_2)^T\mathbf{e}_{12} + \frac{1}{2}(|\mathbf{e}_n^T\dot{\mathbf{x}}_2|^2 - |\mathbf{e}_n^T\dot{\mathbf{x}}_1|^2) + \frac{1}{2}(|\mathbf{e}_r^T\dot{\mathbf{x}}_2|^2 - |\mathbf{e}_r^T\dot{\mathbf{x}}_1|^2) \\ &\quad - \dot{\mathbf{x}}_2 \cdot (\omega_E\mathbf{e}_3 \times \mathbf{x}_2) + \dot{\mathbf{x}}_1 \cdot (\omega_E\mathbf{e}_3 \times \mathbf{x}_1)\end{aligned} \tag{5.81}$$

As a quantity of combined observations, $\tilde{V}_{12}$ includes errors in the observations, ΔV_{12}, due to KBR and orbit error, as well as all other parts of the potential on both sides of the energy balance equation,

$$\tilde{V}_{12} = V_{12}^{(E)} + V_{12}^{(\delta E)} + V_{12}^{(\delta R)} + V_{12}^{(TI)} + E_{12}^{(0)} + \Delta V_{12} + \tilde{V}_{12}^{(F)} - \Delta V_{12}^{(F)}, \tag{5.82}$$

where the observed specific-force energy difference, $\tilde{V}_{12}^{(F)}$, also has an error, $\Delta V_{12}^{(F)}$. The KBR and accelerometer errors, in particular, require careful calibration for systematic biases and drifts [56, 83, 84, 139]. Then, for example, the time-varying potential due to the *hydrological* mass changes may be computed from (5.82) and (5.25) by first removing all modelable and otherwise observable effects (if not negligible) according to

$$\begin{aligned}\tilde{V}_{12}^{(hydro)} &= \tilde{V}_{12} - V_{12}^{(E)} - V_{12}^{(TP)} - V_{12}^{(ET)} - V_{12}^{(OT)} - V_{12}^{(AO)} - V_{12}^{(\delta R)} - V_{12}^{(PT)} \\ &\quad - V_{12}^{(TI)} - \tilde{V}_{12}^{(F)} \\ &= V_{12}^{(hydro)} + E_{12}^{(0)} + \Delta V_{12} - \Delta V_{12}^{(F)}\end{aligned} \tag{5.83}$$

leaving only the system errors, ΔV_{12}, $\Delta V_{12}^{(F)}$, and constant, $E_{12}^{(0)}$. These are estimated by empirical time-wise methods, such as fitting polynomials and periodic error functions to the residuals, $\tilde{V}_{12}^{(hydro)}$, yielding estimates

$$\hat{V}_{12}^{(hydro)} = \tilde{V}_{12}^{(hydro)} - \hat{E}_{12}^{(0)} - \Delta\hat{V}_{12} - \Delta\hat{V}_{12}^{(F)}, \tag{5.84}$$

where the latter three terms are the corresponding error estimates. Care must be exercised to avoid removing hydrological signal in this calibration procedure.
Taking this example further to determine actual mass changes, the in situ potential estimates, $\hat{V}_{12}^{(hydro)}$, may be processed either globally or regionally using space-wise approaches. A global relationship between mass elements, expressed as equivalent water heights, and the associated gravitational potential is given in terms of spherical harmonic coefficients by [154],

$$C_{n,m}^{(hydro)} = \frac{3\rho_w}{\bar{\rho}} \frac{1+k_n}{2n+1} C_{n,m}^{(p)}, \tag{5.85}$$

where, on the right side, ρ_w is the density of water, $\bar{\rho}$ is Earth's mean density, the k_n are load Love numbers for harmonic degrees, n, and the $C_{n,m}^{(p)}$ are spherical harmonic coefficients for a surface density function, $\rho(\phi, \lambda)$. The coefficients on the left side of (5.85) express the potential, analogous to (5.51),

$$\hat{V}^{(hydro)}(r, \phi, \lambda) = \frac{GM}{a} \sum_{n=0}^{n_{max}} \sum_{m=-n}^{n} \left(\frac{a}{r}\right)^{n+1} C_{n,m}^{(hydro)} \bar{Y}_{n,m}(\phi, \lambda), \tag{5.86}$$

up to a maximum resolution, n_{max}, that is consistent with the spatial sampling interval created by the orbits during a particular time interval (such as one month). This linear relationship between data, $\mathbf{y} = \left[\hat{V}_{12}^{(hydro)}\right]$, and parameters, $\xi = \left[C_{n,m}^{(hydro)}\right]$, may be inverted using standard least-squares procedures, where the irregularity of the global data grid (varying slightly in radius, as well as latitude and longitude), presents numerical challenges in the inversion of the normal matrix. These may be overcome in various ways, e.g., using the iterative conjugate gradient methodology

[52]. Monthly (e.g.) solutions then yield a history of the global density function, $\rho(\phi, \lambda)$.

The in situ nature of the potential estimates, $\hat{V}^{(hydro)}$, lends itself to an alternative estimation based on a regional distribution of mascons, $m_j = \rho_w h_j \delta S_j$, $j = 1, ..., J$, representing equivalent water heights, h_j, at surface elements, δS_j. Newton's law of gravitation provides the relationship to the in situ potential difference,

$$\hat{V}_{12}^{(hydro)}(\mathbf{x}_1, \mathbf{x}_2) = G \sum_{j=1}^{J} m_j \left(\frac{1}{l_{2,j}} - \frac{1}{l_{1,j}} \right) = G \rho_w \sum_{j=1}^{J} h_j \delta S_j \left(\frac{1}{l_{2,j}} - \frac{1}{l_{1,j}} \right), \tag{5.87}$$

where $l_{2,j}, l_{1,j}$ are distance from the mascon locations to the satellites. Again, the linear relationship (5.87) may be inverted to solve for the mascons from the data, however, requiring regularization of the instability of downward continuation and the possibly ill-conditioned normal matrix. Section 5.6 briefly reviews the successes of these global and regional estimations from in situ potential difference data.

5.5 Kinematic Orbit Error Analysis

The computation of potential differences according to the energy balance equation, as in (5.81), is based on accurate range-rate measurements between the satellites, as well as accurate three-dimensional orbit state vectors (position and derived velocity). This section analyzes the accuracy requirements in the range-rate, and those of position and velocity, to achieve a certain level of accuracy in the potential difference. Only the principal components, namely, the kinetic energy and main rotation potential terms, are considered since all others are sufficiently small that they do not influence the accuracy requirements.

Linearization of the energy balance equation with respect to range-rate, position, and velocity using differentials yields directly a formulation for the propagation of errors that are presumed for present purposes to be random. Generically, the differential of the potential difference may be written as

$$\delta V_{12} = a_1 \delta \dot{\rho}_{12} + \mathbf{a}_2 \cdot \delta \mathbf{x}_1 + \mathbf{a}_3 \cdot \delta \mathbf{x}_2 + \mathbf{a}_4 \cdot \delta \dot{\mathbf{x}}_1 + \mathbf{a}_5 \cdot \delta \dot{\mathbf{x}}_2, \tag{5.88}$$

where the coefficient, a_1, and vectors of coefficients, $\mathbf{a}_j$, $j = 2, \ldots, 5$, represent appropriate partial derivatives.

Considering only the i-frame and the simple kinetic energy term in which the range-rate has *not* been separated from the velocity vectors,

$$V_{12} = \frac{1}{2}(|\dot{\mathbf{x}}_2|^2 - |\dot{\mathbf{x}}_1|^2) - \dot{\mathbf{x}}_2 \cdot (\omega_E \mathbf{e}_3 \times \mathbf{x}_2) + \dot{\mathbf{x}}_1 . (\omega_E \mathbf{e}_3 \times \mathbf{x}_1), \tag{5.89}$$

the coefficients in (5.88) are $a_1 = 0$ and

$$\begin{cases} \mathbf{a}_2 = -\omega_E \mathbf{e}_3 \times \dot{\mathbf{x}}_1, \\ \mathbf{a}_3 = \omega_E \mathbf{e}_3 \times \dot{\mathbf{x}}_2, \\ \mathbf{a}_4 = \omega_E \mathbf{e}_3 \times \mathbf{x}_1 - \dot{\mathbf{x}}_1, \\ \mathbf{a}_5 = -\omega_E \mathbf{e}_3 \times \mathbf{x}_2 + \dot{\mathbf{x}}_2. \end{cases} \tag{5.90}$$

The magnitudes of $\mathbf{a}_4$ and $\mathbf{a}_5$ are dominated by the orbital velocity in the case of low Earth orbit satellites. For the sake of simplicity it is assumed that all position and velocity component errors are independent and have respective identical variances, σ_x^2 and $\sigma_{\dot{x}}^2$. Then, the variance of the potential difference error is

$$\sigma_{V_{12}}^2 = (\mathbf{a}_2^T \mathbf{a}_2 + \mathbf{a}_3^T \mathbf{a}_3)\sigma_x^2 + (\mathbf{a}_4^T \mathbf{a}_4 + \mathbf{a}_5^T \mathbf{a}_5)\sigma_{\dot{x}}^2. \tag{5.91}$$

Nominal (maximal) values for the state vectors (see the subsequent more detailed analysis) generate the linear relationships between σ_x, $\sigma_{\dot{x}}$ and $\sigma_{V_{12}}$ shown in (Fig. 5.11). For example, a position standard deviation, $\sigma_x \approx 10^{-1}$m, and a velocity standard deviation, $\sigma_{\dot{x}} \approx 10^{-5}\,\mathrm{m/s}$, each contribute about $0.1\,\mathrm{m^2/s^2}$ to the total $\sigma_{V_{12}}$(in the root-sum-square sense). The same analysis holds for the e-frame,where the coefficients, $\mathbf{a}_j$, are transformed according to $\mathbf{a}_j^e = C_i^e \mathbf{a}_j^i$; that is, the variance/covariance propagation is frame invariant.

The high accuracy requirement for velocity illustrated above is not achievable with standard orbital tracking. However, it may be realized by shifting it to the much more

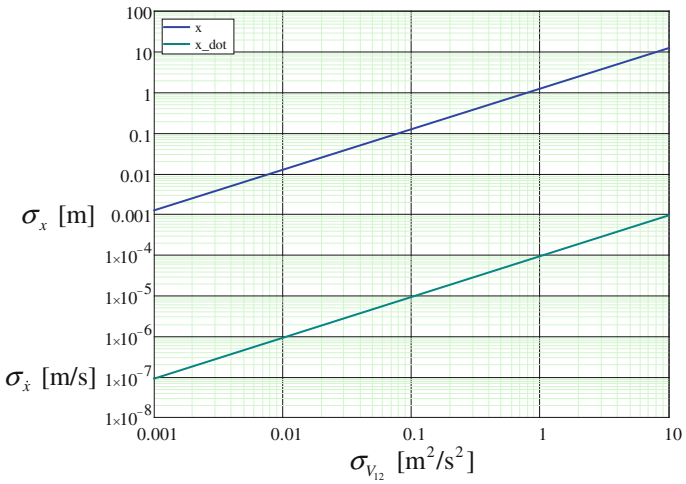

Fig. 5.11 Linear relationships between σ_x, $\sigma_{\dot{x}}$ and $\sigma_{V_{12}}$ based on nominal (maximal) values of GRACE-like orbital state vectors

precise range-rate observations, as shown in the following analysis. In this case, with (5.63), the potential difference is given by (neglecting small terms),

$$V_{12} = \frac{1}{2}\dot{\rho}_{12}(\dot{\mathbf{x}}_1 + \dot{\mathbf{x}}_2)^T\mathbf{e}_{12} + \frac{1}{2}(|\mathbf{e}_n^T\dot{\mathbf{x}}_2|^2 - |\mathbf{e}_n^T\dot{\mathbf{x}}_1|^2) + \frac{1}{2}(|\mathbf{e}_r^T\dot{\mathbf{x}}_2|^2 - |\mathbf{e}_r^T\dot{\mathbf{x}}_1|^2) - V_{12}^{(R0,i,e)}. \tag{5.92}$$

Leaving details to the reader, the coefficients in (5.88) are given for the i-frame by

$$\mathbf{a}_1 = \frac{1}{2}(\dot{\mathbf{x}}_1 + \dot{\mathbf{x}}_2)^T\mathbf{e}_{12}, \tag{5.93}$$

$$\mathbf{a}_2 = -\frac{1}{2}\frac{\dot{\rho}_{12}}{|x_{12}|}\mathbf{E}(\dot{\mathbf{x}}_1 + \dot{\mathbf{x}}_2) + \mathbf{S}_1(\dot{\mathbf{x}}_2\dot{\mathbf{x}}_2^T - \dot{\mathbf{x}}_1\dot{\mathbf{x}}_1^T)\mathbf{e}_n + \mathbf{T}_1(\dot{\mathbf{x}}_2\dot{\mathbf{x}}_2^T - \dot{\mathbf{x}}_1\dot{\mathbf{x}}_1^T)\mathbf{e}_r - \omega_E\mathbf{e}_3 \times \dot{\mathbf{x}}_1, \tag{5.94}$$

$$\mathbf{a}_3 = \frac{1}{2}\frac{\dot{\rho}_{12}}{|\mathbf{x}_{12}|}\mathbf{E}(\dot{\mathbf{x}}_1 + \dot{\mathbf{x}}_2) + \mathbf{S}_2(\dot{\mathbf{x}}_2\dot{\mathbf{x}}_2^T - \dot{\mathbf{x}}_1\dot{\mathbf{x}}_1^T)\mathbf{e}_n + \mathbf{T}_2(\dot{\mathbf{x}}_2\dot{\mathbf{x}}_2^T - \dot{\mathbf{x}}_1\dot{\mathbf{x}}_1^T)\mathbf{e}_r + \omega_E\mathbf{e}_3 \times \dot{\mathbf{x}}_2, \tag{5.95}$$

$$\mathbf{a}_4 = \frac{1}{2}\dot{\rho}_{12}\mathbf{e}_{12} - \mathbf{e}_n\dot{\mathbf{x}}_1^T\mathbf{e}_n - \mathbf{e}_r\dot{\mathbf{x}}_1^T\mathbf{e}_r + \omega_E\mathbf{e}_3 \times \mathbf{x}_1, \tag{5.96}$$

$$\mathbf{a}_5 = \frac{1}{2}\dot{\rho}_{12}\mathbf{e}_{12} + \mathbf{e}_n\dot{\mathbf{x}}_2^T\mathbf{e}_n + \mathbf{e}_r\dot{\mathbf{x}}_2^T\mathbf{e}_r - \omega_E\mathbf{e}_3 \times \mathbf{x}_2, \tag{5.97}$$

where

$$\mathbf{E} = \left(\mathbf{I} - \frac{1}{|\mathbf{x}_{12}|^2}\mathbf{x}_{12}\mathbf{x}_{12}^T\right), \tag{5.98}$$

$$\mathbf{S}_1 = \frac{1}{|\mathbf{x}_1 \times \mathbf{x}_2|}([\mathbf{x}_2\times] - (\mathbf{x}_2 \times \mathbf{e}_n)\mathbf{e}_n^T), \tag{5.99}$$

$$\mathbf{S}_2 = -\frac{1}{|\mathbf{x}_1 \times \mathbf{x}_2|}([\mathbf{x}_1\times] - (\mathbf{x}_1 \times \mathbf{e}_n)\mathbf{e}_n^T), \tag{5.100}$$

$$\mathbf{T}_1 = -\mathbf{S}_1[\mathbf{e}_{12}\times] - \frac{1}{|\mathbf{x}_{12}|}\mathbf{E}[\mathbf{e}_n\times], \tag{5.101}$$

$$\mathbf{T}_2 \quad = -\mathbf{S}_2[\mathbf{e}_{12}\times] + \frac{1}{|\mathbf{x}_{12}|}\mathbf{E}[\mathbf{e}_n\times]. \tag{5.102}$$

Equation (5.94) through (5.97) show that the coefficients, $\mathbf{a}_j$, $j = 2, \ldots, 5$, have elements that may be roughly associated with along-track, cross-track, and radial

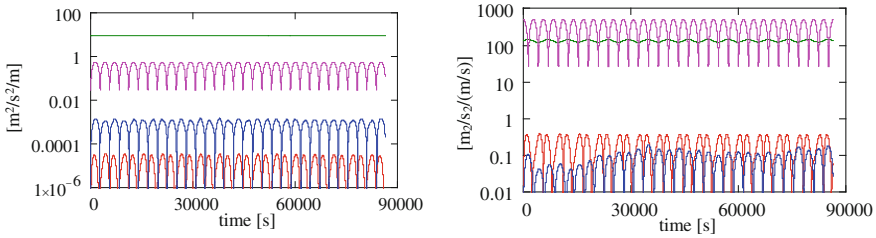

Fig. 5.12 Along-track elements (*red*), cross-track elements (*blue*), radial elements (*green*), and Earth-rotation-rate elements (*magenta*) of the coefficient, $\mathbf{a}_2$ (the same as $\mathbf{a}_3$) *on the left*, and of the coefficient, $\mathbf{a}_4$ (the same as $\mathbf{a}_5$) *on the right*

directions, as well as Earth rotation. Contributions to the potential difference error from the corresponding position and velocity components are thus governed by their relative magnitudes. For example, (Fig. 5.12) shows that the contribution of position uncertainty, scaled by the coefficients, $\mathbf{a}_2$ and $\mathbf{a}_3$, is largely determined by the radial components of velocity and least by their along-track components. Also, the contribution of velocity uncertainty (coefficients, $\mathbf{a}_4$ and $\mathbf{a}_5$) depends mostly on the combination of radial velocity and position scaled by Earth's rotation rate. Thus, just as the radial velocity is a major contributor to the potential difference value (Fig. 5.4), so it is a critical component in the accuracy of the potential difference (assuming commensurate state vector component accuracies). Based on the simulated EGM2008 orbits, the maximum square roots of the coefficients in

$$\sigma^2_{V_{12}} = a_1^2\sigma^2_{\dot\rho_{12}} + (\mathbf{a}_2^T\mathbf{a}_2 + \mathbf{a}_3^T\mathbf{a}_3)\sigma_x^2 + (\mathbf{a}_4^T\mathbf{a}_4 + \mathbf{a}_5^T\mathbf{a}_5)\sigma_{\dot x}^2. \tag{5.103}$$

are $|a_1| = 7660\,\mathrm{m}^2/\mathrm{s}^2$ per m/s, $\sqrt{\mathbf{a}_2^T\mathbf{a}_2 + \mathbf{a}_3^T\mathbf{a}_3} = 12.2\,\mathrm{m}^2/\mathrm{s}^2$ per m, $\sqrt{\mathbf{a}_4^T\mathbf{a}_4 + \mathbf{a}_5^T\mathbf{a}_5} = 726\,\mathrm{m}^2/\mathrm{s}^2$ per m/s. The linear relationships between the observation standard deviations and the potential difference standard deviation are displayed in (Fig. 5.13). The accuracy requirement for the total velocity vectors is reduced by an order of magnitude, whereas, the position errors must be better by an order of magnitude compared to the case without range-rate observations (Fig. 5.11).

The latter increase in accuracy requirement comes from the need to establish along-track, cross-track, and radial directions. A simpler analysis combines this with the velocity accuracy requirement in terms of along-track, cross-track, and radial velocity components. The kinetic energy term in (5.92) then becomes

$$V_{12}^{(K)} = \frac{1}{2}\dot\rho_{12}(v_1 + v_2) + \frac{1}{2}(u_2^2 - u_1^2) + \frac{1}{2}(w_2^2 - w_1^2), \tag{5.104}$$

where

$$\dot{\mathbf{x}}_1 = u_1\mathbf{e}_n + v_1\mathbf{e}_{12} + w_1\mathbf{e}_r, \quad \dot{\mathbf{x}}_2 = u_2\mathbf{e}_n + v_2\mathbf{e}_{12} + w_2\mathbf{e}_r. \tag{5.105}$$

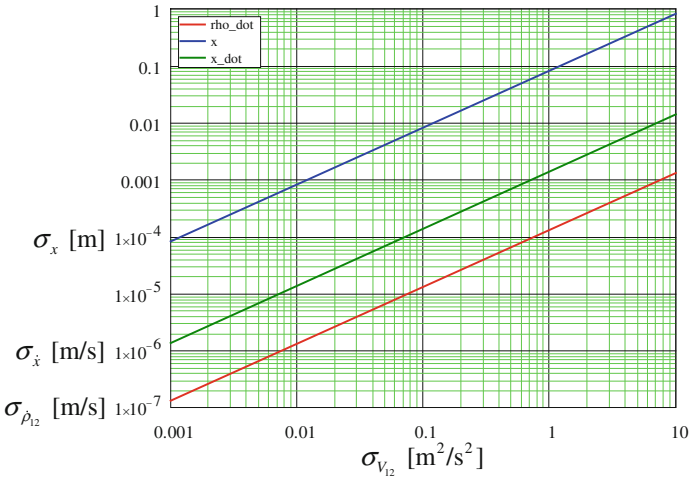

Fig. 5.13 Linear relationships between σ_x, $\sigma_{\dot{x}}$, $\sigma_{\dot{\rho}12}$ and σ_{V12} based on nominal (maximal) values of GRACE-like orbital state vectors

Assuming the component velocity errors are independent and have identical variances per component, the variance in the potential difference is

$$\sigma^2_{V_{12}^{(K)}} = \frac{1}{4}(v_1 + v_2)^2\sigma^2_{\dot{\rho}_{12}} + \frac{1}{2}\dot{\rho}^2_{12}\sigma^2_v + (u_2^2 + u_1^2)\sigma^2_u + (w_2^2 + w_1^2)\sigma^2_w. \qquad (5.106)$$

The maximum square-root values of the velocity coefficients for the EGM2008 simulated orbits are $|\dot{\rho}_{12}|/\sqrt{2} = 0.54\,\mathrm{m}^2/\mathrm{s}^2$ per m/s, $\sqrt{u_1^2 + u_2^2} = 0.24\,\mathrm{m}^2/\mathrm{s}^2$ per m/s, and $\sqrt{w_1^2 + w_2^2} = 185\,\mathrm{m}^2/\mathrm{s}^2$ per m/s. The radial component of velocity needs to be three orders of magnitude more accurate than the other components in order to make the same contribution to the kinetic energy difference error.

5.6 Summary

The energy balance approach to geopotential modeling from satellite-to-satellite tracking has been analyzed through simulations and applied to actual satellite data by a number of investigators. Various studies demonstrated its feasibility in recovering the global field in terms of a spherical harmonic model from either the CHAMP or GRACE missions [52, 164], or other satellite constellations [155]. The earlier studies concentrated on the numerical issues of processing a large global grid of data that involves the inversion of a full normal matrix, for example, by iterative conjugate-gradient techniques. Visser et al. [149] also showed that the approach is particularly sensitive to satellite velocity errors. The regional estimation of equivalent water height mascons from in situ potential differences was investigated by Han [54] whose

simulations validated the ability to obtain improved resolution and accuracy. Similar studies by Ramillien et al. [117] extended the options for optimizing the estimation procedures that must account for local downward continuation and normal matrix stabilization.

Implementation of the energy balance equations using actual precision satellite tracking data were initially achieved by Gerlach et al. [46] for CHAMP (non-SST data), whose spherical harmonic solution to maximum degree, $n_{max} = 60$, agreed in accuracy with the best standard satellite-derived global model available at the time. The analysis by Han et al. [55] of GRACE data showed that a regional solution of equivalent water height mascons over the Amazon River basin yields improved spatial and temporal resolutions compared to the standard GRACE spherical harmonic solution. Another analysis by Han et al. [56] proved that regional estimation from GRACE data can add important constraints on the mass displacements associated with large earthquakes. Many other results similarly demonstrated the utility of the energy balance approach, from early analyses of CHAMP data [2, 136] and its resolution capability [157] to additional analyses of GRACE data that inferred tides under Antarctic ice shelves [53] and estimated the Amazon hydrological cycle [139].

The principal advantage of the energy balance approach is the ability to obtain in situ potential differences. That is, by kinematically tracking a satellite, yielding both position and a derived velocity continually in a coordinate frame (either inertial or Earth-fixed) without the need for a dynamic integration of tracking data, one accumulates a spatial data set of potential differences as if the satellite were equipped with a 'potential-difference-meter'. These data can then be processed further to estimate the global, or more importantly, the regional gravitational field. In particular, one may take direct advantage of the increased data resolution at higher latitudes that is associated with the convergence of polar orbits. The accuracy of the potential differences depends crucially, of course, on the kinematic orbit accuracy, both in velocity and position. Precision low-low satellite-to-satellite tracking, such as with GRACE, reduces the accuracy requirements on the absolute velocity by an order of magnitude. However, it should be noted that range-rates do not sense cross-track and radial components of the absolute or inter-satellite velocity, where the radial component of the latter makes a particularly significant contribution to the potential difference. On the other hand, the radial-velocity contribution is primarily a long-wavelength signal compared to the along-track component, and is thus amenable to strong noise filtering without loss of high-frequency signal.

5.7 Exercises

Data and files needed for the following exercises are available online at:
www.geoq.uni-hannover.de/autumnschool-data
http://extras.springer.com

This exercise is designed to demonstrate that the energy balance formulation can be used to solve for in-situ potential differences using range-rate and state vector data from GRACE. The data are corresponding L1B products for 1 December 2008. The provided data files are:
GNV1B_A.dat: t[s], $\mathbf{x}_1^e$[m], $\sigma_{x_1^e}$[m], $\dot{\mathbf{x}}_1^e$[$^{\mathrm{m}}/_{\mathrm{s}}$], $\sigma_{\dot{x}_1^e}$[$^{\mathrm{m}}/_{\mathrm{s}}$] for GRACE A (trailing)
GNV1B_B.dat: t[s], $\mathbf{x}_2^e$[m], $\sigma_{x_2^e}$[m], $\dot{\mathbf{x}}_2^e$[$^{\mathrm{m}}/_{\mathrm{s}}$], $\sigma_{\dot{x}_2^e}$[$^{\mathrm{m}}/_{\mathrm{s}}$] for GRACE B (leading)
KBR1B.dat: t[s], $\dot{\rho}_{12}$[$^{\mathrm{m}}/_{\mathrm{s}}$], $\delta\dot{\rho}_{12}^{(lighttime)}$[$^{\mathrm{m}}/_{\mathrm{s}}$], $\delta\dot{\rho}_{12}^{(antennacenter)}$[$^{\mathrm{m}}/_{\mathrm{s}}$]
EGM_A.dat: t[s], $\mathbf{x}_1^e$[m], V_1[$^{\mathrm{m}^2}/_{\mathrm{s}^2}$].
EGM_B.dat: t[s], $\mathbf{x}_2^e$[m], V_2[$^{\mathrm{m}^2}/_{\mathrm{s}^2}$].

Remarks:
(a) All GRACE data are given in the Earth-fixed frame.
(b) The GRACE L1B state vector files are not pure kinematic orbits, but are consistent to high accuracy with an a priori global gravitation model. Hence, this exercise is more of a simulation than an actual geopotential determination.
(c) The data have been extracted from GRACE L1B products, where data records have been synchronized in time across the files and extraneous data and metadata have been omitted. The range-rate values require light-time and antenna center corrections: $\dot{\rho}_{12} = \dot{\rho}_{12}^{(raw)} + \delta\dot{\rho}_{12}^{(lighttime)} + \delta\dot{\rho}_{12}^{(antennacenter)}$
(d) The gravitational potential values are obtained from the model, EGM2008 ($N_{max} = 180$), for the points long each orbit.
(e) Specific force and time-integral terms, as well as the pole tide potential are neglected in the tests of this exercise.

Tasks
1. Write the energy balance equations to be tested, both in terms of range-rate and position/velocity observables, and without the range-rate observable. Define all notation.
2. Compute the right-hand side of both equations using the GRACE data given in the files.
3. Compare on a plot the main range-rate term with the other terms in the energy balance equation (formulated for the range-rate) for the first three hours of the orbits. Why are the cross-track and rotation potential terms almost the same?
4. Compare the computed potential differences to the provided EGM2008 data. That is, plot the differences, $V_{12}^{(GRACE)} - V_{12}^{(EGM)}$, with and without the range-rate observable for the entire day's worth of data, and compute the statistics of these differences (mean, standard deviation). Why is the mean not close to zero? What is the cause of the oscillation in these differences?
5. Based on the average of the formal standard errors in position and velocity, $\sigma_x = 3.6 * 10^{-3}$m, $\sigma_{\dot{x}} = 3.45 * 10^{-6}\,^{\mathrm{m}}/_{\mathrm{s}}$ and assuming a range-rate accuracy of $\sigma_{\dot{\rho}_{12}} = 0.1 * 10^{-6}\,^{\mathrm{m}}/_{\mathrm{s}}$, determine the contribution of each error type (position, velocity, and range-rate) to the total error in the potential difference at a point (using the graphic in the lecture notes). How does the total potential difference accuracy thus estimated compare to the standard deviations computed above?
6. Compute the power spectral density (median-smoothed periodogram) of the differences, $V_{12}^{(GRACE)} - V_{12}^{(EGM)}$, with and without the range-rate observable, for the

1-day orbit and with respect to the temporal frequency. Plot both on the same log-log graph. Can you interpret the results? (e.g., what causes the resonance peak at low frequency? What could be the reason for the greater power at very high frequencies when the range-rate observation is included?)

Acknowledgements These lecture notes would not have been completed without the stimulating, helpful, and much appreciated discussions with colleagues, specifically Dr. Junyi Guo, Dr. Kun Shang, and Mr. Nlingi Habana (in particular, who helped with the exercises) of the Division of Geodetic Science, School of Earth Sciences, at the Ohio State University, as well Prof. Shin Chan Han (University of Newcastle), Prof. Srinivas Bettadpur (CSR, University of Texas), and Prof. Jakob Flury and Dr. Majid Naeimi of the Institut für Erdmessung, Leibniz Universität Hannover. Particular gratitude from the author goes to the sponsor of these lectures, the Wilhelm and Else Heraeus Foundation.

References

1. Altamimi, Z., Collilieux, X., & Métivier, L. (2011). ITRF2008: An improved solution of the international terrestrial reference frame. *Journal of Geodesy*, *85*(8), 457–472.
2. Badura, T., Sakulin, C., Gruber, C., & Klostius, R. (2006). Derivation of the CHAMP only global gravity field model TUG-CHAMP04 applying the energy integral approach. *Studia Geophysica et Geodaetica*, *50*(1), 59–74.
3. Baker, R. (1960). Orbit determination from range and range rate data. Technical report, Semi-annual meeting of American Rocket Society, Los Angeles.
4. Balmino, G. (1974). Determination of earth potential by means of space methods. *La Geodynamique Spatiale*, *A76–36176*(17–42), 275–472.
5. Balmino, G., Barthel, G., Castel, L., Halldorson, T., Hufnagel, H., Leibold, G., et al. (1978). Mission/system definition study for a space laser low orbit mission (SLALOM)-Final Report. Technical report, ESA. ESA Contract No. 3483/78/F/DK(SC).
6. Baur, O., Reubelt, T., Weigelt, M., Roth, M., & Sneeuw, N. (2012). GOCE orbit analysis: Longwavelength gravity field determination using the acceleration approach. *Advances in Space Research*, *50*(3), 385–396.
7. Beutler, G. (2005a). Methods of celestial mechanics. Physical, mathematical, and numerical principles (Vol. 1). Springer. ISBN 3-540-40749-9.
8. Beutler, G. (2005b). Methods of celestial mechanics. Application to planetary system, geodynamics and satellite geodesy (Vol. 2). Springer. ISBN 3-540-40750-2.
9. Beutler, G., Mueller, I., & Neilan, R. (1994). The international GPS service for geodynamics (IGS): Development and start of official service on 1 January 1994. *Manuscripta Geodaetica*, *68*, 43–51.
10. Beutler, G., Jäggi, A., Mervart, L., & Meyer, U. (2010a). The celestial mechanics approach: Application to data of the GRACE mission. *Journal of Geodesy*, *84*(11), 661–681.
11. Beutler, G., Jäggi, A., Mervart, L., & Meyer, U. (2010b). The celestial mechanics approach: Theoretical foundations. *Journal of Geodesy*, *84*(10), 605–624.
12. Bjerhammar, A. (1969). On the energy integral for satellites. *Tellus*, *21*(1), 1–9.
13. Björk, A. (1996). *Numerical methods for least squares problems*. Philadelphia, PA: SIAM.
14. Bock, H., Jäggi, A., Dach, R., Beutler, G., & Schaer, S. (2009a). GPS single-frequency orbit determination for low earth orbiting satellites. *Advances in Space Research*, *43*(5), 783–791.
15. Bock, H., Dach, R., Jäggi, A., & Beutler, G. (2009b). High-rate GPS clock corrections from CODE: Support of 1 Hz applications. *Journal of Geodesy*, *83*(11), 1083–1094.
16. Bock, H., Jäggi, A., Meyer, U., Visser, P., & van den IJssel, J., (2011a). GPS-derived orbits for the GOCE satellite. *Journal of Geodesy*, *85*(11), 807–818.
17. Bock, H., Jäggi, A., Meyer, U., Dach, R., & Beutler, G. (2011b). Impact of GPS antenna phase center variations on precise orbits of the GOCE satellite. *Advances in Space Research*, *47*(11), 1885–1893.

M. Naeimi and J. Flury (eds.), *Global Gravity Field Modeling from Satellite-to-Satellite Tracking Data*, Lecture Notes in Earth System Sciences,
DOI 10.1007/978-3-319-49941-3

18. Bock, H., Jäggi, A., Beutler, G., & Meyer, U. (2014). GOCE-Precise orbit determination for the entire mission. *Journal of Geodesy*, *88*(11), 1047–1060.
19. Bouman, J. (2000). Quality assessment of satellite-based global gravity. Ph.D. thesis, TU Delft.
20. Breakwell, J. (1979). Satellite determination of short wavelength gravity variations. Technical report, American Astronomical Society, Provincetown.
21. Brockmann, E. (1997). Combination of solutions for geodetic and geodynamic applications of the global positioning system (GPS). Technical report, Geodätisch-geophysikalische Arbeiten in der Schweiz, Band 55, Schweizerische Geodätische Kommission, Institut for Geodäsie und Photogrammetrie, Eidg. Technische Hochschule Zürich, Zürich. http://www.sgc.ethz.ch/sgcvolumes/sgk-55.pdf.
22. Brockmann, J. (2014). On high performance computing in geodesy -applications in global gravity field determination. Ph.D. thesis, Bonn University.
23. Buchar, E. (1958). Motion of the nodal line of the second Russian Earth Satellite (1957) and flattening of the Earth. *Nature*, *182*, 198–199.
24. Buckreuss, S., Balzer, W., Muhlbauer, P., Werninghaus, R., & Pitz, W. (2003). The TerraSAR-X satellite project. In *Proceedings of IGARSS, Toulouse* (Vol. 5, pp. 30963098).
25. Bulirsch, R., & Stoer, J. (1966). Numerical treatment of ordinary differential equations by extrapolation methods. *Numerische Mathematik*, *8*, 1–13.
26. Colombo, O. (1981). Geopotential modelling from satellite-to-satellite tracking. Technical report, OSU report 317, Columbus.
27. Colombo, O. (1984). *The global mapping of gravity with two satellites* (Vol. 3.7), *New Series*. Delft: Netherlands Geodetic Commission.
28. Dach, R., Brockmann, E., Schaer, S., Beutler, G., Meindl, M., Prange, L., et al. (2009). GNSS processing at CODE: Status report. *Journal of Geodesy*, *83*(3–4), 353–366.
29. Dach, R., Lutz, S., Walser, P., & Fridez, P. E. (2015). *Bernese GNSS software version 5.2*. Astronomical Institute, Universtiy of Bern, Bern Open Publishing.
30. Danby, J. (1988). *Fundamentals of celestial mechanics*. Richmond, Virginia: Willman-Bell Inc.
31. Daras, I., Pail, R., Murböck, M., & Yi, W. (2015). Gravity field processing with enhanced numerical precision for LL-SST missions. *Journal of Geodesy*, *89*(2), 99–110.
32. Dickey, J. (1997). Satellite gravity and the geosphere. Technical report, The committee on earth gravity from space, National Research Council, National Academy Press.
33. Ditmar, P., Kusche, J., & Klees, R. (2003). Computation of spherical harmonic coefficients from gravity gradiometry data to be acquired by the GOCE satellite: Regularization issues. *Journal of Geodesy*, *77*, 465–477.
34. Dow, J., Neilan, R., & Gendt, G. (2005). The international GPS service: Celebrating the 10th anniversary and looking to the next decade. *Advances in Space Research*, *36*(3), 320–326.
35. Drinkwater, M., Haagmans, R., Muzi, D., Popescu, A., Floberghagen, R., Kern, M., et al. (2006). The GOCE gravity mission: ESA's first core explorer. *ESA SP*, *627*, 1–7.
36. Dunn, C., Bertiger, W., Bar-Sever, Y., Desai, S., Haines, B., Kuang, D., et al. (2003). Instrument of GRACE. *GPS World*, *14*(2), 16–28.
37. Eanes, R. (1995). A study of temporal variations in Earths gravitational field using Lageos-1 laser range observations. Ph.D. thesis, University of Texas at Austin.
38. Eanes, R., & Bettadpur, S. (1995). Temporal variability of Earths gravitational field from satellite laser ranging. In *Global gravity field and its temporal variations* (Vol. 116, pp. –41). IAG Proceedings.
39. ESA (1978). SLALOM mission/system definition. Technical report, Contract No. 3483/78/F/DK(SC).
40. Flechtner, F., Morton, P., Watkins, M., & Webb, F. (2013). Status of the GRACE follow-on mission. In U. Marti (Ed.), *Gravity, geoid and height systems* (pp. 117–121). IAG Symposia 141.
41. Flohrer, C., Otten, M., Springer, T., & Dow, J. (2011). Generating precise and homogeneous orbits for Jason-1 and Jason-2. *Advances in Space Research*, *48*(1), 152–172.

42. Förstner, W. (1979). Ein Verfahren zur Schätzung von Varianz- und Kovarianzkomponenten. *Allgemeine Vermessungs-Nachrichten*, *86*, 446–453.
43. Friis-Christensen, E., Lühr, H., Knudsen, D., & Haagmans, R. (2006). Swarm–An Earth observation mission investigating geospace. *Advances in Space Research*, *41*(1), 210–216.
44. Fu, L., Christensen, E., Yamarone, C., Lefebvre, M., Mnard, Y., Dorrer, M., et al. (1994). TOPEX/POSEIDON mission overview. *Journal of Geophysical Research*, *99*(C12), 2436924381.
45. Gaposchkin, E., & Coster, A. (1988). Analysis of satellite drag. *The Lincoln Laboratory Journal*, *1*(2), 203–224.
46. Gerlach, C., Földvary, L., Svehla, D., Gruber, T., Wermuth, M., Sneeuw, N., et al. (2003). A CHAMP-only gravity field model from kinematic orbits using the energy integral. *Geophysical Research Letters*, *30*(20), 2037.
47. Guo, J., Shang, K., Jekeli, C., & Shum, C. (2015). On the energy integral formulation of gravitational potential differences from satellite-to- satellite tracking. *Celestial Mechanics and Dynamical Astronomy*, *121*(4), 415–429.
48. Hackel, S., Montenbruck, O., Steigenberger, P., Balss, U., Gisinger, C., & Eineder, M. (2015a). Galileo orbit determination using combined GNSS and SLR observations. *GPS Solutions*, *19*, 15–25.
49. Hackel, S., Montenbruck, O., Steigenberger, P., Balss, U., Gisinger, C., & Eineder, M. (2015b). Impact of improved satellite dynamic models on reduced dynamic orbit determination. *Journal of Geodesy*, in review.
50. Hajela, D. (1974). Direct recovery of mean gravity anomalies from satellite to satellite tracking. Technical report, OSU report 218, Columbus.
51. Hajela, D. (1978). Improved procedures for the recovery of 50 mean gravity anomalies from ATS6/GEOS-3 satellite-to-satellite range rate observations using least squares collocation. Technical report, OSU report 276, Columbus.
52. Han, S. (2004). Efficient determination of global gravity field from satellite-to-satellite tracking mission. *Celestial Mechanics and Dynamical Astronomy*, *88*, 69–102.
53. Han, S., Shum, C., & Matsumoto, K. (2005a). GRACE observations of M2 and S2 ocean tides underneath the Filchner-Ronne and Larsen ice shelves. *Antarctica. Geophysical Research Letters*, *32*, L20311.
54. Han, S., Shum, C., & Braun, A. (2005b). High-resolution continental water storage recovery from low-low satellite-to-satellite tracking. *Journal of Geodynamics*, *39*(1), 11–28.
55. Han, S., Shum, C., Jekeli, C., & Alsdorf, D. (2005c). Improved estimation of terrestrial water storage changes from GRACE. *Geophysical Research Letters*, *32*, L07302.
56. Han, S., Shum, C., & Jekeli, C. (2006). Precise estimation of in situ geopotential differences from GRACE low-low satellite-to-satellite tracking and accelerometer data. *Journal of Geophysical Research*, *111*, B04411.
57. Hartmann, T., & Wenzel, H. (1995). The HW95 tidal potential catalogue. *Geophysical Research Letters*, *22*(24), 3553–3556.
58. Henriksen, S. E. (1977). *National geodetic satellite program, part 1 and 2* (p. 1019). NASA, Washington DC: Technical report.
59. Hofmann-Wellenhof, B., & Moritz, H. (2005). *Physical geodesy*. Berlin: Springer.
60. Hofmann-Wellenhof, B., Lichtenegger, H., & Wasle, E. (2007). *GNSS–Global navigation satellite systems: GPS, GLONASS, Galileo, and more*. Wien, New York: Springer.
61. Ilk, K., Löcher, A., & Mayer-Gürr, T. (2008). VI Hotine-Marussi symposium on theoretical and computational geodesy. In *Kapitel dowWe need new gravity field recovery techniques for the new gravity field satellites?* (Vol. 132, pp. 3–9). Springer.
62. IPCC (2013). Climate change 2013—The physical science basis. Technical report, Fifth assessment report of the intergovernmental panel on climate change, Cambridge University Press.
63. Izsak, I. (1964). Tesseral harmonics of the geopotential and corrections to station coordinates. *Journal of Geophysical Research*, *69*(12), 2621–2631.

64. Jäggi, A. (2007). Pseudo-stochastic orbit modeling of low earth satellites using the global positioning system. Technical report, Geodätisch-geophysikalische Arbeiten in der Schweiz, Band 73, Schweizerische Geodätische Kommission, Institut for Geodäsie und Photogrammetrie, Eidg. Technische Hochschule Zürich, Zürich. http://www.sgc.ethz.ch/sgc-volumes/sgk-73.pdf.
65. Jäggi, A., Bock, H., Pail, R., & Goiginger, G. (2008). Highly reduced dynamic orbits and their use for global gravity field recovery: A simulation study for GOCE. *Studia Geophysica et Geodaetica*, *52*(3), 341–359.
66. Jäggi, A., Dach, R., Montenbruck, O., Hugentobler, U., Bock, H., & Beutler, G. (2009). Phase center modeling for LEO GPS receiver antennas and its impact on precise orbit determination. *Journal of Geodesy*, *83*(12), 1145–1162.
67. Jäggi, A., Bock, H., Thaller, D., Dach, R., Beutler, G., Prange, L., et al. (2010). Precise orbit determination of low Earth satellites at AIUB. *ESA SP*, *686*, 62.
68. Jäggi, A., Bock, H., & Floberghagen, R. (2011a). GOCE orbit predictions for SLR tracking. *GPS Solutions*, *15*(2), 129–137.
69. Jäggi, A., Bock, H., Prange, L., Meyer, U., & Beutler, G. (2011b). GPS-only gravity field recovery with GOCE, CHAMP, and GRACE. *Advances in Space Research*, *47*(6), 1020–1028.
70. Jäggi, A., Prange, L., & Hugentobler, U. (2011c). Impact of covariance information of kinematic positions on orbit reconstruction and gravity field recovery. *Advances in Space Research*, *47*(9), 1472–1479.
71. Jäggi, A., Bock, H., Meyer, U., Beutler, G., & van den IJssel, J., (2015). GOCE: Assessment of GPS-only gravity field determination. *Journal of Geodesy*, *89*(1), 33–48.
72. Jäggi, A., Dahle, C., Arnold, D., Bock, H., Meyer, U., Beutler, G., et al. (2016). Swarm kinematic orbits and gravity fields from 18 months of GPS data. *Advances in Space Research*, *57*(1), 218–233.
73. Jazwinski, A. (1970). *Stochastic processes and filtering theories*. New York: Academic Press Inc.
74. Jekeli, C. (1999). The determination of gravitational potential differences from satellite-to-satellite tracking. *Celestial Mechanics and Dynamical Astronomy*, *75*, 85–101.
75. Jekeli, C. (2000). *Inertial navigation systems with geodetic applications*. Berlin: Walter deGruyter Inc.
76. Jekeli, C. (2004). High-resolution gravity mapping: The next generation of sensors. *The State of the Planet: Frontiers and Challenges in Geophysics, Geophysical Monograph 150*, *19*, 135–146. R. S. J. Sparks (Ed.).
77. Jekeli, C., & Rapp, R. (1980). Accuracy of the determination of mean anomalies and mean geoid undulations from a satellite gravity mapping mission. Technical report 307, Department of Geodetic Science, The Ohio State University.
78. Jekeli, C., & Upadhyay, T. (1990). Gravity estimation from STAGE, a satellite-to-satellite tracking mission. *Journal of Geophysical Research*, *95*(B7), 10973–10985.
79. Kaula, W. E. (1969). The terrestrial environment: Solid-Earth and ocean physics application of space and astronomic techniques. Technical report, Report of a study at Williamstown/Mass. to NASA, Cambridge Mass.
80. Kaula, W. E (1983). Inference of variations in the gravity field from satellite-to-satellite range rate. *Journal of Geophysical Research*, *88*(B10), 8345–8349.
81. Keating, T., Taylor, P., Kahn, W., & Lerch, F. (1986). Geopotential research mission, science, engineering, and program summary. Technical report, NASA Tech. Memo 86240.
82. Keller, W., & Sharifi, M. (2005). Satellite gradiometry using a satellite pair. *Journal of Geodesy*, *78*, 544–557.
83. Kim, J. (2000). Simulation study of a low-low satellite-to-satellite tracking mission. Ph.D. thesis, University of Texas at Austin, Austin.
84. Kim, J., & Tapley, B. (2002). Error analysis of a low-low satellite-to-satellite tracking mission. *Journal of Guidance, Control, and Dynamics*, *25*(6), 1100–1106.

85. Kim, M. (1997). Theory of satellite ground-track crossovers. *Journal of Geodesy*, *71*, 749–767.
86. Koch, K. (1986). Maximum likelihood estimate of variance components. *Bulletin Geodesique*, *60*, 329–338.
87. Koch, K. (1999). *Parameter estimation and hypothesis testing in linear models*. Berlin: Springer.
88. Krieger, G., Moreira, A., Fiedler, H., Hajnsek, I., Werner, M., Younis, M., et al. (2007). TanDEM-X: A satellite formation for high-resolution SAR interferometry. *IEEE Transactions on Geoscience and Remote Sensing*, *45*(11), 3317–3341.
89. Kusche, J. (2003). A Monte-Carlo technique for weight estimation in satellite geodesy. *Journal of Geodesy*, *76*, 641–652.
90. Lambeck, K. (1988). *Geophysical geodesy: The slow deformations of the Earth*. Oxford: Clarendon Press.
91. Lambin, J., Morrow, R., Fu, L., Willis, J., Bonekamp, H., Lillibridge, J., et al. (2010). The OSTM/Jason-2 mission. *Marine Geodesy*, *33*(Supp 1), 4–25.
92. Lemoine, F., Goossens, S., Sabaka, T., Nicholas, J., Mazarico, E., Rowlands, D., et al. (2013). High-degree gravity models from GRAIL primary mission data. *Journal of Geophysical Research, Planets*, *118*, 1676–1699.
93. Liu, X. (2008). Global gravity field recovery from satellite-to-satellite tracking data with the acceleration approach. Ph.D. thesis, TU Delft.
94. Loveless, F., & Duncan, B. (1976). *Satellite-to-satellite tracking for orbit improvement and determination of a 1 degree x 1 degree gravity field*. National Technical Information Service, US Department of Commerce: Technical report.
95. Mayer-Gürr, T. (2006). Gravitationsfeldbestimmung aus der Analyse kurzer Bahnbögen am Beispiel der Satellitenmissionen CHAMP und GRACE. Ph.D. thesis, Institut für Theoretische Geodäsie der Universität Bonn.
96. Mayer-Gürr, T. (2015). The combined satellite gravity field model GOCO05s. In *EGU General Assembly Conference Abstracts* (Vol. 17, pp. 12364).
97. Mayer-Gürr, T., Ilk, K., Eicker, A., & Feuchtinger, M. (2005). ITG-CHAMP01: A CHAMP gravity field model from short kinematic arcs over a one-year observation period. *Journal of Geodesy*, *78*(7–8), 462–480.
98. Mayer-Gürr, T., Eicker, A., Kurtenbach, E., & Ilk, K. (2010). ITG-GRACE: Global static and temporal gravity field models from GRACE data. In Flechtner et al. (Ed.), *System Earth via geodetic geophysical space techniques*. Berlin: Springer.
99. Mayer-Gürr, T., Rieser, D., Hoeck, E., Brockmann, J., Schuh, W., Krasbutter, I., et al. (2012). The new combined satellite only model GOCO03. In *International Symposium on Gravity, Geoid and Height Systems. GGHS 2012, Venice, Italy*.
100. Meissl, P. (1971). A study of covariance functions related to the earth's disturbing potential. Technical report, OSU report 151, Columbus.
101. Menard, Y., Fu, L., Escudier, P., Parisot, F., Perbos, J., Vincent, P., et al. (2003). The Jason-1 mission. *Marine Geodesy*, *26*(3–4), 147–157.
102. Merson, R., & King-Hele, D. (1958). A new value for the Earth's flattening, derived from measurements of satellite orbits. *Nature*, *182*, 640.
103. Meyer, U., Jäggi, A., Beutler, G., & Bock, H. (2015). The impact of common versus separate estimation of orbit parameters on GRACE gravity field solutions. *Journal of Geodesy*, *89*(7), 685–696.
104. Montenbruck, O. (2000). *Satellite orbits-models, methods, and applications*. Springer.
105. Montenbruck, O., van Helleputte, T., Kroes, R., & Gill, E. (2005). Reduced dynamic orbit determination using GPS code and carrier measurements. *Aerospace Science and Technology*, *9*(3), 261–271.
106. Montenbruck, O., Rizos, C., Weber, R., Weber, G., Neilan, R., & Hugentobler, U. (2013). Getting a grip on multi-GNSS: The international GNSS service MGEX campaign. *GPS World*, *24*(7), 44–49.

107. Moritz, H. (1969). On the determination of the potential from gravity disturbances along a fixed direction. *Tellus*, *21*, 568–571.
108. Muller, P., & Sjogren, W. (1968). Mascons: Lunar mass concentrations. *Science*, *161*(3842), 680–684.
109. NASA. (1972). *Earth and ocean physics applications program* (Vol. II). Technical report, NASA, EOPAP: Rationale and program plans.
110. Newton, I. (1687). *Philosophiae naturalis principia mathematica*.
111. Nievergelt, Y. (2000). A tutorial history of least squares with applications to astronomy and geodesy. *Journal of Computational and Applied Mathematics*, *121*, 37–72.
112. NRC (1979). Applications of a dedicated gravitational satellite mission. Technical report, Panel on gravity field and sea level, Washington D.C.
113. O'Keefe, J. (1957). An application of Jacobi's integral to the motion of an Earth satellite. *The Astronomical Journal*, *62*(1252), 265–266.
114. Pavlis, N., Holmes, S., Kenyon, S., & Factor, J. (2012). The development and evaluation of the Earth gravitational model 2008 (EGM2008). *Journal of Geophysical Research, Solid Earth*, *117*, B04406.
115. Pearlman, M., Degnan, J., & Bosworth, J. (2002). The International laser ranging service. *Advances in Space Research*, *30*(2), 135–143.
116. Petit, G., & Luzum, B. (2010). *IERS technical note no. 36, IERS conventions 2010*. Verlag des Bundesamts für Kartographie und Geodäsie, Frankfurt am Main.
117. Ramillien, G., Biancale, R., & Gratton, S. (2011). GRACE-derived surface water mass anomalies by energy integral approach: Application to continental hydrology. *Journal of Geodesy*, *85*, 313–328.
118. Rapp, R. (1998). Past and future developments in geopotential modeling. In R. Forsberg, M. Feissel, & R. Dietrich (Eds.), *Geodesy on the move, IAG-Symposium* (Vol. 119, pp. 58–78). Berlin: Springer.
119. Reigber, C. (1989). Theory of satellite geodesy and gravity field determination. In *Lecture notes in Earth sciences* (Vol. 25, pp. 197–234). Kapitel Gravity field recovery from satellite tracking data. Springer.
120. Reigber, C., Luhr, H., & Schwintzer, P. (2002). CHAMP mission status. *Advances in Space Research*, *30*(2), 129–134.
121. Reigber, C., Schwintzer, P., Neumayer, K., Barthelmes, F., König, R., Förste, C., et al. (2003). The CHAMP-only earth gravity field model EIGEN-2. *Advances in Space Research*, *31*(8), 1883–1888.
122. Remondi, B. (1993). NGS second generation ASCII and binary orbit formats and associated interpolation studies. In G. L. Mader (Ed.), *Permanent satellite tracking networks for geodesy and geodynamics*. Berlin, Heidelberg, New York: Springer.
123. Rockwell,. (1984). *GPS interface control document, ICD-GPS-200*. Satellite Systems Division: International corporation.
124. Rummel, R. (1975). Downward continuation of gravity information from SST or satellite gradiometry in local areas. Technical report, OSU report 221, Columbus.
125. Rummel, R. (1979). Determination of short-wavelength components of the gravity field by satellite-to-satellite tracking or satellite gradiometry: an attempt to an identification of problem areas. *Manuscripta Geodaetica*, *4*, 107–148.
126. Rummel, R., & van Gelderen, M. (1992). Spectral analysis of the full gravity tensor. *Geophysical Journal International*, *111*, 159–169.
127. Rummel, R., Reigber, C., & Ilk, K. (1978). The use of satellite-to-satellite tracking for gravity parameter recovery. *ESA Space Oceanography, Navigation, and Geodynamics*, *137*, 153–161.
128. Schmid, P., & Vonbun, F. (1974). *The ATS-F/nimbus E tracking and orbit determination experiment*. International Convention and Exposition, New York, NY: In IEEE.
129. Schuh, W. (1996). *Tailored numerical solution strategies for the global determination of the Earth's gravity field*. Technical report, Mitt: Geodät. Instiute der TU Graz.
130. Schwarz, C. (1970). Gravity field refinement by satellite-to-satellite Doppler tracking. Technical report, OSU report 147, Columbus.

131. Seeber, G. (2003). *Satellite geodesy: Foundations, methods, and applications*. de Gruyter.
132. Shampine, L., & Gordon, M. (1975). *Computer solution of ordinary differential equations: The initial value problem*. San Francisco, W.H: Freeman.
133. Sheard, B., Heinzel, G., Danzmann, K., Shaddock, D., Klipstein, W., & Folkner, W. (2012). Intersatellite laser ranging instrument for the GRACE follow-on mission. *Journal of Geodesy*, *86*(12), 1083–1095.
134. Sjogren, W., Laing, P., Liu, A., & Wimberly, R. (1976). Earth gravity field variations from GEOS-3/ATS-6 satellite-to-satellite radio tracking. *EOS Transactions AGU*, *57*(4), 234.
135. Sneeuw, N. (2000). A semi-analytical approach to gravity field analysis from satellite observations. Ph.D. thesis, Deutsche Geodätische Kommission, Reihe C-527, München.
136. Sneeuw, N., Gerlach, C., Foldvary, L., Gruber, T., Peters, T., Rummel, R., et al. (2004). A window on the future of geodesy. In F. Sanso (Ed.), *IAG symposium series* (Vol. 128, pp. 288–293). Kapitel One year of time variable CHAMP-only gravity field models using kinematic orbits. Berlin: Springer.
137. Sośnica, K. (2015). Determination of precise satellite orbits and geodetic parameters using satellite laser ranging. Technical report, Geodätisch-geophysikalische Arbeiten in der Schweiz, Band 93, Schweizerische Geodätische Kommission, Institut for Geodäsie und Photogrammetrie, Eidg. Technische Hochschule Zürich, Zürich.
138. Sośnica, K., Jäggi, A., Thaller, D., Beutler, G., & Dach, R. (2014). Contribution of Starlette, Stella, and AJISAI to the SLR-derived global reference frame. *Journal of Geodesy*, *88*(8), 789–804.
139. Tangdamrongsub, N., Hwang, C., Shum, C., & Wang, L. (2012). Regional surface mass anomalies from GRACE KBR measurements: Application of L-curve regularization and a priori hydrological knowledge. *Journal of Geophysical Research*, *117*, B11406.
140. Tapley, B., Bettadpur, S., Ries, J., Thompson, P., & Watkins, M. (2004a). GRACE measurements of mass variability in the Earth system. *Science*, *305*, 503–505.
141. Tapley, B., Schutz, B., & Born, G. (2004b). *Statistical orbit determination*. Elsevier Academic Press.
142. Tapley, B., Bettadpur, S., Watkins, M., & Reigber, C. (2004c). The gravity recovery and climate experiment: Mission overview and early results. *Geophysical Research Letters*, *1*(9), L09607.
143. Teunissen, P., Kleusberg, A. (1998). *GPS for geodesy*. Springer. ISBN 3-540-63661-7.
144. Torge, W., & Müller, J. (2010). *Geodesy*. Berlin: Walter de Gruyter.
145. van den IJssel, J., Encarnao, J., Doornbos, E., & Visser, P., (2015). Precise science orbits for the Swarm satellite constellation. *Advances in Space Research*, *56*(6), 1042–1055.
146. Van Helleputte, T., Doornbos, E., & Visser, P. (2009). CHAMP and GRACE accelerometer calibration by GPS-based orbit determination. *Advances in Space Research*, *43*(12), 1890–1896.
147. van Loon, J. (2008). Functional and stochastic modelling of satellite gravity data. Ph.D. thesis, TU Delft.
148. Visser, P., & van den IJssel, J., (2015). Calibration and validation of individual GOCE accelerometers by precise orbit determination. *Journal of Geodesy*, *90*(1), 1–13.
149. Visser, P., Sneeuw, N., & Gerlach, C. (2003). Energy integral method for gravity field determination from satellite orbit coordinates. *Journal of Geodesy*, *77*(3–4), 207–216.
150. Vonbun, F., Kahn, W., Wells, W., & Conrad, T. (1980). Determination of 50x50 anomalies using satellite-to-satellite tracking between ATS-6 and APOLLO. *Geophysical Journal of the Royal Astronomical Society*, *61*, 645–657.
151. Švehla, D., & Rothacher, M. (2004). Kinematic precise orbit determination for gravity field determination. In F. Sanso (Ed.), *A window on the future of geodesy* (pp. 181–188). Berlin, Heidelberg, New York: Springer.
152. Wagner, C. (1983). Direct determination of gravitational harmonics from low-low GRAVSAT data. *Journal of Geophysical Research*, *88*(B12), 10309–10321.
153. Wahr, J. (1981). Body tides on an elliptical, rotating, elastic and oceanless earth. *Geophysical Journal of the Royal Astronomical Society*, *64*(3), 677703.

154. Wahr, J., Molenaar, M., & Bryon, F. (1998). Time variability of the Earth's gravity field: Hydrological and oceanic effects and their possible detection using GRACE. *Journal of Geophysical Research*, *103*(B12), 30205–30229.
155. Wang, X., Gerlach, C., & Rummel, R. (2012). Time-variable gravity field from satellite constellations using the energy integral. *Geophysical Journal International*, *190*, 1507–1525.
156. Weiffenbach, G., Grossi, M., & Shores, P. (1976). *Apollo-Soyuz doppler tracking experiment MA-089*. Smithsonian Astrophysical Observatory, Cambridge Mass: Technical report.
157. Weigelt, M., Sideris, M., & Sneeuw, N. (2009). On the influence of the ground track on the gravity field recovery from high-low satellite-to-satellite tracking missions: CHAMP monthly gravity field recovery using the energy balance approach revisited. *Journal of Geodesy*, *83*(12), 1131–1143.
158. Weigelt, M., van Dam, T., Jäggi, A., Prange, L., Tourian, M., Keller, W., et al. (2013). Time-variable gravity signal in Greenland revealed by high-low satellite-to-satellite tracking. *Journal of Geophysical Research, Solid Earth*, *118*, 3848–3859.
159. Wells, W., Conrad, T., & Kahn, W. (1977). Estimation of gravity anomalies with GEOS-3/ATS-6 satellite-to-satellite tracking data. *EOS Transactions*, *58*(6), 371.
160. Wolff, M. (1969). Direct measurement of the Earth's gravitational potential using a satellite pair. *Journal of Geophysical Research*, *74*(22), 5295–5300.
161. Wu, S., Yunck, T., & Thornton, C. (1991). Reduced-dynamic technique for precise orbit determination of low Earth satellites. *Journal of Guidance, Control, and Dynamics*, *14*(1), 24–30.
162. Yunck, T., Wu, S., Wu, J., & Thornton, C. (1990). Precise tracking of remote sensing satellites with the global positioning system. *IEEE Transactions on Geoscience and Remote Sensing*, *28*(1), 108–116. doi:10.1109/36.45753.
163. Zehentner, N., & Mayer-Gürr, T. (2015). Precise orbit determination based on raw GPS measurements. *Journal of Geodesy*, *90*(3), 275–286.
164. Zheng, W., Shao, C., Luo, J., & Hsu, H. (2006). Numerical simulation of Earth's gravitational field recovery from SST based on the energy conservation principle. *Chinese Journal of Geophysics*, *49*, 644–650.
165. Zheng, W., Hsu, H., Zhong, M., & Yun, M. (2012). Efficient accuracy improvement of GRACE global gravitational field recovery using a new inter-satellite range interpolation method. *Journal of Geodynamics*, *53*, 1–7.
166. Zuber, M., Smith, D., Watkins, M., Asmar, S., Konopliv, A., Lemoine, F., et al. (2013). Gravity field of the moon from the gravity recovery and interior laboratory (GRAIL) mission. *Science*, *339*, 668.
167. Zumberge, J., Heflin, M., Jefferson, D., Watkins, M., & Webb, F. (1997). Precise point positioning for the efficient and robust analysis of GPS data from large networks. *Journal of Geophysical Research*, *102*(B3), 5005–5017.